

Mouse Tracheal Epithelial Cells (mTECs) as a Tool to Study the Role of *BPIFA1* in Influenza A Infection.

Name of student Fawaz Aljuhani

A thesis submitted for the degree of Master of Philosophy (MPhil.)

June 2023

University of Sheffield

Faculty of Medicine, Dentistry and Health

Department of Infection, Immunity and Cardiovascular Disease

Supervisors: Professor Colin Bingle

Dr Lynne Bingle

Abstract

The respiratory epithelium is a major physical barrier to infections and provides a robust innate defensive shield through the concerted actions of the mucociliary epithelial layer and its secreted chemical components. Influenza A virus (IAV) is a major human pathogen that overcomes these defences to cause disease. The mechanism that the virus uses to infect the airway remains to be fully elucidated. We have employed primary airway cells grown in 3D cultures as models to understanding the role of epithelial cells in homeostasis and infectious disease. In these cells differentiation occurs when the confluent cell layer develops on the semi-permeable insert with the cells fed with media underneath, termed an air liquid interface (ALI) condition. Studies using mice tracheal epithelial cells (mTECs) at the ALI have recently shown that BPIFA1 (Bacterial Permeability increasing fold containing Family A member 1), a respiratory tract secreted protein, protects the airway from IAV infection. The mechanism for this remains unknown and it was assumed that the infection was occurring through ciliated cells.

In this thesis I have established and validated mTECs grown at an ALI as a tool for infection studies. I conducted a genome-wide transcriptional analysis to investigate global alterations in gene expression as the cells transitioned from isolated cells, through a basal cell intermediate phenotype, to full mucociliary differentiation. The cultures represent a model of the native tracheal epithelium. This analysis identified multiple genes as being up regulated during this process and serves as a resource for target gene identification. Using published single cell RNAseq data we could show that *Bpifa1* expression is seen in several cell types with by far the highest expression being seen in the secretory cells. A comparative expression analysis showed that *Bpifa1* was the most highly expressed member of the larger *Bpif* gene family in mTECs and confirmed that the closest murine paralog of the gene, *Bpifa5*, was not expressed in these cells, and would not be likely to serve a similar function.

Using IF microscopy I confirmed that IAV did not infect *BPIFA1* positive cells in mTEC cultures and was not commonly associated with ciliated cells at the early stages of infection. To address issues of cell specificity, I infected undifferentiated mTECs (lacking the mature epithelial phenotype) and could show that these were infected, despite the absence of ciliated cells. Levels of infection

were less than was seen in differentiated mTECs. A genome wide transcriptional study showed cells of both phenotypes (basal cell intermediate, and full mucociliary differentiation phenotypes) upregulated multiple interferons stimulated genes (ISGs), albeit with lower response in the undifferentiated cells. I identified the gut antimicrobial protein gene Lypd8, as a potential novel ISG. I employed this infection model to establish an assay for IAV infection of undifferentiated mTECs, which can be utilized to examine the role of BPIFA1 in IAV anti-viral responses. To investigate this further, I generated several recombinant BPIFA1 protein expression constructs that exhibit sequence differences in a presumptive functional domain at the N-terminus of the protein for use in this infection assay. Comparative analysis showed that this repeat region is highly variable between species and is longer in rodents. I also generated a series of short peptides corresponding to the repeat region in this domain. Both sets of BPIFA1derived reagents could be investigated for their ability to modulate IAV infection and to define more fully the functional mechanism that BPIFA1 employs against IAV infection. My results show that mTECs are a good model for studies investigating IAV infections. Undifferentiated mTECs can be used in a simple quantitative infection assay to unravel the contributions of specific regions of BPIFA1 in regulating IAV infection.

Statement of Contributions to Data Presented

This thesis uses new and published data to study the role of BPIFA1 in infection with Influenza A virus (IAV) using primary mTEC cultures at an air-liquid interface (ALI). I personally conducted the majority of the experimental work and data analysis as part of fulfilling the thesis requirements. Experimental work involving the primary cell cultures and the recombinant BPIFA1 protein expression constructs was undertaken by me. This involved the establishment, infection and analysis of mTECs at several differentiation stages. The data for the genome-wide transcriptional analyses presented in this thesis were generated from my samples using core technical help and the initial processing of the data were undertaken by Dr Paul Heath and Dr Miraj Chowdhury. My contribution to these datasets was in the analysis and interpretation of differential gene expression, particularly the role of interferon-stimulated genes and the expression profiles of BPIFA1 in different cell types. I used bioinformatics tools to reanalyze and redefine the data. For the fluorescence microscopy I prepared and stained the samples and imaging was performed by a dedicated technician with the help of members of the Bingle lab, particularly Dr Priyanka Anjuan. This clear delineation of data provenance and my analytical contributions assures transparency and recognizes the collaborative nature of scientific research.

List of Abbreviations

ALI – Air Liquid Interface
AMPs antimicrobial peptides
ASL- Airway surface liquid
AT1- Alveolar Type 1 cell
AT2- Alveolar Type 2 cell
BAL- Bronchoalveolar lavage fluid
BPI – Bactericidal / Permeability-increasing
BPIF- Bactericidal / Permeability-increasing fold containing
BPIFA1 - Bacterial permeability family member A1
BPIFB1 - Bacterial permeability family member B1
CETP- cholesterol ester transfer protein
CF Cystic fibrosis
CFTR- Cystic fibrosis Transmembrane Conductance Regulator
DCs - dendritic cells
ENaC – Epithelial sodium channel
HA - Hemagglutinin
HEK cells – Human embryonic Kidney Cells
HPAI - highly pathogenic avian influenza
HDPs - Host defence peptides
hAECs - human airway epithelial cells
HNPs - Human Neutrophil Peptides
IAV – Influenza A Virus
IFN L2- Interferon Lambda 2
ISGs -Interferon stimulated genes

KO-Knockout

LBP- lipopolysaccharide-binding protein

LPLUNC – Long palate, lung and nasal clone

LRT- Lower Respiratory Tract

LUNX - Lung specific protein X

LYPD8 - LY6/PLAUR Domain Containing 8

MCC-Mucociliary Clearance

MMR- macrophage mannose receptors

mTEC – Mouse tracheal Epithelial Cells

MUC5AC – Mucin 5AC

MUC5B - Mucin 5B

NA – Neuraminidase

NASG- Nasopharyngeal carcinoma-related protein

NC-Negative Control

NA - neuraminidase

NE - neutrophil elastase

NK - Natural killer ells

OAZ-1 - Ornithine decarboxylase antitype 1

PAMPs -Pathogen Associated Molecular Patterns.

PC - Positive Control

PCL-Periciliary Layer

pDCs- Plasmacytoid dendritic cells

PLTP- Phospholipid transfer protein

PLUNC- Palate Lung and Nasal Epithelial Clone

PRRs- Pattern recognition receptors

PSP-Parotid secretory protein

RIG-1 Retinoic Acid-Inducible Gene 1

SA - sialic acid

SLFN4 - schlafen 4

SPLUNC1 - short palate, lung, and nasal epithelial clone 1

SPURT - secretory protein in upper respiratory tract

TEKT1 - Tektin 1

TLR2 - Toll-like receptor 2

TLR3 - Toll-like receptor 3

TLR4 - Toll-like receptor 4

TLR7 - Toll-like receptor 7

TLR8 Toll-like receptor 8

URT-Upper Respiratory Tract

vRNP viral ribonucleoprotein

WAP - Whey Acidic Protein

WFDC Whey Four-Disulphide Core

WT-Wild Type

Conferences and presentations

1st year presentation at The University of Sheffield 8th July 2018. "The role of BPIFA1 /SPLUNC1 in influenza virus infection".

DRIP meeting at Medical School at The University of Sheffield 13th of March 2019. "The role of BPIFA1 /SPLUNC1 in influenza virus infection".

British Association for Lung Research (BALR) Annual Conference, Cambridge, UK. 10th-12th.September 2019 "Mouse tracheal epithelial cells (mTECs) for the study of influenza A infection".

3rd year presentation day at The University of Sheffield 14th July 2020. "Functional analysis of BPIFA1 in influenza A infection in mouse tracheal epithelial cells".

ERS Meeting Online e-poster 24th August 2020. "Functional analysis of BPIFA1 in influenza A infection in mouse tracheal epithelial cells (mTECs)".

Acknowledgments

The success of this research-based project needed a lot of labour, guidance, research, and assistance. I was really thankful to work on such a great research project because it helped to improve my knowledge and to learn new experimental protocols. The effective result of this undertaking required a great deal of work, direction, and help. I might want to say first a tremendous thank you to my project supervisor and tutor Prof Colin Bingle whose direction all through every one of these four years of my project was priceless. I'm massively thankful for the chance to work with you as your insight and help empowered me to get familiar with a great deal and procure a new range of abilities which will be exceptionally gainful for my future vocation. Thank you for your understanding and furnishing me with freedom to chip away at this task. I wish that each PhD student could have such coach like you! I might likewise want to say thank you to Dr Lynne Bingle whose help, exhortation, and advice made a difference to my examinations and allowed me to accomplish the most ideal outcome in four years of my investigations. I'm appreciative for the chance to work under such extraordinary management of Prof Colin Bingle and Dr Lynne Bingle as the two of them established an agreeable and driven workplace. I would not forget to remember Dr Priyanka Anujan of her help all through my MPhil. Many thanks to you, I took in a great deal about being a fruitful scientist from you. I would likewise like to say a gigantic thank you to lab specialized help at the University of Sheffield. I might want to offer my thanks to Dr Helen Marriott from the University of Sheffield for giving wild-type mice and Prof James Stewart from the University of Liverpool. A tremendous thank you to all individuals from the Bingle group and my MPhil companions who made each day of my MPhil a pleasant and significant experience. Many thanks to Abdulaziz, Zeyad, Miraj, Renata and Cameron for being magnificent companions and partners. I'm likewise very thankful to my parents, wife, and children for unrestricted love, backing, inspiration, and freedom to live my fantasies; I would have been unable to finish this excursion with no of you! Finally, I want to communicate my appreciation to the Kingdom of Saudi Arabia, Ministry of Health for financing this venture and empowering me to go to various meetings during my MPhil studies.

Contents

Abstract	2
Statement of Contributions to Data Presented	4
List of Abbreviations	5
Conferences and presentations	8
Acknowledgments	9
List of Figures	15
List of Tables	19
1 Introduction	21
1.1 Respiratory System (RS)	21
1.2 Upper Respiratory Tract (URT)	21
1.2.1 Nasal Cavity	21
1.2.2 Pharynx	21
1.3 Lower Respiratory Tract (LRT)	22
1.3.1 Trachea	22
1.3.2 Bronchi	23
1.3.3 Alveoli	24
1.4 Structural Cells of the Respiratory Epithelium	25
1.4.1 Basal Cells	26
1.4.2 Club Cells	27
1.4.3 Goblet (Mucous) Cells	27
1.4.4 Ciliated Cells	28
1.4.5 Neuroendocrine cells	28
1.4.6 Tuft Cells	29
1.4.7 lonocytes	29
1.4.8 Alveolar Type 1 (AT1) Cells	30
1.4.9 Alveolar Type 2 (AT2) Cells	30
1.5 Cellular Differences between Human and Mouse Airway Cells	31
1.6 Immunity	32
1.6.1.2 Anatomical and Chemical Barriers as Frontline Defence Mechanisms	33
1.6.2 Non-Structural (Immune) Cells of the Airways	34

1.6.3 Submucosal Glands	38
1.6.4 Intrinsic Immunity as a Form of Innate Immunity	38
1.6.5 Host defence peptides (HDPs)	39
1.6.5.1 Adaptive Immunity	40
1.6.5.2 Cathelicidins/LL-37	40
1.6.5.3 α -Defensins (Human Neutrophil Peptides (HNPs)	41
1.6.5.4 β-Defensins	41
1.6.5.5 Lactoferrin	42
1.6.5.6 Lysozyme	42
1.6.5.7 Whey Acidic Protein (WAP)/Whey Four-Disulphide Core (WFDC) Proteins	42
1.7 Influenza Virus	43
1.8 Viral Life Cycle	47
1.9 Innate Immune Defence System in the Presence of Influenza	49
1.10 PRRs Involved in Respiratory Viral Infections	51
1.11 TLRs	51
1.11.1 TLR2 and TLR4	52
1.11.2 TLR3	53
1.11.3 TLR7 and TLR8	53
1.12 Retinoic Acid-Inducible Gene 1 (RIG-1) Receptors	53
1.13 IFN Signalling and Antiviral Action	53
1.14 Bactericidal/Permeability-Increasing (BPI) Protein Family	54
1.14.1 PLUNC, Bacterial Permeability-Increasing Fold Containing Family Member A (BBPIF Gene Family	•
1.14.2 Localisation of BPIFA1	56
1.15 Comparative Analysis of BPIF Genes	58
1.16 Functions of BPIFA1	60
1.16.1 Antibacterial Function	60
1.16.2 Immunomodulatory and Chemotactic Functions	61
1.17 Structural Features of BPIFA1	62
1.18 Role of BPIFA1 in Pulmonary Diseases	66
1.18.1 CF	66
1.18.2 COPD	67
1.18.3 Asthma	67

	1.18.4 Idiopathic Pulmonary Fibrosis (IPF)	67
	1.18.5 Mucociliary Clearance	68
	1.19 BPIFA1 and Viral Infection	68
	1.20 Mouse Cell Models for Studying Respiratory Infections	70
	1.20.1 Proliferation of mTECs	70
	1.20.2 Differentiation of mTECs	70
	1.21 ALI Culture of mTECs	71
	1.21.1 mTECs and Infections	71
	1.22 Hypothesis and Aims of the Study	71
2	Materials and Methods	74
	2.1 Direct-Zol RNA Miniprep Protocol	74
	2.2 RNA Gel	74
	2.3 Complementary DNA (cDNA) Synthesis	74
	2.4 Reverse Transcription (RT)-PCR	75
	2.5 DNA Gel Electrophoresis	76
	2.6 RNA Array Analysis	77
	2.6.1 Bioinformatic Analysis	77
	2.7 Generation of mBPIFA1 Constructs	78
	2.7.1 Transformation of Plasmid Construct VR1255 Into Competent Bacteria	78
	2.7.2 Miniprep Extraction of Constructs	79
	2.7.3 Midi-Preparations of Recombinant Plasmids	79
	2.8 Site-Directed Mutagenesis (SDM)	80
	2.9 Synthesis DNA of <i>BPIFA1</i> Constructs	82
	2.10 DNA Sequencing	83
	2.11 Sodium Dodecyl Sulphate–Polyacrylamide Gel Electrophoresis (SDS-PAGE) and Western Blotti	•
	2.12 Dot Blotting	84
	2.13 Cell Line Transfection	84
	2.14 Culture of mTECs	85
	2.14.1 In Vitro Culture of mTECs	85
	2.15 Infection of mTECs With IAV (H3N2)	87
	2.16 ALI Culture Sample Fixation	88
	2.17 Analysis of the Samples From In Vitro Infection Assays	88

2.17.1 Fluorescence Immunocytochemistry	88
2.17.2 Quantification of IAV Staining	90
2.18 Statistical Analysis	90
Chapter 3: Validation of mTEC cultures	91
3.1 Introduction	92
3.2 Aims of the Chapter	92
3.3 Results	93
3.3.1 Description of mTEC Cultures	93
3.3.2 Validation of Gene Expression by RT-PCR	93
3.3.3 SDS-PAGE	97
3.3.4 Confocal Imaging of Cells During Differentiation	98
3.3.5 Gene Expression in Whole-Genome Expression Data Sets	99
3.3.5.1 Most Highly Expressed Genes in the Original, Day 0 and Day 14 Cells	100
3.3.5.2. Transcriptional Changes in the Gene Expression During mTEC Differentiation	103
3.3.5.3. Differential Gene Expression Between the Original and Day 0 Cells	105
3.3.5.4. Differential Gene Expression Between the Day 0 and 14 Cells	109
3.3.5.5 Differential Gene Expression Between the Original and Day 14 Cells	114
3.4 Validation of the Gene Expression During Differentiation	118
3.5 Cell Type Representation in the ALI Differentiated mTECs	119
3.6 Expression of Selected Genes During mTEC Differentiation	122
3.7 High Expression of <i>Bpifa1</i> in the Secretory Cells in the mTECs	124
3.8 Expression of BPIF Family Members in the Differentiated mTECs	127
3.10 Discussion	131
4.1 Introduction	137
4.2 Results	139
4.2.1 Effects of Infection on the mTECs	139
4.2.2 Genome-Wide Analysis of the Gene Expression in the Infected mTECs	141
4.2.3 Expression of selected genes in the IAV-infected mTECs	143
4.2.4 Cell-Specific Infection of the mTECs	146
4.2.5 IAV Infection of the Undifferentiated mTECs	149
4.2.6 Genome-wide transcriptional responses to IAV Infection of undifferentiated and differentiated mTECs	152
4.2.7 Expression of membrane-spanning proteases in the mTECs	

4.3 Discussion	163
4.4 Summary	166
5.1 Introduction	
5.2 Results	169
5.2.1 Sequence Analysis of BPIFA1	169
5.2.2 BPIFA5 is a close paralogue of BPIFA1 but does not conserve the N-terminal regions	172
5.2.4 Generation of FLAG-Tagged BPIFA1 constructs in the VR1255 Vector	175
5.2.5 Production of VR1255 DNA for cloning reactions	176
5.2.7 Generation of FLAG-Tagged mBPIFA1 Mutant Constructs in VR1255	179
5.2.8 Generation of Pig and M. pahari BPIFA1 Flag-Tagged Constructs	183
5.2.9 Transfection of the BPIFA1-VR1255 plasmids into HEK Cells	185
5.2.10 Production and secretion of the BPIFA1-FLAG recombinant proteins	186
5.2.11 Planned experiments with recombinant proteins	188
5.2.15 Discussion	190
6.1 General Discussion	194
6.2 Limitations of the Study	197
6.3 Conclusion	198

List of Figures

- Figure 1.1. Diagram of the respiratory tract
- Figure 1.2. The Alveolar unit.
- Figure 1.3. Epithelial cell types of the airways
- Figure 1.4. Cell lineage relationship obtained from human surface airway epithelium.
- Figure 1.5. Epithelial cell type conservation between human and mouse are not conserved.
- Figure 1.6. An illustration the barriers of immunity pathogens immunity.
- Figure 1.7. The process of mucociliary clearance in the respiratory tract.
- Figure 1.8. Illustration of the timeline history of Influenza virus since 1980's elaborating 6 pandemics at that time
- Figure 1.9. Redrawing Structure and composition of Influenza A Virus
- Figure 1.10. The IAV life cycle in the respiratory tract.
- Figure 1.11. Airway proteases involved with IAV infection.
- Figure 1.12. Innate immune response against the influenza (IAV) infection.
- Figure 1.13. Staining of BPIFA1 in mouse trachea.
- Figure 1.14. Tissue restricted Bpifa1 expression in the mouse.
- Figure 1.15. Tissue restricted BPIFA1 expression in human tissues.
- Figure 1.16. Chromosomal locations of BPIF genes in human and mouse.
- Figure 1.17. Structural similarity between BPIFA1 and BPI.
- Figure 1.18. Superimposition of Mouse and Human BPIFA1 Protein Structures.
- Figure 1.19. Multiple sequence alignment of BPIFA1.
- Figure 2.1. mBPIFA1 gene cloned into VR1255 vector
- Figure 2.2. Overview of mTEC Isolation Process.
- Figure 3.1. Phase contrast images of mTECs during differentiation
- Figure 3.2. End-point RT-PCR of markers in mTECs during ALI differentiation
- Figure 3.3. Secretion of BPIFA1 from mTEC cultures
- Figure 3.4. Immunofluorescence (IF) microscopic detection of β -TUBULIN and BPIFA1 in day 14 mTECs

- Figure 3.5. Heat map of genes differentially expressed during mTEC culture
- Figure 3.6. Differentially expressed genes in uncultured tracheal epithelial (original) cells and day 0 ALI cells
- Figure 3.7. Differentially expressed genes in day 0 and day 14 ALI cells.
- Figure 3.8. Differentially expressed genes in day 14 ALI cells and the original cells
- Figure 3.9. End-point RT-PCR of selected genes in ALI-differentiated mTECs
- Figure 3.10. SPRING representation of gene expression in single mouse tracheal cells.
- Figure 3.11. Cell type specific localisation of selected genes in mTECs
- Figure 3.12. Cell type specific localisation of additional genes in mTECs.
- Figure 3.13. Differential gene expression in original, day 0 and day 14 mTECs
- Figure 3.14: Expression of selected genes in an RNAseq mTEC data set
- Figure 3.15. Absolute expression of Bpifa1 in different mTEC cell populations
- Figure 3.16. The top 20 most highly expressed genes in mouse tracheal secretory cells
- Figure 3.17. Expression of Bpif genes in day 14 mTEC cultures.
- Figure 3.18. Expression pattern of top 50 genes in non-infected mTECs and virus-infected cells.
- Figure 3.19. Expression pattern of top 50 genes in mTEC source cells and virus-infected cells (ALI, Day14).
- Figure 3.20. Expression pattern of top 50 genes in mTEC source cells and cells at ALI on day 14.
- Figure 3.21. Gene Expression Analysis of mTEC Source Cells, non-infected, and IAV-Infected Cells.
- Figure 3.22. Gene Expression Analysis of mTEC Source Cells, non-infected, and IAV-Infected Cells
- Figure 3.23. Gene Expression Analysis of mTEC ALI non-infected, IAV-Infected and mTEC interferon cells.
- Figure 3.24. Gene Expression Analysis of mTEC cells
- Figure 3.25. Gene Expression Analysis of mTEC source, infected and non-infected cells
- Figure 3.26. Gene Expression Analysis of mTEC cells in ALI with DAPT.
- Figure 3.27. Gene Expression Analysis of mTEC source cells and those grown at ALI.
- Figure 3.28. Gene Expression Analysis of mTEC source cells and those grown at ALI.
- Figure 4.1. IAV nucleoprotein staining increases in infected mTEC cells over time

- Figure 4.2. Time and Dose Dependence of IAV Infection in mTECs
- Figure 4.3. Expression of Bpifa1 and Tekt1 during IAV infection in mTECs
- Figure 4.4. Expression of target genes in IVA infected mTEC cells
- Figure 4.5. Schematic representation of IAV infection protocol in differentiated mTECs.
- Figure 4.6. Day 14 infected cells stained with BPIFA1 and IAV
- Figure 4.7. Co-staining of infected mTECs with tubulin and IAV-Np
- Figure 4.8. Schematic representation of IAV infection protocol in undifferentiated mTECs
- Figure 4.9. Co-staining of infected undifferentiated and differentiated mTECs with tubulin and IAV-Np.
- Figure 4.10. Co-staining of infected mTECs with tubulin and IAV-NP in undifferentiated and differentiated m TECs.
- Figure 4.11. Infection of undifferentiated and differentiated mTECs with IAV
- Figure 4.12. Scatter plot of day 0 infected mTECS
- Figure 4.13. Volcano plot of day 0 infected mTECs
- Figure 4.14. Scatter plot of day 14 infected mTECS
- Figure 4.15. Volcano plot of day 14 infected mTECS
- Figure 4.16. Scatter plot of differentially expressed genes in IAV infected mTECs.
- Figure 4.17. Heat map analysis of IAV induced gene in undifferentiated and differentiated Figure 4.18. Heat map data of the top 10 induced genes from day 0 and day 14 mTECs
- Figure 4.19. Membrane spanning proteases gene expression during IAV infection
- Figure 5.1. Comparative analysis of mBPIFA1 by BLAST analysis
- Figure 5.2. Alignment of the N-terminal region of selected rodent BPIFA1 proteins
- Figure 5.3. Evolutionary relationship between BPIFA1 and BPIFA5.
- Figure 5.4. Lack of conservation of N-Terminal domains between rodent BFIFA1 and BPIFA5
- Figure 5.5. Sequences of BPIFA1 for construct production
- Figure 5.6. Schematic diagram of the BPIFA1-FLAG constructs.
- Figure 5.7. Map of mammalian VR1255 plasmid.
- Figure 5.8. VR1255 DNA digest for initiating cloning.

- Figure 5.9. Primers for generation of mBPIFA1-FLAG.
- Figure 5.10. Sequencing of mBPIFA1 long deletion clone from SDM
- Figure 5.11. Alignment of BPIFA1 proteins to be used for functional analysis
- Figure 5.12. Diagnostic digest of BPIFA1 expression constructs
- Figure 5.13. Transient transfections of HEK293T cells
- Figure 5.14. Secretion of mBPIFA1-Flag into HEK conditioned media.
- Figure 5.15. Secretion of different BPIFA1-Flag proteins into conditioned media
- Figure 5.16. Development of a functional assay: BPIFA1 containing ALI secretions block IAV infection
- Figure 5.17. BPIFA1 derived peptides for functional studies

List of Tables

- Table 2.1 The primer pairs used in the study are shown table.
- Table 2.2 Primary antibodies in immunostaining.
- Table 2.3 Secondary antibodies in immunostaining.
- Table 3.1 RNA recovery from HEK cells.
- Table 3.2 The top 50 most highly expressed genes in mTECs at different times points.
- Tale 3.3 Top 50 most differentially expressed genes in original cells compared to day 0 cells.
- Table 3.4 Expression of top 50 most differentially expressed genes in day 0 and compared to day 14 ALI cells.
- Table 3.5 The top 50 genes in original and day 14 cells.
- Table 4.1 The top 50 induced genes in IAV infected mTECs.
- Table 4.2 Expression of selected genes from mTEC RNAseq data.
- Table 4.3 Expression of selected genes from infected whole lung RNAseq data.
- Table 4.5 The top 50 most induced genes between day 0 IAV and day 0 mock infected mTECs.
- Table 4.6 The top 50 most induced genes between day 14 IAV and day 14 mock infected mTECs.
- Table 5.1 Primer sequences used in PCR for Site directed mutagenesis.

Chapter 1: Introduction

1 Introduction

1.1 Respiratory System (RS)

The main function of the RS is gaseous exchange, wherein oxygen is inhaled, and carbon dioxide (CO₂) is exhaled. The respiratory tracts include an upper respiratory tract (URT) and lower respiratory tract (LRT) (Figure 1.1). The URT includes the nasal passage, anterior nares, paranasal sinuses, oropharynx and nasopharynx, while the LRT includes the larynx, trachea, bronchi, bronchioles, and alveoli (Man, de Steenhuijsen Piters et al. 2017)

1.2 Upper Respiratory Tract (URT)

1.2.1 Nasal Cavity

The nasal cavity is mainly responsible for filtering inhaled air, preventing entrance of foreign particles in the RS. Humans breathe mostly through their noses, while rodents are obligate nose breathers. The olfactory receptors present in the nasal cavity allow the sense of smell. Two different kinds of mucosal tissues line the nasal cavity: the respiratory mucosa and olfactory mucosa. Olfactory receptors are present in the olfactory mucosa. Conversely, pseudostratified ciliated columnar epithelia containing goblet cells constitute the respiratory mucosa. Mucus is produced by the secretory glands, and host defence peptides and antibacterial enzymes are found in this secretion (Youssef, Kassem et al. 2018).

1.2.2 Pharynx

The pharynx connects the mouth and nasal cavity to the oesophagus and larynx. It is shaped like a funnel and is made up of three components: the nasopharynx, oropharynx and laryngopharynx (Hennessy 2016). The nasopharynx is present at the back of the nasal cavity and serves as a passageway for air. Pseudostratified ciliated epithelial cells are present in the nasopharynx, which facilitate movement of mucus towards the throat (Dahl and Mygind 1998) (Martin 2017). Next to the nasopharynx is the oropharynx, which works as a pipe for the passage of air and food. This component is covered with a squamous epithelial layer. Finally, at the larynx (also known as the voice box), the respiratory tract separates from the digestive tract (Deshmukh 2020). Stratified squamous epithelia line the larynx, which functions as a channel for air as well as food (Fritz

2019), and are critically important for speech (Nocini, Molteni et al. 2020). The larynx allows the execution of a switching mechanism that functions to ensure that food and air are transported properly.

1.3 Lower Respiratory Tract (LRT)

1.3.1 Trachea

The trachea (or windpipe) is the part of the LRT that starts from the larynx and ends at the midthorax as it divides into two bronchi. It protrudes from the cricoid cartilage, which serves as the base for the larynx (Figure 1.1) (Davies 2014). The wall of the trachea is made up of three different layers: the mucosa, submucosa, and adventitia. The trachea plays many roles including filtering, humidifying and warming air prior to its entry into the lungs (Al-Qadi, Artenstein et al. 2013). The length and diameter of the trachea are around 11 cm and 2.5 cm, respectively. The trachea divides into two bronchi that enter the lungs (Raja 2019). The ciliated cells present in the trachea regulate movement of ions and fluid and remove foreign particles. The goblet/secretory cells present therein secrete mucins, giving rise to a protective boundary. Finally, the tracheal basal cells serve as a stem cell population and are involved in healing following injury (Raja 2019).

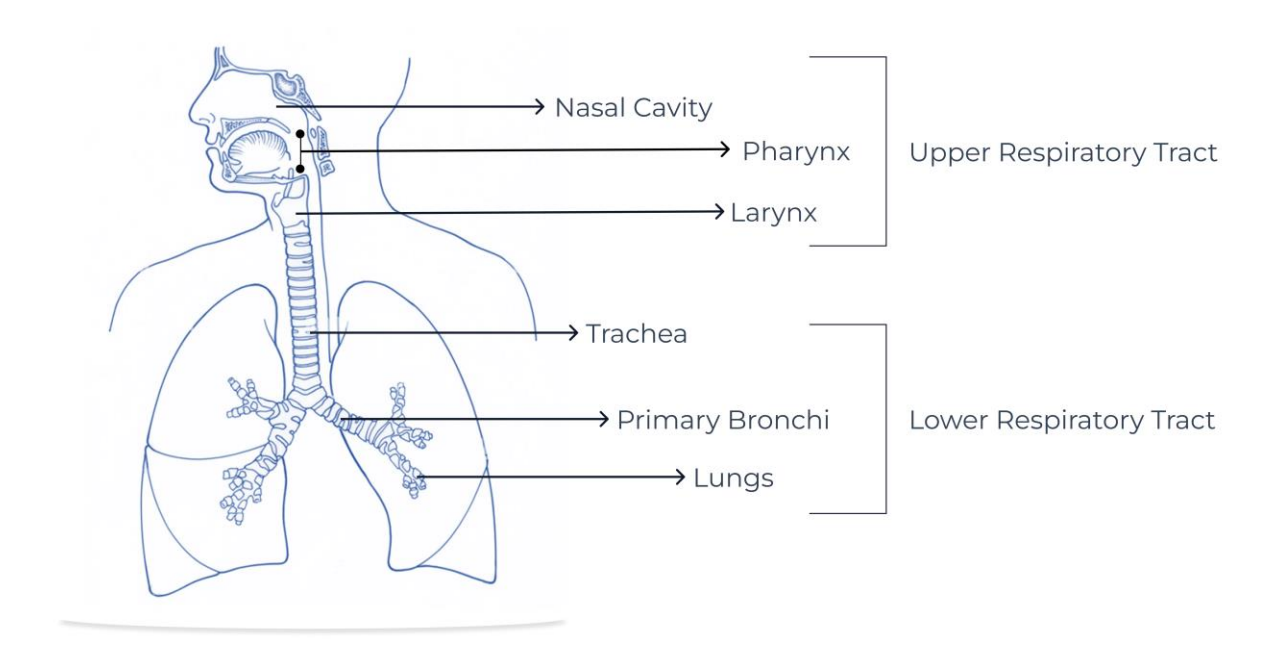


Figure 1.1. The Respiratory Tract

This figure illustrates the lower respiratory tract, which comprises trachea, bronchi and peripheral lung, and the upper respiratory tract (Teirumnieks 2020)

https://creativecommons.org/licenses/by-sa/4.0/

.

1.3.2 Bronchi

The bronchi are divided into several branches: The primary, secondary and tertiary bronchi end in the bronchioles. These air passages connect to the tiny sacs of the alveolar tissue (Frank 2014). The LRT has a pseudostratified columnar epithelial layer containing goblet, basal and ciliated cells (Berube, Prytherch et al. 2010).

1.3.3 Alveoli

The alveoli are the regions of the peripheral lung where gaseous exchange occurs predominantly (Figure 1.2). These bronchiolar ducts end in terminal clumps of alveoli called alveolar sacs. About 300 million gas-containing alveoli are present in the body (Rogers 2010). The alveolar walls are extremely thin and are made up of simple of squamous epithelial cells. Pulmonary capillaries cover the alveoli on their outer side. These capillaries contain blood and exchange gas through alveolar type 1 (AT1) cells that they abut on one side (Yang, Hernandez et al. 2016). The alveoli also contain cuboidal shaped type 2 cells. These cells are mainly responsible for generating a fluid-containing surfactant, which coats the inside of the alveoli that is exposed to gas. The cells also generate some host defence proteins (HDPs).

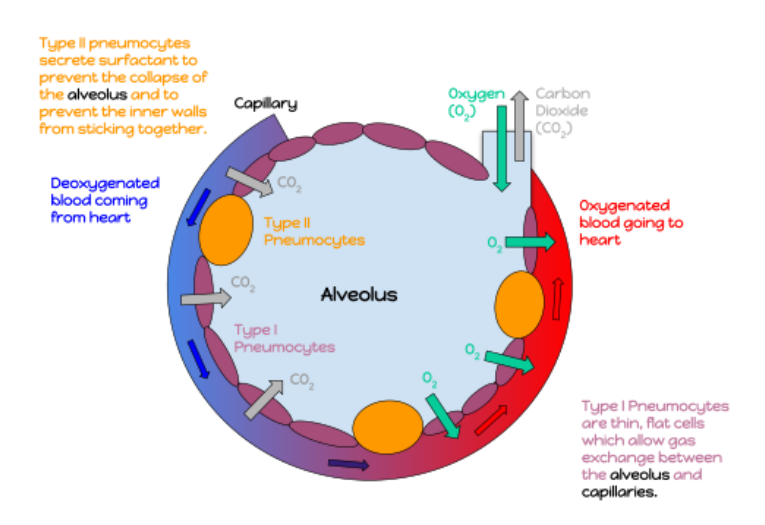


Figure 1.2. Alveolar Unit

The alveolar unit allows gas exchange of oxygen and carbon dioxide between blood and alveolar air. It contains type I and type II pneumocytes, fibroblasts, and macrophage ("Anannotated diagram of an alveolus" by Katherinebutler1331 is licensed under CC BY-SA 4.0. To view a copy of this license, visit https://creativecommons.org/licenses/by-sa/4.0/?ref=openverse.)

(https://creativecommons.org/licenses/by-sa/4.0/).

1.4 Structural Cells of the Respiratory Epithelium

The respiratory epithelium is pseudostratified and lines the tract from the nose to the terminal bronchioles. Multiple cells within the epithelium contribute to its function and are a primary means of lung defence. These cells include basal, supra-basal, goblet, club, and ciliated cells and pulmonary ionocytes as shown in Figure 1.3. The lineage relationships between the airway cells have been undergoing some revision in recent studies conducted with single-cell RNA sequencing (scRNAseg). These studies have shown that basal cells first divide into club cells. Goblet cells arise from club cells and then divide into multiciliated cells. When scRNAseq was undertaken in the airways of humans, additional cells were also identified including deuterosomal cells (a type of ciliated cell) and hybrid mucous-multiciliated cells (Guo, Du et al. 2019). In chronic respiratory disorders, such as chronic obstructive pulmonary disease (COPD), asthma, and cystic fibrosis (CF), the number of goblet cells is increased, while that of ciliated cells is decreased (Cohn 2006) (Curran and Cohn 2010). The cells in the respiratory tract have long been thought to exist in a defined classification, but some differences of opinion exist among authors concerning the usage of different names and the precise division into distinct cell types. For example, (Schiller, Montoro et al. 2019) Schiller et al. (2019) defined club cells as those that express SCGB1A1, MUC5AC and MUC5B, whereas other authors consider cells to be club cells if they express only SCGB1A1 (Schiller, Montoro et al. 2019). Another sub-type of club cell, which was seen to have much higher levels of immune system regulatory genes, was also found (Zaragosi, Deprez et al. 2020). The use of scRNAseq has allowed some revision of the interrelationships between different epithelial cell types as shown in Figure 1.4.

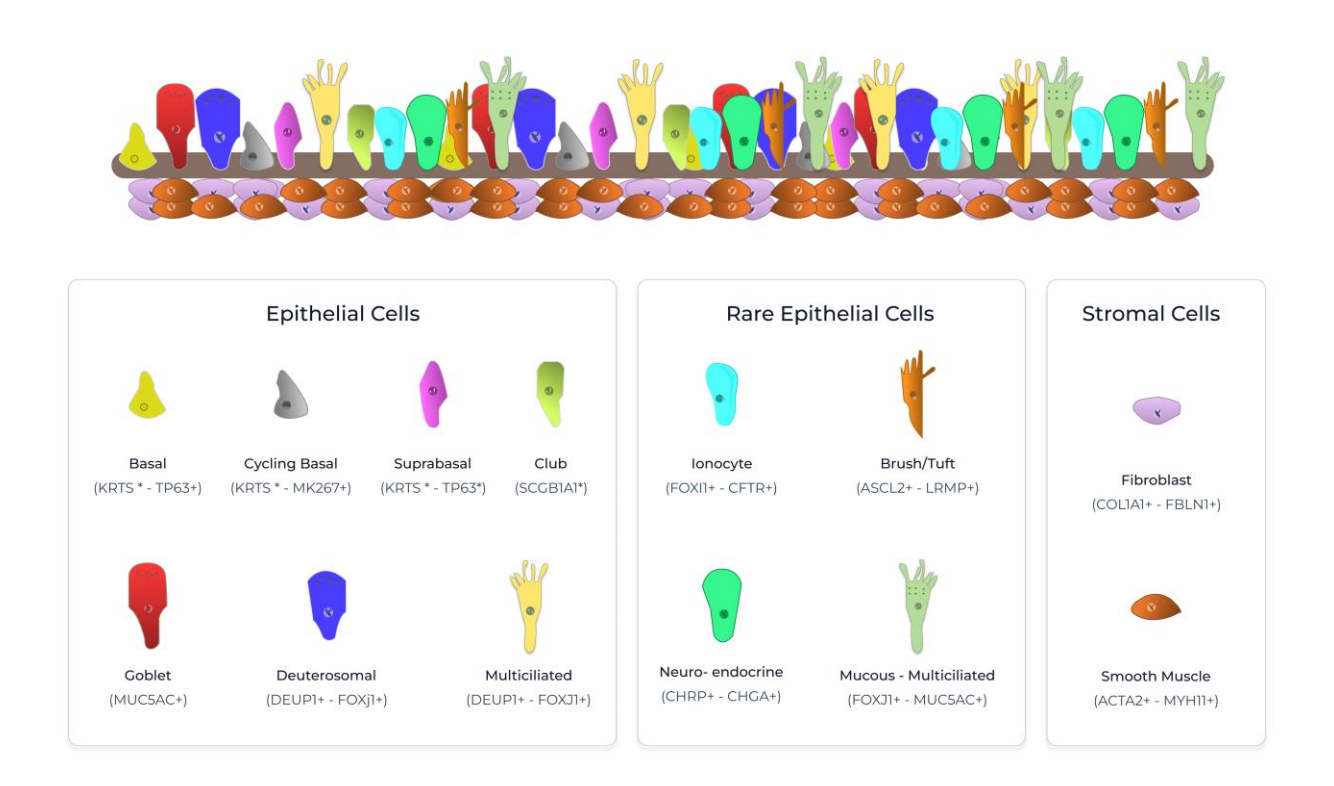


Figure 1.3. Types of Epithelial Cells in the Airways

This schematic diagram illustrates various types of epithelial cells along with rare epithelial and stromal cells (Montoro, Haber et al. 2020) .

The respiratory epithelium outside of the alveolar space is pseudostratified. This means that all epithelial cells directly sit on the basement membrane. These cells include large numbers of ciliated, goblet, club/serous and basal cells as well as rarer brush and neuroendocrine cells (NECs) and the recently identified ionocytes. These cell types are described below.

1.4.1 Basal Cells

Basal cells are found at the bottom of the epithelial layer and can generate all epithelial cells in the airways (Figure 1.3). The transcription factor *TP63* is expressed in basal cells and, along with certain keratins, marks this cell population (Morimoto 2010) (Siebel 2017). The NOTCH signalling pathway is needed for sustaining and differentiating basal cells (Rock 2009). This is verified by

the fact that basal cells express NOTCH ligands such as JAG1 and JAG2. When NOTCH signalling is activated in basal cells, these cells differentiate into secretory cells (Stupnikov, Yang et al. 2019). Conversely, in the absence of NOTCH signalling, ciliated cells are formed from basal cells (Whitsett and Alenghat 2015).

1.4.2 Club Cells

Club cells are present within the bronchiolar and tracheal epithelia. Initially, they were known as Clara cells, but this name is no longer used (Winkelmann and Noack 2010) (Lynch 2016). These cells are located next to ciliated cells, and their numbers vary depending on the exact location in the airways (Figure 1.3). They play a considerable secretory role and are responsible for generating pro-inflammatory cytokines and immune proteins that regulate innate immunity and play homoeostatic function (Whitsett and Alenghat 2015). Club cells also produce glycosaminoglycans, are a significant site of expression of xenobiotic-metabolising enzymes including cytochrome p450s and play a role in the reduction of oxidative stress (Dean and Snelgrove 2018). The most established marker for these cells is SCGB1A1, which is identified in part because of its ability to bind to polychlorinated biphenyls (Nordlund-Moller, Andersson et al. 1990). Overall, club cells are involved in safeguarding the lining of the bronchioles (Whitsett and Alenghat 2015).

1.4.3 Goblet (Mucous) Cells

Goblet cells situated within the conducting epithelium secrete mucin glycoproteins, principally the gel-forming mucins MUC5AC and MUC5B, and lipids onto the epithelial wall (Rogers 2003) (Taherali, Varum et al. 2018). These cells have mucin-containing granules and exhibit a characteristic morphology that gave rise to the term 'goblet cell'. Goblet cell products facilitate the entrapment and clearance of inspired irritants, microorganisms and particles (Ivanova, Sotirova et al. 2022). A recent single-cell analysis has reclassified goblet cells into goblet, mucous and serous cells based on specific gene signatures, and this distribution appears different between mice and humans (Travaglini, Nabhan et al. 2020). This cell population is substantially responsive to infection and allergy and has the capacity to alter its phenotype in diseases. If

NOTCH signalling increases SAM-pointed domain Ets-like factor (SPDEF) levels, the production of mucins is regulated, and mucous cell metaplasia, hyperplasia or dysplasia occurs (Chen, Korfhagen et al. 2009) (Rajavelu, Chen et al. 2015) (Parekh, Nawroth et al. 2020). SPDEF is therefore essential for differentiation of the goblet cell. Goblet cells and submucosal glands are strongly influenced by environmental components such as allergens and bacterial contaminants. If mucus overproduction is not controlled, lung inflammation can occur, consequently resulting in airway obstruction and chronic lung disease (Whitsett and Alenghat 2015, Whitsett 2018).

1.4.4 Ciliated Cells

The ciliated cells present in the respiratory epithelium are typically elongated columnar cells, and each cell has around 150–250 motile cilia on its apical surface (Ghanem, Laurent et al. 2020). Ciliated cells are responsible for mucociliary clearance, which is the process by which airway secretions are moved from the lungs into the pharynx and swallowed. The cilia present on the cell surface move to propel particles and pathogens out of the airways through coordinated beating (Bastola, Young et al. 2021). Geminin coiled-coil domain-containing protein 1 (*GMNC*), multiciliate differentiation and DNA synthesis associated cell (*MCIDAS*) and forkhead box J1 (FOXJ1) are key transcription factors that regulate the development of cilia and deuterosomes (organelles involved in multiciliated cell centriole expansion) (Whitsett 2018). Other genes required for ciliogenesis include *MYB*, *RFX2* and *RFX3* (*Arbi*, *Pefani* et al. 2016, *Campbell*, *Quigley* et al. 2016). Classical ciliated cells appear to be derived from basal cells through a range of intermediate cells including deuterosomal and mucous—deuterostomal cells (Figure 1.4).

1.4.5 Neuroendocrine cells

The respiratory Neuroendocrine cells (NEC) are known to have both neural and endocrine functions. They are known to play a role in the regulation of airway function, including epithelial cell proliferation and differentiation (Klimov, Cherevko et al. 2022). After injury, these cells stimulate other cells to initiate repair of the bronchial epithelium and appear to act as sensor cells that control immune responses in the airways (Ouadah, Rojas et al. 2019, Croasdell Lucchini,

Gachanja et al. 2021). Mutant mice deficient in NECs exhibit a poor response to allergy. They express CGRP and ASCL1 as marker genes (Branchfield, Nantie et al. 2016).

1.4.6 Tuft Cells

Tuft cells, also known as brush cells, are rare and solitary chemosensory cells found in the respiratory epithelium (Davis and Wypych 2021). They recently have come under examination owing to the discovery of them having connections to type 2 immunity, mediating chemosensing, modulating inflammation and producing acetylcholine (Branchfield, Nantie et al. 2016). Tuft cells appear to act as a conduit between ligands from the external space through taste-like signalling pathways for the generation of output, which is a unique feature among airway epithelial cells (Kotas, O'Leary et al. 2023).

1.4.7 Ionocytes

Pulmonary ionocytes have been recently identified in several scRNAseq studies and shown to express a higher level of cystic fibrosis transmembrane conductance regulator (CFTR), the transporter protein for chloride ions, than other cells present in the airways. Therefore, these cells seem to play a role in the physiology of regulating airway surface fluid and can be potential players in the pathogenesis of CF. When *Foxi1*, an ionocyte transcription factor, is eliminated from ionocytes, the expression of *cftr* is lost in mice (Montoro, Haber et al. 2018). Ionocytes arise from precursor basal cells, and *Foxi1* is expressed in the basal cells of the airways after injury (Hawkins and Kotton 2018, Plasschaert, Zilionis et al. 2018).

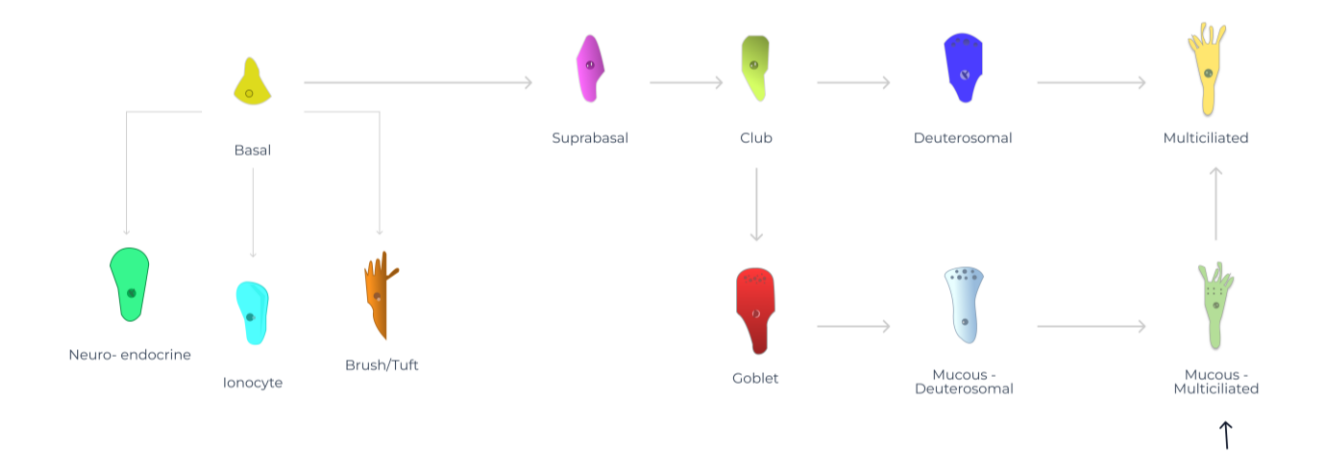


Figure 1.4. Lineage Relationship of Cells from Human Airway Epithelia

This figure shows the lineage relationships of individual cell types found in the trachea and the large airways in recent single-cell RNA sequencing studies. Adapted from (Zaragosi, Deprez et al. 2020).

1.4.8 Alveolar Type 1 (AT1) Cells

AT1 cells exhibit structural and anatomical characteristics needed to allow effective gaseous exchange (Figure 1.2). The substantially thin membrane present between the pulmonary capillaries and alveoli allows exchange of gas through passive diffusion (Saha and Chong 2021). AT1 cells play a crucial role in maintaining homoeostasis of the alveoli, as they allow passage of ions and water required by the epithelial layer of the alveoli (Agnese, Calvano et al. 2002). At the molecular level, NK homeobox 2-1 (*NXK2.1*) is required for the formation and regulation of AT1 cells (Torre and Flores 2020).

1.4.9 Alveolar Type 2 (AT2) Cells

AT2 cells are found in the alveolar region of the lungs. They contribute to the maintenance and repair of the alveolar epithelial barrier that separates the air spaces of the lungs from the blood vessels (Olajuyin, Zhang et al. 2019). These cells substantially contribute to the production and secretion of proteins and surfactant lipids (Mezoughi 2021). Infection and injury affect the number and secretory potential of AT2 epithelial cells. The surfactant that these cells produce is

involved in lowering the surface tension of the cell surface, thereby preventing alveolar collapse in case of expiration atelectasis (Ghati, Dam et al. 2021). The role of AT2 cells in host defence against pathogens has also been established. By secreting cytokines, they allow inflammatory cells to initiate an immune response (Kumar, Zhang et al. 2004, Pasrija and Naime 2021). AT2 cells have also been identified as progenitors of the alveolar epithelium.

1.5 Cellular Differences between Human and Mouse Airway Cells

Recent scRNAseq studies have highlighted a potentially important difference in the airway epithelial cells seen between mice and humans based on gene expression signatures (Travaglini, Nabhan et al. 2020). Human cells could be classified into more distinct cell types with a noticeable expansion of basal cell types as well as identification of two ciliated cell types. The division of secretory cells into the goblet, serous and mucous cell types seen in humans could not be detected in mice. This suggests that lung cells have undergone significant diversification during mammalian evolution (Figure 1.5).



Figure 1.5. Non-Conservation of the Epithelial Cell Types between Humans and Mice

The molecular cell types in humans and mice defined by gene expression are aligned. Red text shows the lineage related to specific expansions, while blue text shows the cells that are more abundant in humans. The asterisk shows the cell types absent in mice. This image is modified from that presented by (Travaglini, Nabhan et al. 2020).

1.6 Immunity

Immunity is classified into four distinct types: physical and chemical barriers, intrinsic immunity, innate immunity, and adaptive immunity (Figure 1.6). Any invading pathogen must overcome all these barriers to establish an infection.

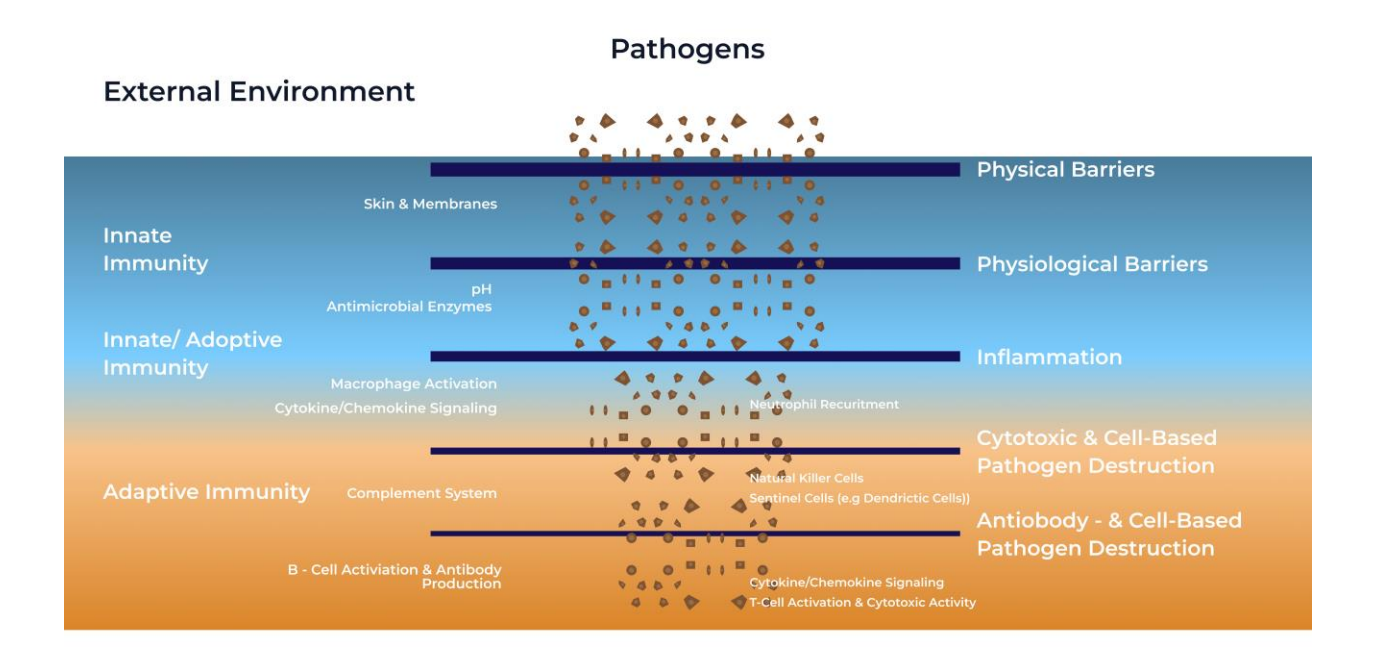


Figure 1.6. Barriers of Immunity against Pathogens

Physical and chemical barriers, intrinsic immunity, innate immunity, and adaptive immunity are the four branches of the human immune system. Initially, defence is initiated with the physical barrier in the form of skin, hair within the nose and cilia within the respiratory tract. Thereafter, different cells, such as macrophages and neutrophils activate the innate immune response. Antigen-presenting cells then act as a link between innate immunity and adaptive immunity. Finally, infections resolved by any of the previous barriers face adaptive immunity, in which pathogen-specific immune responses are generated through the production of antibodies this image adapt (arcr.niaaa.nih.gov).

1.6.1 Barriers of the Epithelial Airways

1.6.1.1 Function of the Physical Barrier

The ciliated cells in the respiratory epithelium clear the mucus released by the goblet cells. The loss or dysfunction of these cells can lead to various diseases, such as CF and COPD (Kusak 2018). The contributors to mucus clearance are mucin proteins, periciliary fluids and cilia (via the orchestrated action from ciliated cells) (Knowles and Boucher 2002, Vareille, Kieninger et al. 2011). The mucociliary escalator works by maintaining a flow of mucus gel in the airways, which entraps pathogens and various other particles from the LRT and moves them to the pharynx from where they are swallowed (Lever 2021). Two fluid layers constitute the airway surface layer: the top mucus (gel) layer, which is interlinked with pathogens, and the second lower layer, known as the periciliary layer (PCL) or sol layer, which surrounds the cilia. The PCL has a low viscosity to enable beating to occur more easily. Clearance of mucus is achieved with the movement of cilia in a metachronal wave form (Wanner, Salathe et al. 1996, Bustamante-Marin and Ostrowski 2017) (Figure 1.7).

The importance of the mucociliary escalator can be seen from the fact that it acts as a barrier against infection and clears out about 100,000 bacteria per day in healthy lungs (Gozzi-Silva, Teixeira et al. 2021). The loss of functionality of cilia causes disorders, such as CF, asthma, and primary ciliary dyskinesia (Braiman and Priel 2008, Horani, Brody et al. 2014, Tilley, Walters et al. 2015). Airway cells synthesise and secrete mucins. MUC5B and MUC5AC are the major proteins, but others include MUC1, MUC4, MUC16, MUC20, MUC21 and MUC22 (Bonser and Erle 2017). MUC5B is mostly expressed in submucosal gland goblet cells. Meanwhile, the production of MUC5AC (Okuda, Chen et al. 2019), a protein that is a major component of the gel-forming mucus layer in the respiratory tract, is usually decreased in the airways of patients with COPD and CF (Whitsett 2018).

1.6.1.2 Anatomical and Chemical Barriers as Frontline Defence Mechanisms

As outlined above, the respiratory epithelial cells are a significant component of the immune response. When there are breaches of this natural barrier, pathogenic agents can gain entry

to the epithelium. Respiratory epithelial cells secrete multiple innate defence proteins onto their apical surface, thereby contributing to the formation of mucus.

Several specific immune cells collaborate in immune defence. Elie Metchnikoff was the first individual to document the phagocytic ability of macrophages for maintaining natural or innate immunity. Phagocytosis is employed by mononuclear phagocytes and neutrophils for the absorption of microbes. Large particles are also cleared by this process, which means that phagocytosis covers infective factors (viruses and bacteria) (Gordon, Crocker et al. 1986, Rosales 2020).

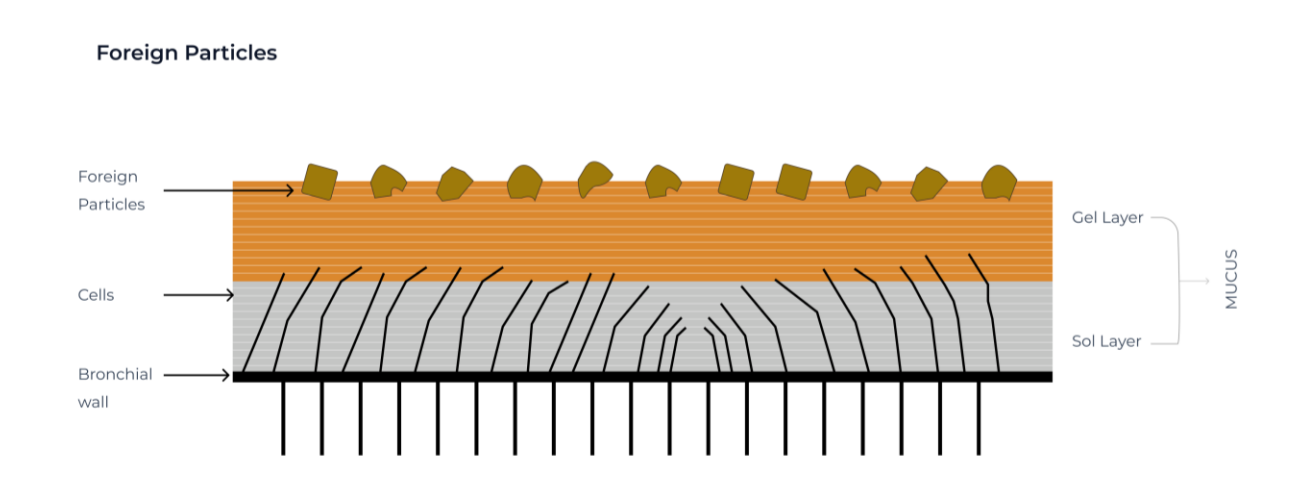


Figure 1.7. Process of Mucociliary Clearance in the Respiratory Tract

Inhaled microbes are trapped in the gel-forming mucus layer by binding to lectins and are then cleared from the body by the coordinated movement of cilia on multiciliated cells in the pulmonary epithelium.

1.6.2 Non-Structural (Immune) Cells of the Airways

1.6.2.1 Dendritic cells

The dendritic cells (DCs) provide a functional connection between innate and adaptive immune systems. DCs are produced from bone marrow progenitor cells and found in all tissues. After DCs entrap an antigen, they become activated and start their migration to the lymphoid tissues of the body (Zanna, Yasmin et al. 2021). Naïve T cells are presented with the antigen protein on the surface of DCs in collaboration with the major histocompatibility complex (MHC) peptide. T cell

antigen receptors on T cells bind to the MHC–peptide complex on the surface of DCs, which are known as antigen-presenting cells (Wu, Wei et al. 2020). This process is known as the DC-mediated T-cell activation system (Banchereau and Steinman 1998). The activation of DCs leads to the differentiation of T cells towards mature effector and memory T cells. Non-activated DCs are capable of presenting antigens to T cells; however, without stimulatory signals, the likelihood of DCs activating the immune response is reduced (Heath and Carbone 2001, Shahverdi, Masoumi et al. 2022). Thus, DCs require activation to become fully functional and contribute to the regulation of tolerance. The lungs contain a diverse population of DCs that regulate the immune response to viral infections (Zanna, Yasmin et al. 2021). One sub-type — conventional DCs — are responsible for capturing and processing antigens and consequently for presenting them on their surface in a form that can be recognised by T cells. DCs in the lungs are also known to interact with other immune cells such as macrophages and natural killer (NK) cells to promote antiviral immunity. For instance, after capturing antigens, DCs migrate to the regional lymph nodes where they present the antigens to T cells, which will consequently differentiate into effector T cells, such as CD8+T cells, which can recognise and kill virus-infected cells.

1.6.2.2 Mast cells

Mast cells express high-affinity immunoglobulin E receptors (FCER1) and are strategically located in various compartments of the lungs. Their role is of importance in various disorders involving inflammation and the immunoglobulin super antigens related to cancer. For example, in lung cancer, mast cells can be found in high numbers in the tumour microenvironment and can promote cancer progression (Cristinziano, Poto et al. 2021). The life cycle of mast cells begins in the bone marrow where they evolve from pluripotent stem cells and circulate as immature cells until they reach their destination and convert into mature cells (Ishizaka 1993, Cordes, Cante-Barrett et al. 2022).

1.6.2.3 Alveolar and airway macrophages

Alveolar and airway macrophages (AMs) play a critical role in the immune defence by phagocytosis of inhaled particles and microorganisms (Bissonnette 2020). Macrophages have a

lifespan of months to years (Murphy 2016). They are resistant to apoptosis while residing in the tissues (Gordon and Pluddemann 2018) and their density varies across various tissue types. Certain stimuli can increase the tissue density of macrophages. They are the primary regulators of innate immunity and are usually the first line of defence against pathogens entering the tissues (Brubaker, Bonham et al. 2015).

AMs are found in the lung alveoli and protect against the pathogens entering the body through breathing The AMs primarily protect against bacteria that are inhaled during inspiration. Once the bacteria reach alveoli, their opsonization occurs. This is followed by a local migration of macrophages, which attach to and engulf the bacteria. Once inside the macrophages, the bacteria are quickly lysed by the hydrolytic enzymes and proteases found in the lysosomes (Flannagan, Heit et al. 2016). AMs are considered to be critical for the removal of innocuous particles silently and induction of the protective immune system to eliminate pathogens. They are involved in reducing inflammatory responses and maintaining homoeostasis within the lungs. Apoptotic cells along with inhaled particles are phagocytised by these cells. The immune responses of AMs are controlled by the secretions of lung epithelial cells. CD200, secreted by epithelial cells maintains the quiescent state of AMs (Bissonnette 2020) therefore, coordination between epithelial cells and macrophages is critical for respiratory immune responses. In contrast, neutrophils are the main leucocytes during respiratory immune response against viral infections (Liu, Pang et al. 2017). Such infections result in a higher expression of chemokines, which attract neutrophils to the site of inflammation. Similarly, viral infections are responsible for increasing the expression of epithelium-binding proteins on the neutrophils surface (Haddad, Gaudet et al. 2019). The binding of neutrophils to respiratory epithelial cells induces damage to the surface, which is typically observed in viral infection.

1.6.2.4 Resident macrophages

Resident macrophages clean the tissues of invading pathogens and dead and apoptotic cells. They also release certain chemicals to regulate the local inflammatory response. After ingesting pathogen, macrophages trap it in phagosomes. In the next step, a fusion of phagosome with lysosome occurs, which exposes the trapped pathogen to digestive enzymes. Thus, a slow death

and digestion of the ingested pathogen occurs. They also train the adaptive immune response by ensuring the delivery of bacterial peptides to helper T cells (He, Zhou et al. 2005). Further, they release chemotactic molecules to recruit inflammatory and the other phagocytic cells (Fung, Mangan et al. 2013).

1.6.2.5 Neutrophils

Neutrophils regulate phagocytosis and the immune response. They are highly abundant in the blood, contain granules with digestive enzymes, and are among the first responders to a bacterial infection (Mohamed and Alawna 2020). Neutrophils have a short lifespan with tactile properties and constitutes more than two third of all white blood cells (Rosales 2018). They ingest and hydrolyse bacteria by releasing reactive oxygen species (ROS). Various ROS generated by neutrophils include nicotinamide adenine dinucleotide phosphate (NADPH), superoxide, and related species (Brubaker, Bonham et al. 2015). Neutrophils have secretory granules, which contain host defence peptides (HDPs) lactoferrin, cathelicidin (LL-37), defensin and lysozyme (Kanashiro, Hiroki et al. 2020). They can also create anti-bacterial extracellular traps comprising of hydrolytic proteins, histones, and decondensed chromatin (Sollberger, Choidas et al. 2018). Endothelial activation is generally the first step required for recruiting neutrophils. This is followed by the adhesion of the neutrophils to endothelium (Brubaker, Bonham et al. 2015). Next, an extravasation or migration of neutrophils through the gaps in endothelial cells towards extracellular tissues occur. The local chemotactic factors guide the neutrophils to invading pathogens. Next, the neutrophils perform phagocytosis, which is governed by the immunoglobulins deposition in the tissues and their subsequent recognition by the receptor proteins (Brubaker, Bonham et al. 2015). Once the pathogen is trapped within the phagosome, various hydrolytic enzymes and ROS are released to digest and kill the pathogen (Ulfig and Leichert 2021).

1.6.2.6 Fibroblasts and smooth muscle cells

Fibroblasts and smooth muscle cells are also important cells in the lungs, playing a role in the maintenance and repair of the lung structure via extracellular matrix-producing myofibroblasts

and secretory matrix fibroblasts (Ushakumary 2021). Interstitial resident fibroblasts direct the behaviour of the epithelial stem cell niche to perform repair function (Ushakumary 2021). Furthermore, they undergo different stages of differentiation along with specific gene expression during injury repair response. For example, $Axin2 + PDGFR\alpha^+$ fibroblast sub-types greatly contribute to regeneration (Zepp, Zacharias et al. 2017). Further, smooth muscle cells contribute not only as contractile units but also towards remodelling of the epithelium by releasing inflammatory cytokines, growth factors and proteases (Chung 2005). Both fibroblasts and smooth muscle cells demonstrate immunomodulatory properties by producing a variety of chemokines, cytokines, and growth factors that can influence the inflammatory response in the lungs (Choreno-Parra, Thirunavukkarasu et al. 2020).

1.6.3 Submucosal Glands

The area from the trachea down to the bronchioles is rich in submucosal glands. These glands secrete large quantities of mucins and proteins onto the airway surface, which boost the immune response in the airways (Ostedgaard, Price et al. 2020). Multiple cell types are present in the submucosal glands, including ciliated, serous, myoepithelial, basal and goblet cells (Whitsett and Alenghat 2015). CFTR, a key protein that maintains balance between fluids and electrolytes and movement of mucus gel by ciliary activity (Whitsett 2018), is produced by the submucosal gland. MUC5B is the most highly expressed gel-forming mucin (more so than MUC5AC). The glands also produce a variety of innate immune and antimicrobial peptides including lysozyme, lactoferrin, β -defensins and surfactant proteins (SP-A and SP-D).

1.6.4 Intrinsic Immunity as a Form of Innate Immunity

Innate immunity is the first line of defence after pathogens enters the body. It is considered a non-specific type of the immune system, as it responds to all germs and foreign agents in a similar fashion. Importantly, it rapidly acts against pathogens; therefore, it is vital to counter the spread of pathogenic agents. Intrinsic antiviral immunity inhibits viral replication and assembly in cells, thereby becoming a barrier against viruses. Although intrinsic immunity is attributed to the restriction factors inherent in certain types of cells, the factors are prone to induction by viral

infection (Goldstein and Scull 2022). Regarding their mechanism, intrinsic viral restriction factors are able to recognise viral components in a way that is different from pattern-recognition receptors (PRRs), which work by inhibiting viral infection via the induction of interferons (IFNs) and different antiviral proteins (Giovannoni, Bosch et al. 2020). Intrinsic antiviral factors directly and indirectly stop viral replication. (Yan and Chen 2012). IFNs are cytokines produced in response to invading microbes. Type I and III IFNs are expressed in multiple cell types following the recognition of viral particles. The expression of L-12 is reserved for immune cells, such as T cells and NK cells (Fensterl and Sen 2009). The interferon-stimulated gene (ISG) PKR is an IFN-induced kinase that regulates the innate immunity pathway for defence against influenza viral infection (Fensterl and Sen 2009). Different factors achieve such function through different fashions. For example, the E3 ubiquitin ligase tripartite motif (TRIM) 5α achieves this function by uncoating the HIV capsid as it targets the incoming HIV coat. Meanwhile, the deaminase APOBEC3G can inhibit viral replication by editing the viral genome (Wolf and Goff 2008).

1.6.5 Host defence peptides (HDPs)

HDPs, also known as AMPs antimicrobial peptides, prevent microbial growth and are secreted by both epithelial and inflammatory cells (Nakashige 2015). Host defence peptides as proteins with cationic properties were first described in the 1960s (Simmaco, Kreil et al. 2009). In the 1980s, several HDPs were identified, including cropin, defensins and magainin, which are small HDPs found in various organisms. Cropin was first isolated from moths (Hultmark, Steiner et al. 1980), defensin from human neutrophils (Ganz, Selsted et al. 1985) and magainin from amphibians (Zasloff 1987). Since then, numerous other HDPs have been discovered.

The respiratory epithelial cells produce multiple HDPs with activities against bacterial, fungal, and viral pathogens. Some of these proteins are generated from inactive pro-peptides, such as α -defensins produced by neutrophils (Prasad, Fiedoruk et al. 2019). These pro-peptides, which are approximately 90 amino acids in length, are processed by cell proteases (Thakur, Sharma et al. 2022). This processing results in the production and accumulation of the mature cationic defensin protein in the primary granules of neutrophils. Examples of some HDPs are described below.

1.6.5.1 Adaptive Immunity

The most common form of adaptive immunity is the production of antibodies. Antibodies are produced by B cells, which require activation by helper T cells or CD4 T cells. Antibodies can perform their function through different mechanisms. The most common mechanism is neutralisation, in which binding of pathogenic elements such as bacteria and viruses to their target cells is prevented (Webb, Bernshtein et al. 2021). Furthermore, antibodies can prevent the entry of bacterial toxins into the host cells. As bacterial cells multiply outside the host cells, antibodies activate different phagocyting cells, which can digest bacterial cells. The coating of bacterial cells by specific antibodies is known as opsonisation. Phagocytic cells contain Fc receptors, which recognise the antibodies bound to bacterial cells (Achkar and Casadevall 2013). Alternatively, the complement system, in which a series of proteins are activated in a sequence, can be activated when antibodies are bound on the surface of pathogens. This leads to the binding of complement proteins to pathogens and subsequent binding of complement protein receptors on phagocytes, resulting in phagocytosis of pathogens. Adaptive immunity encompasses antibody-driven responses of B cells, helper T cells and cytotoxic T cells in four phases: encounter, activation, attack, and memory (McCreary, Bariola et al. 2022). Both of them play a crucial role in viral infections (Iwasaki and Medzhitov 2010). T cells can identify infected cells and eradicate them through cytolysis and the secretion of toxic substances. This T cellmediated toxicity contributes to mitigating viral infections and is a key aspect of adaptive immunity. Moreover, adaptive immunity includes the process of memory, resulting in a quicker and more effective response to pathogens upon subsequent exposure and thus providing better protection against future infections (Iwasaki and Medzhitov 2010, Maini and Burton 2019).

1.6.5.2 Cathelicidins/LL-37

Cathelicidins are small cationic peptides with antimicrobial properties that are found in a variety of species (Kosciuczuk, Lisowski et al. 2012). The first cathelicidin was isolated from a *Hyalophora cecropia* moth and named cecropin (Hultmark, Steiner et al. 1980). Another cathelicidin – magainin – was isolated from the skin of a *Xenopus laevis* frog (Zasloff 1987). Since then, multiple cathelicidins have been identified from a range of species (Kosciuczuk, Lisowski et al. 2012),

including high-activity cathelicidin from *Bungarus fasciatus* snakes (cathelicidin-BF) (Wang 2008, Utkin, Siniavin et al. 2022). Human cathelicidin (also known as LL-37) is the sole cathelicidin with both anti-inflammatory and antibacterial properties. Cathelicidins are produced as inactive propertides that are bound to domains before secretion. The highest concentration of cathelicidins is found in the secondary granules within neutrophils, which are triggered by proteolytic cleavage after merging with phagosomes and the action of the granulocyte neutrophil elastase (NE) (Dutta and Das 2016).

LL-37 has antimicrobial activity against various types of pathogens. It works in several ways: by directly killing pathogens by permeabilising their cell membranes and disrupting their internal structures; by modulating the host immune response by recruiting and activating immune cells and by acting as a chemoattractant to recruit immune cells to fight invading pathogens (Thakur, Sharma et al. 2022). LL-37 also has anti-inflammatory properties, modulating the release of proinflammatory cytokines and chemokines and promoting wound healing (Jiang, Liao et al. 2020). It also plays a role in the host defence against cancer by inhibiting cancer cell growth and promoting cancer cell apoptosis.

1.6.5.3 α-Defensins (Human Neutrophil Peptides (HNPs)

HNPs have bacteria-killing activity against both gram-positive and gram-negative bacteria. They also modulate the immune response by stimulating both cytokines and chemokines (Nagaoka, Suzuki et al. 2010). HNPs exhibit strong activity against several types of pathogens (influenza A virus [IAV] and HIV).

1.6.5.4 β-Defensins

There are 33 different genes that code for β -defensin peptides in the human genome. However, the airway epithelium expresses only β -defensins 1–4 (Rayner, Makena et al. 2019). β -defensins exhibit a broad activity against bacteria, fungi, and enveloped viruses (Hosseiniyan Khatibi, Kheyrolahzadeh et al. 2020). For example, β -defensins 1 and 2 have bactericidal activity against *Escherichia coli* and *Pseudomonas aeruginosa*. In healthy individuals, β -defensins are not typically present in airway secretions (Manicassamy, Manicassamy et al. 2010). However, in patients with

respiratory illness or following infection, there is an increase in β -defensin levels in airway fluid. This is because the presence of pathogens triggers the production and release of these peptides by epithelial cells as a part of the host defence mechanism (Chen, Schaller-Bals et al. 2004, Cane, Tregidgo et al. 2021).

1.6.5.5 Lactoferrin

Lactoferrin is a protein that binds to iron and is present in the circulation and mucosal secretions. It can generate an iron-deficient environment that hampers the microbial growth. Lactoferrin has a direct bactericidal effect on microorganisms and can cause an increase in immunoglobulin A activity (Ellison 1994, Ward and Conneely 2004). The antimicrobial activity of lactoferrin has been found to increase synergistically when integrated with lysozyme (Tavares, Antunes et al. 2020).

1.6.5.6 Lysozyme

Lysozyme is an antimicrobial enzyme that is involved in the host defence against pathogens in various body secretions. It has proteolytic activity against the peptidoglycan found in the bacterial cell walls, which causes cell death (Varela-Fernandez, Garcia-Otero et al. 2022). It acts as a glycoside hydrolase and breaks down the β -1,4 linkages between N-acetylmuramic acid and N-acetyl-D-glucosamine residues, which are key elements of gram-positive bacterial cell walls (Nguyen 2018). Lysozyme found in the respiratory tract is released by epithelial cells and submucosal glands, and the level directly correlate with bactericidal activity of the airways (Widdicombe 2019, Kelly and McLoughlin 2020). Additionally, the combined effect of lysozyme and human secretory leucocyte peptidase inhibitor (SLPI) has been shown to increase antibacterial activity, demonstrating a synergistic function between these proteins (Zegels, Van Raemdonck et al. 2010).

1.6.5.7 Whey Acidic Protein (WAP)/Whey Four-Disulphide Core (WFDC) Proteins

The major whey protein in milk is WAP, which is essential for regulating the production of mammary epithelial cells (Bhat, Ahmad et al. 2020). WAP is a prototypic member of the FDC domain-containing protein family; members of this family with a similar structure of disulphide

bonds are referred to as WFDC proteins (Bingle and Vyakarnam 2008, Wegen, van Heek et al. 2022). The PI3 gene in humans encodes a protein called elafin or peptidase inhibitor 3, which is an elastase-specific protease inhibitor with a single WFDC domain (Nugteren and Samsom 2021). The SLPI is known for its antiprotease activities, and as a part of the innate immune response. SLPI has antiprotease and antimicrobial activities against bacteria and fungi. It is an important molecule in the functioning of the innate immune system that controls the proliferation, differentiation, and cycle of myeloid cells. The primary physiological function of SLPI and elafin is the blockage of NE, but they also act as potent inhibitors of various other proteinases (Scott, Weldon et al. 2011). WFDC2 is another member of this family, which is highly expressed in the trachea, lungs, and kidneys (Bingle, Cross et al. 2006); however, its function remains unclear. Elafin and SLPI have antibacterial properties and can induce a macrophagic response to the lipopolysaccharides (LPSs) of bacteria. Human lungs, nose, and trachea express both elafin and WFDC2 (Bingle, Cross et al. 2006). SLPI also promotes wound healing in mice skin (Ashcroft, Lei et al. 2000, Farr, Ghosh et al. 2020). It has anti-inflammatory properties and has been reported to obstruct macrophage/monocyte pro-inflammatory functions (Jin, Nathan et al. 1997). In the lungs of LPS-treated mice, elafin has been found to block inflammatory responses (Vachon, Bourbonnais et al. 2002).

1.7 Influenza Virus

The influenza virus was isolated in 1933 by British scientists Smith, Andrews, and Laidlaw. This virus is related to the *Orthomyxoviridae* family of viruses and is an enveloped virus that includes eight RNA segments in which the genetic material of the virus is encoded (Shtyrya, Mochalova et al. 2009). Influenza has been a prominent part of history because of its involvement in pandemics and various seasonal epidemics (Neumann, Noda et al. 2009). Once a person is infected, there is rapid replication of the virus in the initial 7 days, which can lead to intense pulmonary distress. The virus replicates until the immune responses are instigated (Baum and Paulson 1990, Imai, Kuba et al. 2008). From the three genera of influenza viruses (A, B and C), human pathology is predominantly associated with genera A and B (Iwasaki and Pillai 2014, Neumann and Kawaoka 2015).

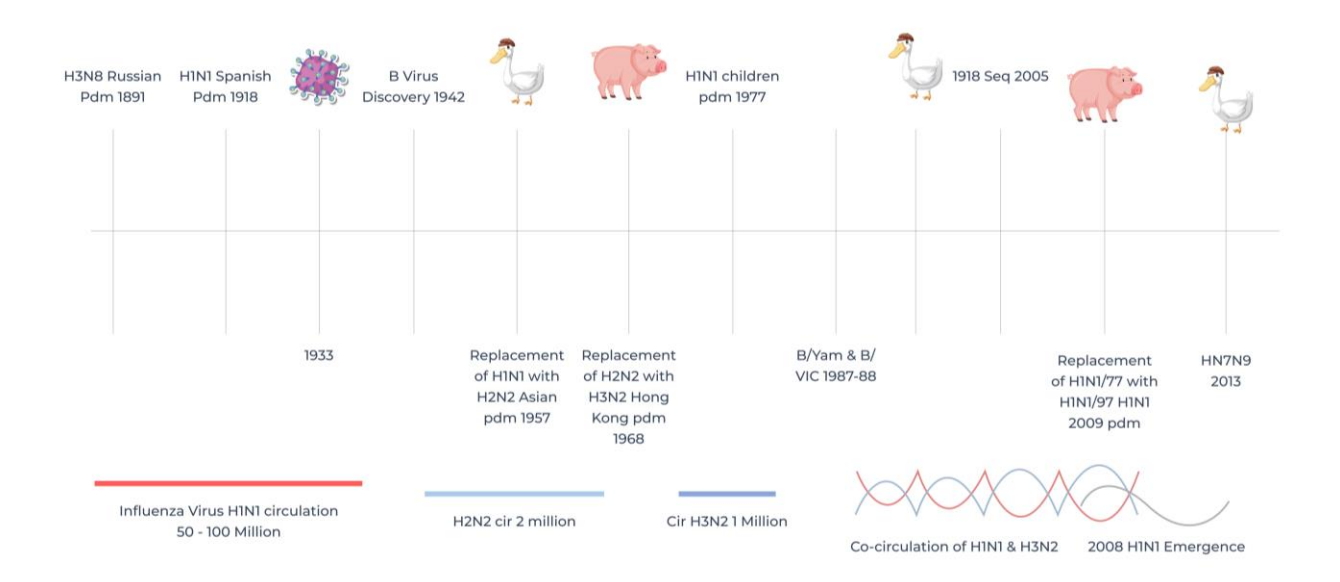


Figure 1.8. Timeline History of the Influenza Virus Since the 1890s Elaborating Six Pandemics (Francis et al., 2019)

The A genus of the virus has two different viral surface glycoproteins: haemagglutinin (HA) and neuraminidase (NA). HA facilitates the early stage of the viral life cycle by facilitating the entry of the virus into host target cells. It is synthesised in an inactive form, which is cleaved to become active by proteases, a hallmark of all diseases (Bertram 2010). Conversely, NA is responsible for releasing the virus from host cells and is an enzyme that cleaves sialic acid (SA) from the glycoprotein group. There are 19 variations of HA (H1–H19) and nine types of NA (N1–N9) (Tong, Li et al. 2012). The combination of these glycoprotein subgroups determines the ability of the virus to be transmitted from one host species to another. They bind with host cells through receptors with SA residues. HA protein sequence in humans has shown that HA specifically binds to SA residues that end with α 2,3-galactose β 1,4-*N*-acetyl glucosamine (SA α 2,3Gal) or SA α 2,6Gal (Slepushkin, Staber et al. 2001). SA α 2,3Gal is present on the surface of goblet cells and SA α 2,6Gal on the surface of ciliated cells (Allen and Ross 2018).

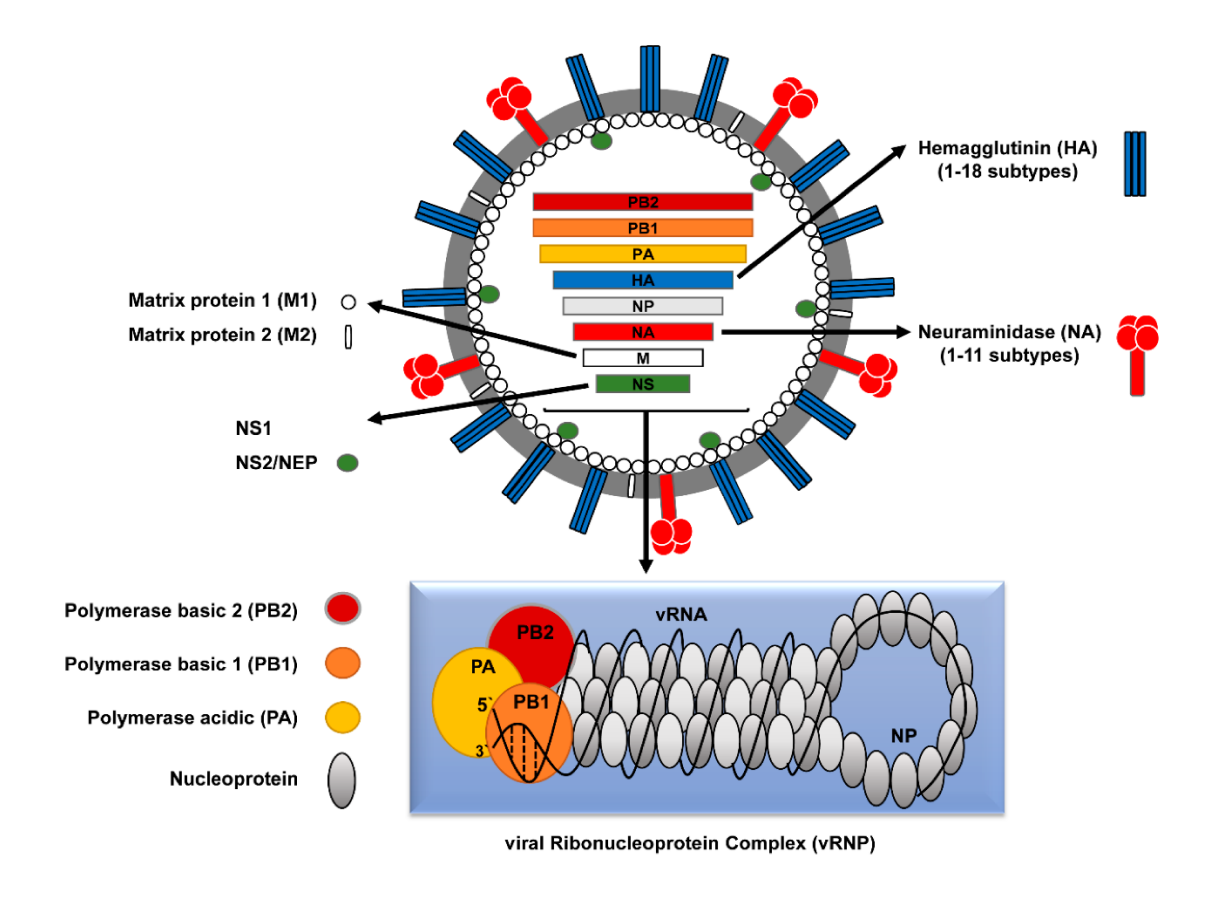


Figure 1.9. Structure and Composition of Influenza A Virus

Influenza A virus comprises HA and NA as well as M2, PB1, PB2, PA and NP (https://upload.wikimedia.org/wikipedia/commons/0/04/Viruses-10-00497-g001.png) licence ("Viruses-10-00497-g001" by Ahmed Mostafa, Elsayed M. Abdelwhab, Thomas C. Mettenleiter, and Stephan Pleschka is licensed under CC BY 4.0. To view a copy of this license, visit https://creativecommons.org/licenses/by/4.0/?ref=openverse.).

IAV enters host cells through the HA protein, which binds to SA present on the cell surface membrane. NA is a surface protein with glycoside hydrolase enzyme activity (Rogers, Paulson et al. 1983, Nie, Stadtmuller et al. 2020) that acts as a receptor-damaging enzyme and helps in removing viral particles from targeted cells. The name of HA derives from its ability to clump red blood cells together, as noted by Hirst in 1942. The HA protein is the main target of neutralising antibodies generated through vaccination and is considered a primary surface antigen of IAV.

However, IAV often generates mutations of susceptible HA epitopes, leading to modifications in its antigen structure, which can cause a lack of recognition by the non-specific immune system. NA is therefore often targeted by therapeutic inhibitors for IAV, such as peramivir, oseltamivir and zanamivir (Spanakis, Pitiriga et al. 2014).

The cell surface SA-terminating glycans act as receptors for HA on the surface of IAV (Byrd-Leotis, Lasanajak et al. 2021). The linkage specificity of SA plays a critical role in IAV's cross-species transmission, with avian viruses binding to $\alpha 2,3$ -linked sialylated glycans and human viruses preferring $\alpha 2,6$ -linked sialylated glycans (Karakus, Pohl et al. 2020). Research has explored the binding and structural properties of IAV and its glycan receptors as well as the effects of mutations in HA. Historical data on IAV are based on its ability to cause agglutination of red blood cells from different species, bind to carbohydrates and interact with other types of ligands. There is a difference in the presence of SA among different species at the site of infection. For example, $\alpha 2,3$ SA is found in mice, while $\alpha 2,6$ SA is found in humans (Byrd-Leotis, Jia et al. 2019).

Viruses that infect humans bind to host cell surface oligosaccharides that have the NeuAcα2,6Gal structure, while viruses that infect birds bind to those with the NeuAcα2,3Gal structure (Rogers, Paulson et al. 1983, Thompson, de Vries et al. 2019). Studies have shown that Sambucus nigra and Maackia amurensis lectins can differentiate between NeuAcα2,6Gal and NeuAcαGal, making them important markers. It has been found that human viruses identify SA linked to galactose through the α 2,6 linkage (Rogers, Paulson et al. 1983), while avian viruses identify SA through the α2,3Gal linkage (Suzuki 1994, Matrosovich, Gambaryan et al. 1997, Ayora-Talavera 2018). This explains why humans can be infected by only a few viruses. The receptor-binding site of the influenza virus consists of variable amino acids, and it is the differences in this region that determine the preferential identification of the SA-Gal linkage and the host species the virus infects. The HA protein limits the host range of the influenza virus. Ciliated epithelial cells are the major target of infection for the influenza virus, but the virus can also infect alveolar cells and macrophages (Shieh, Blau et al. 2010). The binding of HA to ciliated epithelial cells occurs through the α 2,3 linkage (Lewis 2022), while the α 2,6 linkage is more commonly associated with nonciliated cells. Accordingly, viral replication can occur in non-ciliated cells in both the small and large airways (Childs, Palma et al. 2009, Edwards, Tata et al. 2022).

1.8 Viral Life Cycle

The IAV life cycle can be distinguished into various stages, including 1) the entry into the host cell, 2) entry of viral ribonucleoprotein (vRNP) into the nucleus of the host cell, 3) transcription and replication of the viral genome, 4) export of vRNP from the host cell nucleus and budding and assembly over the plasma membrane of the host cell (Figure 1.10). Spikes are created by the HA homotrimer on the viral cell membrane, which then attach to the SA present on the cell membrane of the host cell (Samji 2009, Kuhaudomlarp and Imberty 2022).

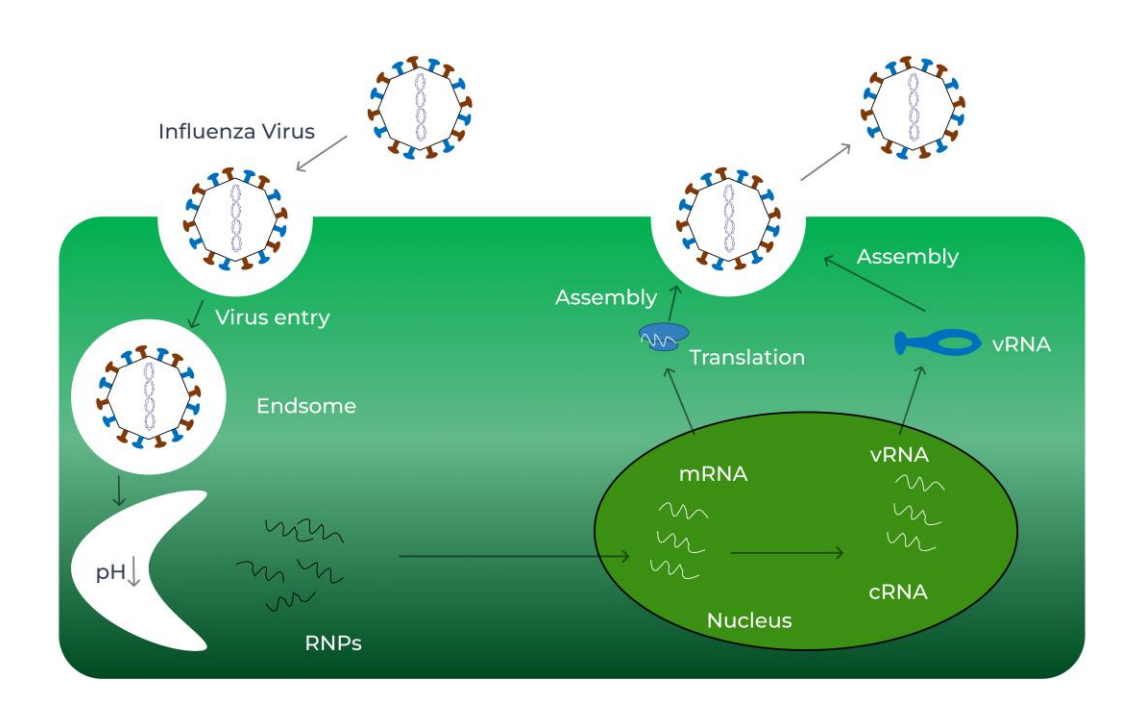


Figure 1.10. Life Cycle of IAV in the Respiratory Tract

There are nine steps to complete the infection process: binding, fusion, reverse transcription, integration, transcription, translation, assembly, binding, and release of the virus via membrane airway proteases regulating viral infections (Londrigan, Short et al. 2015).

In human airway epithelial cells (hAECs), influenza viral infection and replication requires proteolytic activation at multiple stages by cellular proteases – HA-activating proteases.

(Figure 1.11). HA connects with N-acetyl neuraminic acid-containing cell surface receptors to trigger the infection.

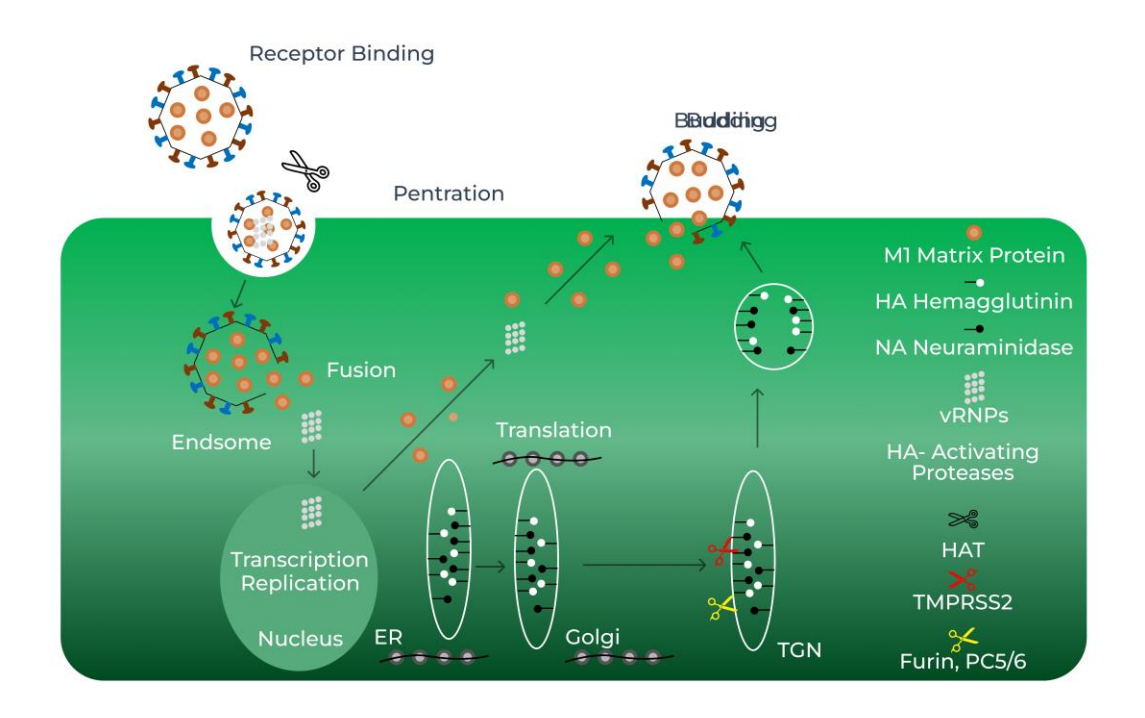


Figure 1.11. Airway Proteases Involved in IAV Infection

The influenza virus binds to surface receptors and is engulfed as an endosome. VRNPs are transported into the host cell nucleus with active transcription and replication. Newly formed viral proteins are processed in the Golgi apparatus. Finally, new viruses emerge from cells as vRNPs and capsid proteins are packaged through exocytosis (Garten, Braden et al. 2015). During viral replication, HA is involved in receptor-mediated endocytosis, which leads to the fusion of endosomal and viral membranes in acidic pH, causing the discharge of vRNPs into the cytoplasm (termed as uncoating). This allows vRNPs to enter the nucleus, resulting in the replication and transcription of the viral genome. The cellular machinery then translates viral mRNAs. The HA, NA and M2 proteins are accepted by the cellular endoplasmic reticulum and transported to the plasma membrane. Internal viral proteins are synthesised at free ribosomes and then imported into the nucleus to be combined as new vRNPs. These vRNPs then exit the nucleus for

transmission to the plasma membrane, where new virions are formed through the self-assembly of viral proteins. NA helps to split N-acetyl neuraminic acid from carbohydrate moieties when progeny virions are released. The proteolytic activation of HA occurs at specific time points during viral replication, as represented by scissors in Figure 1.11 (closed scissor: enzymatically inactive protease; open scissors: active protease; truncated scissor: soluble protease). Furin in the trans-Golgi network (TGN) is used to cleave HA at a multi-basic cleavage site. During both attachment and access to the cell and budding and assembly of progeny virus, the plasma membrane's HAT or the TGN's TMPRSS2 cleaves HA at a monobasic cleavage site (Bottcher-Friebertshauser, Garten et al. 2014).

1.9 Innate Immune Defence System in the Presence of Influenza

The influenza virus invades the mucociliary layer of the respiratory tract through the oral or the nasal route. The response against the virus by the immune system is initiated either by macrophages or DCs (Perrone, Plowden et al. 2008, Garcia-Caballero, Rasmussen et al. 2009, Manicassamy, Manicassamy et al. 2010). The host's receptors contain some evolutionary primitive proteins known as PRRs, which signal the immune response against the virus and bacteria, and helps detect the molecules associated with tissue damage, also known as damage-associated molecular patterns (DAMPs). The timely detection of these molecules is essential for initiating and enhancing the inflammatory response (Iwasaki and Medzhitov 2015) .

The innate immune response is triggered by active sensing of pathogen-associated molecular patterns (PAMPs) by PRRs. A rapid initiation of complex signalling pathways follows, which initiates the inflammatory response generated by triggering molecules. Together, these reactions facilitate the apoptosis of pathogens. The Toll-like receptors (TLRs), including TLR1/2 and TLR4, are classical example of RRRs (Lumb 2020). They are a part of the TLR family, which bind to PAMPs, and are critical in the defence of innate immunity (Ward and Conneely 2004). The different signalling molecules induced by PRRs include chemokines, eicosanoids and proinflammatory and type I IFNs. Chemokines attract NK cells, monocytes, neutrophils, and other immune cells to the infected site, where they work together with macrophages to degrade and remove infected dead cells. Fever and anorexia associated with influenza are mainly caused by

the actions of eicosanoids and pro-inflammatory cytokines (Kroes, Miranda-Bedate et al. 2022). IFNs are released by various immune cells, such as plasmacytoid DCs and macrophages as well as epithelial cells. These molecules cause the neighbouring cells to reduce protein synthesis, so that they do not become infected with the rampaging virus (Jewell, Vaghefi et al. 2007, Hogner, Wolff et al. 2013) . The role of ISGs is not fully understood, and the function of some remains unclear (Jewell, Vaghefi et al. 2007, Schoggins 2019).

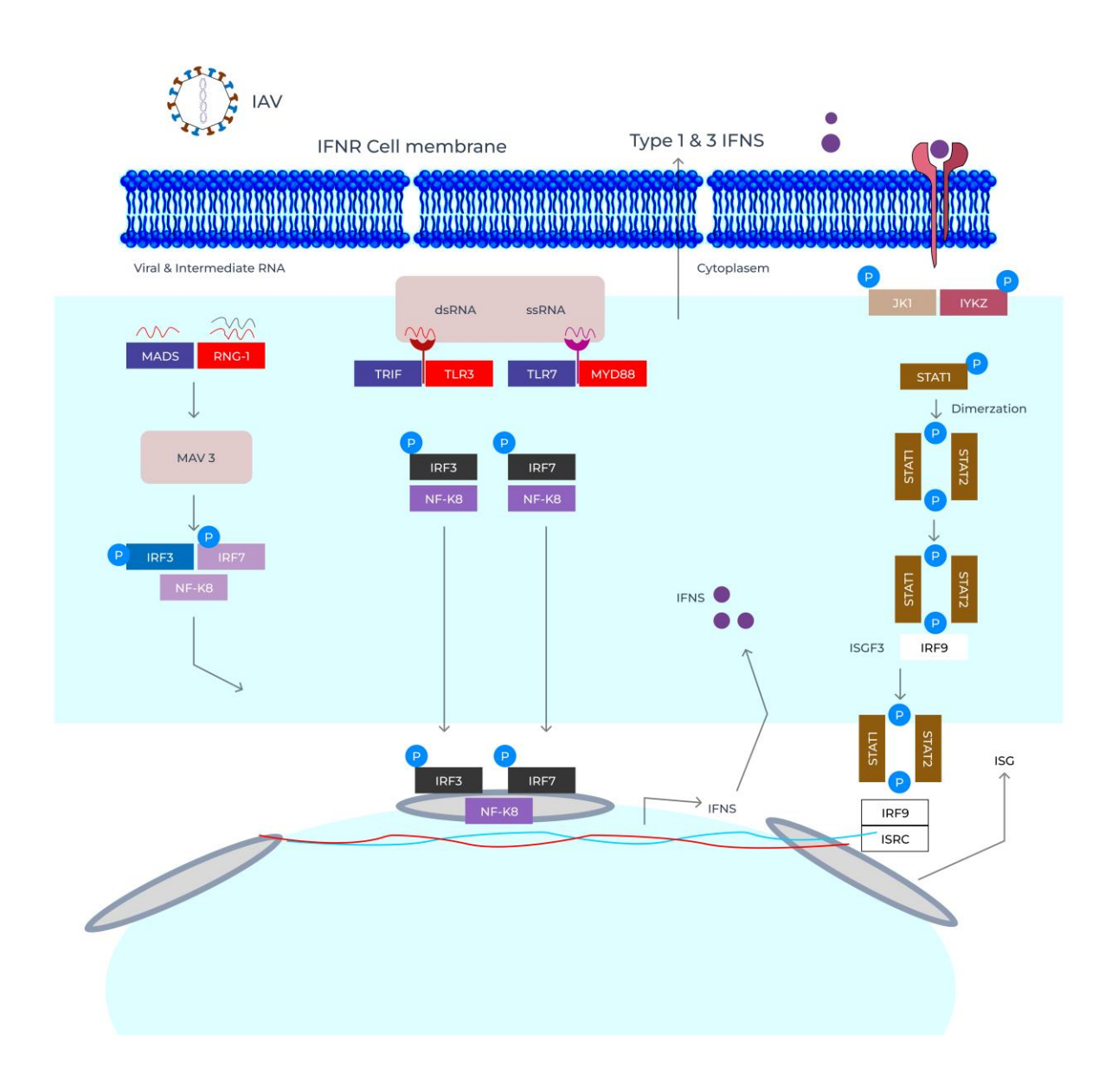


Figure 1.12. Innate Immune Response Against IAV Infection

The presence of IAV results in the release of type I and III IFNs, which then activate the JAK/STAT pathway, leading to the expression of more IFNs. Similarly, innate immune response requires an increased synthesis of IFNs against viral infection can be induced by the presence of viral or intermediate RNA. These RNA molecules form complexes with transcription factors such as NF-kB, leading to the activation of IFN gene expression. Adapted from (Chen, Liu et al. 2018).

1.10 PRRs Involved in Respiratory Viral Infections

PRRs play a crucial role in detecting viral infections in the respiratory tract (Iwasaki and Medzhitov 2004). These receptors are expressed by various innate immune cells and are designed to identify PAMPs (related to microbial pathogens) and DAMPs (related to cellular components). As a part of the evolutionarily old immune system, PRRs develop before the adaptive immunity and can induce effective antiviral responses (Zhang, Li et al. 2022). Type I IFNs (IFN- β and multiple IFN- α molecules) are among the most crucial factors for antiviral responses triggered by PRRs (Takeda 2005).

The activation of PRRs also leads to the maturation of DCs, which enhances the expression of CD80, CD86 and CD40, thereby regulating antigen-specific CD8+ T cell responses (Sakuragi, Liao et al. 2022). Overall, PRRs play a vital role in the defence mechanism of the respiratory tract against viral infections (Butler, Lager et al. 2014).

1.11 TLRs

TLRs are the most extensively studied family of conserved PRRs that give rise to innate immune reactions. The TLR proteins that are most frequently associated with influenza are TLR2, 3, 4, 7 and 8. The glycoproteins in viral membranes can be identified by cell surface proteins, such as TLR2 and TLR4 (Li and Wu 2021). Conversely, TLR3 and TLR7 are the intracellular proteins responsive to double-stranded viral RNA (dsRNA) (Keynan 2011), while TLR8 can identify single-stranded viral DNA (Iwasaki and Pillai 2014). The viral activation of TLR4 leads to the expression of inflammatory cytokines (Medzhitov, Preston-Hurlburt et al. 1997, Veloso, Fernandez et al. 2022). TLR4 also senses LPS molecules that are carried in the serum by LPS-binding protein (LBP). LPS monomers are transferred by LBP to the GPI-linked cell surface protein, CD14, over the

plasma membrane surface (Ulevitch and Tobias 1995, Richard 2023). The small MD-2 protein, which is related to the extracellular domain of TLR4, is also required by the LPS recognition complex (Shimazu 1999, Tam 2022). The TLR4, MD-2 and CD14 complexes directly bind to LPS (Shimazu 1999, Poltorak 2000). B cells carry out LPS recognition via the RP105 cell surface receptor that is associated with TLR4. The largest range of ligands is identified by TLR2 receptors, such as bacterial lipoproteins and peptidoglycans (Takeuchi, Kawai et al. 2001, Narayanankutty, Sasidharan et al. 2020). Downstream signals are generated following the binding of TLR2 to a ligand, such as myeloid differentiation primary response gene 88 (MyD88) and MyD88 adaptor-like protein (Bowie and Unterholzner 2008).

1.11.1 TLR2 and TLR4

According to Nelli et al. (2010), TLR4 on the cell surface may be capable of recognising viral surface glycoproteins HA and/or NA. While TLR4 primarily responds to molecular signatures produced by microbes such as LPS, studies have shown that viral infections can also trigger it (Van Poucke, Nicholls et al. 2010). High replication of viral antigens may result in hyper-activation of TLR4, leading to increased inflammation and oxidative damage to the lungs. An example of such a case is H5N1 viral infection (Peiris, Cheung et al. 2009). However, pre-stimulation of TLR4 has been shown to provide protection against lethal highly pathogenic avian influenza (HPAI) (Meraz 2014). The TLR2 and TLR4 pathways have also been found to be effective against different strains of influenza viruses, as pre-stimulation of both pathways provides protection against the PR8 virus (Barjesteh, O'Dowd et al. 2020), while pre-stimulation of TLR2 affects only the HA molecule of the 1918 Spanish influenza, with no effect from a TLR4 agonist. Thus, TLR4-regulated signalling targets HPAI viruses, while TLR2 is associated with protection against Spanish influenza (Nicholls 2013). The complex innate signalling involved in reinforcing the response to different strains of the influenza virus highlights the importance of further studies on the pathways involved in controlling influenza infections and inducing pathogenesis. These studies may help in developing effective strategies to prevent human infection with highly pathogenic influenza viruses (Nicholls 2013).

1.11.2 TLR3

TLR3 can identify viral dsRNA that has been endocytosed, which can consequently be degraded via phagocytosis (Alexopoulou, Holt et al. 2001, Schulz, Diebold et al. 2005). TLR3 initiates the production of pro-inflammatory cytokines in respiratory epithelial, which are involved in the action of CD4 and CD8 T cells to destroy the virus (Le Goffic, Balloy et al. 2006).

1.11.3 TLR7 and TLR8

Viral derived ssRNA is identified by TLR7 and TLR8. The MYD88 adaptor is involved in TLR7 response, which induces the regulatory transcription factor NF- κ B or IFN7 (Tykalová 2022), through which type I IFNs are modulated, and pro-inflammatory cytokines are induced (Seo, Pritzl et al. 2012) (Seo et al., 2012). TLR7 is involved in restricting influenza infection, inducing B cells instead of T cells (Heer 2007). TLR8 in humans occurs in monocytes and macrophages and is involved in the stimulation of IL-2 and, potentially, IFN α (Ablasser, Poeck et al. 2009).

1.12 Retinoic Acid-Inducible Gene 1 (RIG-1) Receptors

Viral nucleic acids are associated with another type of PRR, known as RIG-1-like receptors (RLRs). This group of PRRs comprises cytoplasmic RNA helicases, including MDA5, RIG-1 and LGP2 (Meng, Chanda et al. 2017). The specificity of the ligand encountered determines the connection between MDA5 and RIG-I with viral RNA, which consequently triggers signalling and induction of inflammatory cytokines and type I IFN (Pichlmair, Schulz et al. 2006, Kawai 2008). Like TLRs, RLRs distinguish between host 'self' RNA and 'non-self' RNA of foreign pathogens.

1.13 IFN Signalling and Antiviral Action

The activation of PRRs and RLRs due to viral nucleic acids initiates downstream signalling leading to the transcription of cytokines, IFNs and chemokines (Guy and Bowie 2022). These factors are responsible for activating neutrophils, macrophages and maturing DCs. Type I IFNs (IFN- α and IFN- β) are considered the most effective inducers in the innate immune system response (Matsumiya and Stafforini 2010). In the case of influenza infection, type I IFNs mainly control viral replication, while TNF- α , IL-1 β and IL-8 mobilise immune cells to the infected area, causing

inflammation. Type I IFNs impact IFN α/β receptors on both infected and adjacent cells, triggering the antiviral signalling cascade of tyrosine kinase 2 and Janus kinase 1 and phosphorylating STAT1/2, which initiates the transcription of ISGs (Fernandez-Sesma, Marukian et al. 2006, Picca, Calvani et al. 2020). These IFN-activated genes induce further ISG proteins, including antiviral proteins such as MxA, which inhibit IAV replication; viperin, which stops virus budding in the host and restricts replication; tetherin, which restricts virus assembly and OAS, which activates RNase L to stop virus replication in the RNA (Garcia-Sastre 2011, Nicholls 2013). Taken together, IFNs and ISGs are critical mediators in the host response to IAV.

1.14 Bactericidal/Permeability-Increasing (BPI) Protein Family

BPI was first identified as an antibacterial protein present in neutrophils. It is effective against gram-negative bacteria (Weiss, Elsbach et al. 1978, Townsend, Dyer et al. 2020). In humans, there are three other well characterised BPI-related proteins: LBP, cholesteryl ester transfer protein (CETP) and phospholipid transfer protein (PLTP). BPI and LBP are involved in bacterial infection and inflammation and CETP and PLTP in lipid transport in the bloodstream (Holweg, Schnare et al. 2011). CETP, LBP and PLTP are found in the liver; however, BPI is principally released from the primary granules of neutrophils. These proteins, which are sized from 55 to 60 kDa, conserve a structural fold similar to a boomerang that is made up of two domains: N-terminal and C-terminal domains (Beamer 2003). The N-terminal domain of BPI is considered the active area of the BPI molecule, as it is the part involved in toxicity to gram-negative bacteria. This region of LBP binds to LPS. In 1999, a protein related to BPI – palate, lung and nasal epithelial clone (PLUNC) – was identified in the embryonic, palatal, tracheal and nasal epithelia of mice (Weston, LeClair et al. 1999, Liu, Wang et al. 2021) (Weston et al., 1999; Liu et al., 2021) and subsequently in the trachea of humans (Bingle and Bingle 2000). Soon after, PLUNC was recognised as a member of a small family of genes (Bingle and Craven 2002).

1.14.1 PLUNC, Bacterial Permeability-Increasing Fold Containing Family Member A (*BPIFA1*) and the BPIF Gene Family

PLUNC was first identified in a study aimed at discovering proteins involved in closure of the palate during growth of mouse embryo (Weston, LeClair et al. 1999). At the time, two related proteins were already known: the salivary-enriched parotid secretory protein (Madsen and Hjorth 1985) and submandibular gland protein B (Mirels and Ball 1992). Later studies identified multiple human PLUNC genes located on chromosome 20q11 (Bingle and Craven 2002, Mulero, Boyle et al. 2002, Bingle, LeClair et al. 2004). The human genome has 11 PLUNC family members, while the mouse genome has 14, but there are species-specific variations, including some pseudogenes (Bingle 2011). The PLUNC gene locus evolved from the deletion and duplication events (Bingle 2004). PLUNC genes are largely restricted to mammals, although some are present in birds (LeClair, Nomellini et al. 2004, Chiang, Veldhuizen et al. 2011). There are two types of PLUNC proteins: short PLUNC (SPLUNC) proteins with about 250 amino acids and long PLUNC (LPLUNC) proteins with around 450 amino acids (Bingle, Singleton et al. 2002). SPLUNC proteins are structurally like the N-terminal domain of BPI, while LPLUNC proteins have two domains that share structural similarity with the domains of BPI. Based on these similarities, a nomenclature was established: Single domain-containing proteins were renamed BPIFA, while two domaincontaining proteins became BPIFB proteins (Bingle, Bingle et al. 2011). The original (S)PLUNC protein was renamed BPIFA1; this term will be used throughout this thesis.

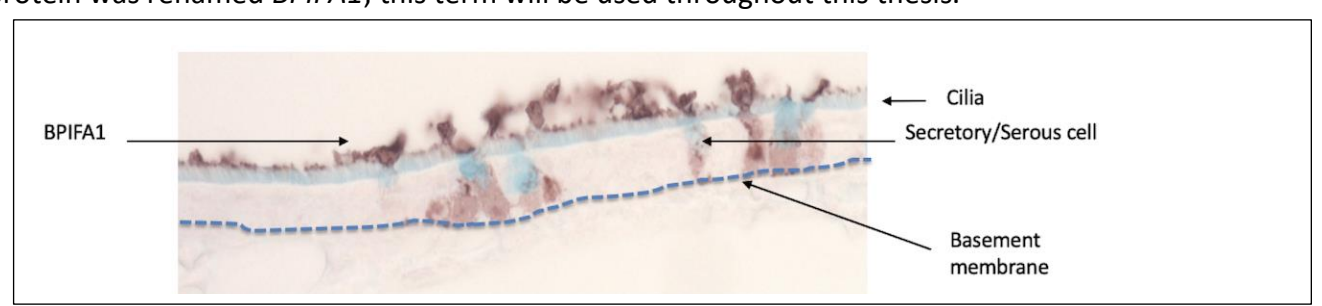


Figure 1.13. Staining of BPIFA1 in Mouse Trachea

The brown stain represents BPIFA1, while the blue stain indicates Alcian Blue. The image shows that the protein is produced by secretory cells. Image from Maslinda Musa.

1.14.2 Localisation of BPIFA1

Weston et al. (Weston, LeClair et al. 1999) described the expression of Bpifa1 in the nasal epithelium and palate of an embryonic murine model as well as in the trachea. BPIFA1 is localised in the respiratory epithelium and Bowman's glands of the nasal passages and in the trachea in the large airways of adult mice (Figure 1.13). It is produced by non-ciliated cells and found in the serous glands of the posterior region of the tongue (Musa, Wilson et al. 2012). BPIFA1 has been shown to strongly stain the epithelium of murine middle ear (Mulay, Chowdhury et al. 2021) and is also found in human middle ear (Hadzhiev, Yordanov et al. 2017). In humans, BPIFA1 is localised in non-ciliated epithelial cells and is also seen in submucosal ducts and submucosal gland serous cells as well as in the small glands in the posterior part of the tongue (Bingle, Cross et al. 2005). BPIFA1 is absent in the epithelium of the bronchioles, but there is a significant increase in BPIFA1 levels in the airways of patients with cystic fibrosis (Bingle, Barnes et al. 2007). BPIFA1 is also present in nasal lavage fluid and abundant in airway secretions (Ghafouri, Kihlstrom et al. 2003). It is also seen in the salivary glands, particularly in the ducts and mucous cells of the acini as well as in saliva (Vargas, Speight et al. 2008). Overall, BPIFA1 exhibits a high degree of tissue restriction, which is illustrated by the expression data from BioGPS (Figures 1.14 and 1.15). The highest expression of BPIFA1 can be noted in the lungs, trachea, heart, and nasal cavity.

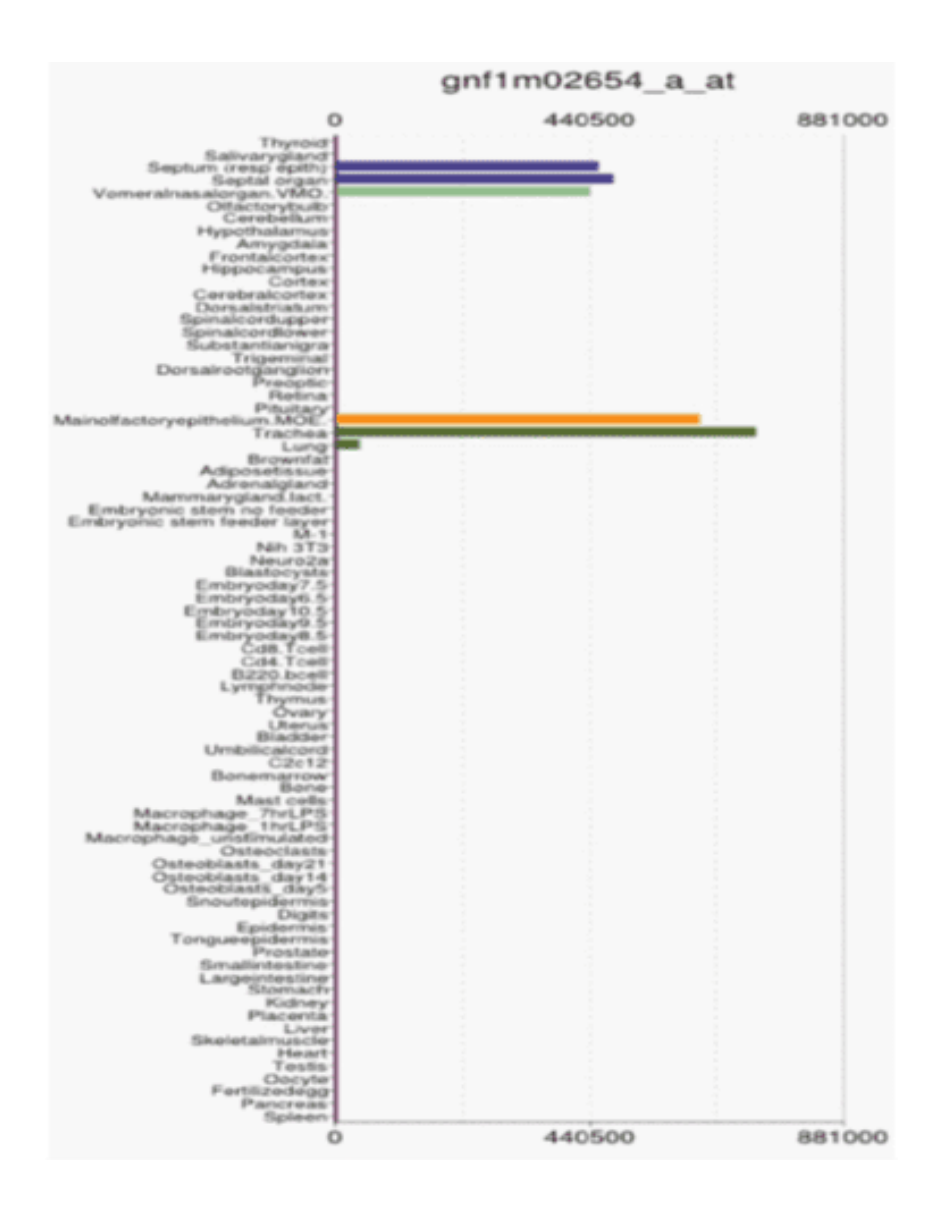


Figure 1.14. Tissue-Restricted Bpifa1 Expression in Mice

Restricted sites of expression are seen in the microarray data of *Bpifa1* from adult mice. The expression of *Bpifa1* is limited to just the nasal cavity, lungs, and trachea (i.e. upper airways). The BioGPS portal was accessed to obtain the image, which was formulated based on data from Su et al. (2004).

Figure 1.15. Tissue-Restricted BPIFA1 Expression in Human Tissues

Bpifa1 is expressed in limited tissues. Human tissue microarray data reveal that there is restricted



expression of *BPIFA1*. The BioGPS portal was accessed to obtain the image, which was formulated based on data from Su et al. (2004).

1.15 Comparative Analysis of BPIF Genes

As previously discussed, *BPIF* family genes are divided into including *BPIFA* and *BPIFB* (Vachon, Bourbonnais et al. 2002, Bingle, Bingle et al. 2011). These genes are located in a single locus on

mouse chromosome 2 and human chromosome 20 (Bingle, Singleton et al. 2002, Bingle, Bingle et al. 2011) (Figure 1.16). The human locus contains 11 *BPIF* genes, including three pseudogenes (*BPIFA4P*, *BPIFB5P* and *BPIFB9P*) (Bingle, Bingle et al. 2011). The mouse locus has 14 *Bpif* genes, with one pseudogene (*Bpifa2f-ps*) (Bingle 2011).

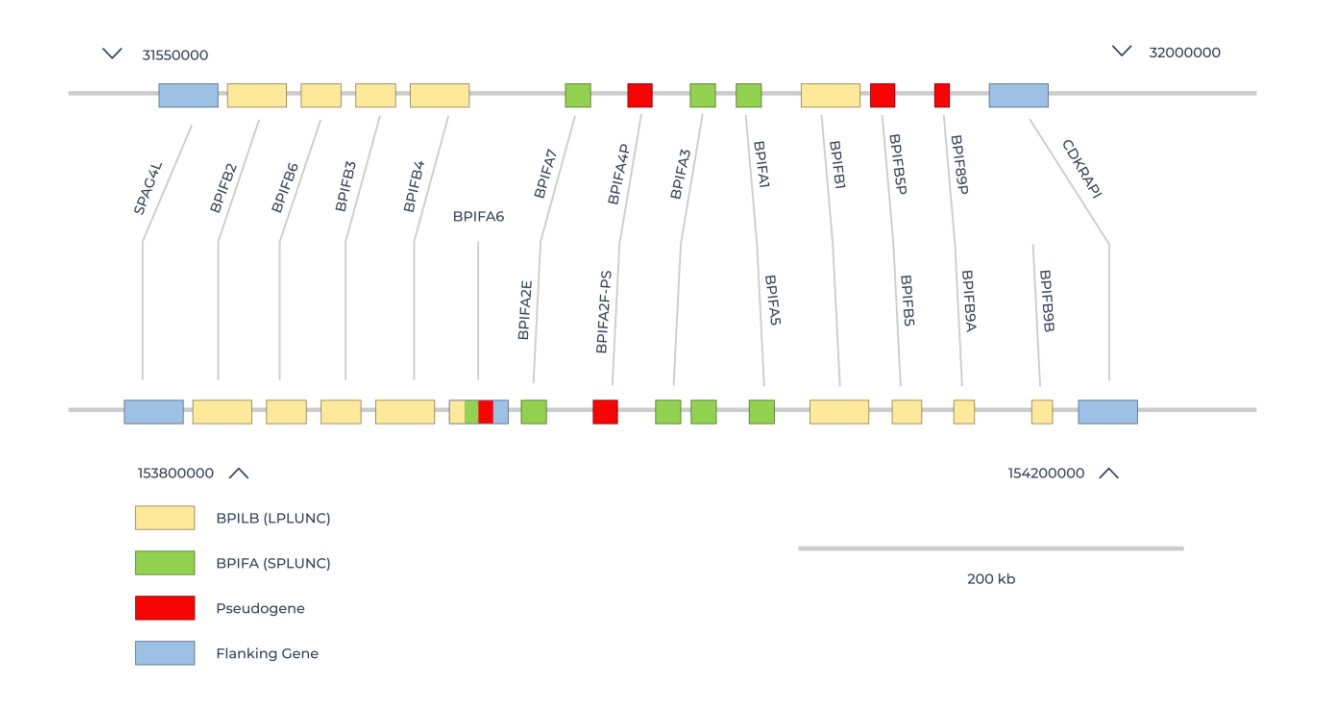


Figure 1.16. Chromosomal Locations of BPIF Genes in Humans and Mice

The *BPIF* genes are found on chromosome 20 in humans and chromosome 2 in mice. Lines signify orthologues of individual genes, while arrowheads signify the chromosomal locations of human and mouse genes. *BPIFA* genes are shown as green boxes, *BPIFB* genes as yellow boxes and *BPIF* pseudogenes as shaded boxes. *SPA4L* and *CDK5RAP1* are adjacent to the loci of both mouse and human *BPIF* genes. Scale bar, 200 kb. Adapted from (Bingle, Bingle et al. 2011) .

The quantity of *BPIF* genes in mammalian species differs, and it is only in mammals that the complete cohort of *BPIF* genes is identified (Bingle, LeClair et al. 2004, Bingle, Bingle et al. 2011).

BPIFA1 is found in all mammals as a functional gene. Various paralogues show extremely low sequence similarity (Bingle 2004).

1.16 Functions of BPIFA1

BPIFA1 has been shown to have multiple functions associated with homoeostasis of the respiratory tract, including antimicrobial, immunomodulatory and surfactant functions. BPIFA1 is also involved in clearing the mucociliary passages and maintaining the airway surface liquid (ASL) regulation (Abdelwahab, Reidel et al. 2020) (Abdelwahab et al., 2020). Lastly, BPIFA1 may also contribute to antiviral defence.

1.16.1 Antibacterial Function

BPIFA1 and the BPIF family of proteins were initially believed to contribute to host defence. Multiple studies have explored the role of BPIFA1 in antimicrobial host defence, and the results suggest that BPIFA1 can restrict bacterial growth and exhibit antimicrobial activity. For instance, BPIFA1 inhibits P. aeruginosa growth in a dose-dependent manner by creating small pores in the bacterial outer membrane (Sayeed, Nistico et al. 2013). BPIFA1 also demonstrates antibacterial activity against Mycoplasma pneumoniae by reducing P1 adhesion expression, which plays a crucial role in the adherence of bacteria to host epithelial cells (Gally, Di et al. 2011). BPIFA1 helps to regulate the surface tension of airway secretions as an endogenous surfactant, thereby maintaining low mucosal surface tension and providing anti-biofilm defences (Al Katy 2019). Experiments with genetically deficient Bpifa1-/- mice showed that they were more susceptible to Klebsiella pneumoniae infections (Liu, Bartlett et al. 2013). BPIFA1 also acts as a shield against Neisseria meningitidis infections by preventing biofilm formation, adherence, and invasion of 16HBE14 epithelial cells (Mashbat, Bellos et al. 2020). Individuals with CF have a high risk of developing Burkholderia cepacia complex infections. In a previous study, Burkholderia cenocepacia strain J2315 was administered to both Bpifa1-/- knockout mice and their wild-type (WT) littermates, and the results showed that the bacterial burden in the lungs of Bpifa1-/- mice was higher than that in the lungs of WT mice (Kim 2016). Similarly, incubation of BPIFA1knockdown primary human bronchial epithelial cells (HBECs) with J2315 resulted in a higher

bacterial burden than did that of non-transduced HBECs. The study also suggested that BPIFA1—ENaC interaction could prevent the cellular invasion of J2315 (Ahmad, Kim et al. 2020).

Studies have shown that BPIFA1 reduces the creation of bacterial biofilm. Recombinant BPIFA1 may interfere with the creation of biofilm in vitro with *P. aeruginosa (Gakhar, Bartlett et al. 2010)*. In a previous study, there was greater creation of bacterial biofilm with polarised mouse primary airway epithelial cells from *Bpifa1*-/- mice than with epithelial cells from WT mice. This study also noted that biofilm biomass was inhibited by BPIFA1 in a dose-related manner (Liu, Bartlett et al. 2013).

1.16.2 Immunomodulatory and Chemotactic Functions

Studies on the significance of fluctuations in BPIFA1 levels in lung inflammation have been conducted. The chemotactic and immunomodulatory properties of BPIFA1 have also been evaluated. When LPS was administered to Bpifa1-/- mice, there was a disruption in neutrophil recruitment into the lungs and the transmigration of neutrophils across the airways (Britto, Niu et al. 2019). A transcriptomic analysis that distinguished between WT and Bpifa1^{-/-} mice showed a downregulation of Cxcl9 and Cxcl10 in Bpifa1-/- mice with acute lung inflammation and lower protein levels in the bronchoalveolar lavage (BAL) of *Bpifa1*-/- mice (Britto, Niu et al. 2019). In vitro recombinant hBPIFA1 showed chemotactic function, as it could induce the migration of phagocytic cells towards infection sites when exposed to P. aeruginosa (Sayeed, Nistico et al. 2013). BPIFA1 also increased the rate of neutrophil migration (Sayeed, Nistico et al. 2013). Another study showed a significant increase in neutrophil infiltration after mice were exposed to P. aeruginosa (Lukinskiene, Liu et al. 2011). The BAL fluid of mice infected with P. aeruginosa showed an increased number of macrophages 6 h after infection compared with that of Bpifa1-/mice. Additionally, a significant decrease in the number of neutrophils in the BAL of WT mice was observed after exposure to *P. aeruginosa* compared with that of *Bpifa1-/-* mice (Liu, Di et al. 2013). Bpifa1^{-/-} mice also showed a significant decrease in NE activity compared with WT mice (Liu, Di et al. 2013).

1.17 Structural Features of BPIFA1

Protein threading studies on BPIFA1 and other family members predicted structural similarities with BPI (Bingle and Craven 2002). The first published BPIF structure for horse LATHERIN/BPIFA4 confirmed the presence of an extended β -barrel-like structure (Vance, McDonald et al. 2013). Subsequently, two groups determined the structure of human BPIFA1 and confirmed a high degree of structural similarity with the N-terminal domain of BPI (Ning, Wang et al. 2014). The two proteins only share 12% identity over this region (Figure 1.17).

The structure of mouse BPIFA1 has also been described (Little and Redinbo 2018) (Little et al., 2018), reconfirming the structural relationship (Figure 1.18). Mouse and human BPIFA1 share 66% identity over the region of the structure figure.

BPIFA1 is a glycine—leucine-rich protein, and glycine linkers may provide BPIFA1 with a large amount of conformational flexibility. The glycine—leucine-rich part of BPIFA1 is related to the hydrophobic core of the protein, which enables the binding of BPIFA1 to hydrophobic lipids (Bingle and Craven 2002). BPIFA1 has also been shown to interact with lipids present in airway surfactants (Ning, Wang et al. 2014).

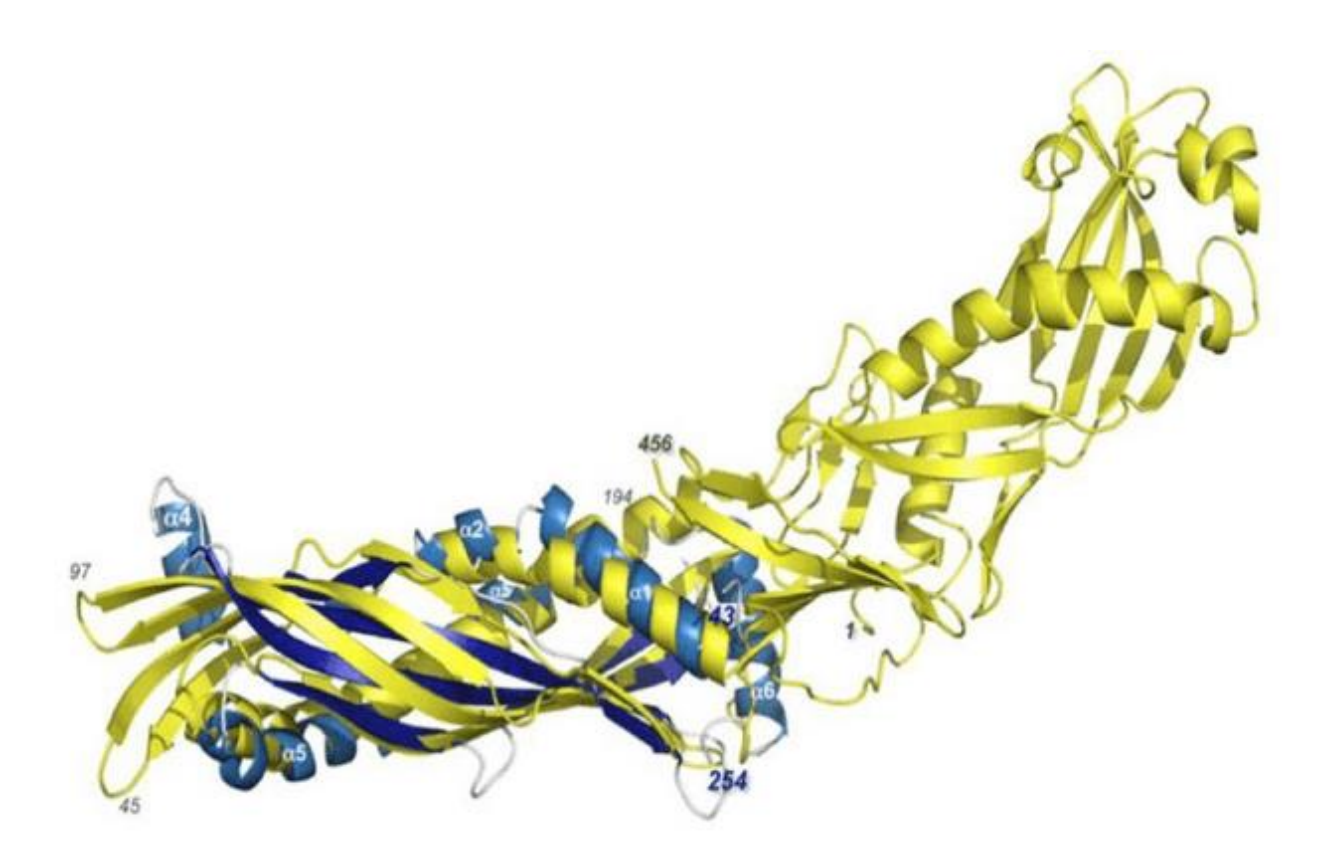


Figure 1.17. Structural Similarity Between BPIFA1 and BPI

This figure shows the structural similarity between human BPIFA1 (blue) and the N-terminal half of human BPI (yellow). Residues 43–254 of *BPIFA1* are superimposed over residues 1–194 of BPI. The amino acid sequence of the two proteins in this region is 12% (Garland, Walton et al. 2013).

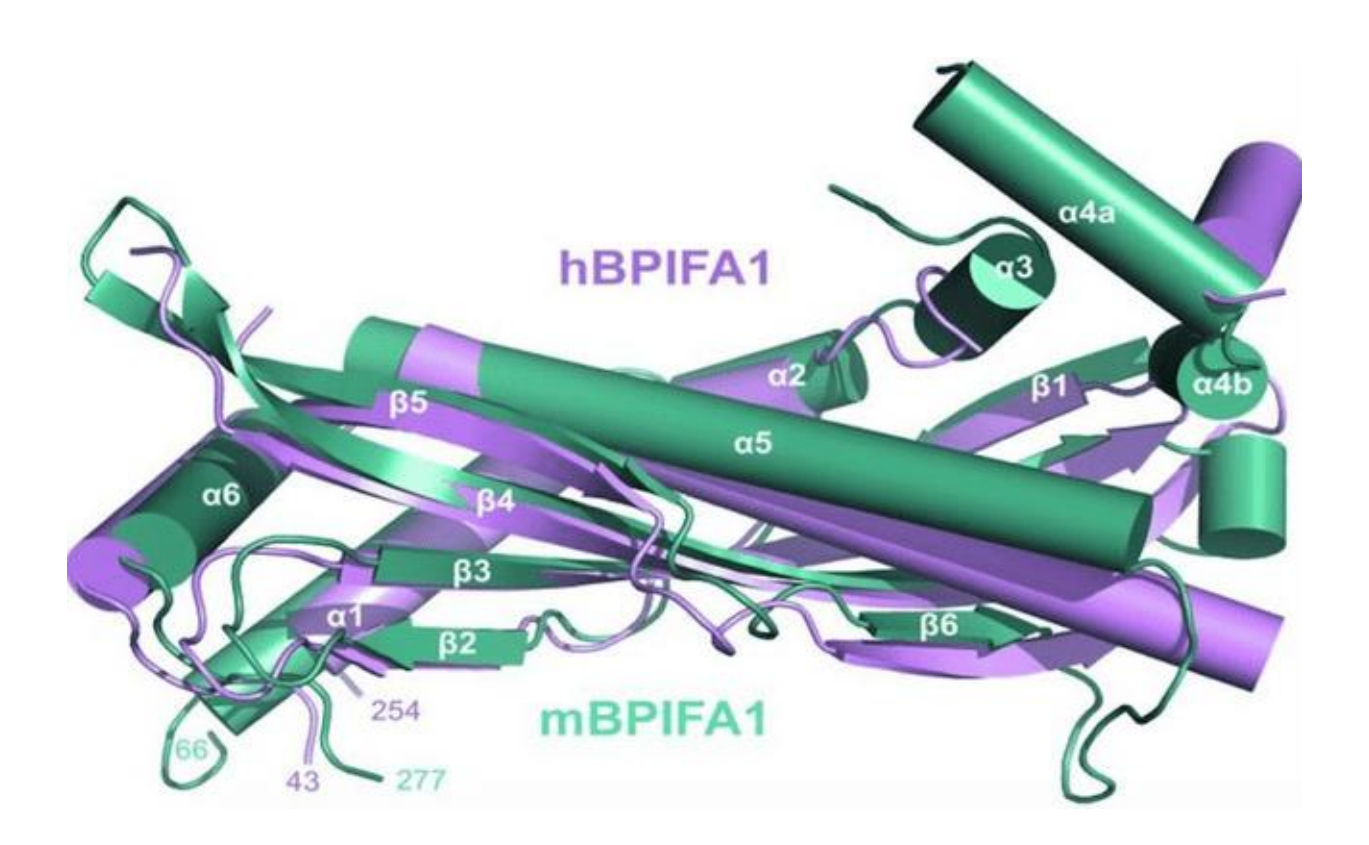


Figure 1.18. Superimposition of Mouse and Human BPIFA1 Protein Structures

The teal structure represents the superposition of mBPIFA1, while the pink structure depicts the superposition of hBPIFA1 monomers (Little and Redinbo 2018).

BPIFA1 has a length of 256 amino acids in humans and 278 amino acids in mice. The extreme N-terminal sequence of mouse BPIFA1 contains a PLPL repeat region, which is absent in the sequence of human BPIFA1 (Weston, LeClair et al. 1999, Bingle and Bingle 2000). A subsequent study has found that the N-terminal sequence of BPIFA1 showed significant variability among rodent species (Leeming, Kipar et al. 2015). Interestingly, this variable N-terminal region is absent in the crystal structure of either human or mouse BPIFA1, indicating that BPIFA1 may have a poorly defined and flexible structure. This structural variability between the proteins in various species could have implications, as discussed in the functional section.

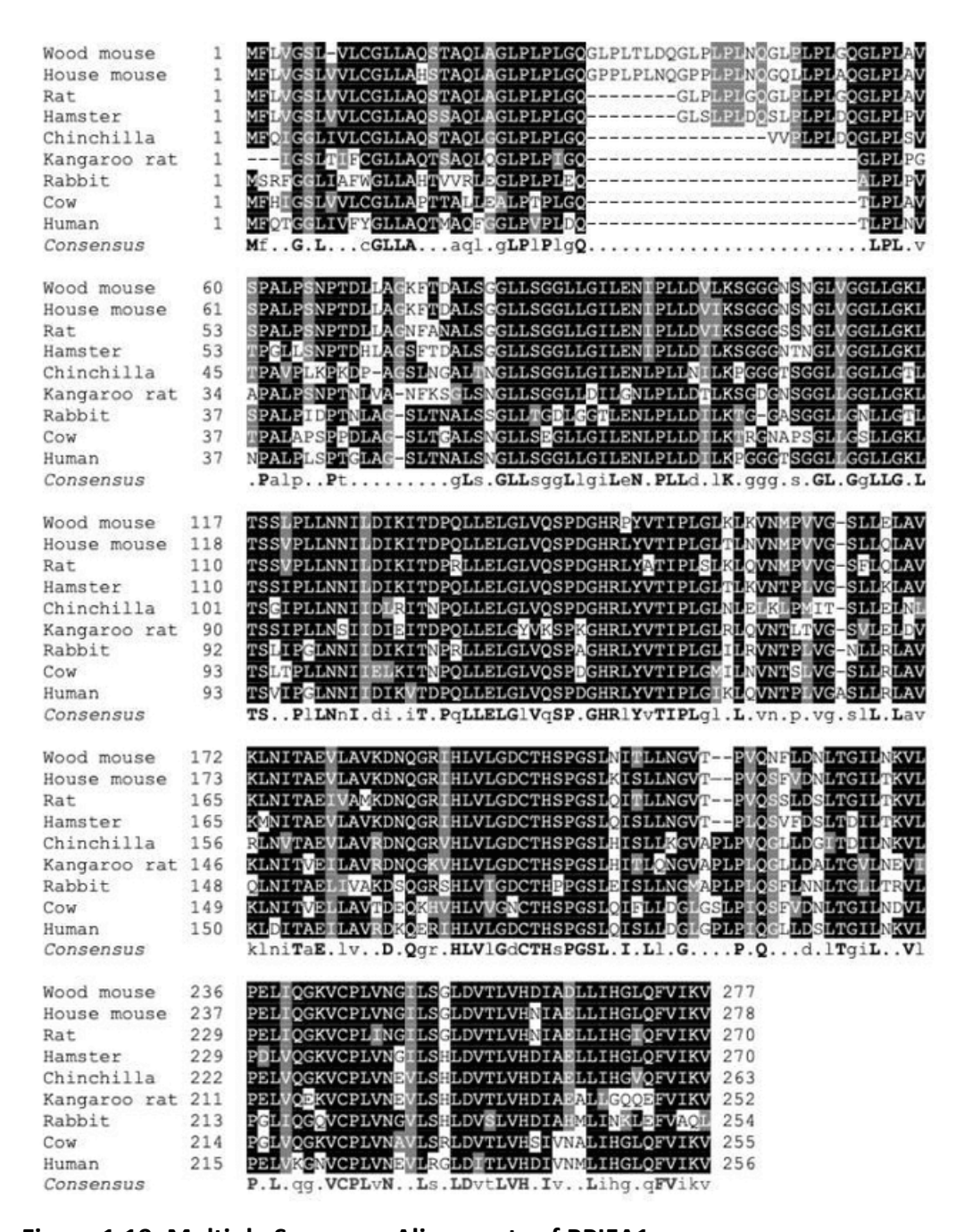


Figure 1.19. Multiple Sequence Alignments of BPIFA1

When BPIFA1 was analysed with respect to its sequence alignment, a significantly lower homology was observed in the N-terminal than in its remaining parts (Leeming, Kipar et al. 2015).

1.18 Role of BPIFA1 in Pulmonary Diseases

Several studies have evaluated BPIFA1 in respiratory diseases. As described previously, BPIFA1 is primarily expressed by upper airway epithelial cells. However, the expression pattern of BPIFA1 changes in patients with pulmonary diseases.

1.18.1 CF

CF is a genetic disorder that affects multiple systems of the body and is characterised by the build-up of thick mucus in various organs including the intestines, respiratory tract, liver and bile ducts, sweat glands and exocrine pancreas (Wilschanski and Durie 2007). It is caused by a disruption in the *CFTR* gene. Any malfunction in CFTR leads increases the ENaC activity and the absorption of mucus by cells, causing higher salt and water concentrations (Sharma, Verma et al. 2001). This results in the impairment of cilia movement and production of thick mucus. The role of BPIFA1 in CF remains unclear; however, a considerable increase in BPIFA1 mRNA and protein levels has been observed in the respiratory tracts of patients with CF compared with individuals without CF (Britto 2022). Staining of BPIFA1 in the small airways of patients with CF has also been reported to significantly increase compared with that in the airways of individuals without CF (Bingle, Barnes et al. 2007). This increased staining in the small airways of patients with CF may be attributed to phenotypic modifications of the airway epithelium (Bingle, Barnes et al. 2007).

CF is partially caused by dysregulation of ENaC linked to a lower ASL volume and greater mucus dehydration (Garland, Walton et al. 2013). This may compromise the regulation of ENaC because of the lower pH of ASL and weakened activity of BPIFA1 in the airways of patients with CF (Garland, Walton et al. 2013). Furthermore, the antimicrobial properties of BPIFA1 decline because of the lower pH and higher elastase level in individuals with CF, leading to a greater bacterial burden in the airways (Garland, Walton et al. 2013). A peptide derived from BPIFA1 may be a target for the treatment of CF (Terryah, Fellner et al. 2018).

1.18.2 COPD

COPD is a chronic lung disorder characterised by inflammation, leading to airflow obstruction within the lungs. It is associated with the generation of mucus, coughing and wheezing sounds during breathing. Prolonged exposure to hazardous gases or particles from cigarette smoke is a major risk factor for COPD (Murthy 2005).

(Di, Harper et al. 2003) Di et al. (2003) showed that BPIFA1 expression was elevated in the submucosal glands, epithelial surface, and sputum of patients with COPD than in healthy controls. The levels of BPIFA1 vary in the airways of active smokers and COPD patients. Ghafouri et al. (2003) (Ghafouri, Kihlstrom et al. 2003) reported significantly higher BPIFA1 levels in the nasal fluids of smokers than of non-smokers. In another study, elevated BPIFA1 levels were found in the sputum of COPD patients but not in that of healthy smokers (Baraniuk, Casado et al. 2015). Cigarette smoking has been suggested to be related to increased BPIFA1 levels in the airways, as elevated amounts of the BPIFA1 protein were found in the URT of smokers compared with non-smokers (De Smet, Seys et al. 2018). Furthermore, BPIFA1 protein staining and gene expression were shown to increase as the clinical stage of COPD increased.

1.18.3 Asthma

Asthma is characterised by chronic inflammation that causes airway hyper-responsiveness and airflow limitation in most patients, resulting in symptoms such as chest tightness, wheezing, coughing and breathlessness (Lee, Hwang et al. 2018). There are limited data on BPIFA1 levels in patients with asthma, with one study suggesting reduced protein levels (Wu, Huang et al. 2017). BPIFA1 expression in the nasal epithelium of patients with asthma may also be regulated by genetic differences in the *BPIFA1* gene (Schaefer, Li et al. 2019).

1.18.4 Idiopathic Pulmonary Fibrosis (IPF)

IPF is a chronic inflammatory condition leading to progressive pulmonary tissue fibrosis, with a life expectancy of approximately 5 years from diagnosis (Policelli 2016). The role of BPIFA1 in IPF is not well understood. A study found higher expression of *BPIFA1* in patients with IPF than in healthy individuals (Yang, Burch et al. 2007). The distribution of BPIFA1 in IPF-affected tissue was

found to differ from that in healthy tissue, with expression in bronchial columnar, mucous and bronchial and bronchiolar epithelia in IPF-affected tissue but not in healthy tissue (Garcia 2018). Additionally, patients with IPF showed elevated expressions of both BPIFA1 and BPIFB1 in the lungs (Bingle, Wilson et al. 2012).

1.18.5 Mucociliary Clearance

As BPIFA1 can affect mucociliary clearance, it has been considered a key factor in host defence. (Liu, Di et al. 2013) Liu et al. (2013) found that there was a considerable decrease in the expression of critical mucin genes (*Muc5ac* and *Muc5b*) in *Bpifa1*-/- mice as well as *Scgb1a1* (*Liu, Bartlett et al. 2013*). This is a key finding because these proteins are major components of the lining fluid in the airways and regulate mucociliary clearance. *Bpifa1* loss also decreased *Foxj1* expression, a marker of ciliated cells (Liu, Bartlett et al. 2013). This observation suggests that there is a significant decrease in the ability to support mucociliary clearance when BPIFA1 is absent in the airways (Liu, Bartlett et al. 2013). When the expression of chinchilla *Bpifa1* was silenced by mucociliary clearance of the Eustachian tube was ineffective (McGillivary 2010). The relationship between BPIFA1 and surfactant properties appears to be critical for ensuring that the Eustachian tube works effectively in non-typeable *Haemophilus influenzae*-induced otitis media (McGillivary 2010).

1.19 BPIFA1 and Viral Infection

The regulation of BPIFA1 expression appears to be impacted by viral infections. A study using a murine model showed that the levels of BPIFA1 in BAL fluid were significantly low in mice infected with IAV (Britto, Liu et al. 2013). However, another study found that the levels of *Bpifa1* were significantly higher in the pulmonary tissues of mice infected with murine herpesvirus 68 (MHV-68) 14 days post-infection. Seven days after the infection (Al Katy 2019) *Bpifa1* expression in the bronchiolar epithelium of MHV-68-challenged wood mice decreased significantly, while that in the bronchi, bronchioles and tracheal epithelium increased compared with those of control wood mice (Leeming, Kipar et al. 2015). The mechanism behind the expression of BPIFA1 in the terminal bronchioles without the RNA is not yet understood (Leeming, Kipar et al. 2015). In a previous

study, the load of human rhinovirus 1B was found to be significantly higher in the lung tissue of *Bpifa1*-/- mice than in that of controls (Wu, Jiang et al. 2014). Recombinant BPIFA1 was also shown to induce apoptosis of Epstein–Barr virus (EBV)-infected B cells, reducing the expression of EBV latent membrane protein 1. This finding suggests that BPIFA1 supports host defence against EBV-triggered nasopharyngeal epithelial cancer, although the mechanism is unknown (Zhou, Cui et al. 2007).

Previous studies from the host laboratory have suggested that BPIFA1 functions in host defence against IAV infection. IAV induced a larger weight loss and a much higher viral titre of lung tissues in *Bpifa1*-/- mice than in WT controls. In addition, the spread of IAV to the lung parenchyma was more rapid in *Bpifa1*-/- mice. The alveoli and bronchiolar epithelia were found to stain for IAV 24 h after infection in *Bpifa1*-/- mice but not in controls. These findings suggest that *Bpifa1* may contribute to the innate and intrinsic immune responses.

The function of BPIFA1 has been previously evaluated in mouse tracheal epithelial cells (mTECs) of both *Bpifa1*-/- and WT mice to understand the contribution of BPIFA1 in the airway epithelium. Phenotype analysis showed similarities between the cells, suggesting that the difference in IAV binding and infection is based on the presence or absence of Bpifa1 rather than on the number of cells expressing receptors. BPIFA1-positive cells did not appear to be the initial site of infection, implying that the protein does not only synthesise cells but also protects the epithelial surface. Bpifa1-/- cultures showed relatively higher importation rates of IAV RNPs into the nucleus of cells and increased viral binding compared with controls. The lower levels in the RNP import assay than the binding assay suggests that BPIFA1 plays a crucial role in reducing the initial binding of IAV to normal airway ciliated epithelial cells and its subsequent entry into them. As BPIFA1 is secreted into the PCL (Kesimer, Ehre et al. 2013), the protein forms a part of an IAV infection barrier that provides protection to the epithelial surface. However, the mechanism of interaction between BPIFA1 and virus particles and cell type specificity of mTEC infection has not yet been investigated. Nonetheless, the data highlight a significant role of BPIFA1 in providing protection against IAV infections in murine models.

1.20 Mouse Cell Models for Studying Respiratory Infections

The air–liquid interface (ALI) culture model has been found to be an effective representation of *in vitro* and *in vivo* airway biology, as it simulates the exposure of cells to both air and liquid. The ALI system consists of a basolateral compartment separated by a porous permeable filter, where cells are cultured on the apical surface until they become confluent and form an apical microenvironment (Cei, Doryab et al. 2021). The basal surface provides access to media to keep cells fed, and humidification of the apical side leads to the differentiation of cells and the secretion of mucus and apical fluids onto the epithelial surface. This makes ALI culture a valuable tool in respiratory disease research, as it closely resembles the epithelial compartments present *in vivo*. Unlike cell lines, which are generally unable to differentiate into other cell types, ALI is suited to investigate the role of airway epithelial cells in the development of respiratory tract and related diseases (Wang, He et al. 2018).

1.20.1 Proliferation of mTECs

The proliferation of mTECs plays a crucial role in their differentiation and function in the airway epithelium. Early studies have indicated that multiple growth factors, such as insulin, epidermal growth factor and retinoic acid, are essential for the formation of cilia and the differentiation of mucous cells (Green 1977). The progenitor cell population needs to be expanded to ensure sufficient cell numbers for proper differentiation. During the initial stages of cell culture, both basal and differentiated club cells are present, but after a few days, only basal cells adhere to the membrane (Green 1977, Allen-Hoffmann, Schlosser et al. 2000). The methods used for the proliferation of mTECs are consistent with those used for cells from other species (Lechner 1985, Wu, Zhao et al. 1997).

1.20.2 Differentiation of mTECs

Cell differentiation occurs only when the cell layer becomes confluent. mTECs are differentiated into an epithelium mimicking upper airway under ALI conditions (You, Richer et al. 2002, Horani, Nath et al. 2013). This differentiation promotes the development of multiple cell types including ciliated and secretory cells. Their marker proteins can be seen during the differentiation phase,

but the actual amount varies (You, Huang et al. 2004, Bustamante-Marin and Ostrowski 2017). A small number of goblet cells can be seen using MUC5AC, for example, which can be increased when IL-13 is added to the media. For example, staining of cytokeratin 14 is present in large amounts at the beginning of differentiation but is lost as the cells differentiate (You, Richer et al. 2002, Tyner, Kim et al. 2006).

1.21 ALI Culture of mTECs

1.21.1 mTECs and Infections

As differentiated mTECs have a phenotype like that seen in the native airways, they can be a suitable model for infection studies. In my host laboratory, such cells have been used for infection with IAV and bacterial pathogens (Akram 2014, Caikauskaite 2018). In the case of IAV infection when TECs from WT and *Bpifa1*-/- mice were infected with X31 virus, loss of BPIFA1 was shown to cause an increase in the infection of the cells, suggesting that the protein has an antiviral defence function in the airway epithelium (Akram 2014). The mechanism for this and the identity of the cells that are initially infected have not yet been identified.

1.22 Hypothesis and Aims of the Study

The background of this study highlights the important role of innate molecules and structural cells in protecting the lungs from viral infections. BPIFA1, a secreted protein in ASL, is one of the most significant components of ASL and has multiple protective functions. BPIFA1 protects the epithelium and is secreted against non-ciliated epithelial cells in the airways. Previous research suggests that BPIFA1 may defend against IAV infections.

The hypothesis of this study is that BPIFA1 plays a critical role in protecting the lungs from IAV infection by functioning as a constituent of ASL and shielding the epithelium.

The main aim of this study is to understand the role of BPIFA1 in protecting the lungs from IAV infection. This will be achieved by:

1- Establishing and validating mTEC cultures for use in IAV infection studies,

- 2- Performing a genome-wide analysis of mTEC differentiation,
- 3- Analysing transcriptional responses to IAV infection in undifferentiated and differentiated mTEC cultures and
- 4- Generating and validating BPIFA1-based reagents for functional studies.

The overall goal of this study is to use mTECs as a tool to study the role of BPIFA1 in IAV infection.

Chapter 2: Materials and Methods

2. Materials and Methods

2.1 Direct-Zol RNA Miniprep Protocol

The Direct-zol RNA miniprep system from Zymo Research was used to obtain high-quality RNA directly from TRI-Reagent samples. The system eliminates impurities and results in a small final volume (6–15 uL) of RNA that is ready for downstream analysis. The following protocol was followed: An equivalent volume of 100% ethanol was added to the TRI-Reagent samples and then centrifuged in a microfuge for 30 s. The pellet was added to a filter and centrifuged again for 30 s. The flow-through was discarded, and 400 μ L of RNA wash buffer was added to the column, which was then centrifuged at maximum speed for 30 s. The flow-through was discarded again. Thereafter, 5 μ L of DNase (to digest genomic DNA), along with 35 μ L of DNA digestion buffer, was added to the column matrix and incubated at room temperature for 15 min. Further, the column was centrifuged for two minutes after adding 700 μ L of RNA wash buffer. The column was transferred to an RNase-free tube, and the RNA was eluted using DNase/RNase-free solution, followed by centrifugation in the microfuge for 30 s. The RNA was quantitated using a Nanodrop spectrophotometer, and the samples were stored frozen.

2.2 RNA Gel

The quality of the RNA removed from the cells was examined using denaturing electrophoresis. In an RNase-free conical flask, 0.5 g of RNase-free agarose was dissolved in 36 mL of RNase-free distilled water in a microwave. Thereafter, 5 mL of 10× MOPS and 9 mL of formaldehyde were added, and the gel was poured into the tray. Further, 1× MOPS was included to the tank. RNA samples of 2–5 μ L were with an equivalent volume of denaturing RNA loading dye (Sigma), heated at 70°C for 5 min and loaded. The gel was operated at 70 V for 20 to 30 min until the gel had moved an adequate distance to solve the 18 and 28S ribosomal RNA bands. A UV transilluminator was then used to observe the gels.

2.3 Complementary DNA (cDNA) Synthesis

CDNA synthesis was performed using a master mix comprising AMV RT buffer (5 μ L) at a concentration of 1×, RNase inhibitor (0.25 μ L) at a concentration of 20 U/ μ L, DNTPs (0.5 μ L) at a

concentration of 10 mM, AMV RT (0.25 μ L) at a concentration of 40 U/ μ L and Oligo RT (0.5 μ L) at a concentration of 0.1 μ M (all from Promega). In most cases, 200 ng of RNA was used. The total volume was 20 μ L with RNase-free water. The RT reaction mix was placed in a PCR machine and subjected to a temperature of 42°C for 60 min, followed by a temperature of 95°C for 5 min. The samples were stored frozen until use. Negative RT controls were created by excluding either RNA or AMV RT from the samples.

2.4 Reverse Transcription (RT)-PCR

RT-PCR testing was conducted using either Maxima Hot Start (Thermo Fisher) or FastGene Optima HotStart (Flowgene) PCR mixes. These systems utilise a hot start enzyme in a ready-to-use reaction mix, requiring only the addition of cDNA and specific primers. The master mix consisted of 10 μ L of Hot Start mix, 7 μ L of water and 1 μ L of forward and reverse oligonucleotides. A total of 19 μ L of the master mix was added to 1 μ L of cDNA.

Table 2.1. Primer Pairs Used

Primer	Sequence		
Bpifa1 F	ACA GAG GAG CCG ACG TCT AA		
BPIFA1 R	CCA AGA AAG CTG AAG GTT C		
TEKT1 F	CAG TGC GAA GTG GTA GAC G		
TEKT1 R	TCC ACC TGG ATT TCC TCC TG		
OAZ1 F	ACA GAG GAG CCG ACGTCT AA		
OAZ1 R	CCA AGA AAG CTG AAG GTT C		
LYPD8 F2	GCA ATG CCA CCC ACT CTG AA		
LYPD8 R2	GAG GGC TTC TGG GTG AAG CG		
SLFN4 F1	GAA GGC AGC TGT GTG AAG AG		
SLFN4 R1	GAG GGC TTC TGG AGA GCA TA		
IFNL2 F	GAC AAG AAC CCA AGC TGA CC		
IFNL2 R	ACC TCA GGT CCT TCT CAA GC		

The samples were run on this standard cycle. Heat activation was initiated at 94°C for 5 min, after which 30 cycles of denaturation were performed at 94°C for 1 min, annealing at 60°C for 1 min and extension at 72°C for 1 min. Thereafter, a final extension was performed at 72°C for 7 min. The samples were then kept in an ice box until they were run on the gel.

2.5 DNA Gel Electrophoresis

Electrophoresis was then applied to resolve the PCR reaction products. Depending on the size of the DNA products, electrophoresis was conducted in 0.7-2.5% (w/v) agarose gels. Agarose and $50 \, \text{mL}$ of $1 \times \text{TAE}$ buffer was mixed, after which the mixture was boiled in a microwave. Thereafter, $0.5 \, \mu\text{g/mL}$ ethidium bromide (Sigma) was added when the temperature of the gel decreased to $55-60\,^{\circ}\text{C}$, and the gel was poured into a casting tray. Electrophoresis buffer ($1 \times \text{TAE}$) was added

to the tank, and the gel was inserted, so that the wells were placed at the negative pole of the tank. The standard comprised Hyperladder DNA markers (I or IV) (4–5 μ L) (Bioline). Electrophoresis was performed at 70 to 90 V for 45 min to 1 h, after which the gel was imaged using a Bio-Rad system.

2.6 RNA Array Analysis

The total RNA (three samples each at individual time points) was evaluated for quantity and quality using the Nanodrop and Agilent Bionalyser 600. We used 200 ng of RNA for the analysis on the Clariom S Mouse GeneChip (Thermo Fisher) as instructed by the manufacturers. The cDNA was constructed from the mRNA and a T7 polymerase binding site was added at the 3' end of the RNA molecule. We generated the antisense RNA using T7 polymerase and purified the product with a magnetic bead quantified on the Nanodrop. Thereafter, 15 ug of the RNA was used as the template to generate sense DNA, which incorporated into a hybridisation solution following biotin labelling and incubated with the GeneChip. After a hybridisation wash with the fluidics station, a fluorescent signal was generated, which corresponds to the hybridisation of the labelled material to the oligonucleotide probes on the chip. Scanning was performed on a GeneChip 7000G scanner, and the images were collected as CEL files.

2.6.1 Bioinformatic Analysis

The microarray data in the CEL files were analysed using the Affymetrix Expression Console software, which includes several tools for data analysis. We obtained the gene level summary data using the robust multi-array algorithm, which processes expression data from Affymetrix arrays. Differentially expressed genes were identified using the Limma package with the criteria of an absolute fold change greater than 2 and a limma-adjusted p-value less than 0.05. The statistical models included correction for batch effects, and p-values were adjusted using the Benjamini and Hochberg method. The results were visualised with multidimensional scaling plots generated using the Limma package. We performed the gene ontology analyses with the ClusterProfiler package to unravel the important signalling pathways enriched among the differentially expressed genes.

2.7 Generation of mBPIFA1 Constructs

The construct of mBPIFA1 cloned into the VR1255 vector was provided by Professor Colin Bingle/Renata Caikauskaite.

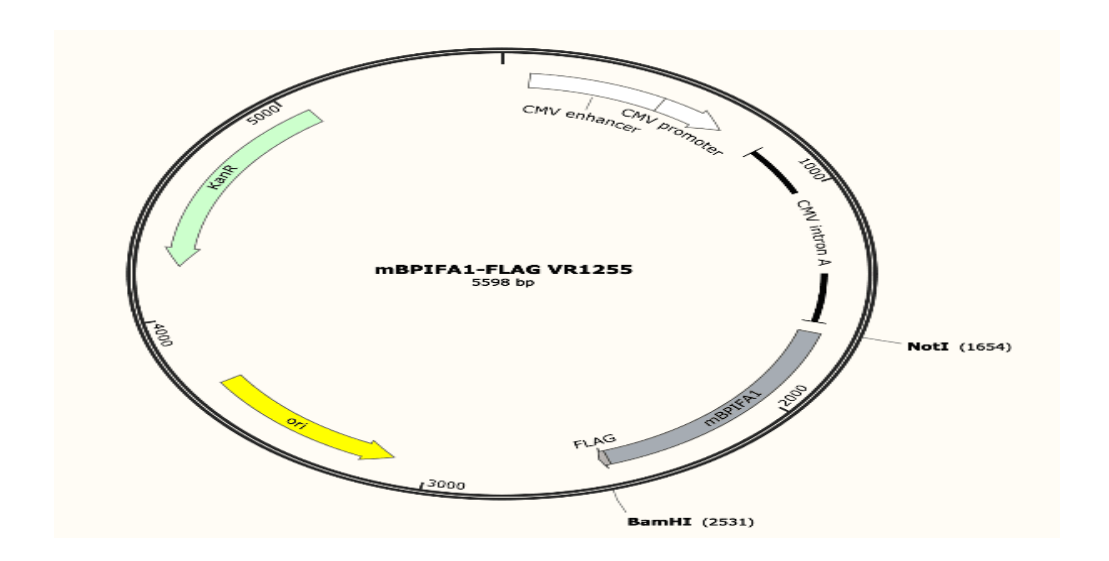


Figure 2.1. *MBPIFA1* **Gene Cloned into the VR1255** The sequence of *mBPIFA1* is cloned between the restriction sites of *BamH*I and *Not*I. 'Ori' indicates the origin of replication, while '*KanR*' is the gene-encoding product responsible for kanamycin resistance.

2.7.1 Transformation of Plasmid Construct VR1255 Into Competent Bacteria

A total of 3 μ L of plasmid (1 ng/ μ L) was mixed with 17 μ L of competent *E. coli* cells (TOP10 One Shot cells, Invitrogen), which was then gently stirred and cooled on ice for 30 min. Heat shock was applied to the plasmid and competent *E. coli* cell mixture for 45 s at 42°C, after which it was kept on ice for 5 to 10 min. Thereafter, 100 μ L of SOC medium was added and then incubated for 1 h at 37°C. A 100 μ L sample including 50 μ g/mL kanamycin and 40 μ L IPTG/X-gal mixture was plated over the LB agar plate via aseptic methods and incubated at 37°C overnight. A sterile pipette tip was used to collect bacterial colonies, which were then re-inoculated into 2 mL LB medium and 50 μ g/mL ampicillin. Lastly, we performed an overnight culture with continuous shake in an incubator at 37°C.

2.7.2 Miniprep Extraction of Constructs

The Isolate II Plasmid Mini Kit (Bioline) was used to carry out the process in accordance with the instructions by the manufacturer and the high-copy plasmid DNA protocol to obtain the recombinant construct from the bacterial cells.

A total of 1.5 mL of *E. coli* LB culture was centrifuged for 30 s at 11,000 × g to harvest the bacterial cells, and resuspension was performed in 250 μ L of buffer P1. Thereafter, 250 μ L of lysis buffer P2 was added to the cells and mixed by inverting the tube slowly six to eight times. Following a 5 min incubation, 300 μ L of neutralisation buffer P3 was added followed by a thorough mixing of the cocktail. Centrifugation was conducted for 5 min at 11,000 × g. The sample supernatant was placed on the spin column and centrifuged at 11,000 × g for 60 seconds. Further, 600 μ L of wash buffer PW2 was used to wash the column, which was then centrifuged at 11,000 × g for 60 seconds. The column was spun for another 2 min. The spin column was placed in a clean tube to elute the plasmid DNA using 50 μ L of elution buffer-P or water. After it was centrifuged at 11,000 × g for 1 min, the plasmid DNA was quantified and stored in the fridge/freezer until it was needed.

2.7.3 Midi-Preparations of Recombinant Plasmids

The ZymoPURE Plasmid Midi-Prep Kit was used to generate plasmid preparations. Overnight growing of bacteria that consisted of the target plasmid DNA in 100 mL LB broth (comprising the relevant antibiotic, 50 μ g/mL kanamycin for the VR1255 vector and 50 μ g/mL ampicillin for the CT-GFP-TOPO vector) was initiated. This was conducted in a shaking incubator at 37°C and at 225 rpm. Next, 50 mL of the LB broth was centrifuged for ten minutes at 5000 × gat room temperature, followed by the discarding of the supernatant.

There was an addition of 8 mL of ZymoPURE P1 to the bacterial cell pellet for the extraction of plasmid DNA, after which there was resuspension of the cells with the help of a bench top vortex. Further, 8 mL of buffer P2 was added, and the tube was immediately inverted six times to mix the contents. The tube was then incubated at room temperature for 2 to 3 min. This was followed by the addition of 8 mL of buffer P3 and gentle mixing of the contents by inverting the tube six times. Thereafter, the lysate was placed in a syringe filter and filtered into a 50 mL tube. Binding buffer (8 mL) was added to the cleared lysate and was mixed by inverting the tube. The

centrifugation protocol provided by the manufacturer was followed to remove the plasmid DNA, and an elution buffer was used to elute the plasmid DNA.

For long-term bacterial storage, 0.5 ml of the left-over LB broth was taken and gently stirred with 0.5 ml of sterile glycerol, after which it was stored at a freezing temperature of -80°C.

2.8 Site-Directed Mutagenesis (SDM)

SDM was utilised to generate mutations inside the m*BPIFA1* gene to extract the four N-glycosylation sites using the Q5 Site-Directed Mutagenesis Kit according to the manufacturer's recommendations.

The first step was _.

Step	25 μL RXN	Concentration	
Q5 hot start of 2× master	12.5 μL	1×	
mix			
10 μM forward primer	1.25 μL	0.5 μΜ	
10 μM reverse primer	1.25 μL	0.5 μΜ	
m <i>BPIFA1</i> 1–25 ng/μL	1 μL	1-25 ng/μL	
RNase-free water	9 μL		

The second step was end-point PCR.

Step	Temperature	Time
Initial denaturation	98°C	30 s
25 cycles	98°C	10 s
	50-72°C	10-30 s
	72°C	20-30 s
Final extension	72°C	2 min
Hold	4°C	

The third step was KLD reaction.

Step	Volume	Concentration
m <i>BPIFA1</i>	1 μL	
2× KLD enzyme mix	5 μL	1×
10× KLD enzyme mix	1 μL	1×
H ₂ O-free water	3 μL	

The last step was transformation, in which 5 μ L of KLD mix was added to 12.5 μ L of *E. coli* and incubated on ice for 30 min. The samples were heat shocked at 42°C for 30 s and incubated on ice for 5 min. Thereafter, 150 μ L of SOC was added with gentle shaking at 37°C for 1 h, after which 100 μ L was plated on agar with kanamycin antibiotic overnight.

Primers were obtained lyophilised, and sterile water was used to re-suspend them at a final stock primer concentration of 1 μ g/ μ L. The stock primers were then diluted at a ratio of 1:10 with sterile water, which provided a primer dilution of 0.1 μ g/ μ L for PCR. The following reagents were mixed to carry out the PCRs in 10 μ L reaction volumes: 1 μ L VR1255 construct DNA (including the cloned mBPIFA1 gene), 1 μ L each primer, 2 μ L nuclease-free water, and 5 μ L master mix. The following conditions were used for PCR: starting denaturation of 98°C for 30 s, followed by 25 cycles of 98°C denaturation for 10 s; 60°C annealing for 20 s and 72°C extension for 1 min and 45 s. The last extension was performed at 72°C for 2 min, and the reaction temperature was kept at 4°C until use.

2.9 Synthesis DNA of BPIFA1 Constructs

The production of the *BPIFA1* sequences was outsourced from Biomatik (http://www.biomatik.com), which is specialised in the production of synthetic constructs.

DNA constructs were produced in a pBSK (+) simple, amp-resistant vector. The constructs were validated through sequencing and restriction digestion performed by the company. The inserts were modified to consist of the A1F1NotI and A1RSTOP sequences, flanking each side of the gene in a manner like the original PCR reactions. A Kozak sequence was part of the A1F1NotI sequence as well as an ATG start codon needed to produce protein. The Notl site permitted restriction digestion for cloning. A stop codon was included at the extreme 3' end to halt protein synthesis. The construct also contained a FLAG-tag sequence, which is an artificial sequence for recognition by a highly specific antibody. This allows for the easy purification of large proteins. Additionally, the construct included a BamHI site, enabling the removal of the mutated sequence for subsequent sub-cloning through digestion with BamHI and NotI restriction enzymes. The mutant construct was transformed into E. coli cells, which were cultured inside LB agar (consisting of ampicillin at a concentration of 50 μg/mL), and the plasmid DNA was removed via miniprep purification as explained earlier. Once the mutant plasmid DNA was extracted, NotI and BamHI restriction sites were used for its digestion to sub-clone it into the VR1255 vector. Before subcloning, the digested DNA was run on an agarose gel to confirm the digestion. The desired DNA band of an appropriate size was then isolated from the gel using a sterile scalpel, and the DNA was recovered using the DNA extraction kit.

After the DNA was purified from the agarose gel slice, the DNA Nanodrop was used to measure it, and its purity was examined. The purified DNA was sub-cloned into the VR1255 vector by performing the litigation reactions at different insert–vector ratios. The ligated plasmid was transformed into $\it E. coli$ cells through the heat shock method. After the heat shock treatment, the cells were cultured overnight at 37C° in LB agar plates that included 50 $\mu g/mL$ kanamycin. On the next day, colonies were selected and cultured in LB broth overnight at 37C°. The plasmid DNA was removed by centrifuging and lysing the cells using the Isolate II Plasmid Mini Kit. The cloning

of the DNA into the appropriate site of the VR1255 vector was confirmed, and the alignment of the cloned DNA was checked via sequencing.

2.10 DNA Sequencing

Sequencing of the DNA was undertaken in the Core Genomics Facility, University of Sheffield, using specific forward and reverse primers depending on the vector.

2.11 Sodium Dodecyl Sulphate-Polyacrylamide Gel Electrophoresis (SDS-PAGE) and Western Blotting

Western blotting permits the identification of proteins by carrying out antibody detection. In this study, 12% resolving gels and stacking gels were used. After the gels were assembled, samples of ALI apical washes were created by mixing the same volume of sample with SDS loading 2× SDS lysis buffer (10 mL), 1M DTT (dithiothreitol) (1 mL), 20% SDS solution (1 mL), glycerol (2 mL), Tris-HCL (0.5 M, pH 6.8, 1.25 mL), 0.2% bromophenol blue (200 µL) and one protease inhibitor tablet in water (4.55 mL). Further, 25 μL of the samples and 25 μL of the SDS buffer were used. The temperature of the samples was increased to 95°C, and the samples were loaded into the gel, after which the gel was placed in the tank that consisted of immunoblotting running buffer (Tris [30.3 g], glycine [2.9 g], 20% SDS solution [50 mL] and water [1000 mL]). Thereafter, the gel was run at 60 V, and the samples were permitted to pass through the stacking gel. The power was increased to 150 V (or 200 V) until the sample dye at the start had run towards the end of the gel. On each gel, a ColorPlus Pre-stained Protein Ladder (NEB) was used as the standard ladder. A piece of polyvinylidene difluoride (PVDF) membrane (8.5×6.5 cm) and six pieces of Whatman paper were also utilised. The Whatman paper was kept in the transfer buffer, and the gel was removed from the running instrument. The short plate was removed to allow for accessibility of the gel. The stacking gel was carefully removed while removing the resolving gel. The transfer buffer (Tris [2.9 g], glycine [1.4 g], 20% SDS solution [925 µL], methanol [100 mL] and water [500 mL]) was kept on the gel to prevent the gel from becoming dry.

The transfer was subsequently established by combining three pieces of Whatman paper and the PVDF membrane, while ensuring that there were no air bubbles between the gel and the PVDF

membrane. This was kept in the Bio-Rad semi-dry blotter at 25 V for 20 min for a single gel. When two gels were used, the time was 25 min.

After protein transfer to the membrane was completed, the membrane was treated with 5% skimmed milk in TBS Tween for 1 h at room temperature to prevent non-specific binding. Thereafter, it was washed three times in TBS Tween for 15 min each. The primary antibody, rabbit anti-BPIFA1, was then added to the membrane in 5 mL of blocking buffer and incubated overnight in a cold room. On the following day, the membrane was washed thrice in TBS Tween for 15 min each. The secondary antibody, mouse anti-rabbit HPR, was then added to the membrane in 5 mL of blocking buffer and incubated for 1 h at room temperature on a rolling platform. The membrane was then washed extensively with TBS Tween. ECL solution (2 mL) was added to the membrane and allowed to stand for 5 min before imaging to develop the image. The image was captured using a suitable exposure time on the chemiluminescence high-resolution system in the Image Lab software.

2.12 Dot Blotting

Cell secretion samples (10 μ L) were placed on a PVDF membrane from Millipore and allowed to air-dry. The membrane was blocked in 5% skim milk in 1× TBS Tween buffer for 1 h using an orbital shaker. The following steps were performed via the SDS-PAGE method using polyclonal rabbit anti-mouse BPIFA1 as the primary antibody and polyclonal goat anti-rabbit BPIFA1 as the secondary antibody. The results were visualised using the Bio-Rad ChemiDoc XRS+ System. Densitometry was performed to analyse the results, and quantification was conducted using the ImageJ-win32 programme. Finally, data analysis and statistical tests were conducted.

2.13 Cell Line Transfection

On the following day, HEK293 cells, which the human epithelial kidneys use to produce viral vectors, were transfected in 12-well plates using a standard calcium phosphate protocol. Four hours prior to transfection, the low glucose DMEM growth medium was replaced with a fresh growth medium. A mixture of $3.8 \,\mu\text{L}$ of CaCl₂ (at a $2.5 \,\text{M}$ concentration) and $1.52 \,\mu\text{g}$ of the BPIFA1-VR1255 construct was combined in an Eppendorf tube. The DNA/CaCl₂ mixture was then added

dropwise to a bijou tube, while the mixture including 38 μ L of 2× HEPES-buffered saline was slowly stirred. The tube was then incubated for 20 min at room temperature. The HEK293T cells were transfected via dropwise addition of the transfection–DNA mixture and incubated for 18 h at 37°C and 5% CO₂. Next day, the medium with the transfection–DNA mixture was removed, and the cells were washed with PBS (in the absence of calcium and magnesium chloride from Sigma-Aldrich). A fresh DMEM growth medium (500 μ L) was then added. The cells were incubated for 30 h at 5# CO2 at 37°C. The conditioned medium and the samples were centrifuged for five min at 1000 g to remove debris, and 25 μ L of the conditioned medium was lysed in 25 μ L of 2× SDS lysis buffer. The transfected cell samples were lysed in 100 μ L of 2× SDS lysis buffer. The samples were then analysed for protein expression using western blotting. After BPIFA1 production and secretion were confirmed, the conditioned medium samples were collected daily for 4 days. The cells were washed with PBS to obtain the conditioned media with FBS serum, and a fresh serum-free medium was added. For 3 days, serum-free conditioned medium samples were obtained for western blotting analysis.

2.14 Culture of mTECs

The steps involved in culturing the mTECs are illustrated in Figure 2.2. In the first step, the cells were grown until they reached confluence. In the second step, ALI media were added, and the cells were elevated into the air. From day 0 to day 14, the cells underwent differentiation. They were ready to be used in the experiments at this stage.

2.14.1 In Vitro Culture of mTECs

Various protocols have been formulated in the past few years to facilitate the separation and culture of mouse mTECs, so that they function as a model of the murine airways. In this study, epithelial cells were removed from C57BL/6 mice. When the cells were removed from mouse trachea, they were cultured at an ALI using the technique presented by (Horani, Nath et al. 2013). The use of such cells has recently been mentioned by the Bingle Laboratory (Akram 2015). A brief overview of the protocol is presented subsequently.

For mouse dissection, Field Lab staff members euthanised the mice, and the researcher carefully removed the tracheas to avoid contamination. The tracheas were placed in mTEC media, and the fibrous tissue was removed under the microscope using forceps. The trachea was then cut horizontally under the microscope and placed in a 15 mL tube with mTEC basic and pronase for overnight digestion. On the next day, the cells were washed with mTEC basic media containing 10% FBS, treated with DNase to prevent cell clumping and neutralised with mTEC basic media with 10% FBS. The cells were plated on a Petri dish and incubated for 4 h. The non-adherent cells were removed, and the media were collected, while the fibroblasts were cultured in mTEC basic media with 10% FBS. The epithelial cells were counted using a haemocytometer and then plated over collagen-coated trans-wells at 30,000 cells/well. For cell culture, mTEC basic media with retinoic acid and 10 mM ROCKi were used. During this phase, the cells were lysed for RNA extraction. After 3 days without mobility, the cells were confluent and cultured in ALI using specified ALI mTEC media in the lower chamber for 14 days until differentiation occurred (Figure 2.1). In the latter part of this study, a proprietary media system was used: PneumaCult-Ex Plus for submerged growth and PneumaCult ALI for differentiated growth. These media contained specific nutrients, growth factors and other components essential for the optimal growth and proliferation of mTECs but no BPE. They were designed to produce a mucociliary phenotype in the airway cells in ALI cultures (Rayner, Makena et al. 2019). For transcriptional and protein analyses, washes and cell lysates were obtained. The surface of the cells was washed to obtain apical washes, which were kept frozen until needed. The washed cells were directly lysed using TRI-Reagent to obtain lysates for RNA extraction, which were also kept frozen until needed. MTEC original cells and fibroblasts served as negative controls.

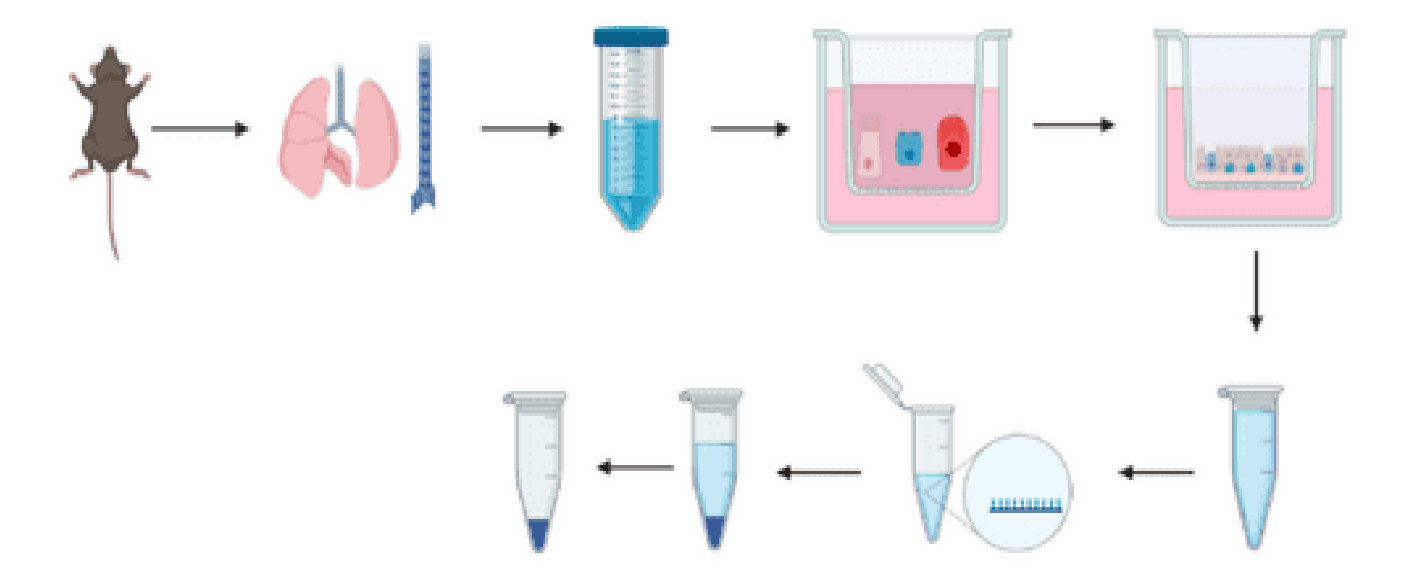


Figure 2.2. Overview of the mTEC Isolation Process

This figure illustrates the steps involved in the isolation and culture of mTECs. The process begins with euthanasia and dissection of mice to extract the trachea. The trachea is then cleaned and placed in media with pronase for digestion. On the following day, the cells are seeded in transwells and maintained in a submerged state until they reach confluence. At this stage, the cells are transferred to ALI media and kept for 14 days during which the media are changed every 2 days, and washed cells are collected. Finally, the RNA is extracted from the cells using TRI-Reagent and stored at -80° C for future analysis.

2.15 Infection of mTECs With IAV (H3N2)

The H3N2 strain of the IAV (A/X-31) was obtained from Professor James Stewart at the University of Liverpool. The virus titre was determined in the laboratory of Professor Stewart using a plaque assay on Madin–Darby canine kidney IAV infection and provided at a known concentration. The virus was added to the apical surface of the cells for 1 h and then removed, and the culture continued as needed. Thereafter, the apical media were removed; the cells were washed, and the trans-well was fixed.

2.16 ALI Culture Sample Fixation

Warm (37°C) PBS was used to wash the apical surface of the trans-well membrane, and the sample was kept in the incubator for incubation for 30 min. Following the incubation, the medium was removed from the basal compartment. Further, 300 μ L of 10% buffered formalin was added to the apical chamber and 700 μ L to the basolateral compartment of the trans-well and incubated at room temperature for one hour. PBS was used to wash the apical and basolateral compartments of the trans-well three times (equilibrated at room temperature) by carrying out repeated pipetting. In the last step, there was addition of 300 μ L of PBS to the apical chamber and 700 μ L of PBS to the basolateral chamber.

2.17 Analysis of the Samples From In Vitro Infection Assays

2.17.1 Fluorescence Immunocytochemistry

From the two compartments of the trans-wells, PBS was aspirated. PBS with 0.5% Triton X was used to dilute 300 μ L of permeabilization/blocking buffer (goat serum or rabbit serum based on the source of detection antibody) at a ratio of 1:10 and then added to the apical surface. Thereafter, the plate was kept on a shaker with 80 revolutions per minute for one hour at room temperature. The permeabilization/blocking buffer was removed from the apical surface. The apical as well as basal surfaces were washed once with PBS. The primary antibody in the permeabilization/blocking buffer was developed as illustrated in Table 2.2, and 300 μ L of primary antibody solution was added to the apical chamber trans-wells. The plate was then kept on a shaker overnight in a cold room at 80 rpm.

Table 2.2. Primary Antibodies in Immunostaining

Primary antibody	Manufacturer	Dilution
BPIFA1 (Rabbit Ab,	Prepared in a laboratory	1:200
polyclonal)	(Musa et al., 2012)	
FOXJ1 (Mouse Ab,	Affymetrix eBioscience	1:200
monoclonal)	(2A5)	
β-tubulin (Mouse Ab,	Sigma (T5201)	1:100
monoclonal)		

After overnight incubation, the primary antibody was removed from the apical surface. PBS was used through pipetting to wash the apical and basal surfaces thrice. The method shown in Table 2.3 was used to create the secondary antibody solution, and 300 μ L of antibody solution was included in the apical chamber of the trans-well, after which the plate was covered in aluminium foil. The plate was subsequently kept on a shaker for 1 h at room temperature and 80 rpm.

Table 2.3. Secondary Antibodies in Immunostaining

Secondary antibody	Dilution
Alexa Fluor 568 Goat anti-rabbit Ab. Cat No. A11011. (Red)	1:200
Alexa Fluor 488 Goat anti-mouse Ab. Cat No. A11001. (Green)	1:200

The secondary antibody was diluted in PBS and used to wash the apical and basal surfaces of the trans-well under dim light. The membrane containing the cells was carefully cut out using a scalpel and held in place on a microscope slide using forceps, with the cells facing upwards. A single drop of 4,6-diamidino-2-phenylindole (DAPI) mounting medium (Vectashield, Vector Laboratories) was added to the top of the cells and allowed to sit for 2 min at room temperature.

The coverslip was then placed onto the slide, and any excess DAPI was spread out around the edges. The coverslip was secured to the slide using nail polish and left to set for 30 min at room temperature. The slides were then removed and analysed using the Olympus FV1000 Confocal Microscope.

2.17.2 Quantification of IAV Staining

The Olympus FV1000 Confocal Microscope was used to analyse IAV staining in the mTECs. A 40× magnification was employed to capture an image of eight contiguous fields that encompassed the entire membrane. The ImageJ software was utilised to examine and combine Z-stacks to produce a single image with highest intensity. The mean integrated fluorescence was calculated using the ImageJ software to analyse the signal intensity.

2.18 Statistical Analysis

Statistical analyses were performed where necessary. The expression values of the individual genes were compared across the samples using a paired t-test. One- and two-way analyses of variance were conducted. The analyses were performed using the GraphPad Prism 8 software (GraphPad Software, Inc.). For the statistical analysis of the genes, data were compared using a t-test in the GraphPad Prism 8 software. A P-value of <0.05 was considered statistically significant.

Chapter 3: Validation of mTEC cultures

3.1 Introduction

The airway epithelium consists of several types of cells derived from multipotent basal cells. It performs the homoeostatic function of the respiratory tract, and its modelling in culture is important, as most established cell lines lack differentiation capacity. Primary airway cells grown in 3D cultures and derived from human or mouse trachea, nasal passage or middle ear are considered good models of the airways and have been used in previous studies to understand the role of airway epithelial cells and infectious diseases (Ugonna, Bingle et al. 2014, Lu, Anujan et al. 2019, Mulay, Chowdhury et al. 2021). These studies are based on established protocols (Clarke, Burns et al. 1992, Davidson, Kilanowski et al. 2000, You, Richer et al. 2002), which are influenced by methods for other species (Lechner 1985). Essential growth factors, such as insulin, epidermal growth factor and retinoic acid, promote cell differentiation and cilia formation (Green 1977). Mouse cell culture involves a sufficient number of cells, the proliferation of the progenitor cell population and the attachment of a small number of basal cells to the membrane (Green 1977, Allen-Hoffmann, Schlosser et al. 2000). Epithelial cells differentiate when they are exposed to the ALI condition, which is achieved by a confluent cell layer and feeding media from below. ALI promotes the formation of cilia and the differentiation of mucociliary epithelium, which can be monitored through cell-specific markers (You, Huang et al. 2004, Bustamante-Marin and Ostrowski 2017). The differentiation process is marked by a transcriptional programme, which transforms cells from a basal cell phenotype to a mucociliary epithelium with ciliated and secretory cells (Ross, Dailey et al. 2007). MTECs are differentiated into upper airway-like epithelia under ALI conditions by changing the media and moving the cells to ALI. Samples are taken prior to culture, during confluence and at various times during culture. After 14 days of differentiation, the cells become suitable for experiments.

3.2 Aims of the Chapter

The overall aim of this chapter was to generate cellular tools for the functional analysis of influenza infection in mTECs. The specific objectives were as follows:

- 1. To perfect the dissection technique for isolating mTECs,
- 2. To establish and validate ALI culture conditions and

3. To characterise the transcriptional programme of mTECs during differentiation.

3.3 Results

3.3.1 Description of mTEC Cultures

The culture conditions for mTECs were previously established in the host laboratory (Akram et al., 2014), but I needed to perfect the technique. On average, approximately 150,000 mTECs were isolated per trachea. An average of eight mice per batch was used, and more than 40 batches of cells were made.

Initially, the established protocol was used, which involved culturing the isolated cells in the presence of a ROCK inhibitor (Y-27632) to improve the multiplication of airway epithelial basal cells (Horani, Nath et al. 2013) (Horani et al., 2013) prior to ALI lift. However, during the study, a proprietary media system was used: PneumaCult-Ex Plus for submerged growth and PneumaCult ALI for differentiated growth. These contained specific nutrients, growth factors and other components essential for the optimal growth and proliferation of mTECs. This medium was specifically designed to produce a mucociliary phenotype in differentiated murine airway cells in ALI cultures (Rayner, Makena et al. 2019).

A seeding density of 30,000 cells per trans-well was used, as this was found to be optimal. Within 5–7 days of seeding, a confluent monolayer was achieved, and the cells were imaged using phase-contrast microscopy (Figure 3.1).

3.3.2 Validation of Gene Expression by RT-PCR

Owing to the limited number of cells generated from the mice, the standard differentiation culture conditions utilised 24-well trans-wells with a surface area of 0.33 cm². This resulted in an average of approximately 100,000 cells per trans-well present in the cultures. To ensure that sufficient RNA could be isolated from this cell number, I initially tested the extraction procedure using HEK cells. Initially, the host laboratory used TRI-Regent for RNA isolation; however, the low recovery rate and the presence of contaminants that interfered with PCRs posed a concern, and so the laboratory switched to using the Direct-zol Microprep Kit (Zymo) for RNA isolation during this study.

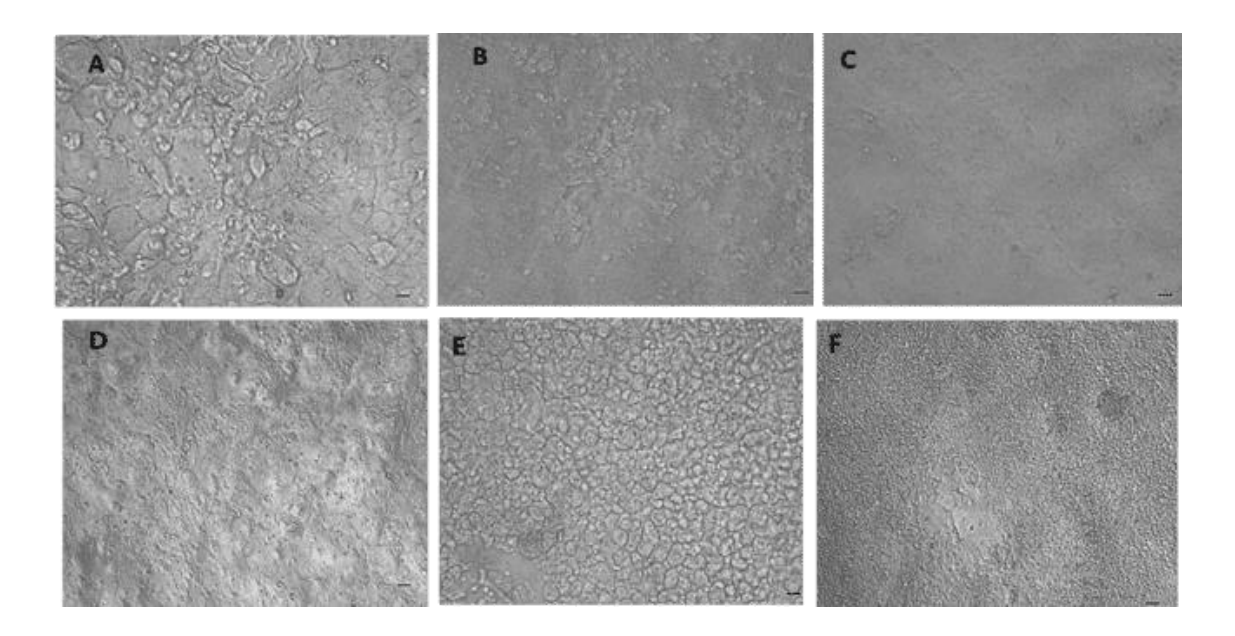


Figure 3.1. Phase-Contrast Images of mTECs During Differentiation

(A) All day 0 cells (B) All day 2 cells (C) All day 6 cells (D) All day 7 cells (E) All day 1

(A) ALI day 0 cells. (B) ALI day 2 cells. (C) ALI day 6 cells. (D) ALI day 7 cells. (E) ALI day 14 cells. (F) ALI day 14 cells 50 μm (lower magnification).

Preliminary studies showed that 100,000 HEK cells could yield up to 5 ug of RNA (Table 3.1). When mTECs were used at different stages of culture, relatively low yields of RNA were initially recovered from primary cells in 0.3 cm² trans-wells, and in some samples, essentially no RNA was recovered. Over time and with technical improvements, up to 2 ug of RNA per trans-well was recovered. Given that only 200–500 ng of RNA was needed for RT-PCR, there was sufficient RNA recovered for the protocol.

For validation of the cultures, end-point RT-PCR was performed to verify the differentiation of mTECs grown at the ALI. This was performed on cells on ALI day 0 (a cell population of progenitor cells) and ALI days 3, 7, and 14 (containing fully differentiated respiratory epithelium), and the original cells obtained before culture were established (containing airway epithelial cells found in the original tissue as well as contaminating cells isolated from the trachea). A fibroblast cell preparation separated from the same mice was used as a control in the PCRs. Each cell

preparation was validated in this manner (with PCRs generally being made on original, day 0 and day 14 cells). A representative gel is shown in Figure 3.2.

Table 3.1. RNA Recovery from HEK Cells

Replicate	Cell Counts	RNA in 15 µl
	1x10 ⁶	7.28
3,000 mile me mo	5x10 ⁵	2.004
Replicate 1	3x10 ³	1.045
	1x10 ⁵	0.225
	5x10 ⁴	0.2755
	2.5x10 ⁴	0.1952
	1x10 ⁶	6.53
	5x10 ⁵	2.246
Replicate 2	3x10 ³	1.2
	1x10 ⁵	0.837
	5x10 ⁴	0.286
	2.5x10 ⁴	0.262

Total RNA was extracted from HEK cells using the Direct-zol RNA Microprep Kit. The number of cells was progressively decreased for the RNA extractions. RNA was eluted in 15 μ L of water prior to quantitation and is displayed as the total ug of RNA recovered.

.

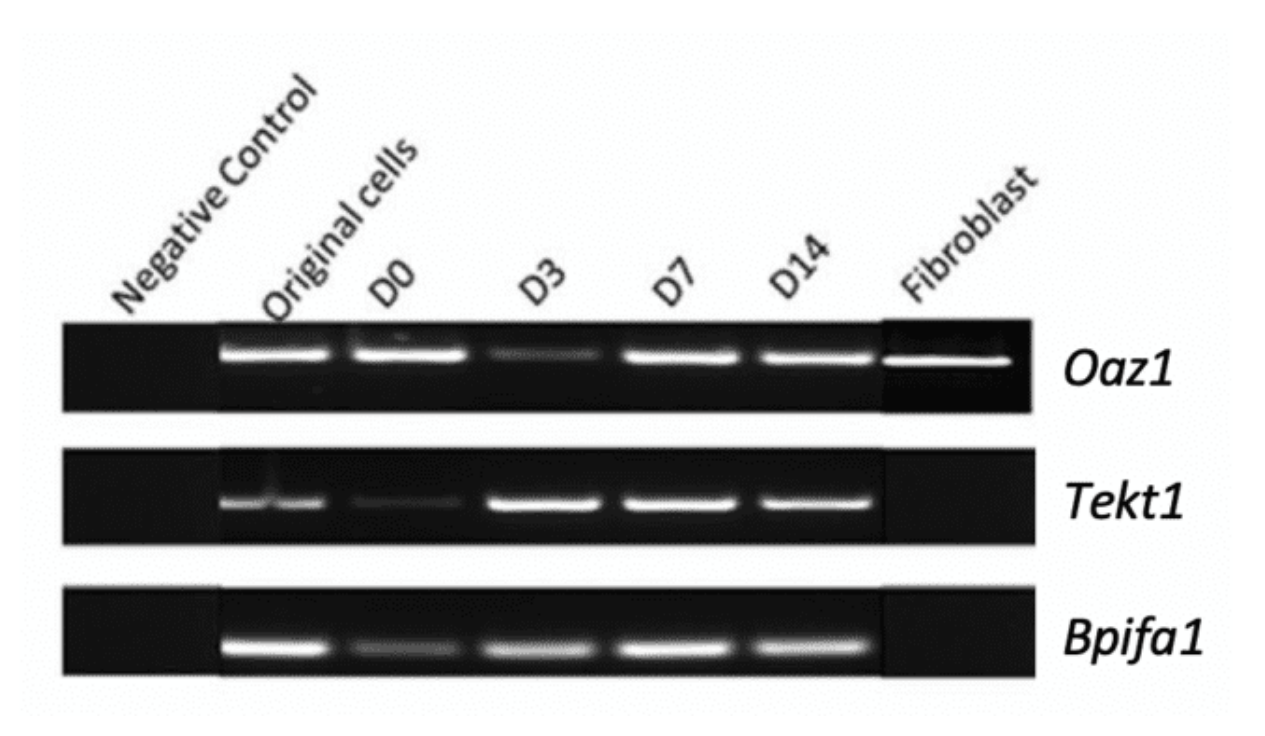


Figure 3.2. End-Point RT-PCR of Markers in mTECs During ALI Differentiation

On days 0, 3, 7 and 14 of ALI culture, mTEC RNA samples were collected, and the expression of epithelial markers was evaluated. Primers for ornithine decarboxylase antizyme 1 (*Oaz1*; internal control), *Bpifa1* (secretory cell marker) and Tektin 1 (*Tekt1*; ciliated cell marker) were used. The positive control was obtained from the original samples of airway epithelial cells that were collected from the trachea before plating. The negative control was RNA from fibroblast cultures that were obtained from the mouse trachea during dissection. The products generated were analysed via 2% agarose gel electrophoresis. This gel is representative of several similar experiments performed to confirm cellular differentiation.

Oaz1, which is considered a housekeeping gene owing to its stable expression across multiple tissue samples (De Jonge 2007), served as the control for all PCRs performed. It was consistently expressed in each sample, including in the fibroblasts, mTECs and ALI cultured cells on days 0, 7 and 14. However, lower Oaz1 expression was observed on day 3, which may have been due to a lack of sufficient cDNA amount during sample preparation or some other technical reason.

Tekt1 is a marker for ciliated cells and is a crucial structural protein found in the axoneme of motile cilia (Ryan, Failler et al. 2018). On day 0, the low expression of *Tekt1* suggests a scarcity of

ciliated cells in the culture, but the expression increased over time; on day 14, its expression level could be compared to that of the original cells, implying the presence of differentiated ciliated cells in the culture.

Bpifa1 was used as a marker for secretory differentiation in the cultures. On day 0, some expression of Bpifa1 was observed, indicating that cells exhibit some degree of differentiation at this time. However, this expression decreased on day 3 but appeared to increase again on days 7 and 14. Mouse fibroblast cDNA served as the negative control and did not express either of the differentiated cell markers, as expected. The end-point PCR suggested that the cells were induced to undergo differentiation during the culture.

3.3.3 SDS-PAGE

The secretion of *Bpifa1* was studied to determine whether functional cell differentiation had occurred in the ALI culture. *Bpifa1* is released by the secretory cells of the airway epithelium and serves as a marker for secretory differentiation. Western blotting was performed on apical washes obtained from mTECs on ALI days 2, 7, 9, 12 and 14. Equal volumes of apical wash were added to each lane. Figure 3.3 shows that a band of around 25 kDa, indicative of Bpifa1, was present on the gel. *Bpifa1* was not detected in the washes obtained on ALI day 0, but its expression started increasing from day 2 to day 14, indicating the presence of differentiating secretory cells releasing *Bpifa1* at these times.

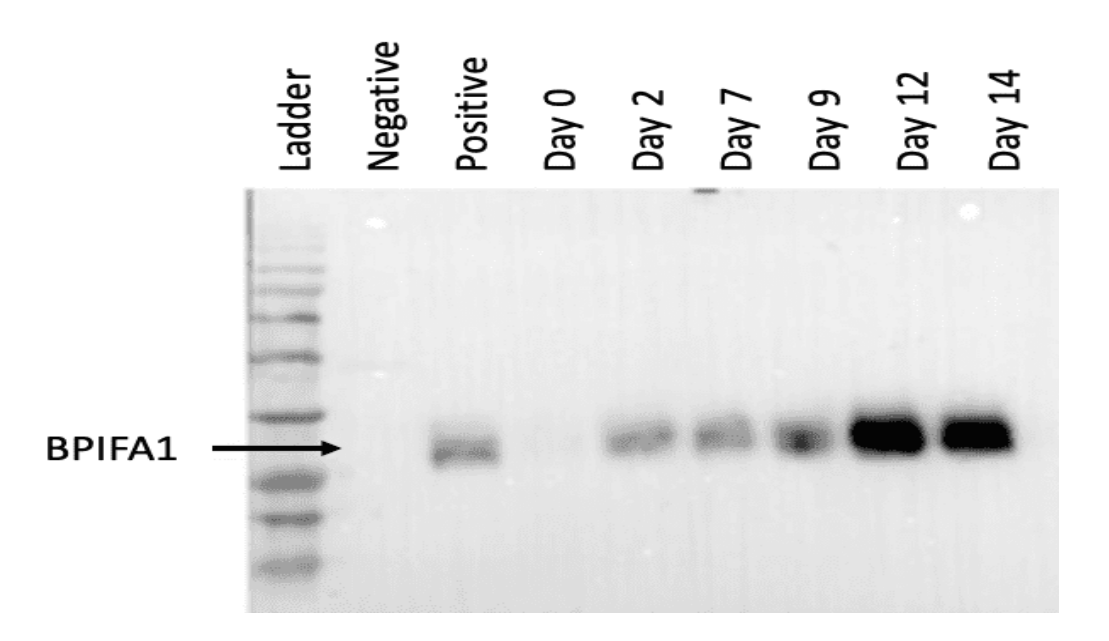


Figure 3.3. Secretion of BPIFA1 From mTEC Cultures

Samples of apical washes from a batch of cells were western blotted to demonstrate the secretion of BPIFA1 by ALI cultured mTECs. The same volume of apical wash collected from the cells on the indicated days was loaded in each well. The position of BPIFA1 is indicated by the band at approximately 25 kDa. Mouse bronchoalveolar lavage fluid was used as the positive control and SDS loading buffer as the negative control. The gel is representative of three individual experiments.

3.3.4 Confocal Imaging of Cells During Differentiation

Confocal imaging was performed to visualise distinct airway epithelial cells in the differentiated ALI culture on day 14. The mTECs on the trans-well membranes were fixed with 10% formalin and stained with antibodies to BPIFA1 (marker the secretory cells) and β -tubulin (a well-accepted marker for cilia) and counterstained with DAPI to visualise the cell nuclei. The stained cells were then imaged under confocal microscopy. TEKT1 was not used, as it serves as a standard marker for ciliated cells in expression studies but is not commonly used to visualise the presence of cilia themselves.

As shown in Figure 3.4, day 0 and 14 mTECs were stained with β -tubulin and BPIFA1. As expected, staining of both markers was absent from day 0 mTEC cultures (A), whereas both proteins were

detected in the day 14 sample (B). The localisation of these two proteins did not overlap. This is consistent with previous data from the laboratory that showed β -tubulin and BPIFA1 in different cell types (Akram 2015).

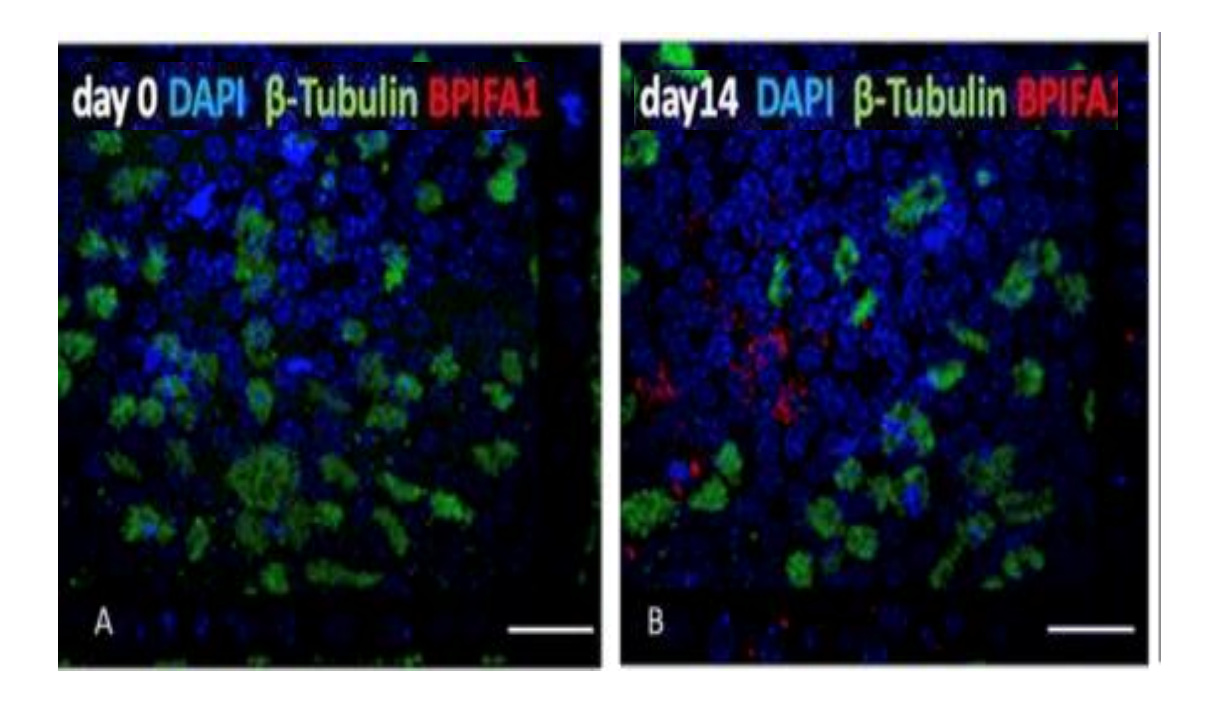


Figure 3.4. Immunofluorescence Microscopic Detection of β -Tubulin and BPIFA1 in the day 14 mTECs

These images depict cell differentiation of secretory and ciliated cells taken from mTECs cultured at the ALI. The day 0 and 14 cells were stained with antibodies to β -tubulin (green) and BPIFA1 (red). Blue represents DAPI. Scale bar, 50 μ m.

3.3.5 Gene Expression in Whole-Genome Expression Data Sets

When the mTEC cultures were confirmed to be differentiated, as expected, the global transcriptional changes in the cells were studied. Samples of the original (freshly isolated uncultured) tracheal cells, confluent cultures of cells prior to ALI lift (ALI day 0) and ALI cells that had been cultured for 14 days were isolated. In these experiments, triplicate samples were used from matched isolations, meaning that the three samples were matched with individual batches of cells. Total RNA was extracted using the Zymo system as previously described, and the quality

was determined using the Agilent Bioanalyser. Only RNA with an RNA integrity number (RIN) of above 8 was used for the analysis.

Microarray analysis was undertaken by Doctor Paul Heath at SITraN, University of Sheffield, using the Mouse Clariome S microarray assay (Thermo Fisher Scientific). In the murine model system, this array can identify the expression of >20,000 well-annotated genes. The Transcriptome Analysis Console (TAC) 4.02 (Thermo Fisher Scientific) was used for the conversion of the Clariome S data to Excel spreadsheet data. The next step consisted of analysing the data in Microsoft Excel to determine the difference in the intensity, fold change and p-value of the genes. The genes that were differentially expressed underwent further analysis using the Venny 2.1.0 software. Database for annotation, visualisation and integrated discovery (Meredith, Zemmour et al. 2015) (Meredith et al.) version 6.8 (Dennis, Sherman et al. 2003) and the TAC tool on version 4.02. A log2 intensity of <5 was considered as negative for expression and a log2 intensity of >5 as positive for expression (Miller, Dye et al. 2019). Robust multi-array average-linear models for microarray data were used to normalise and background correct the microarray data in the TAC tool. The bioinformatic analysis was undertaken by another PhD student (Miraj Chowdhury). I worked to analyse the output of this process. Owing to some unforeseen issues in the RNA array facility, the final number of samples used in the analysis was 2 for the original and day 0 samples and 3 for the day 14 samples.

3.3.5.1 Most Highly Expressed Genes in the Original, Day 0 and Day 14 Cells

The initial analysis aimed to identify the genes with the highest expression levels in the mTECs at different time points. The top 50 genes in terms of expression levels are listed in Table 3.2. The absolute gene expression levels of these genes ranged from 17.24 to 18.79 (log2) in the original cells, from 17.42 to 19.1 (log2) in the day 0 cells and from 17.15 to 18.92 (log2) in the day 14 cells.

Table 3.2. Top 50 Most Highly Expressed Genes in mTECs at Different Time Points

	Top 50^{th} genes in Original , Day 0 and Day 14					
NO	Original	Exp	Day 0	Exp	Day 14	Exp
1	Bpifa1	18.79	ND1	19.1	Cyp2f2	18.92
2	Anxa1	18.775	Krt7	18.675	ND1	18.86
3	Scgb1a1	18.705	Fth1	18.62	ND5; CYTB	18.786
4	ND3	18.66	S100a11	18.605	ND4; ND4L	18.7833
5	Cldn4	18.635	Нѕра8	18.52	Fth1	18.7333
6	COX2	18.615	Bsg	18.49	Hspa8	18.716
7	Rpl13a,Snord32a,Snord33, Snord34, Mir5121	18.535	ND4, ND4L	18.485	COX2	18.57
8	Actb	18.53	Ly6e	18.485	Gstm1	18.42
9	Cbr2	18.53	Gsto1	18.395	ND3	18.36
10	Emp1	18.44	2610528A11Rik	18.365	Tmem176b	18.343
11	Ubc, Uba52	18.435	ND5; CYTB	18.36	Serinc3	18.296
12	Actg1, Mir6935	18.41	COX2	18.34	Gsto1	18.213
13	Scgb3a1	18.305	Rps6	18.31	S100a11	18.18
14	Ubb,Gm1821	18.3	Cyp2f2	18.31	Ly6e	18.1433
15	Reg3g	18.285	Anxa1	18.225	Gm11032	18.133
16	Tmsb4x	18.195	Actb	18.22	Rpl13a,Snord32a,Snord33,Snord34, Mir5121	17.94
17	Gm11032	18.165	Gm11114	18.15	Rpl4	17.926
18	S100a11	18.145	Rpl13a,Snord32a,Snord33,Snord34, Mir5121	18.14	Rps6	17.886
19	F3	18.085	Cd81	18.03	Ubb; Gm1821	17.85
20	Serpinb2	18.08	Rpl28	17.975	Rpl28	17.846
21	Rps6	18.05	Serinc3	17.94	Prdx1	17.763
22	Hbb-bt,Hbb-b2	18.03	Eef2	17.92	Slc3a2	17.746
23	Hbb-bs, Hbb-b1	17.965	Slc2a1	17.915	Gclc	17.716
24	Rmrp	17.965	Itm2b	17.9	Krt7	17.696
25	Actn4	17.935	Pkm	17.89	Gsta3	17.686
26	Eif1	17.835	Mal	17.885	Cyp2a5, Cyp2a4	17.686
27	Cyp2a5, Cyp2a4	17.815	Egln3	17.88	Rpl23	17.676
28	Hnrnpk	17.765	Ndrg1	17.875	Pabpc1	17.633
29	Slc3a2	17.71	Igfbp7	17.855	Ср	17.633
30	Lyz2	17.68	Uba52	17.825	Anxa1	17.61
31	Krt7	17.675	Rplp1	17.79	Actb	17.61
32	Gm1821	17.645	Pabpc1	17.755	Uba52	17.523
33	Eef2	17.64	Psca	17.74	Eef2	17.5
34	Aldh1a1	17.575	Pdzk1ip1	17.69	Itm2b	17.4733
35	Scgb3a2	17.565	Ubb; Gm1821	17.68	Rps23	17.45
36	Hspa5	17.545	Rps23		Bsg	17.413
37	Pabpc1	17.545	Cnfn	17.645	Mgst1	17.396
38	Dstn	17.505	Tmsb4x	17.63	Rpl21	17.393
39	Cdh1	17.495	Ecm1; Mir7014	17.615	Gclm	17.366
40	Krt8	17.485	Krt6a; Krt6b	17.61	Mal2	17.346
41	Ifi202b; Ifi205	17.48	Rpl18a	17.6	Aldh1a1	17.346
42	Gprc5a	17.455	Aldoa	17.595	Scgb1a1	17.336
43	Rpl12, Snora65	17.42	ND3	17.54	Rpl12, Snora65	17.326
44	Tsc22d1	17.38	Slc38a2	17.53	Tmem176a	17.283
45	Gstm1	17.365	Rpl4	17.51	Ftl1	17.2733
46	Errfi1	17.34	Cox7c	17.465	Lamp2	17.26
47	Cyr61	17.34	Tspan1	17.46	Slc25a5	17.223
48	Lgals3	17.25	Capns1	17.425	Gm11114	17.193
49	Ly6e	17.245	Plp2	17.42	Rp16	17.166
<i>50</i>	Plaur	17.235	Mal2	17.415	Bpifa1	17.15

This table presents the log2 expression levels of the top 50 most highly expressed genes in the mTECs measured at three different time points: original cells (n=2), day 0 of ALI culture (n=2) and day 14 of ALI culture (n=3). The expression levels are presented as log2 intensity values, which allow the comparison of the fold changes in expressions of gene. The original cell data serve as the baseline gene expression before the isolated cells were cultured. The day 0 data represent the gene expression immediately after the cells were exposed to the ALI culture conditions, while the day 14 data represent the expression levels of the genes after 14 days of exposure to the ALI culture conditions.

The simple representation of the data in this format suggests that the three cell populations have quite different gene expression profiles. *Bpifa1* was the most highly expressed gene in the original cells; it did not appear in the day 0 list but appeared in the top 50 highly expressed genes in the day 14 cells. *Nd1* was the most highly expressed gene in the day 0 cells and was the second most highly expressed gene in the day 14 cells. *Cyp2f2* was the most highly expressed gene in the day 14 cells and was also in the top 15 list in the day 0 cells. *Anxa1*, *Nd3*, *Cox2*, *Sa100a11* and *Actb* were included among the top 50 highly expressed genes at all three time points. Similar to *Bpifa1*, *Scgb1a1* was also substantially highly expressed in the original and day 14 cells but was not seen in the day 0 cells. Two other secreted globin genes – *Scgb3a1* and *Scgb3a2* – were also highly expressed in the original cells but were not included in the list in the other two conditions. Another secretory protein gene – *Reg3g* – followed a similar expression pattern. The high expression of these abundant secretory genes reflects the fact that the cell population contains a substantial number of differentiated secretory cells.

Among the most highly expressed genes in the original cells were two β-globin genes (*Hbb-bt/Hbb-b2* and *Hbb-bb/Hbb-b1*), which are generally highly expressed in red blood cells. This finding suggests that red blood cells contaminate the original cell preparation and that these disappear in day 0 and 14 samples. The list of most highly expressed genes in the day 0 samples appeared to contain fewer secretory proteins and was dominated by enzymes including components of the mitochondrially encoded NADH ubiquinone oxidoreductase complex (encoded by *Nd1*, *Nd3*, *Nd4* and *Nd5*) as well as *Gsto1*, *Cyp2f2*, *Aldoa* and *Cox7c* in addition to ribosomal protein genes including *Rsp6*, *Rpl28*, *Rplp1*, *Rsp*, *Rpl18* and *Rpl4*.

The list of most highly expressed genes in the day 14 cells also contained many enzymes found in the day 0 cells but also showed a return of some epithelial secretory cell products including *Cp, Scgb1a1* and *Bpifa1. Fth1*, which encodes the iron transport protein ferritin, was highly expressed in both day 0 and 14 cells.

Overall, the high expression of the secretory genes in the original and day 14 cells highlights the presence of differentiated secretory cells, while the shift towards more enzymes in the day 0 cells reveals the effects of the ALI culture conditions.

3.3.5.2. Transcriptional Changes in the Gene Expression During mTEC Differentiation

A heat map was generated to obtain an overall view of differential gene expressions at the three different time points (Figure 3.5). The genes with high or low differential expression (either high or low) in the original vs day 0, original vs day 14 or day 0 vs day cells 14 were used. When visualised in this manner, the gene expression was generally well conserved between the replicate samples in each condition; however, the gene expression seen in the day 14 replicate 3 was somewhat different from that seen in the other two replicates. This suggests that something unexpected may have happened during the culture of this sample, which resulted in differences in the gene expression data in this batch.

The heat map showed that 9780 genes were differentially expressed. Unsupervised hierarchical clustering showed several distinct patterns in the image. As the heat map revealed complex relationships between the groups, the genes were broadly grouped into a few representative regions. The genes grouped in the A region included those highly expressed in both the original and day 14 cells, which might be expected to include genes expressed in the epithelial layer. The genes grouped in the B region included those highly expressed in the day 14 cells, but which were more lowly expressed the original cells. The genes grouped in the C region included those highly expressed in the day 14 cells, but which were more lowly expressed in the day 0 cells and not expressed in the original cells. The genes grouped in the D region included those substantially highly expressed in the primitive cells, but which were lowly (or not) expressed in the epithelial cells during culture. Many genes in group E were highly expressed in the day 0 cells but had a low or limited expression in either of the other two conditions.

Differential gene expression between paired situations was evaluated to obtain a better understanding of some gene expression changes: original vs day 0, day 0 vs day 14 and original vs day 14.

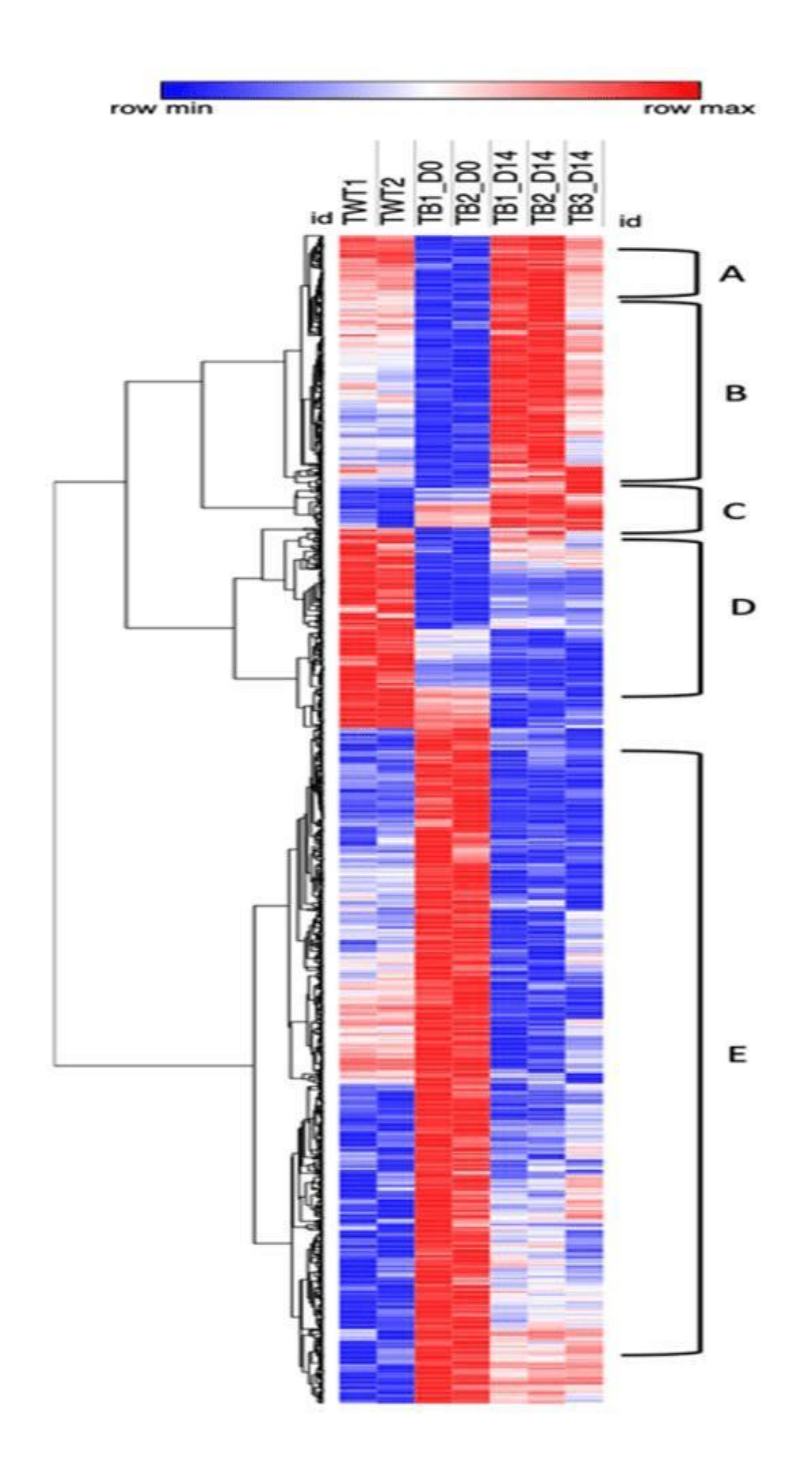


Figure 3.5. Heat Map of Genes Differentially Expressed During mTEC Culture

The heat map displays the genes that showed differential expressions between the original, day 0 and day 14 samples, wherein significant differences in the expression levels were observed between two conditions. The brackets (A–E) categorise the genes with broadly distinct expression patterns. The brackets (A–E) are added somewhat arbitrarily. They represent a categorisation of the genes based on the pattern of expression and the differences seen between the conditions. TWT1 and TWT2 represent the original cells, wherein TWT stands for wild type. TB1-D0, TB2-D0, TB1-D14, TB2-D14 and TB3-D14 represent different sample conditions taken on days 0 and 14. The number after TB (1, 2 or 3) indicates replicates within the samples.

3.3.5.3. Differential Gene Expression Between the Original and Day 0 Cells

Figure 3.6 shows the overall gene expression differences between the original cells isolated from the trachea and sampled prior to culture and those when confluent cultures were established on the transwells prior to ALI culture (day 0). These genes are mostly located in region C in Figure 3.5. Analysis of the differential gene expression between these two conditions would be expected to identify gene signatures of the cell population that was in the original cell isolate taken from the protease digestion of entire tracheal tissues (red dots). This would include red blood cells, inflammatory cells and mesenchymal cells as well as cells from tissues surrounding the trachea when it was dissected. The genes that were more highly expressed in the day 0 cells are shown as green dots. These represent the cells expressed in the growing epithelial cells, as the contaminating cells will have been lost from the cells at this stage.

Table 3.3 displays the top 50 genes that were most differentially expressed between the original cells and the cells grown to confluence on the trans-wells. The top four genes on the list, Hbb-bs/Hbb-b1, Hba-a2/Hba-a1, Hba-a1/Hba-a2 and Hbb-bt/Hbb-b2originate from RNA in contaminated red blood cells. The expression of these genes was significantly lower in the day 0 cells as red cells are lost.

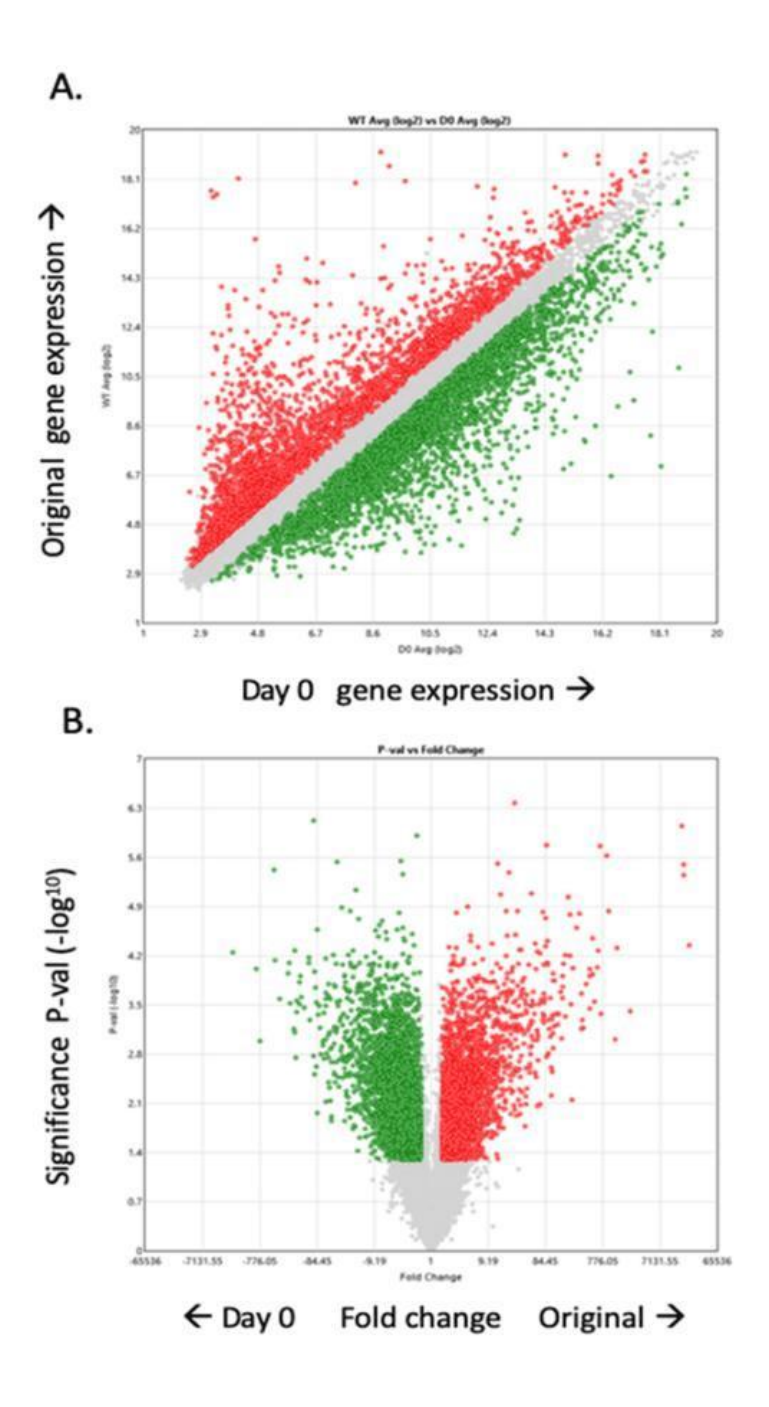


Figure 3.6. Differentially Expressed Genes in Uncultured Tracheal Epithelial (Original) Cells and ALI Day 0 Cells

This figure depicts the comparison of the differentially expressed genes between the uncultured tracheal epithelial cells (original) and ALI day 0 cells. The scatter plot in panel A displays the log2 intensity values of the genes that showed a differential expression. The volcano plot in panel B illustrates the significance of these differentially expressed genes, with 9586 genes shown. Each

dot in the plot represents the expression level of a particular gene. The genes that were significantly differentially expressed are marked with either green dots (indicating overexpression in the day 0 cells) or red dots (indicating overexpression in the original cells). ALI, air—liquid interface

Table 3.3. Top 50 Most Differentially Expressed Genes in the WT Compared with the Day 14 Cells

NO	Genes	WT	. D14	Fold Difference
1	Hbb-bs, Hbb-b1	17.965	3.216	-14.748
2	Hba-a2, Hba-a1	17.065	3.393	-13.671
3	Hba-a1, Hba-a2	17.14	3.473	-13.666
4	Hbb-bt,Hbb-b2	18.03	4.406	-13.623
5	Serpinb2	18.08	6.433	-11.646
6	Lipf	13.815	3.633	-10.181
7	Dcn	14.68	4.613	-10.066
8	Tg	14.45	4.513	-9.936
9	Cd74, Mir5107	15.055	5.243	-9.811
10	Sbpl	14.19	4.616	-9.573
11	Gm10591	13.775	4.243	-9.531
12	Plau	15.79	6.38	-9.41
13	Krt75	14.815	5.46	-9.355
14	Fosb	14.615	5.553	-9.0616
15	H2-Aa	14.605	5.55	-9.055
16	Dcpp3	12.81	3.85	-8.96
17	Bpifb1	15.71	6.856	-8.853
18	Tmprss11b	14.035	5.19	-8.845
19	Nr4a3	12.78	3.953	-8.826
20	H2-Ab1	13.865	5.12	-8.745
21	Cd53	13.87	5.17	-8.7
22	Dmbt1	13.28	4.606	-8.673
23	H2-Eb1	12.715	4.046	-8.668
24	Ccl22	12.835	4.286	-8.548
25	Cldn1	13.515	5.01	-8.505
26	Gm13304, Gm21541, Ccl21b	12.58	4.26	-8.32
27	Gm13304	12.59	4.376	-8.213
28	Krt16	13.94	5.776	-8.163
29	Gm7897	12.77	4.773	-7.996
30	Krt23	16.355	8.373	-7.981
31	Sell	12.235	4.30	-7.931
32	Glycam1	11.54	3.846	-7.693
33	Serpinb1a	15.84	8.476	-7.363
34	117r	11.955	4.6	-7.355
35	Cxcr4	13.22	5.98	-7.24
36	Cytl1	11.215	3.976	-7.238
37	Csrnp1	12.65	5.42	-7.23
39	Dcpp2, Dcpp1	12.635	5.41	-7.225
40	Rgs1	11.635	4.443	-7.191
41	Plek	12.09	4.903	-7.186
42	Rgs2	10.805	3.626	-7.1783
43	Ms4a4c	11.265	4.14	-7.125
44	Satb1	12.81	5.69	-7.12
45	Jun	15.54	8.483	-7.056666667
46	Spi1	12.025	5	-7.025
47	Cd69	11.875	4.853	-7.021666667
48	Prss23	13.435	6.433	-7.001666667
49	Dpt	10.675	3.683	-6.991666667
50	Samsn1	11.405	4.4633	-6.941666667

This table presents the average expression value (log2) in the day 0 and WT samples and the differential expression between the two.

Within the list of genes are several secretory gene products derived from the tracheal epithelium: *Bpifb1*, *Bpifa1*, *Sftpa1*, *Scgb3a1* and *Scgb3a2* from the secretory cells. The list also contains several genes known to be expressed in the tracheal submucosal glands including *Lipf*, *Dcpp3* and *Dcpp2*, which are goblet cell markers (Sountoulidis, Liontos et al. 2020). The list also contains some thyroid and thymocyte enriched genes including *Tg*, *Nr4a3* and *Sell*, which probably arise from the contamination of the tracheal tissue during the initial dissection stage.

Finally, several genes in the list, including *Gm10591*, *Ccl21*, *Cd53*, *Ccl22Fosb*, *Spi1* and *Rgs1*, are known to be highly expressed in inflammatory cells including neutrophils, macrophages, mast cells and lymphocytes.

3.3.5.4. Differential Gene Expression Between the Day 0 and 14 Cells

Figure 3.7 shows the overall gene expression differences between the confluent monolayer cultures established on the trans-wells prior to ALI culture (day 0) and day 14 ALI culture. The genes are mostly located in regions A and B in Figure 3.5.

The analysis of the differential gene expression among the two conditions was expected to identify a signature of the genes that were highly expressed in the day 14 differentiated cells (red dots) than the undistinguishable basal cells that were the improved confluent monolayer preceding the ALI culture (green dots).

The top 50 most differentially expressed genes in the day 14 cells compared with those grown to confluence on the transwells (day 0) are shown in Table 3.4. The most differentially expressed gene in these cells was flavin-containing monooxygenase 3 (*Fmo3*), followed by *Cdhr3* and *SEC14*-like lipid-binding 3 (*Sec14l3*). The list was dominated by the genes associated with ciliated cells: *Cdhr3*, *Tppp3*, *Rsph4a*, *Sntn*, *Cd177*, *Spata18*, *Ccdc146*, *Tmem232*, *Odf3b*, *Ak7*, *Cfap126*, 1700040L02Rik, *Adgb*, *Dynlrb2*, *Gm281*, *Ubxn10*, *Cfap16*, *Fam216b*, *Erich2*, *Nek5*, *Cdhr4*, *Stoml3*,

Lrrc34, 1700013F07Rik, Tcte1, Ccdc153, Kcnrg, Spef2, Elmod1, Dnah5, Meig1, Ccdc108, Lrguk and
Rgs22.

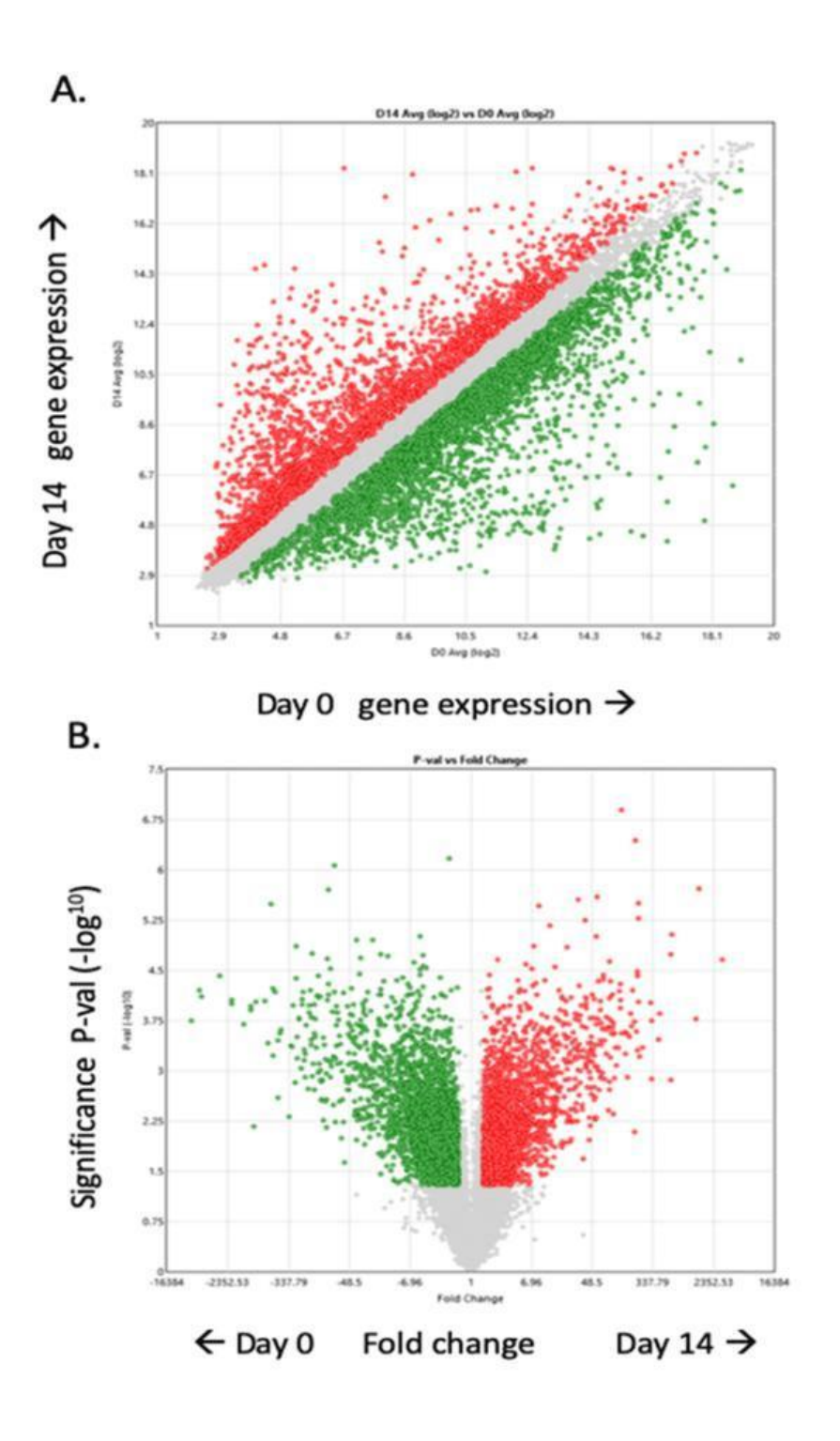


Figure 3.7. Differentially Expressed Genes in the ALI Day 0 and 14 Cells

(A) Scatter plot showing the log2 intensity values of the differentially expressed genes. (B) Among these genes, 9586 genes are shown by the volcano plot. Each dot represents the expression of a gene. Coloured dots represent the significantly differentially expressed genes. The green dot

indicates overexpression in the day 0 cells, and the red dot indicates overexpression in the ALI day 14 cells.

Bpifa1 was the most differentially expressed secretory gene seen in the list, but other secretory genes were seen including *Lyz1* and *Lyz2*. The list also included several enzymes including *Fmo3*, *Sec14l3*, *Cyp2a4* and *Aox1*.

Table 3.4. Expression of the Top 50 Most Differentially Expressed Genes in the Day 0 Cells Compared with the ALI Day 14 Cells

NO	Genes	AvG D0	AvG D14	Fold Change
1	Fmo3	6.845	16.766	9.921
2	Cdhr3	4.565	14.07	9.505
3	Sec14l3	4.305	13.073	8.768
4	Тррр3	5.09	13.643	8.553
5	Lyz2	8.015	16.536	8.521
6	Bpifa1	8.875	17.15	8.275
7	Rsph4a	4.65	12.433	7.783
8	Sntn	3.57	11.316	7.746
9	Cd177	4.08	11.573	7.493
10	Spata18	4.865	12.243	7.378
11	Ccdc146	4.335	11.643	7.308
12	Tmem232	3.715	10.913	7.198
13	5330417C22Rik	5.155	12.256	7.1016
14	Odf3b	3.7	10.766	7.066
15	Ak7	4.77	11.793	7.023
16	Cfap126	7.92	14.893	6.973
17	1700040L02Rik	5.485	12.433	6.948
18	Adgb	4.035	10.97	6.935
19	AU040972	5.89	12.803	6.913
20	DynIrb2	4.96	11.796	6.836
21	Gm281	4.61	11.353	6.743
22	Sult1d1	9.185	15.92	6.735
23	Lyz1	3.87	10.513	6.643
24	Cyp2a4	8.59	15.153	6.5633
25	Ubxn10	6.145	12.703	6.558
26	Cfap161	3.515	10.06	6.545
27	Fam216b	4.565	11.093	6.528
28	Fam161a	4.75	11.203	6.453
29	Erich2	5.03	11.48	6.45
30	Nek5	6.01	12.396	6.386
31	Cdhr4	5.63	12.016	6.386
32	Stoml3	3.855	10.23	6.375
33	Lrrc34	3.89	10.233	6.343
34	1700013F07Rik	4.95	11.256	6.306
35	Tcte1	3.825	10.126	6.301
36	Ccdc153	4.945	11.246	6.301
37	Kenrg	6.085	12.366	6.281
38	Spef2	4.43	10.71	6.28
39	Elmod1	4.51	10.67	6.16
40	Dnah5	4.26	10.373	6.113
41	Meig1	5.75	11.84	6.09
42	Ccdc108	4.735	10.803	6.068
43	Ccdc170	3.82	9.84	6.02
44	Adh7	11.065	17.026	5.961
45	Lrguk	4.635	10.583	5.948
46	Cfap61	4.98	10.85	5.87
47	Cfap53	5.02	10.883	5.863
48	Aox1	7.66	13.48	5.82
49	SIc16a12	5.945	11.74	5.795
50	Rgs22	4.505	10.29	0.304

The average expression value (log2) is shown for both day 0 and 14 cells as well as the differential expression and p-value between the two.

3.3.5.5 Differential Gene Expression Between the Original and Day 14 Cells

Figure 3.8 shows the overall gene expression differences between the original cells isolated from the trachea and sampled prior to culture and ALI day 14 cells established on the trans-wells.

Table 3.5. Top 50 Genes in the Original and Day 14 Cells

NO	Genes	AvG D0	AvG D14	Fold Change	
1	Fmo3	6.845	16.766	1.456	
2	Cdhr3	4.565	14.07	1.741	
3	Sec14I3	4.305	13.073	1.760	
4	Тррр3	5.09	13.643	1.605	
5	Lyz2	8.015	16.536	1.347	
6	Bpifa1	8.875	17.15	1.301	
7	Rsph4a	4.65	12.433	1.639	
8	Sntn	3.57	11.316	1.906	
9	Cd177	4.08	11.573	1.741	
10	Spata18	4.865	12.243	1.583	
11	Ccdc146	4.335	11.643	1.673	
12	Tmem232	3.715	10.913	1.821	
13	5330417C22Rik	5.155	12.256	1.528	
14	Odf3b	3.7	10.766	1.816	
15	Ak7	4.77	11.793	1.579	
16	Cfap126	7.92	14.893	1.305	
17	1700040L02Rik	5.485	12.433	1.480	
18	Adgb	4.035	10.97	1.716	
19	AU040972	5.89	12.803	1.437	
20	DynIrb2	4.96	11.796	1.540	
21	Gm281	4.61	11.353	1.589	
22	Sult1d1	9.185	15.92	1.248	
23	Lyz1	3.87	10.513	1.738	
24	Cyp2a4	8.59	15.153	1.263	
25	Ubxn10	6.145	12.703	1.399	
26	Cfap161	3.515	10.06	1.836	
27	Fam216b	4.565	11.093	1.584	
28	Fam161a	4.75	11.203	1.550	
29	Erich2	5.03	11.48	1.510	
30	Nek5	6.01	12.396	1.403	
31	Cdhr4	5.63	12.016	1.438	
32	Stoml3	3.855	10.23	1.723	
33	Lrrc34	3.89	10.233	1.712	
34	1700013F07Rik	4.95	11.256	1.513	
35	Tcte1	3.825	10.126	1.725	
36	Ccdc153	4.945	11.246	1.514	
37		6.085	12.366	1.392	
38	Kcnrg Spef2	4.43	10.71	1.593	
39					
40	Elmod1 Dnah5	4.51 4.26	10.67	1.571 1.614	
41	Meig1	5.75	11.84	1.412	
41	Ccdc108	4.735	10.803	1.530	
		3.82			
43	Ccdc170	3.82 11.065	9.84	1.705	
44	Adh7		17.026	1.179	
45 46	Lrguk	4.635	10.583	1.538	
46	Cfap61	4.98	10.85	1.485	
47	Cfap53	5.02	10.883	1.479	
48	Aox1	7.66	13.48	1.277	
49	SIc16a12	5.945	11.74	1.381	
50	Rgs22	4.505	10.29	1.548	

The gene expression analysis between the original and day 14 cells, as depicted in Figure 3.7, was expected to highlight the gene signatures of the original cell population sourced from the entire tracheal tissue protease digestion (represented by red dots). The green dots in the figure indicate the genes with a higher expression in the day 14 cells, which probably correspond to the genes highly expressed in the differentiated epithelial cells.

Table 3.5 presents the differential gene expression between the days 0 and day 14 cells. The α-globin and β-globin genes (*Hbb-bs*, *Hbb-b1*, *Hba-a1*, *Hba-a2*, *Hbb-bt*, *Hba-a1* and *Hbb-b2*) were highly expressed in the original cells and lowly expressed in the day 14 cells. This finding suggests that red blood cells contaminate the initial cell preparation of the original cells and are then lost after culture. Additionally, the genes *Sftpa1*, *Bpifb1*, *Scgb3a1*, *Scgb3a2*, *Plek*, *Il7r*, *Gfpt2*, *Pdk4*, *Dmbt1*, *Samsn1*, *Cd69*, *Ms4a4c++*, *Cytl1*, *Il2rg*, *Il2rg*, *Satb1*, *H2-Eb1*, *Sbpl*, *Cd53*, *H2-Aa*, *Nr4a3*, *Cd74*, *H2-Ab1*, *Sell*, *Glycam1*, *Tg* and *Sbpl* were from the haemoglobin group. *Lipf*, *Dcpp3* and *Dcpp1* were markers of goblet cells, while *Lyz1*, *Lyz2*, *Fmo3* and *Sec14l3* were the other differentially expressed genes.

The genes *Cd53*, *Gm10591*, *Ccl21b*, *Ccl22*, *Fosb*, *Spi1*, *Rgs2* and *Rgs1* were highly expressed in inflammatory cells including mast cells, neutrophils, macrophages, and lymphocytes.

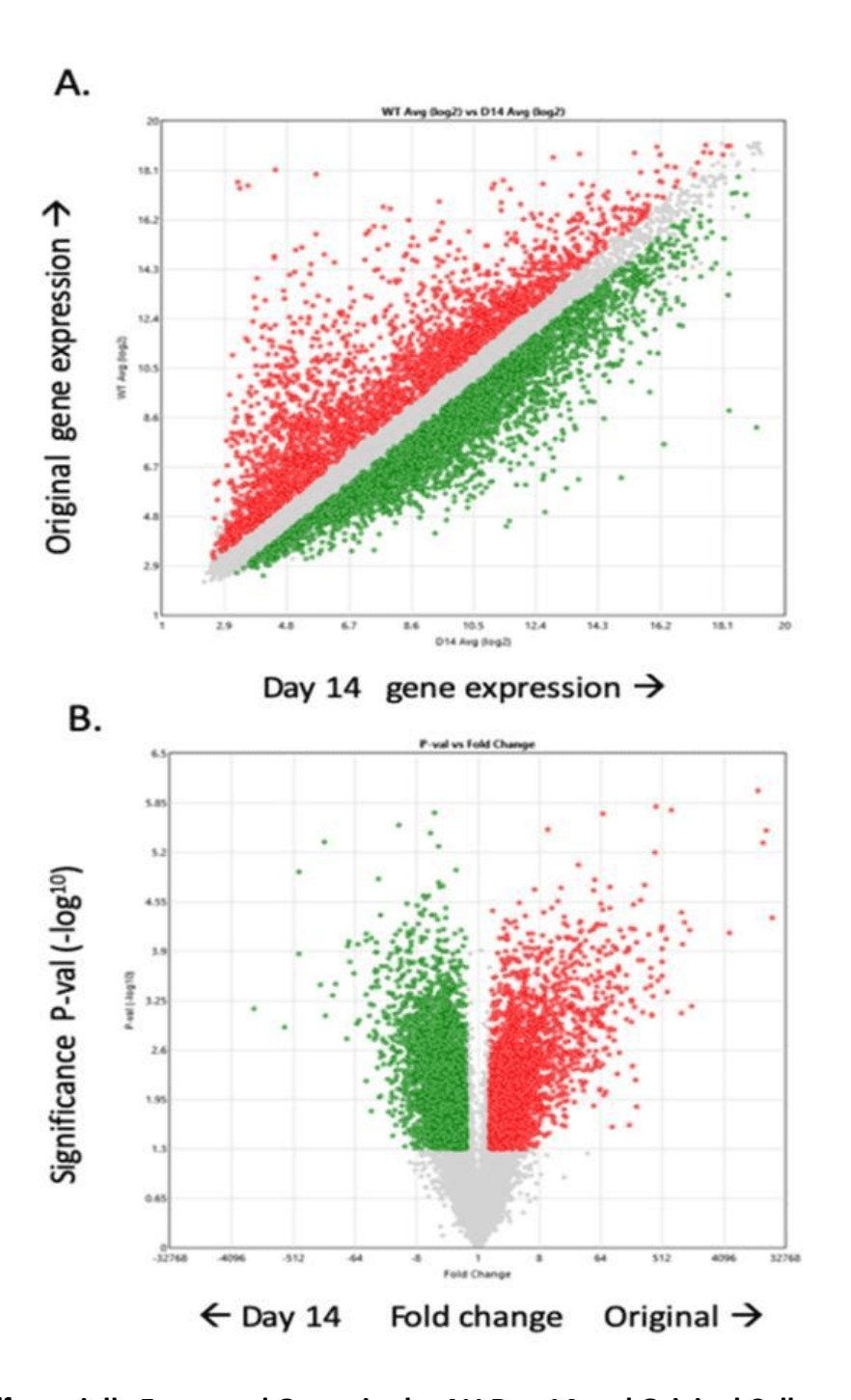


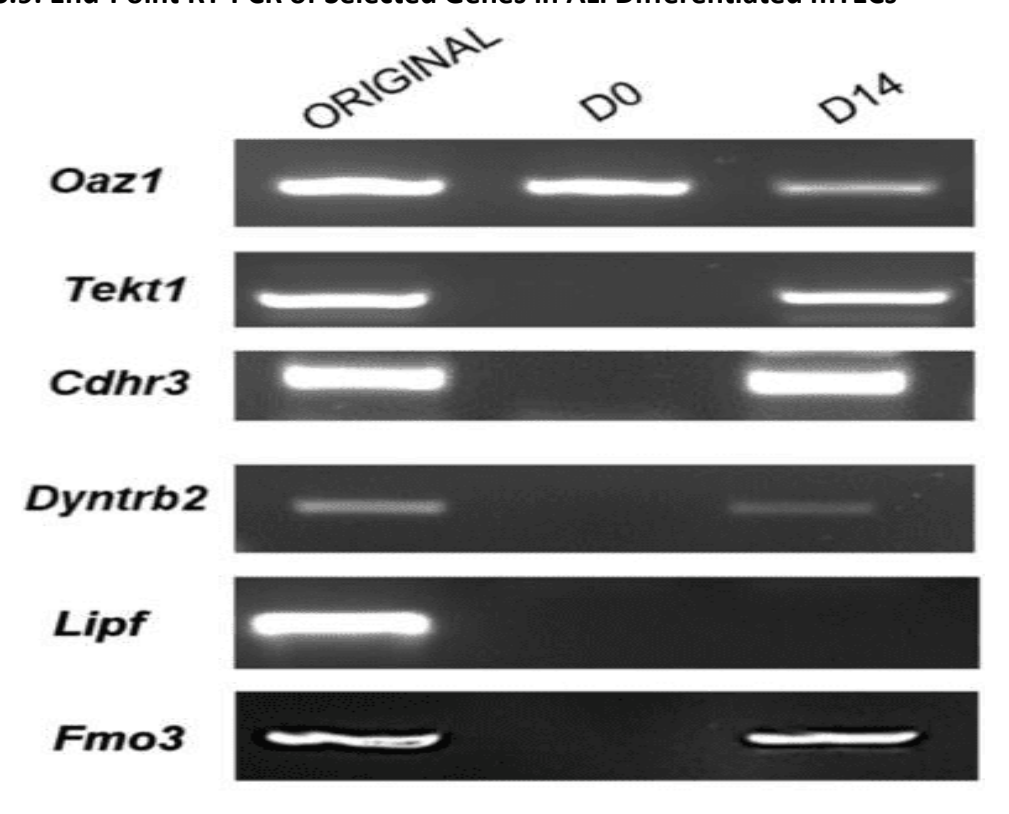
Figure 3.8. Differentially Expressed Genes in the ALI Day 14 and Original Cells

(A) Scatter plot showing the log2 intensity values of the differentially expressed genes. (B) Among these genes, 9568 genes are shown by the volcano plot. Each dot represents the expression of a gene. Coloured dots represent the significantly differentially expressed genes. The green dot indicates overexpression in the day 14 cells, and the red dot indicates overexpression in the original cells.

3.4 Validation of the Gene Expression During Differentiation

As the array analysis identified many genes that were differentially expressed under the different culture conditions, end-point RT-PCR was conducted with selection of the genes using a different set of cDNAs. Notably, end-point RT-PCR is a qualitative method of measuring gene expression, but in this study, it was used to differentiate between the genes expressed at high and low levels. *Lipf*, a gene highly expressed in the original cells, and *Fmo3*, *Cdhr3* and *Dynlrb2*, three genes upregulated in the day 14 cells, were selected. Primers for the ciliated cell marker gene *Tekt1* and the internal control gene *Oaz1* were also used. The data in Figure 3.9 support the differential expression of these genes during the culture. *Lipf* showed a high expression in the original cells but a decreased expression in both day 0 and 14 cells. Conversely, the expression of the other three genes decreased in the original cells but increased in the day 14 cells.

Figure 3.9. End-Point RT-PCR of Selected Genes in ALI Differentiated mTECs



RT-PCR was undertaken on samples of the original, day 0 and day 14 cells with primer pairs to *Oaz1*, *Tekt1*, *Cdhr3*, *Dynlrb2*, *Lipf* and *Fmo3*. The products were resolved using 2% agarose gels.

3.5 Cell Type Representation in the ALI Differentiated mTECs

Data from arrays and PCR provide information on the total gene expression but not on the cell types that express individual genes. However, data on cell-specific gene expression can be obtained from scRNAseq. In this type of analysis, cells are defined based on their gene expression profiles. A recent scRNA analysis of freshly isolated mTECs has identified at least eight distinct cell types (Plasschaert, Zilionis et al. 2018) (Figure 3.10). With the published mTEC scRNAseq data that are accessible on a public browser, it is possible to identify gene expression in distinct cell types.

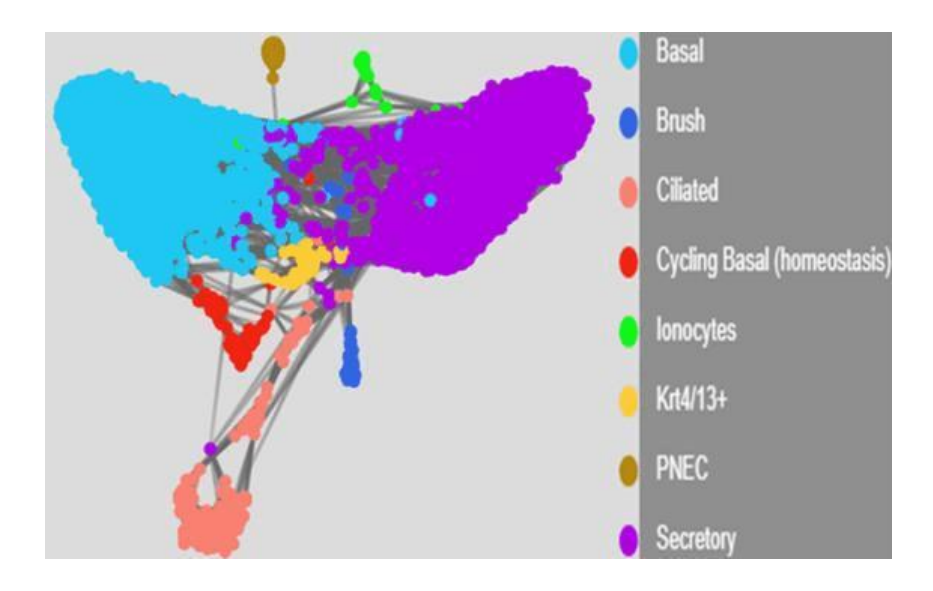


Figure 3.10. SPRING Representation of Gene Expression in Single Mouse Tracheal Cells

Mouse tracheal epithelial cells were isolated, dissociated and collected for scRNAseq. The image presents a SPRING plot of scRNAseq data for the mouse tracheal epithelial cells from the study by (Plasschaert, Zilionis et al. 2018). Different cell types are represented by different colours.

The cell types that expressed several genes from the data set were identified. In the figure, each dot represents a single cell, and the intensity of green corresponds to the level of gene expression

of an individual gene in a single cell. The absolute intensity of each gene varies across each image. Black dots represent the cells with no expression.

As expected, *Oaz1* expression was seen across most cell types in the viewer (Figure 3.11), and *Tekt1* was restricted to the ciliated cells. *Cdhr3* and *Dynlrb2* expression was also largely restricted to the ciliated cells. Fmo3 expression was seen across both the basal cell and the secretory cell population. *Lipf* expression was limited to a substantially small number of cells and was extremely low.

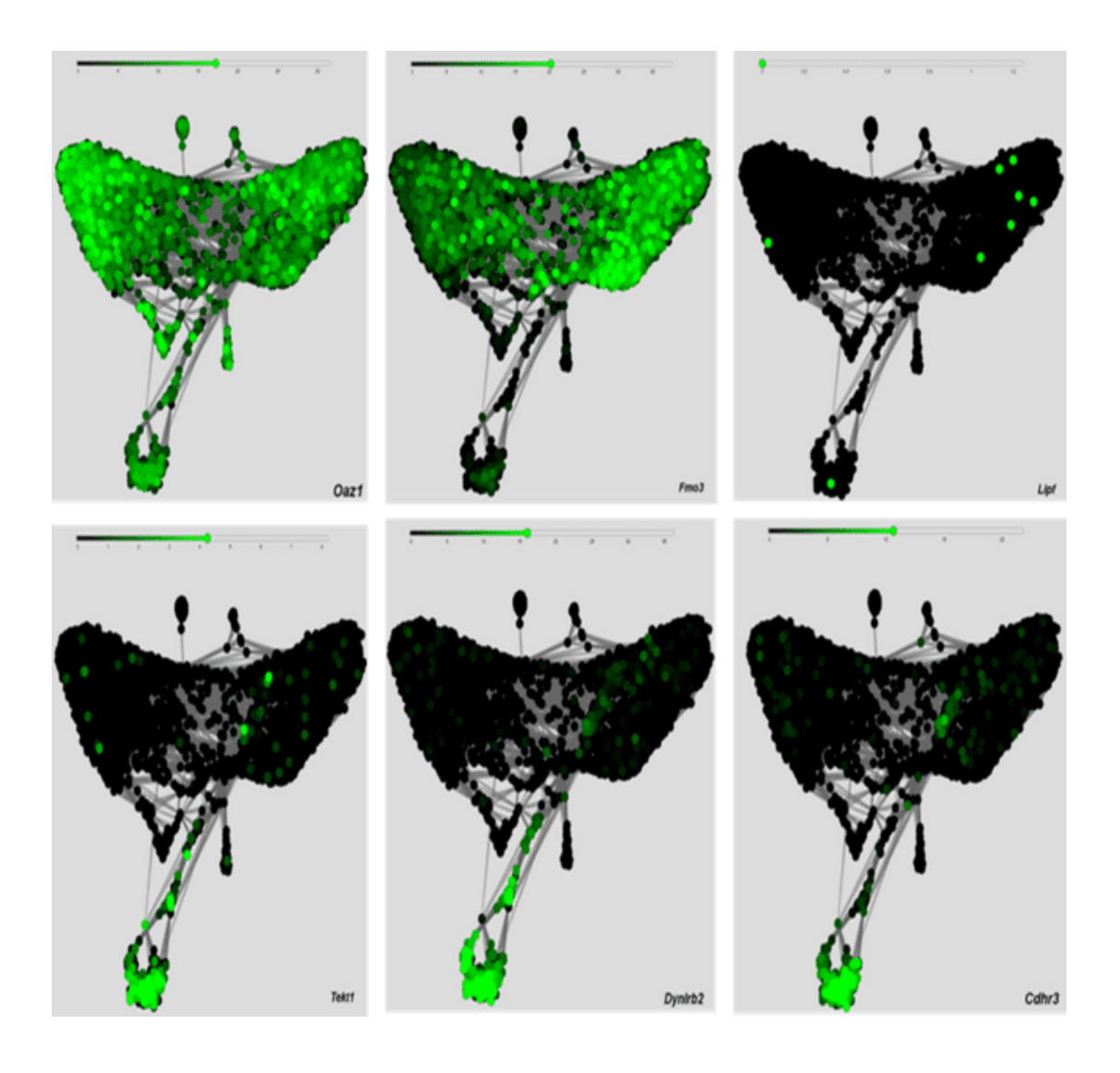


Figure 3.11. Cell-Specific Localisation of Selected Genes in mTECs

The figure shows a representation of the gene expression of *Oaz1*, *Tekt1*, *Cdhr3*, *Dynlrb2*, *Lipf* and *Fmo3* in single-cell data from mouse tracheal cells. Green intensity represents the gene expression levels, while green bars at the top of each image indicate the absolute expression levels (Kleintools, 2020).

A similar analysis was applied to several airway genes that were shown to be highly differentially expressed in the original cells (Figure 3.12). *Bpifa1*, *Bpifb1*, *Lyz2*, *Scgb3a1* and *Sftpa1* were seen to be expressed predominantly in the secretory cells, with some lower expression of *Bpifa1* also noted in the basal cells. *Sec14l3* was expressed in the basal and secretory cells but was also robustly expressed in the ciliated cells.

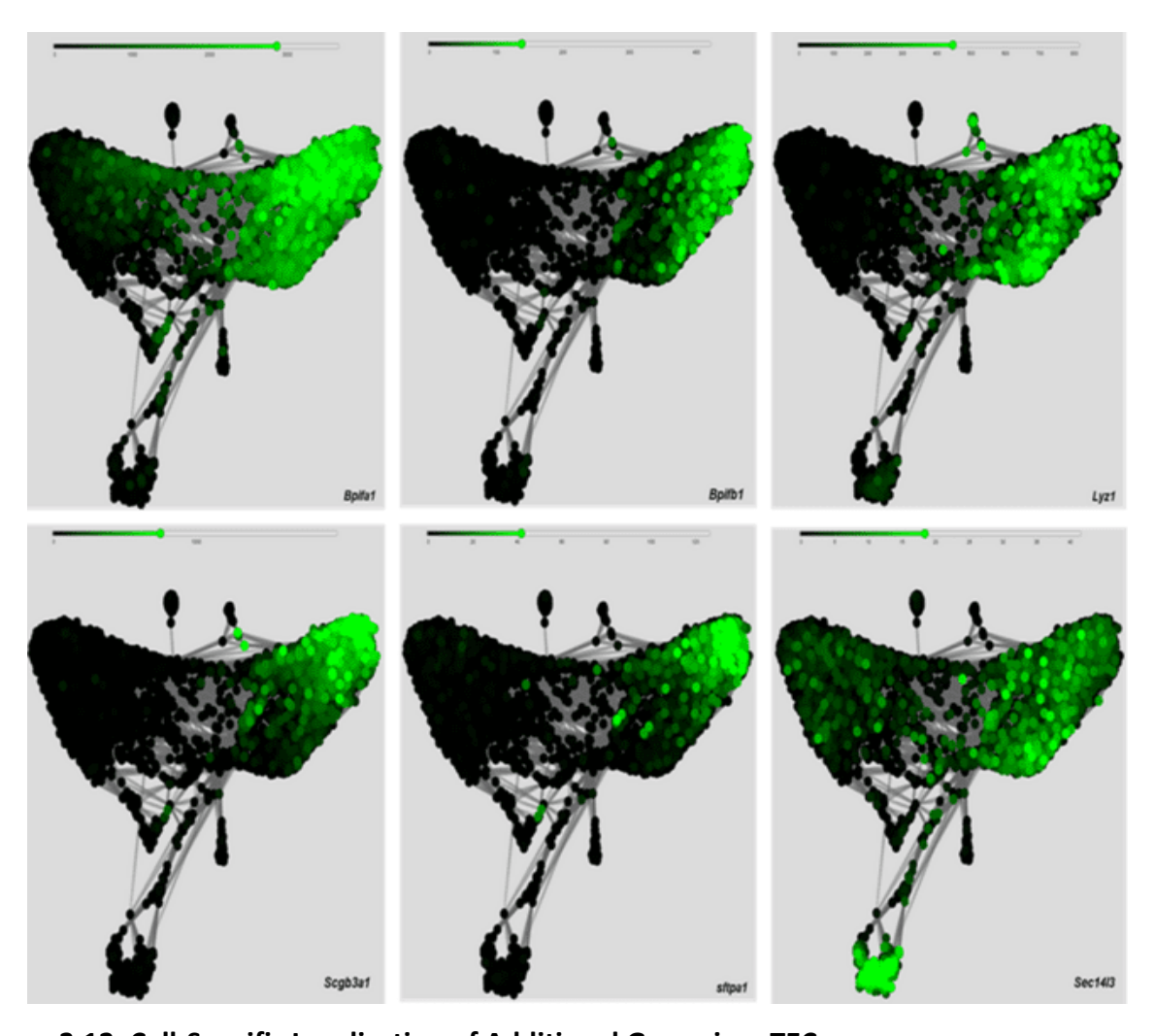


Figure 3.12. Cell-Specific Localisation of Additional Genes in mTECs

The figure shows the gene expression of *Bpifa1*, *Bpifb1*, *Lyz2*, *Scgb3a1*, *Sftpa1* and *Sec14l3* in single-cell data from mouse tracheal cells. Green intensity represents the gene expression levels, while green bars at the top of each image indicate the absolute expression level.

3.6 Expression of Selected Genes During mTEC Differentiation

The expression of the selected genes in the array data under the three different conditions was plotted to exhibit the relative expression of these genes (Figure 3.13). Genes with expression levels below 5 log2 were not considered to be reliably expressed. In most cases, a high expression in the original cells was associated with a high expression in the day 14 differentiated cells. The two clear exceptions were *Lipf* and *Bpifb1*. Both genes exhibited a high expression in the original cells but a generally reduced expression in the day 14 cells. In the case of *Lipf*, expression was completely absent in the day 14 cells.

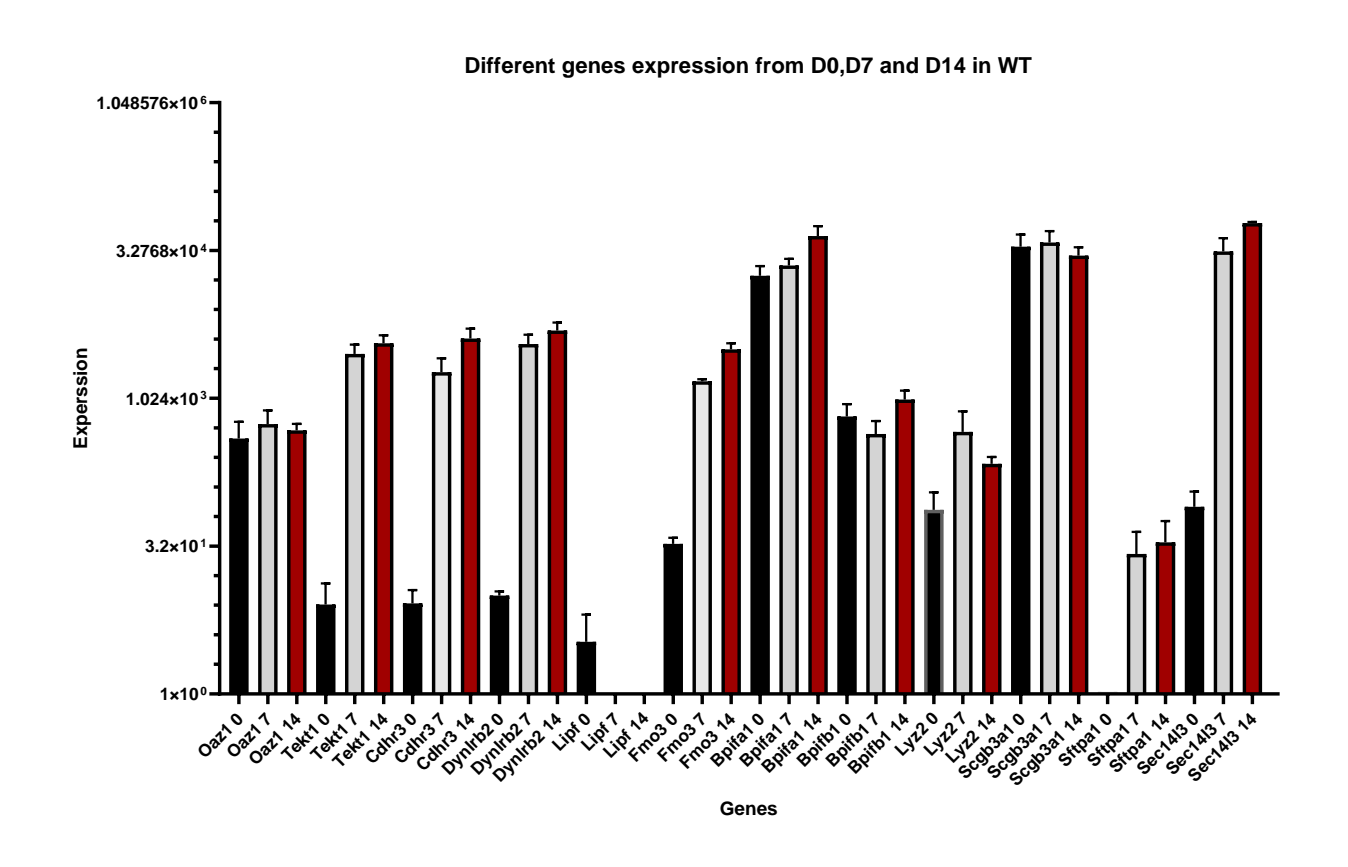


Figure 3.13. Differential Gene Expression in the Original, Day 0 and Day 14 mTECs

The genes expression includes Oaz1, *Tekt1*, *Cdhr3*, *Dynlrb2*, *Lipf, Fmo3*, *Bpifa1*, *Bpifb1*, *Lyz2*, *Scgb3a1* and *Sec14l3*. This data shows SEM and error bars in this experiment done on 3 biological replicates.

The data obtained from the culture of the mTECs were compared with a partially comparable data set obtained through RNAseq analysis of bulk sample mTECs grown under the standard culturing protocol in BGEM media for up to 14 days of ALI growth. Notably, RNAseq generally provides more accurate data on expression levels than do array studies.

The changes in the expression of *Oaz1*, *Tekt1*, *Cdhr3*, *Fmo3*, *Lipf and Dynlrb2* during the ALI mTEC differentiation are shown in Figure 3.14. As expected, the expression level of *Oaz1* remained consistent throughout the time course. Meanwhile, *Tekt1*, *Cdhr3*, *Fmo3* and *Dynlrb2* showed a significantly increased expression. The expression of Lipf was either extremely low or absent at both time points of differentiation.

The data for *Bpifa1*, *Bpifb1*, *Lyz2*, *Scgb3a1* and *Sec14l3* (Figure 3.14) revealed a slightly different pattern. *Bpifa1* expression was notable in the day 0 cells and further increased in the day 14 cells, in line with the present data. However, *Bpifb1* expression was low at both time points, contrasting the elevation seen in the present data from day 0 to day 14. *Sec14l3* expression increased by day 14, while *Sftpa1* was barely expressed on day 0 but showed a slightly higher expression on day 14.

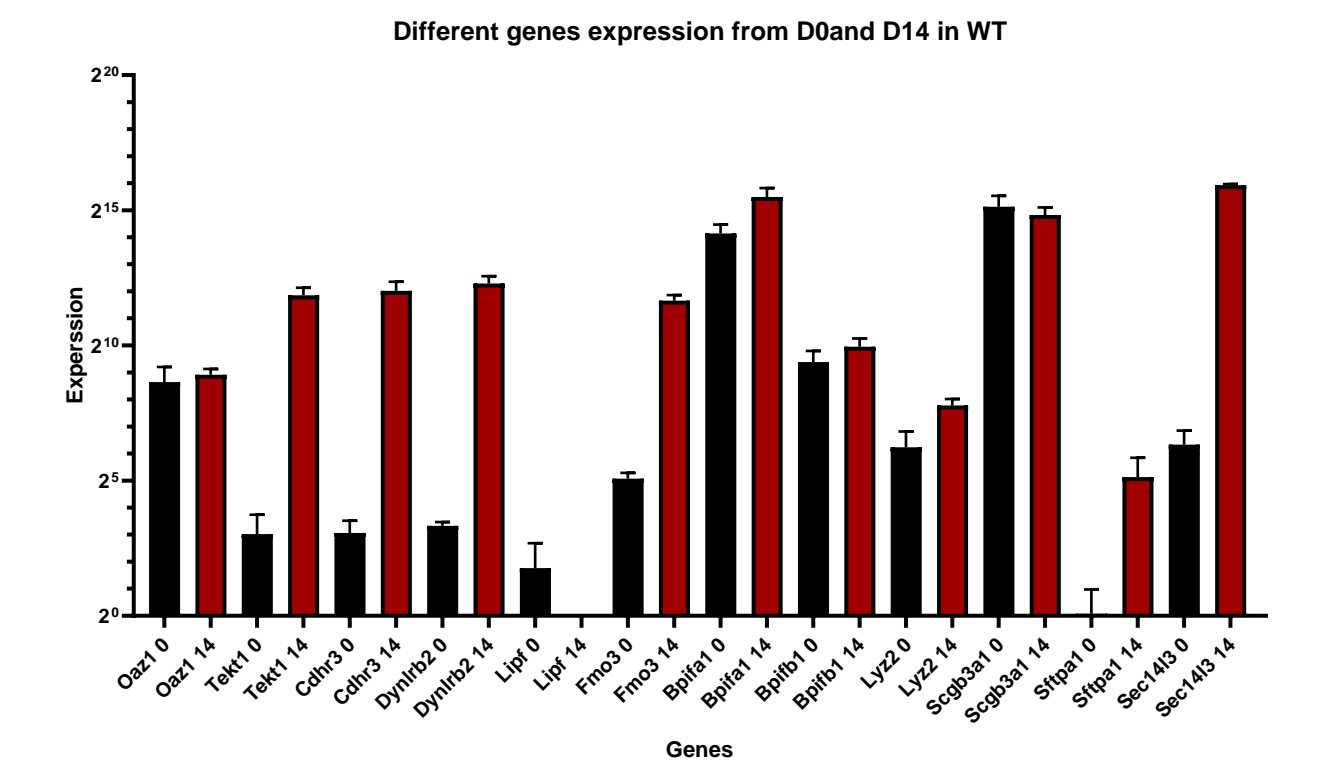


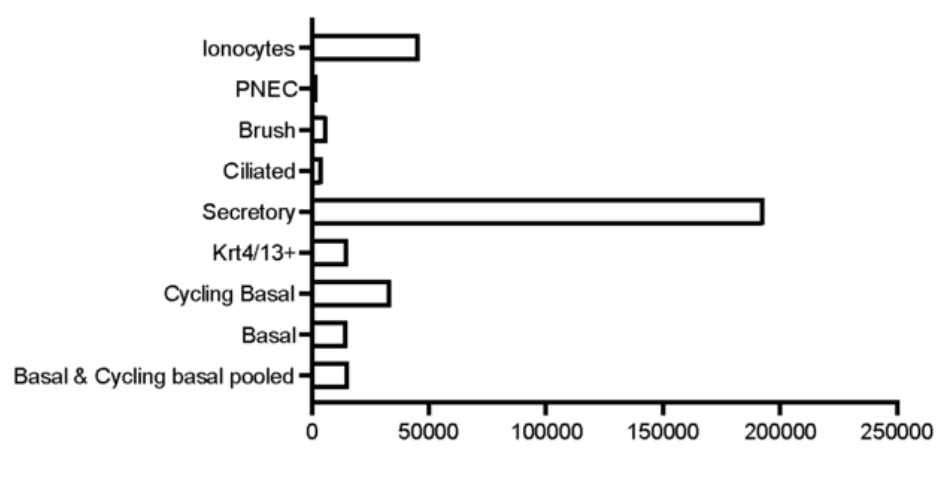
Figure 3.14. Expression of Selected Genes in an RNAseq mTEC Data Set

This figure shows day 0 and 14 gene expression data for Oaz1, *Tekt1*, *Cdhr3*, *Dynlrb2*, *Lipf*, *Fmo3*, *Bpifa1*, *Bpifb1*, *Lyz2*, *Scgb3a1*, *Sftpa1* and *Sec14l3*. The day 14 cells showed a significantly higher expression of *Tekt1*, *Cdhr3*, *Dynlrb2*, *Sftpa1*, *Sec1413*, *Fmo3* and *Lyz2*. In contrast, only *Lipf* was expressed at a lower level in the day 0 cells. This data shows SEM and error bars. The experiment was done on 3 biological replications.

3.7 High Expression of Bpifa1 in the Secretory Cells in the mTECs

The analysis of the scRNAseq data sets allowed the investigation of the site of expression of *Bpifa1* in the tracheal cells. The expression data for *Bpifa1* in each cell type were extracted from the study by (Plasschaert, Zilionis et al. 2018) Plasschaert et al. (2018) (Figure 3.15). *Bpifa1* expression was seen in several cell types, with the highest expression seen in the secretory cells. Consistent with the data shown in Figure 3.12, expression was also seen in the other cells, including basal cells and ionocytes. Consistent with previous work and the staining shown in Figure 3.4, ciliated cells were not found to express *Bpifa1*.

Bpifa1 in mTEC cell populations



Mean expression in cluster (transcripts per million TPM)

Figure 3.15. Absolute Expression of *Bpifa1* in Different mTEC Populations

Expression data for *Bpifa1* were extracted from scRNAseq data from the mouse tracheal epithelial cells from the study by (Plasschaert, Zilionis et al. 2018). The different epithelial cell types are as described in Figure 3.10.

As *Bpifa1* was predominantly expressed in the secretory cells, further analysis was performed to determine the 20 most highly expressed genes in this cell type. The results, shown in Figure 3.16, demonstrated that *Bpifa1* was the most highly expressed gene in the secretory cells, exhibiting a higher expression than *Scgb1a1* and *Reg3g* by a significant margin.

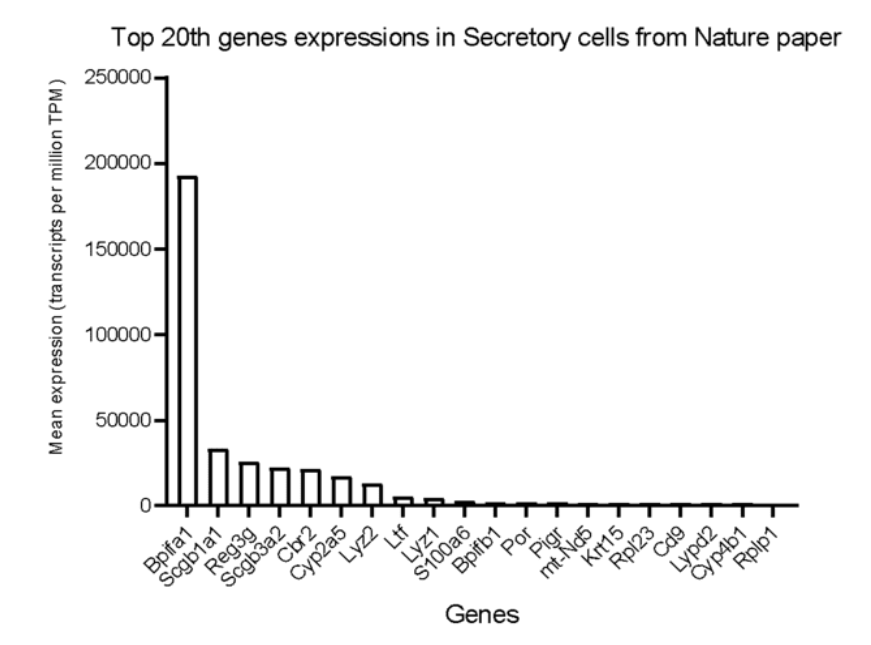


Figure 3.16. Top 20 Most Highly Expressed Genes in Mouse Tracheal Secretory Cells

ScRNAseq expression data for mouse tracheal secretory cells were extracted from the study by

(Plasschaert, Zilionis et al. 2018).

3.8 Expression of BPIF Family Members in the Differentiated mTECs

The previous analysis demonstrated that *Bpifa1* was highly expressed in the secretory cells in the trachea. The expression levels of various *Bpif* family members were investigated to confirm that other members of the *Bpif* gene family were not highly expressed in the differentiated mTECs (Figure 3.17). It was important to confirm the expression of other members of the *Bpif* gene family in the differentiated mTECs to ensure that the observed high expression of *Bpifa1* in the secretory cells was not a general trend among the entire *BPIF* gene family but rather a specific characteristic of *Bpifa1*. The results showed that among the members, *Bpifa1* was the most highly expressed gene in the mTECs on day 14. *Bpifa1* was followed by *Bpifb1*. The rest of the genes showed expression levels at or below the threshold for positive expression (<5 log2). Notably, *Bpifa5* was not expressed in these cells. Although data at this ALI time point were clear, further cell culture beyond 14 days may lead to additional cell differentiation and potentially higher gene expression levels.

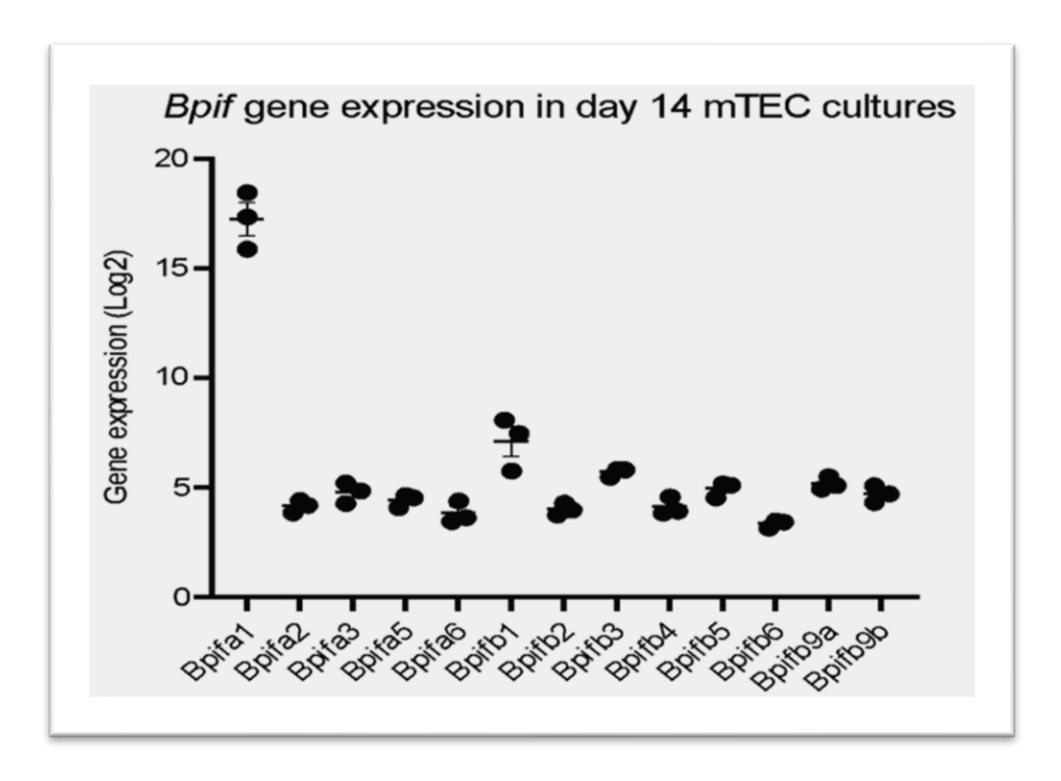


Figure 3.17. Expression of *Bpif* **Genes in Day 14 mTEC Cultures**. Expression of *Bpif* genes in Day 14 mTEC cultures is shown in Figure 3.17. The highest expression of the *Bpif* family in D14 of mTec cultivators is *Bpifa1*, followed by *Bpifb1*. However, the expression levels of *Bpifa2*, *Bpifa3*, *Bpifa6*,

Bpifb2, and *Bpifb5* are nearly the same. Additionally, *Bpifab6* has the lowest expression, while *Bpifb5, Bpifb9a,* and *Bpifb9b* have the same expression in turn.

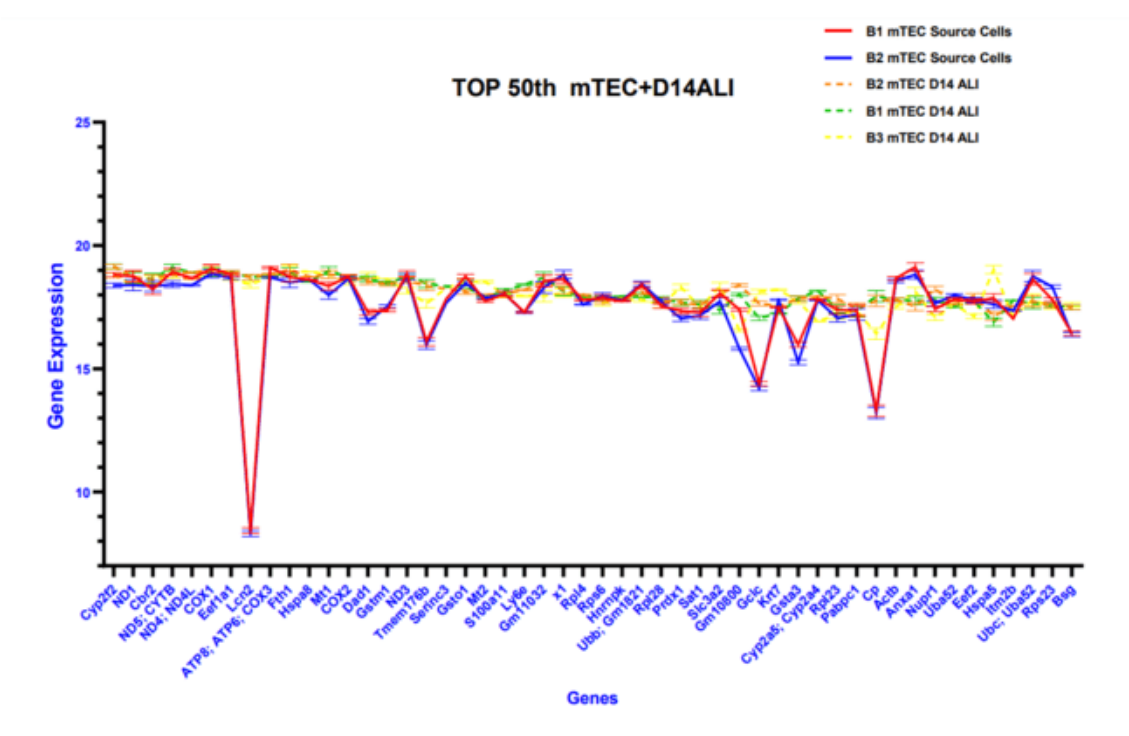


Figure 3.18. Expression Pattern of the Top 50 Genes in the mTEC Source Cells and ALI Day 14 Cells non-infected. The graph results present two replicates (B1 and B2) for the mTEC source cells and three replicates (B1, B2 and B3) for the ALI day 14 mTECs. The x axis presents the gene IDs, while the y axis shows the expression in folds. The lowest expression

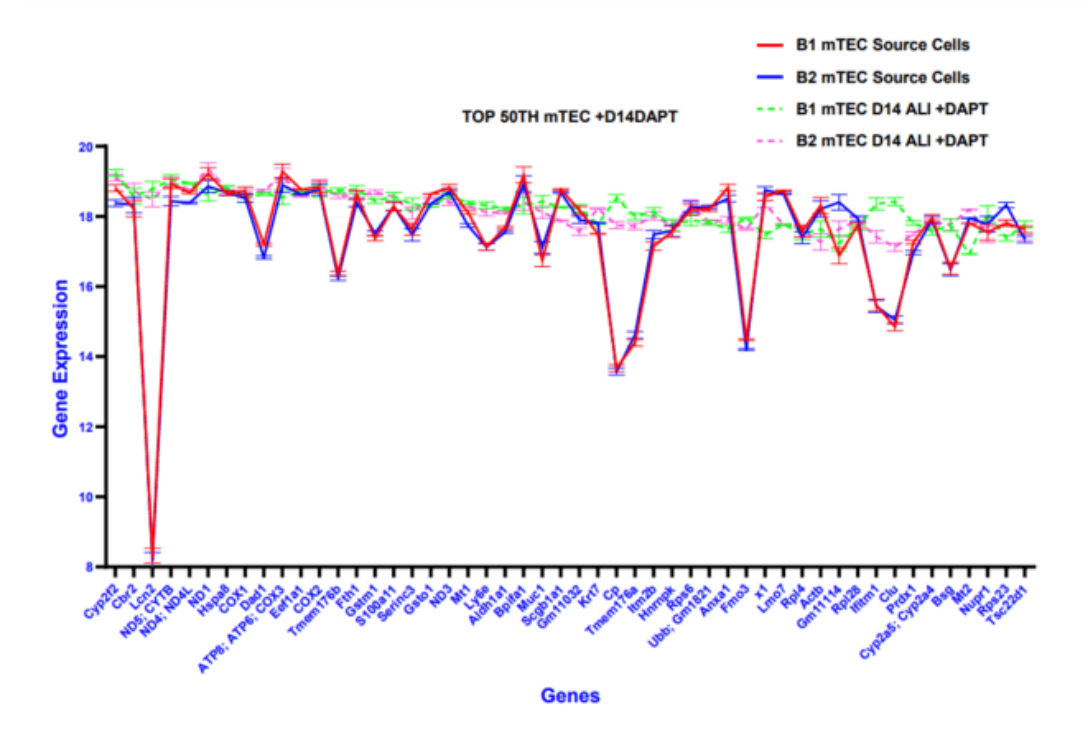


Figure 3.19 Gene Expression Analysis of mTECs cultured at the ALI with DAPT

The graph presents the expression of the top 50 genes in the mTEC source cells and mTEC+ day 14 DAPT cells. The x axis presents the gene IDs, while the y axis shows the expression.

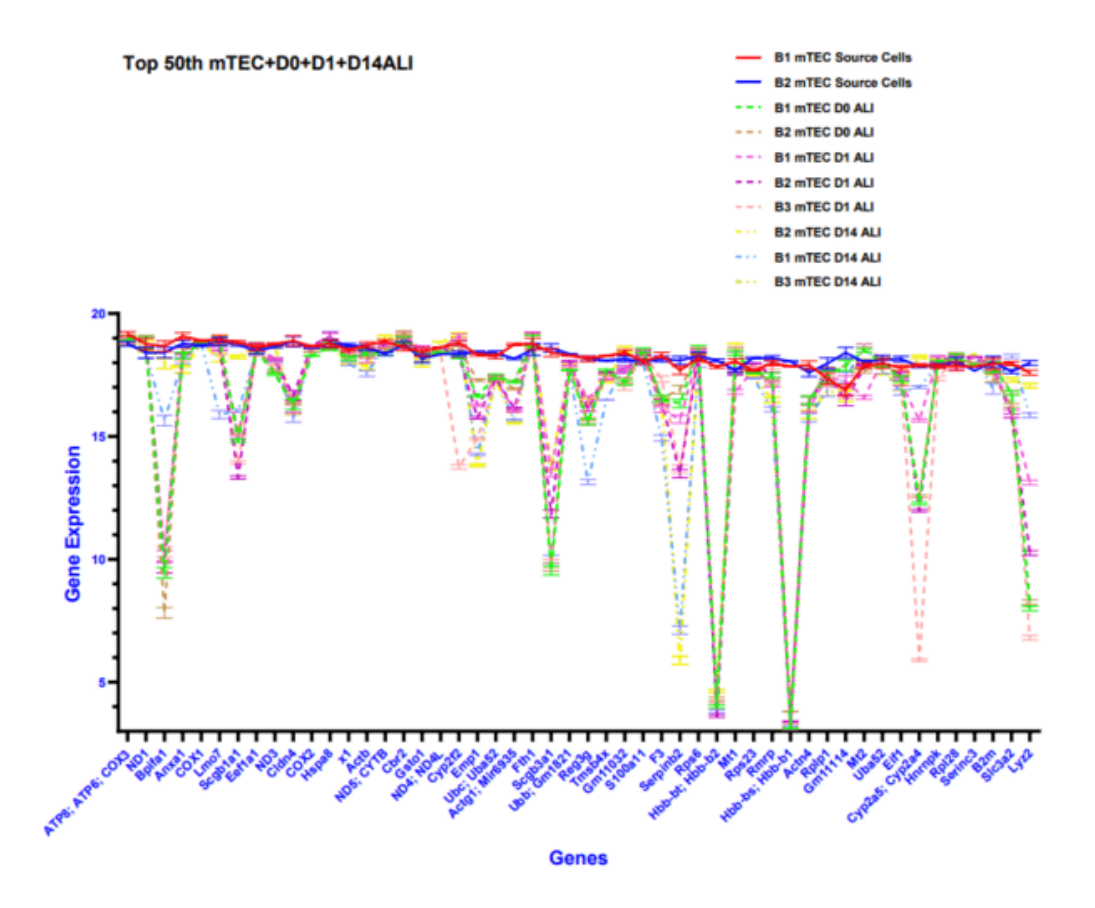


Figure 3.20 Gene Expression Analysis of the mTEC Source Cells and ALI-Grown Cells. This graph shows the gene expression of the top 50 genes in the mTEC source cells and ALI-grown cells (D0, D1 and D14). There are two replicates each for the mTEC source cells and ALI day 0 mTECs and three replicates each for the ALI day 1 and 14 mTECs. The x axis presents the gene IDs, while the y axis shows the expression.

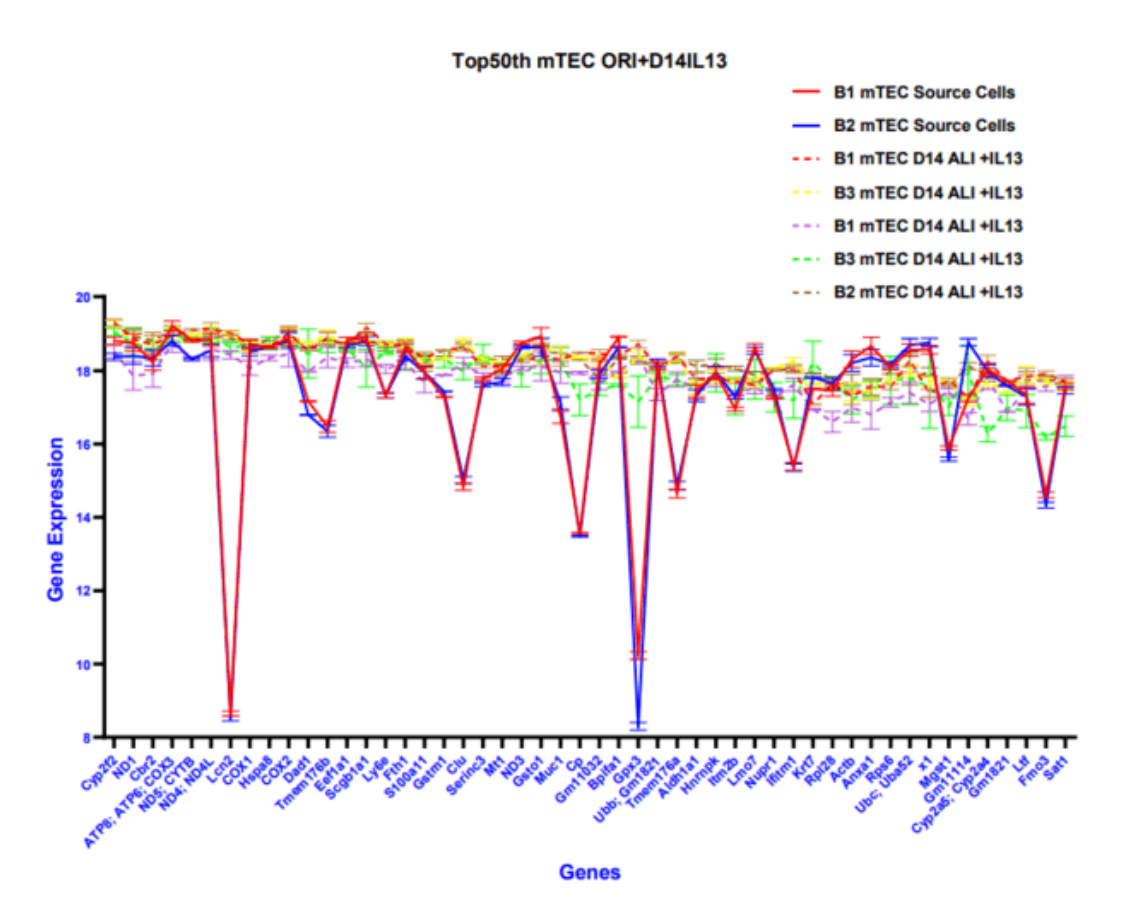


Figure 3.21. Gene Expression Analysis of the mTEC Source Cells and ALI-Grown Cells. The graph depicts the difference in the gene expression between the source cells and cells grown with IL-13 at the ALI. The x axis presents the gene IDs, while the y axis shows the expression.

3.10 Discussion

The airway epithelium constitutes the protective lining of the major airways – the trachea, bronchi, and bronchioles – and enables them to perform their key function of allowing air to access the alveolar space where gas exchange takes place. This protective function is mediated

by the multiple distinct cell types found within this layer, including secretory cells that secrete components of the apical lining fluid, ciliated cells that facilitate the elimination of particles and pathogens through the mucociliary escalator and specialised cells that regulate other important pathways. The secretion of various proteins or peptides by the airways epithelium is essential for defending against pathogens and strengthening the initial innate defence system.

BPIFA1 is a glycoprotein expressed in the submucosal glands and epithelium of the human and mouse lungs (Bingle, Cross et al. 2005, Musa, Wilson et al. 2012). This protein has been hypothesised to play a role in host defence based on its structural similarity with BPI and LBP; subsequent studies have confirmed its critical role in the host response to viruses.

However, notably, lung or airway-derived cell lines may not accurately represent the complex airway epithelium under standard tissue culture conditions. This is because the cell-specific genes expressed in many airway cell types are often not seen in the majority of lung cell lines, and *BPIFA1* expression is limited to a few established cell lines (Bingle and Bingle 2000).

Previous studies have shown that BPIFA1 is localised in serous/secretory cells both *in vitro* and *in vivo* (Bingle, Cross et al. 2005, Musa, Wilson et al. 2012), and differentiated mTECs have been used to address the role of BPIFA1 in the host response to viruses.

At the beginning of this study, it was crucial to demonstrate that differentiated mTECs could be generated in an ALI culture. After multiple attempts, these cells were successfully isolated and cultured, with very rare instances of infection during isolation. The same techniques and media used in previous studies in the host laboratory were used to culture the cells at the ALI and allow for differentiation. Notably, different isolation and culture techniques may result in variations in differentiated cell populations (Clarke, Burns et al. 1992, Davidson, Kilanowski et al. 2000, You, Richer et al. 2002).

The differentiation was validated using RT-PCR, which involved isolating RNA from the trans-wells with a small surface area. The Direct-zol MicroRNA Kit from Zymo was used for RNA isolation. The system was validated using HEK cells, and the number of cells needed for the isolation was determined. Despite some instances of technical errors or limited cell numbers causing difficulties in RNA recovery, the system was used throughout this study.

In addition to RT-PCR, western blotting, and immunofluorescence (IF) microscopy were utilised to validate the cultures. *BPIFA1* secretion was studied through western blotting of apical washes of the cell surface, which recovered enough airway secreted proteins to allow the identification of *BPIFA1*. The presence of increasing amounts of *BPIFA1* in the apical washes from days 2 to 14 of ALI culture indicated the intact function of secretory cells in the cultures. Cell staining showed an increase in the numbers of both secretory and ciliated cells during differentiation. The analysis showed that mTECs were successfully reproducibly isolated and differentiated.

A similar analysis was conducted as described by (Ross, Dailey et al. 2007) for human bronchial cells at the ALI to further understand the transcriptional profile of the cells during different stages of growth and the gene changes that occur during mucociliary differentiation. In this study, a ciliary gene signature was identified, with *BPIFB1* and *BPIFA1* being the two most highly induced genes in the differentiated cells. There have also been similar previous studies on mTECs, with the best results generated by Nemajerova et al. (2016).

In my study, freshly isolated tracheal cells, which were uncultivated and likely contained a broader representation of tracheal cells, were also analysed. This type of sample had not been used in previous studies. As anticipated, the freshly isolated cells expressed genes associated with various immune cells such as neutrophils (*Cd53*), macrophages (*Ccl22*), mast cells (*Fosb*) and lymphocytes (*Spi1* and *Rgs1*). Additionally, there was a significant expression of the haemoglobin genes, indicating contamination of the initial cell preparation with red blood cells.

As the cells were cultured on the transwells, the expression of these genes was lost, as this culture system does not allow for the growth of inflammatory cells or red blood cells. Further, some genes highly expressed in the original cells originated from non-pulmonary tissue, such as thymus and spleen tissues, which may have been a result of inadequate removal of non-lung tissue from the trachea during dissection and cleaning prior to cell isolation. Any remaining contaminating tissue would have contributed to the isolated cell population, but these cells were likely lost as the cultures grew (El-Kassas, Alboraie et al. 2023).

The original cell population showed a strong expression of some epithelial genes that were not present in the cells collected at other time points. Among them were *Bpifb1* and *Lipf*. *Bpifb1* is *related to Bpifa1* and is a gene that is highly expressed in goblet cells and submucosal glands in

both humans and mice (Musa, Wilson et al. 2012). *Lipf* encodes gastric lipase, an enzyme previously considered to be expressed only in gastric chief cells, but it has recently been identified as a marker for airway submucosal gland cells (Sountoulidis, Liontos et al. 2020). It is likely that these genes arise from tracheal submucosal gland cells, which were lost during culture in this study. Although the expression of the *Bpifb1* gene increased in the day 14 cells, it did not return to its level in the original cells. Notably, both genes were also highly expressed in freshly harvested middle ear epithelial cells, another cell population that may contain minor mucosal gland cells but were lost upon culture (Mulay, Chowdhury et al. 2021).

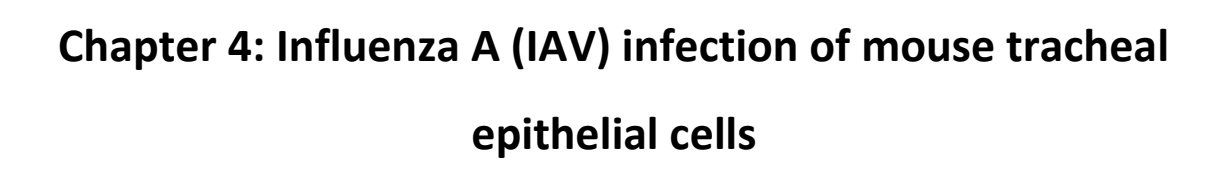
The original cells also expressed high levels of genes associated with secretory cells, with *Bpifa1* being the most differentially expressed secretory gene. Other secretory genes, including *Lyz1* and *Lyz2*, as well as secretoglobins and the surfactant gene *Sftpa1*, were also highly expressed. The original cell population had a strong expression of multiple enzymes, including *Fmo3*, *Sec14l3*, *Cyp2a4* and *Aox1*. In conclusion, the original cell population had a strong epithelial cell signature and a mix of expressed genes.

The day 0 cells had an undifferentiated cell profile, largely resembling basal cells. Under the ALI conditions, the most notable change in the day 14 cells was the expression of the ciliary genes, as previously seen in differentiating airway cells (Ross, Dailey et al. 2007). Some secretory genes, including *Bpifa1*, were also expressed.

Recent scRNAseq data and the web-based SPRING viewer from the Klein laboratory were used to gain a deeper understanding of the cell types expressing several candidate genes. The viewer identified eight distinct cell types based on gene expression data from single freshly isolated mouse tracheal cells and was used to determine the cell types expressing the unknown genes. The viewer allowed the detection of expression in an interactive image and extraction of raw data. It showed that *Bpifa1* was the most highly expressed gene in the secretory cell group, expressed at levels over five times higher than the next gene, *Scgb1a1*. The high level of expression was consistent with data from the original cells and with previous data showing robust staining of *BPIFA1* in mouse tracheal cells (Musa, Wilson et al. 2012) (Musa et al., 2012). *Bpifa1* was also expressed in other cell types, including basal cell sub-types and ionocytes. It will be important to look for co-localisation with an ionocyte-specific marker, such as FOXI1, to further

understand the expression of *Bpifa1* in ionocytes. Some of the other genes highlighted, such as *cdhr3*, are already known to be expressed in ciliated cells. I believe that combining bulk transcriptomic data with single-cell expression data will be a valuable avenue for identifying novel cell-specific genes.

The present data also showed conclusively that *Bpifa1* was the most highly expressed member of the wider gene family in the differentiated mTECs. This confirms previous data (Musa, Wilson et al. 2012) that *Bpifa1* is a major *Bpif* gene in the mouse respiratory tract and further confirms that it is the most appropriate family member to study with respect to respiratory host defence.



4.1 Introduction

As described earlier, IAV is a widespread and significant cause of mortality and morbidity globally. According to recent estimates, IAV causes 250,000 to 500,000 deaths annually worldwide (Zhang and Nawata 2017). IAV targets the respiratory epithelial cells, where it enters and initiates its replication cycle, eventually leading to its release from the infected cells and further spread in the airways. The RS serves as the primary target of IAV, and the virus must overcome the lung defence mechanisms to successfully establish an infection. One of the major innate immune defence mechanisms is the mucosal epithelium, which acts as a physical barrier against foreign pathogens (Eierhoff, Hrincius et al. 2010). IAV can bypass these defences and reach the epithelial cells, which are the targets for infection. The series of steps through which the virus infects the respiratory epithelial cells and how the host protects the cells from the virus are not fully understood yet.

Previous studies in our laboratory have focused on the role of the respiratory secretory protein *BPIFA1* in protecting against IAV infections. BPIFA1 is a glycoprotein that is highly expressed in the submucosal glands and respiratory epithelium of the upper airways in both human and mice. Britto et al. (Britto and Cohn 2015) showed that BPIFA1 provides protection against a variety of pathogens, including bacteria and viruses, leading to the hypothesis that *BPIFA1* functions as a regulator of airway mucosal host defence.

The main hypothesis of the present study is that *BPIFA1* plays a role in regulating IAV infections in the airways. This was tested using murine models, including *Bpifa1* deficient mice in a collaboration between the host laboratory and Professor James Stewart's laboratory at the University of Liverpool. The *in vivo* studies were conducted at the University of Liverpool, where the mice were infected intranasally, while the *in vitro* studies were performed at Sheffield. In the previous chapter, mTEC cultures were established and validated, and the changes in transcription that occur during differentiation were described.

At the start of this study, it was already known that differentiated mTECs could serve as a model for IAV infection. Figure 4.1 shows how viral infection of the cells could be followed by staining cultures with an antibody to IAV nucleoproteins (IAV-NPs). The images suggested that IAV

infection did not occur in *BPIFA1*-positive secretory cells, as the two antibodies did not initially appear to stain the same cells. After longer infections, more cells became infected, and *BPIFA1* protein staining was reduced. Further, some co-localisations of the two proteins were seen.

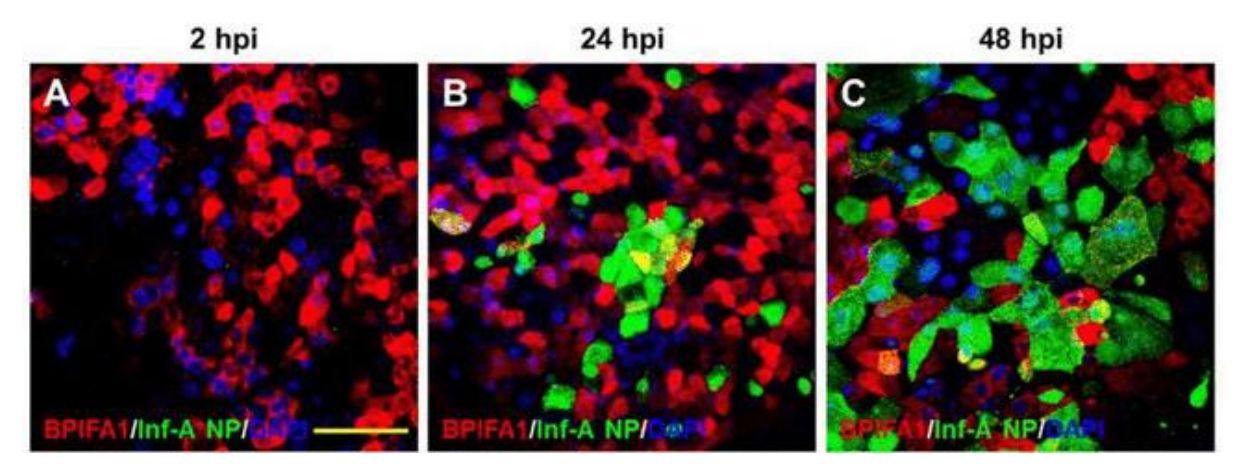


Figure 4.1. IAV-NP Staining Increases in Infected mTECs Over Time

IAV infection at an MOI of 0.5 was followed up over time via microscopy. IAV-NP staining (green) increased over time in the infected mTECs and did not overlap with *BPIFA1* staining (red) for the most part. Adapted from Akram et al. (2018). IAV-NP, IAV nucleoprotein

Previous studies had also shown that IAV infection of *Bpifa1*-/- mTECs was more severe and resulted in more rapid cell death and that loss of the protein removed a protective function, which resulted in the cells becoming infected more readily. These findings suggest that BPIFA1, secreted from secretory cells, contributes to the protective apical fluid layer in the airway epithelium, providing defence against IAV infection *in vitro*. It was also suggested that IAV infects ciliated cells, as these cells have been identified as targets for other respiratory viruses (Ugonna, Bingle et al. 2014, Wu, Yang et al. 2016).

These observations left several questions, which were addressed in this chapter. What cell types in the mTEC cultures are the initial targets of infection? Could we study the transcriptional responses of the infected mTECs?

The main focus of this chapter was as follows:

1. To better understand the effect of IAV infection on mTECs,

- 2. To identify the cell types specifically infected with the virus and
- 3. To investigate the transcriptional consequences of IAV infection on mTECs.

4.2 Results

4.2.1 Effects of Infection on the mTECs

Prior work from the host laboratory had established protocols for infection of mTECs with the H3N2 mouse adapted IAV X31 strain (Akram et al 2018) As expected, these studies showed that infection was proportional to both the infecting dose (multiplicity of infection [MOI] of 0.5–5.0) and duration of infection (2–72 h) (Figure 4.2). Infections for >72 h were difficult to study, as large numbers of cells became infected by that time and began to die, and *BPIFA1* protein staining was reduced.

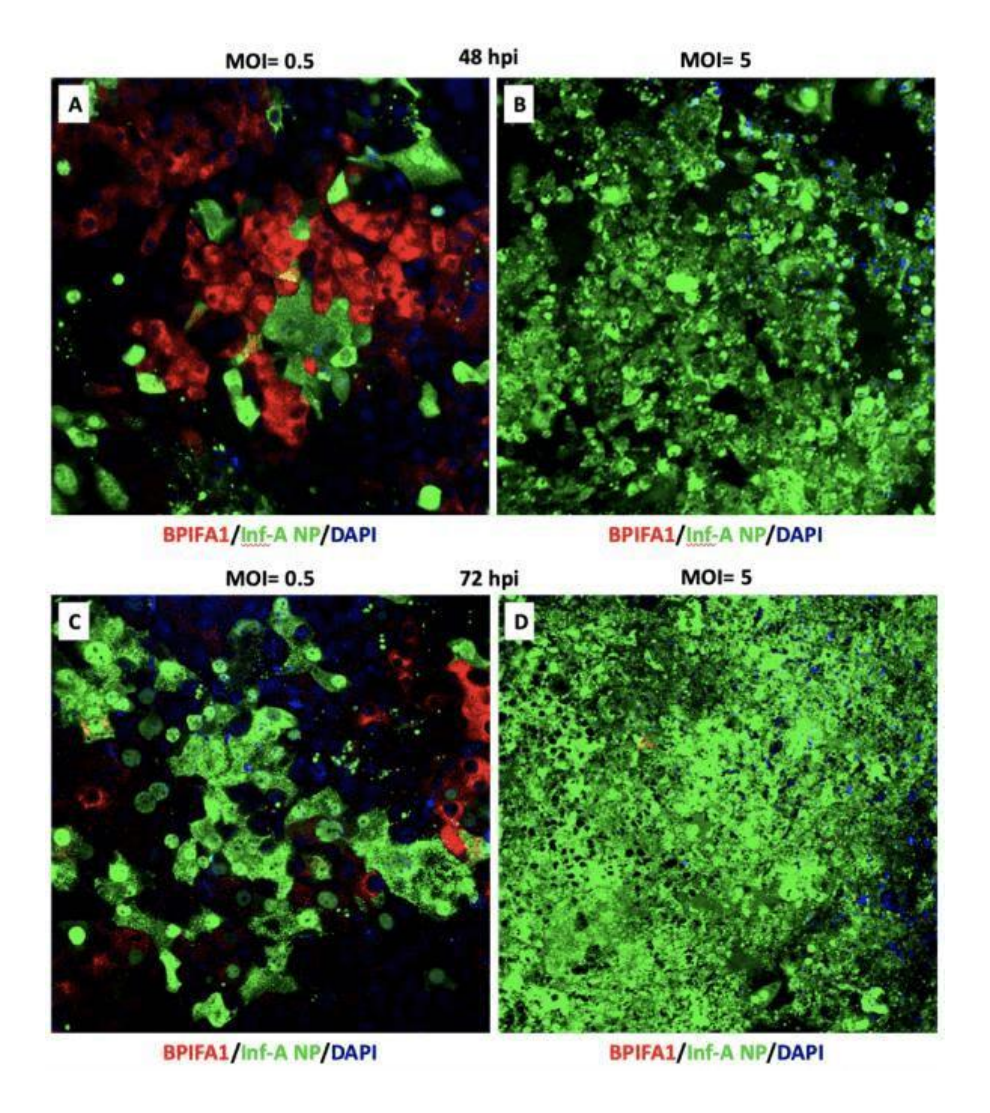


Figure 4.2. Time and Dose Dependence of IAV Infection in mTECs

As the time of infection and dose of IAV increased, Inf-A NP staining (green) became more pronounced. Additionally, BPIFA1 staining (red) progressively decreased in the cells over time. Adapted from Khondoker Akram. Inf-A NP, IAV nucleoprotein

The staining of BPIFA1 was shown to decrease during IAV infection, leading to the hypothesis that gene expression could also change over the same period. End-point PCR was performed to study the expression of *Bpifa1* and *Tekt1* during IAV infection in the mTECs.

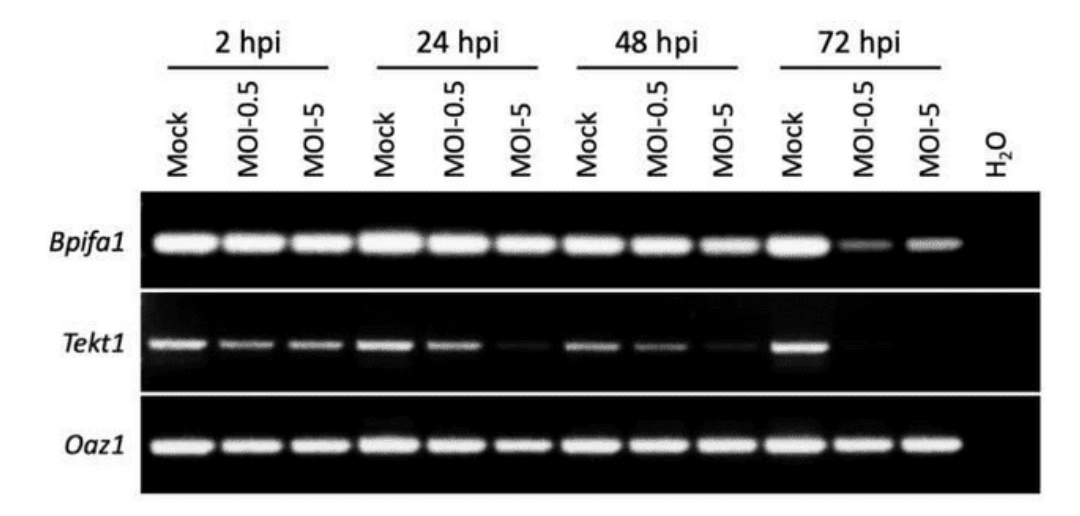


Figure 4.3. Expression of *Bpifa1* and *Tekt1* During IAV Infection in mTECs

The results of a single end-point PCR experiment, as depicted in Figure 4.3, show the expression of *Bpifa1* and *Tekt1* during IAV infection at two doses (0.5 and 5 MOI) and four time points (2, 24, 48 and 72 h). The expression of *Bpifa1* and *Tekt1* was analysed using primers specific to each gene, and *Oaz1* primers served as an internal control (n=1).

The data suggest that both *Bpifa1* and *Tekt1* expression is reduced in a dose- and time-dependent manner, with the loss of *Tekt1* (which was less highly expressed than *Bpifa1* in the uninfected cells) appearing more pronounced. Notably, the analysis involved a single end-point PCR and was non-quantitative. The expression of *Bpifa1* decreased most notably after 72 h with both doses of the virus.

4.2.2 Genome-Wide Analysis of the Gene Expression in the Infected mTECs

Prior to my project, RNA samples were generated by Khondoker Akram and sent to the Centre for Genomic Research at Liverpool University for Illumina HiSeq analysis to examine the genomewide transcriptional response of the mTECs to IAV infection. The analysis was performed on RNA samples taken at 24 h and with an MOI of 0.5. The data underwent cleaning and initial analysis at the University of Liverpool and were presented in the form of annotated Excel spreadsheets. The results showed that 224 genes were upregulated more than two log2-fold in the infected mTECs. The analysis using DAVID (https://david.ncifcrf.gov/) showed that these genes were predominantly correspond to the host response to the virus. Table 4.1 displays the top 50 induced genes in the data set. Many of these genes were not expressed in the uninfected mTECs but were highly elevated following infection. Ifnb1, Ifnl2 and Ifnl3 were the most highly induced genes, with many well-established ISGs present in the list. Some genes, such as Rsad2, Ifit3 and 1830012016Rik, were expressed in the uninfected cells but still highly induced in the infected cells. Ifit3 was the most highly expressed gene in the infected cells. Other highly induced genes included members of the pyrin domain-containing (Pyd) family, such as Pydc4 and Pydc3, and members of the Schafen gene family, including Slfn4 and Slfn5. The list also contained some unexpected genes, such as the olfactory receptor protein Olfr56, also known as IFN-Y inducible protein 47, and Lypd8, a gene previously not associated with viral infection and not previously considered to be an ISG.

Table 4.1. Top 50 Induced Genes in the IAV-Infected mTECs

	Gene	Mock	IAV	Log2FoldChange	P val	P adj
1	Ifnb1	0	315.1012061	Inf	6.87E-26	1.52E-23
2	Ifnl2	0	232.6448157	Inf	2.44E-21	4.50E-19
3	IfnI3	0	216.9388366	Inf	3.09E-20	5.33E-18
4	Cxcl11	1.045130553	901.1305521	9.751909155	3.00E-43	1.99E-4
5	Pydc4	1.045130553	612.5331858	9.19496103	2.53E-35	9.07E-33
6	Slfn4	2.090261105	1147.5181	9.100618026	3.68E-47	3.14E-4
7	Gm12250	10.45130553	3436.664557	8.361182063	9.24E-61	5.52E-5
8	Cxcl10	76.29453034	14719.44731	7.591928154	1.15E-67	2.06E-63
9	Phf11b	34.48930824	5675.748205	7.362517585	8.62E-60	3.09E-5
10	116	5.225652763	729.3464055	7.124849117	2.97E-34	9.51E-3
11	Rsad2	381.4726517	50012.74564	7.034572367	1.13E-64	1.01E-6
12	Phf11a	10.45130553	1351.695828	7.014943561	9.54E-43	6.10E-4
13	Pydc3	4.180522211	513.3891926	6.940225948	2.29E-29	5.62E-2
14	Gbp4	39.714961	4752.040308	6.902720677	6.98E-55	1.39E-5
15	Ifit3	1698.337148	161825.5743	6.574172927	7.09E-60	3.09E-5
16	Mx2	181.8527162	17022.3365	6.548514792	3.34E-57	9.96E-5
17	Gm8979	3.135391658	285.6524953	6.509471654	4.03E-21	7.37E-1
18	SIfn5	38.66983045	3515.194452	6.506252249	9.24E-50	1.10E-4
19	1830012016Rik	1074.394208	88603.31797	6.365765387	4.16E-57	1.07E-5
20	Ifit2	358.4797796	27673.93521	6.270492254	5.02E-55	1.13E-5
21	Gbp3	354.2992573	27054.53066	6.254757962	9.12E-55	1.63E-5
22	AI607873	96.15201084	7258.125602	6.238136183	2.47E-51	3.40E-4
23	tigp1	376.2469989	27554.17712	6.194447158	4.20E-54	6.84E-5
24	Olfr56	3.135391658	221.8469551	6.144775273	6.49E-17	9.45E-1
25	H2-Q8	16.72208884	1085.675807	6.020694482	2.45E-35	8.96E-3
26	Mpeg1	274.8693353	17705.54659	6.009311604	2.90E-51	3.72E-4
27	Gm14446	1289.691102	79359.36763	5.943303062	5.75E-52	8.59E-4
28	Gbp10	94.06174974	5786.671683	5.942981813	2.43E-47	2.18E-4
29	Gbp5	67.93348592	3989.318697	5.875875685	7.11E-45	5.31E-4
30	Gm4841	18.81234995	1063.098462	5.820451338	4.86E-34	1.48E-3
31	Oas3	108.6935775	6053.673328	5.799472224	4.47E-46	3.48E-4
32	Gm7609	32.39904713	1784.591878	5.783498985	2.38E-38	1.04E-3
33	Gbp6	195.4394133	10632.94787	5.765676375	1.48E-47	1.66E-4
34	Ifi203	205.8907189	11040.3217	5.744759603	1.85E-47	1.96E-4
35	Gzma	4.180522211	217.9204603	5.703974678	7.04E-16	9.56E-1
36	Mndal	264.4180298	13746.65823	5.700116583	2.05E-47	2.04E-4
37	Cmpk2	415.9619599	20721.09458	5.638504806	2.31E-47	2.18E-4
38	Gm5431	119.144883	5847.532352	5.617039041	3.78E-44	2.71E-4
39	Isg15	475.5344014	23110.36665	5.602846625	4.81E-47	3.92E-4
40	Oas2	198.574805	8522.456921	5.42351491	2.54E-43	1.75E-4
41	Lypd8	10.45130553	447.620405	5.420520731	4.72E-23	9.62E-2
42	Oasl1	182.8978467	7566.355442	5.370488556	1.50E-42	9.25E-4
43	Gm4951	184.9881078	6962.65687	5.234133494	7.83E-41	4.25E-3
44	Apol9a	296.8170769	10799.82389	5.185289879	2.77E-41	1.60E-3
45	Gldc	6.270783316	222.8285788	5.151144798	9.00E-16	1.19E-1
46	Apol9b	310.4037741	10897.98626	5.133771668	1.03E-40	5.36E-3
47	Tgtp2	871.6388809	30494.14009	5.128657672	8.23E-42	4.92E-3
47	F830016B08Rik	99.2874025	3431.756438	5.111192673	2.71E-37	1.08E-3
49	Mnda	685.6056425	23431.3576	5.094917753	3.12E-41	1.74E-3
50	Gbp9	210.0712411	7159.963232	5.091001604	2.20E-39	1.07E-3

This table presents the expression level as fragments per kilobase of transcript per million mapped reads (FPKM) ranked according to the p-value. The yellow- and green-highlighted genes are those validated by PCR.

4.2.3 Expression of selected genes in the IAV-infected mTECs

The following IAV-induced genes were selected for validation studies: *Ifnl2*, *Slfn4* and *Lypd8*. Table 4.2 shows the expression of these genes in the IAV-infected and non-infected mTEC RNAseq data along with that of the housekeeping gene *Oaz1* as well as *Bpifa1* and *Tekt1*. In absolute terms, *Bpifa1* was the most highly expressed gene. Neither the expression of *Bpifa1* nor that of either *Oaz1* or *Tekt1* dropped significantly following IAV infection. As shown in Table 4.1, the expression of *Ifnl2*, *Slfn4* and *Lypd8* was significantly elevated in the infected cells.

Table 4.2. Expression of Selected Genes From mTEC RNAseq Data

	p p adj
Gene Mock Infected log2 Fold	p paaj
Oaz1 536.151973 440.749039 -0.2826846 0.433559	9 1
Tekt1 702.327731 590.937464 -0.2491389 0.479538	1
Bpifa1 33744.1302 29412.3908 -0.1982125 0.531324	7 1
Ifnl2 0 232.644816 Inf 2.44E-	21 4.50E-19
Slfn4 2.09026111 1147.5181 9.10061803 3.68E-	3.14E-44
Lypd8 10.4513055 447.620405 5.42052073 4.72E-	9.62E-21

This table shows the expression of selected genes (expressed as FPKM) Fragments per kilobase per million in the IAV-infected and non-infected mTEC RNAseq data along with the housekeeping genes.

End-point PCR was conducted to confirm the induction of three ISGs (*Ifnl2*, *Slfn4* and *Lypd8*) in response to IAV infection in the mTECs for over 72 h to validate the RNAseq results. The results showed that the expression of these genes markedly increased after 24 h compared with that of the control samples and remained elevated at 48 and 72 h. This finding confirms the RNAseq data. However, it appeared that there was a decrease in the expression of *Tekt1* in the infected cells compared with that in the control samples at 72 h.

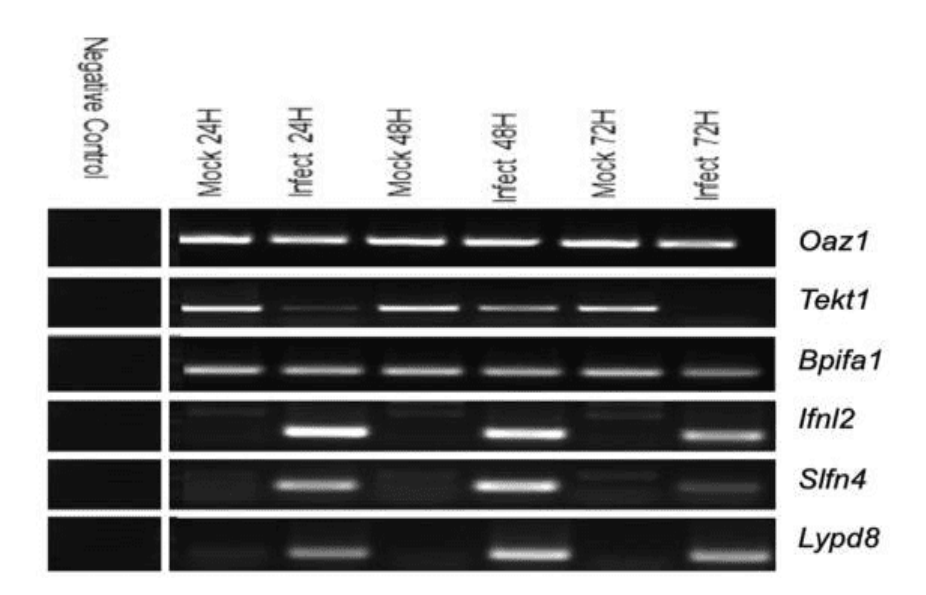


Figure 4.4. Expression of Target Genes in the IAV-Infected mTECs

RT-PCR was conducted using cDNA generated from mTEC cultures that were either infected with IAV (MOI of 0.5) or mock infected for 24, 48 or 72 h. The primers used to amplify the genes were *Oza1*, *Tekt1*, *Bpifa1*, *Infl2*, *Slfn4* and *Lypd8*. The reaction products were then separated via 2% agarose gel electrophoresis and visualised. (n =1)

In parallel with the RNAseq experiment with the mTECs, Professor James Stewart's laboratory at the University of Liverpool also undertook RNAseq from the entire lungs of C57/BL6 mice infected with IAV X31 and sampled at 4 days post-infection. Gene expression data were extracted on the same six genes from the total lung data set to determine whether there was a conservation of transcriptional responses in the context of the entire lungs (Table 4.3). In contrast to what was seen in the mTECs, there was a significant reduction in *Bpifa1* expression in the lungs after IAV infection, alongside a slight reduction in *Tekt1* expression. Further, the expression of *Slfn4* and *Lypd8* was also significantly induced in the infected lungs, whereas that of *Ilfn2* was not significantly induced.

Table 4.3. Expression of selected genes from infected whole-lung RNAseq data

Gene	Mock	Infected	log2 Fold	р	p adj
Oaz1	467.125484	603.100657	0.36858865	0.46677286	1
Tekt1	1062.48149	749.177445	-0.5040583	0.30679859	1
Bpifa1	35018.8405	3885.98426	-3.1717794	6.47E-10	2.19E-07
IfnI2	0.91593232	6.83400178	2.89941772	0.31802165	1
Slfn4	217.07596	11059.9776	5.67100469	1.70E-22	6.90E-19
Lypd8	8.2433909	757.719948	6.52228301	7.04E-20	2.38E-16

This table presents the RNAseq data (FPMK) from the infected and mock-infected whole-lung tissues such as *Bpifa1* in mock is highest than infected *Lypd8* is high expression infected also, *Slfn4* is same.

Taken together, these differential gene expression patterns may play important roles in the host response to IAV infection.

4.2.4 Cell-Specific Infection of the mTECs

The approach initially used to further understand the type of cells involved in IAV infection in mTEC cultures was to use a lower MOI of 0.1. The media used was also switched to the PneumaCult ALI culture media, as this media has specifically been designed for optimal differentiation of cultures and is easier to use and should produce less variability in cell growth (Schweitzer, Crue et al. 2021). The protocol for this study is illustrated in Figure 4.5.

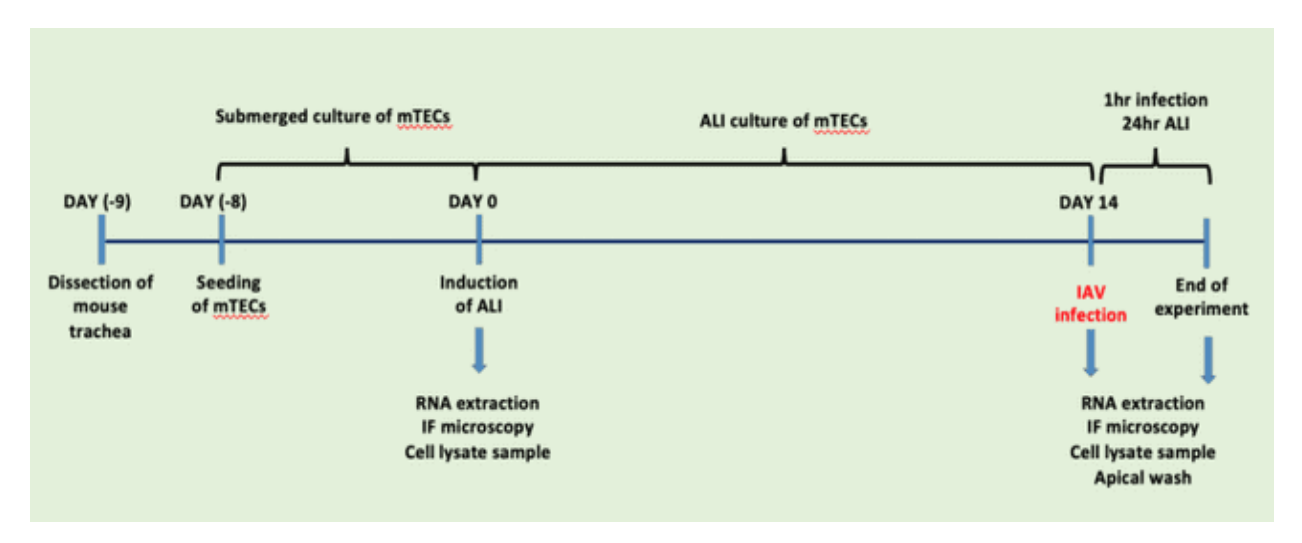


Figure 4.5. Schematic representation of the IAV infection protocol in differentiated mTECs. The protocol is detailed in the materials and methods section.

The mTECs were cultured submerged in PneumaCult Expand⁺ media on trans-well inserts until they became confluent. They were then raised to the ALI and were fed from underneath the semi-permeable transwell with PneumaCult ALI media. The cells were cultured in these conditions until day 14, and at this stage, they were differentiated. The cells were infected with 0.1 MOI of X31 IAV and were sampled at 24 h.

Initially, IF microscopy was used to confirm that the cells cultured in the PneumaCult ALI media differentiated as described before and could be infected with IAV.

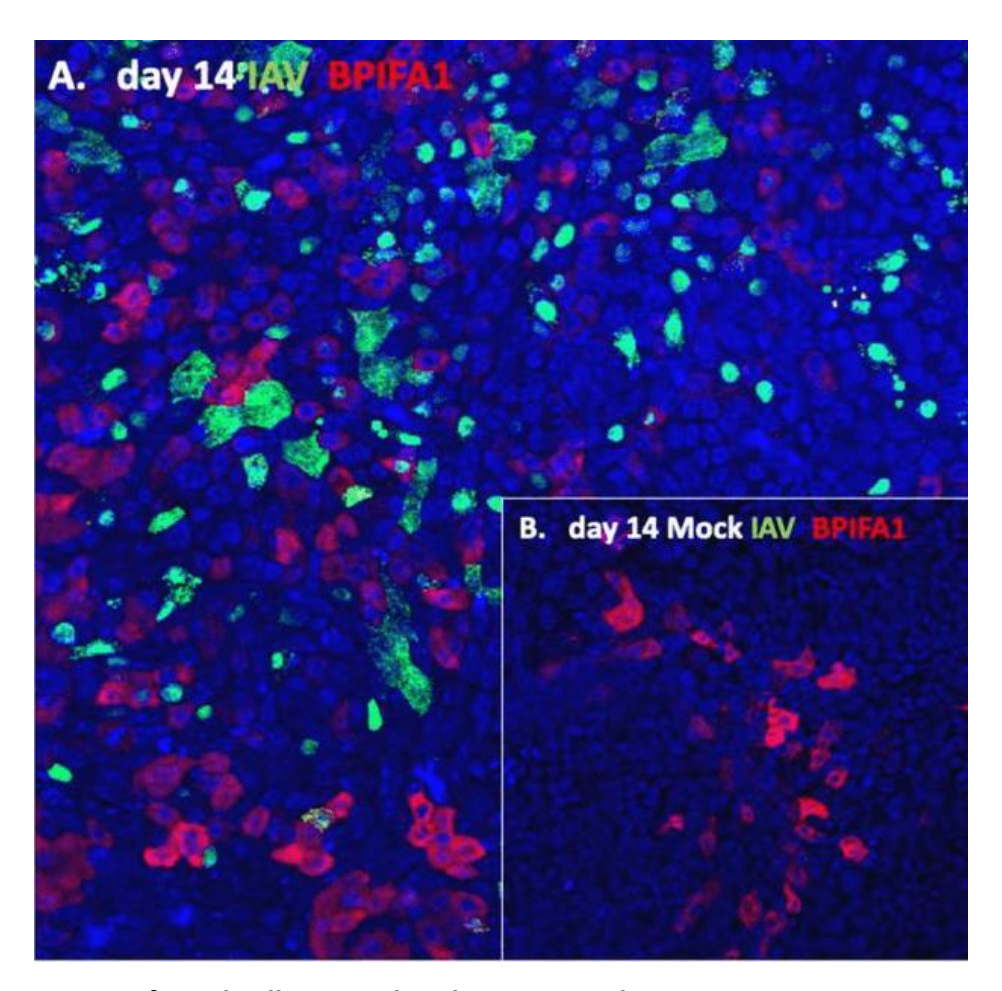


Figure 4.6. Day 14 infected cells stained with BPIFA1 and IAV.

(A) BPIFA1^{+ve} cells (red) are mostly not stained for IAV (green), suggesting that the virus mostly infects other cell types. (B) BPIFA1 staining (red) in the mock-infected cells. The cells were infected with an MOI of 0.1 and stained after 24 h.

The cells grown in the PneumaCult ALI media stained for BPIFA1, confirming that they had undergone differentiation in this media like previous results. The cells infected with IAV on day 14 could be seen using an antibody to IAV-NP. At this dose and time point, most of the stained cells showed no clear overlap of BPIFA1 and IAV staining. The lack of co-staining of IAV and BPIFA1 led to the consideration that infection initially occurred in the ciliated cells. The infected transwell mTEC cultures were stained with an antibody to acetylated TUBULIN as a marker for ciliated cells and with an antibody to IAV.

Figure 4.7 shows images of the culture of the ALI day 14 IAV-infected mTECs. Abundant ciliated cells are visible (shown in red) alongside a strong signal for IAV infection (green). The higher-magnification image in panel B shows a limited amount of co-localisation of the two signals (shown in yellow) in the images. The transwells appear to show some cells exhibiting overlaying of red signals (representing the cilia axoneme) on top of the green IAV signals within the cytoplasm, suggesting that some IAV infection is seen in the ciliated cell population.

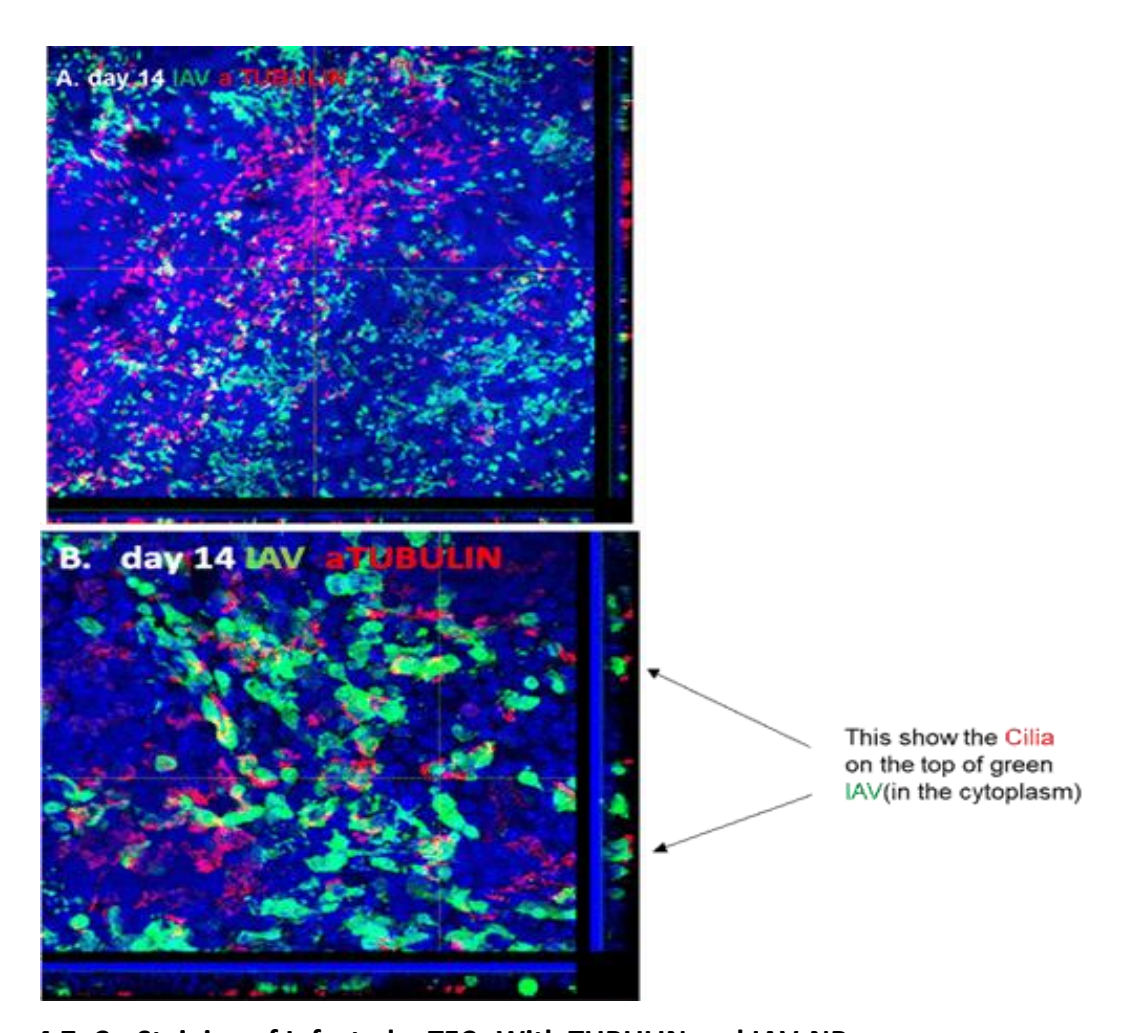


Figure 4.7. Co-Staining of Infected mTECs With TUBULIN and IAV-NP

ALI day 14 differentiated mTECs were infected with IAV and imaged 24 h later as described in the materials and methods section. Acetylated TUBULIN is shown in red, IAV-NP in green and nuclei in blue. The images were taken at two magnifications.

4.2.5 IAV Infection of the Undifferentiated mTECs

With the observation from the differentiated ALI mTECs suggesting a potential infection of IAV in the BPIFA1^{-ve} secretory cells and a proportion of ciliated cells, the susceptibility of the undifferentiated mTECs to IAV infection was investigated. These cells lacked a differentiated phenotype and were cultured on transwells as previously described until they reached confluence in an undifferentiated state. The cultures were then infected with 0.1 MOI of X31 IAV and sampled 24 h later. The experimental design is illustrated in Figure 4.8.

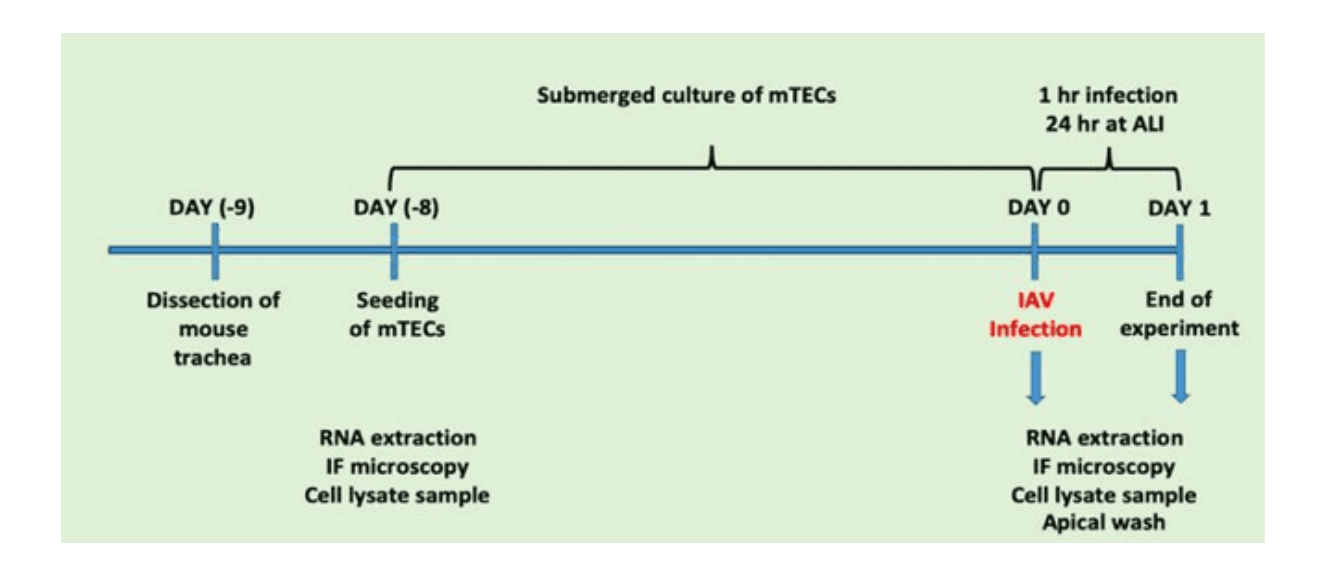


Figure 4.8. Schematic representation of the IAV infection protocol in the undifferentiated mTECs

The protocol is detailed in the materials and methods section. Initially, IAV infection was directly compared between the day 0 mTECs and ALI day 14 cultured cells. Figure 4.9 shows that IAV staining was seen in both cell cultures. Ciliated cells were absent in the day 0 infected mTECs. This observation shows that mTECs do not need to be differentiated to be infected by IAV.

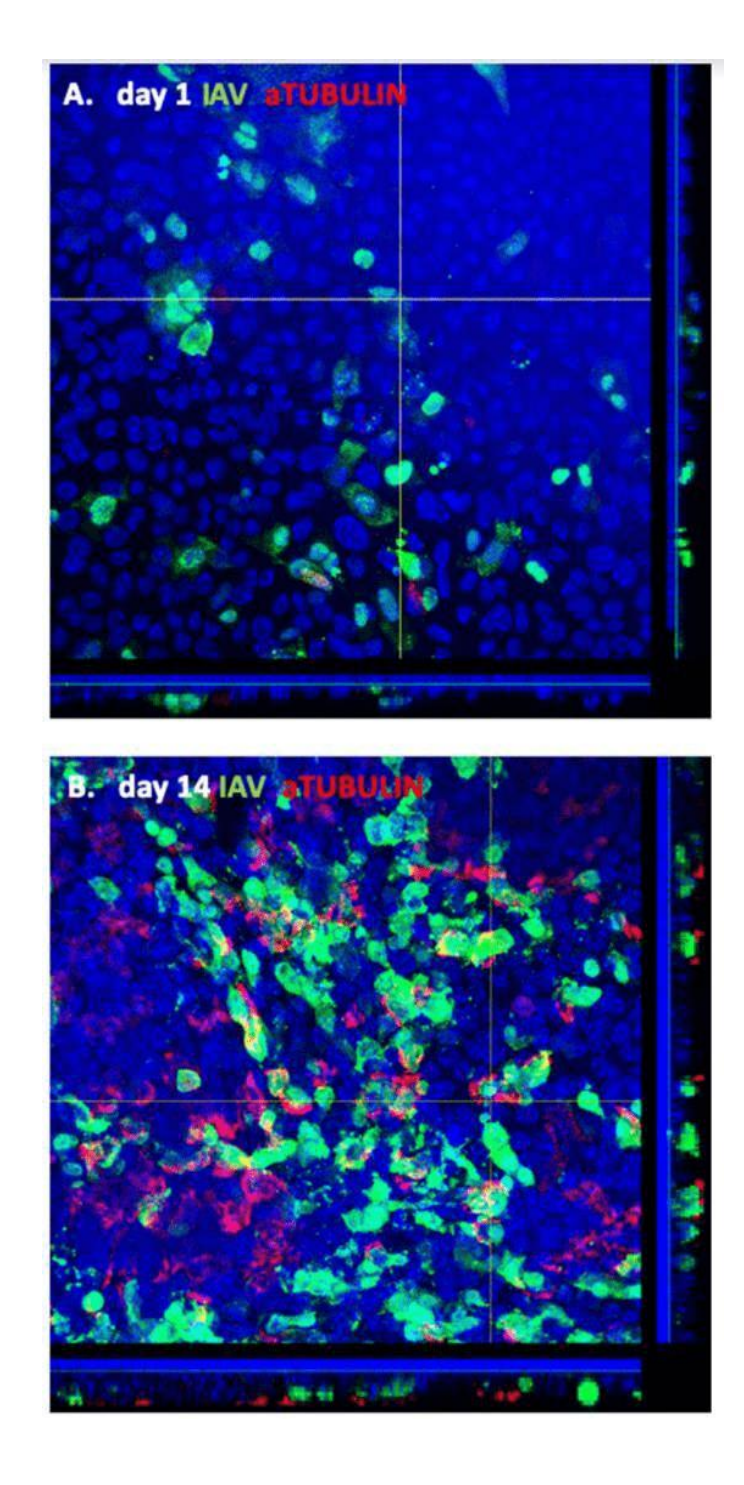


Figure 4.9. Co-staining of infected undifferentiated and differentiated mTECs with TUBULIN and IAV-NP

After the establishment that the undifferentiated cells could be infected with IAV, the level of infection was quantitated in the two conditions. Triplicate experiments (using three different cell preparations from different batches of mice) were conducted, in which the day 0 and day 14 cells

were infected with 0.1 MOI of X31 virus, and infections were allowed to proceed for 24 h. At this time, the experiment was stopped, and the trans-wells were stained with IAV and acetylated TUBULIN. It has previously been shown that the amount of IAV-NP staining can be used as a surrogate marker for the levels of virus in cells.

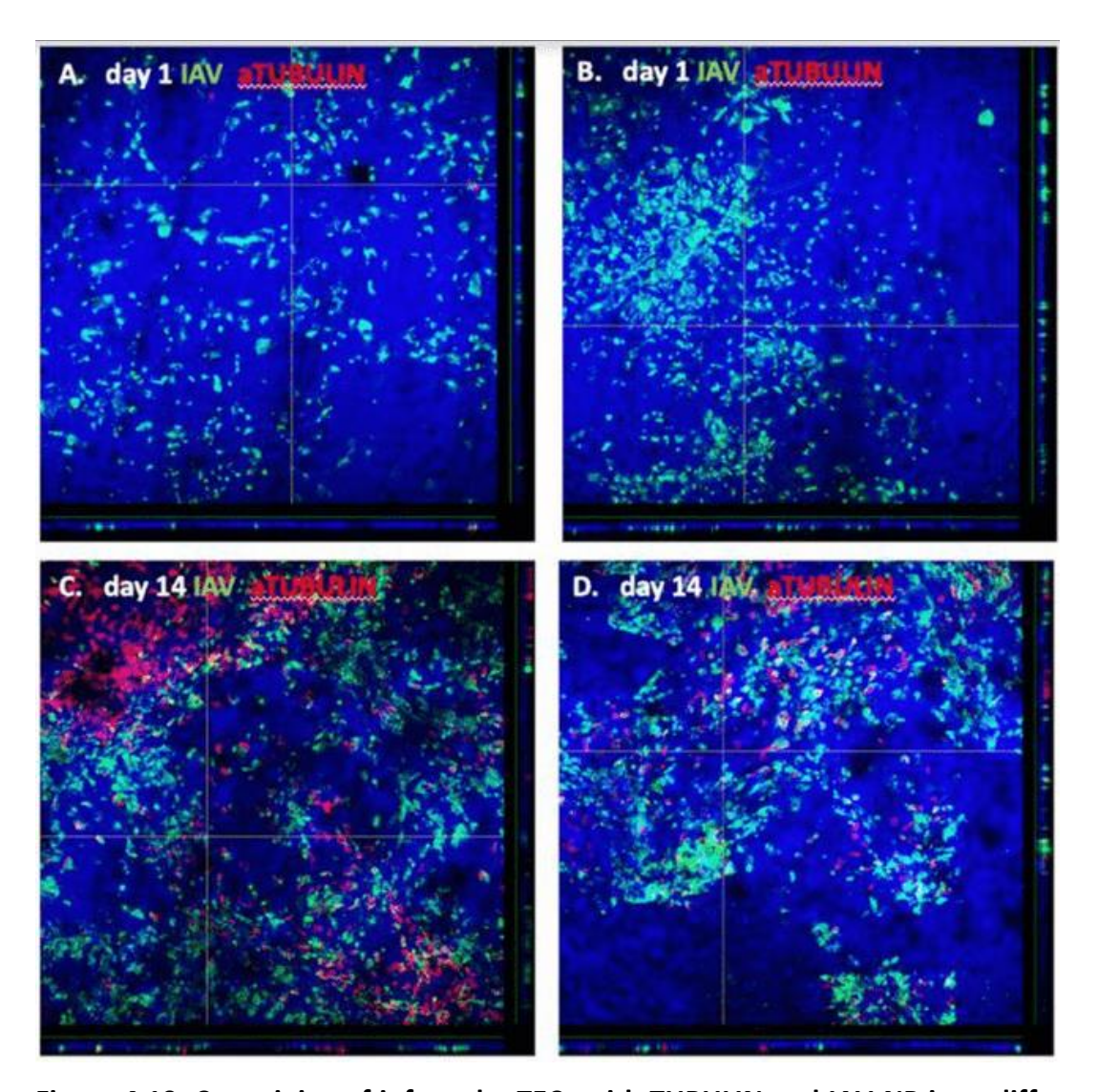


Figure 4.10. Co-staining of infected mTECs with TUBULIN and IAV-NP in undifferentiated and differentiated mTECs

Figure 4.10 shows images of the day 1 and day 14 cells stained with IAV. The images suggest that IAV infection is variable across cultures. A total of 12 images (four from each experimental replicate in each condition) were obtained for quantitation as described in the materials and

methods section. Figure 4.11 confirms that the day 0 undifferentiated cells were readily infected by IAV X31 but at a lower level than the day 14 differentiated cells.

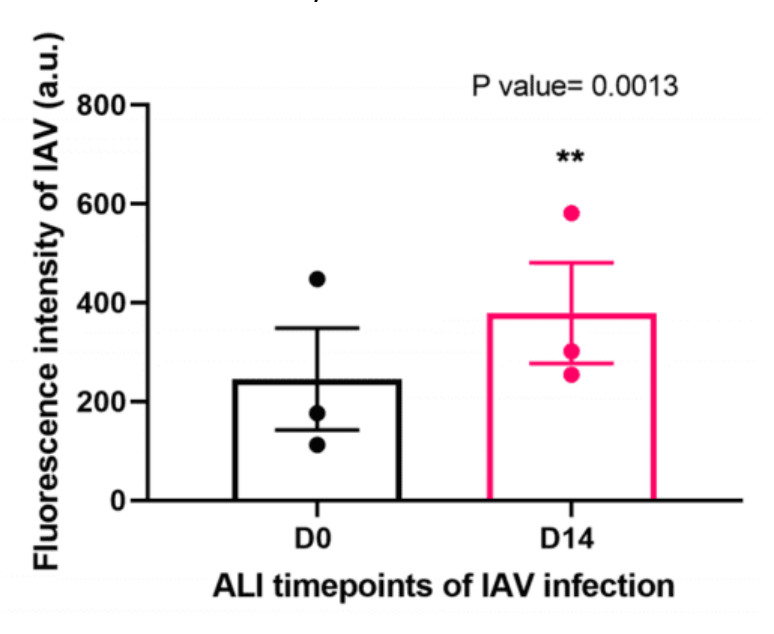


Figure 4.11. Infection of undifferentiated and differentiated mTECs with IAV.

IAV-stained and -infected mTEC cultures were imaged, and IAV staining intensity was quantitated by used immunofluorescence of IAV staining NP nucleoprotein of IAV as a green across four fields from each of the three replicates experiments (n=3).

4.2.6 Genome-wide transcriptional responses to IAV Infection of undifferentiated and differentiated mTECs

The genome-wide transcriptional responses towards IAV infection in the day 0 (undifferentiated) and day 14 (differentiated) cells were evaluated to examine the consequences of the infection in the undifferentiated mTECs more thoroughly. In the day 0 cultures, IAV infected the basal cells, which are the progenitor cells of the airway epithelium (Rock 2009) whereas the day 14 cells were differentiated, yielding an increased number of ciliated and secretory cells.

The undifferentiated cells were infected on day 0 when they had become confluent, but samples were taken 24 h after when the cells had been at the ALI for 1 day.

Triplicate samples of biological replicates were collected from the same isolations used for the IAV imaging experiments. Total RNA was extracted using the Zymo system, and the quality was assessed using the Agilent Bioanalyser. Only RNA samples with an RIN greater than 8 were used

for further analysis. Microarray analysis was performed by Doctor Paul Heath at SITraN, University of Sheffield, using the Mouse Clariome S microarray assay (Thermo Fisher Scientific). The initial data analysis was performed by another PhD student in the laboratory (Miraj Chowdhury) as previously described in Chapter 3. Owing to some unforeseen issues, data were not available for all samples at each time point, and only two samples from the day 14 infected cells could be used for the analysis.

The gene expression of the day 0 mock-infected cells and day 0 IAV-infected cells from the microarray analysis was represented in scatter and volcano plots (Figures 4.12 and 4.13). The dots on the plot indicate the expression of 6819 genes, with highly differentially expressed genes represented by coloured dots. Green dots represent the overexpressed genes in the day 0 mock-infected cells, while red dots indicate the overexpressed genes in the day 0 IAV-infected cells. The further the red dots are from the midline, the higher the gene induction. The results showed that among the day 0 mock-infected cells, 3146 genes were highly expressed, while 3673 genes were lowly expressed; among the day 0 IAV-infected cells, 2880 genes were highly expressed, while 3939 genes were lowly expressed.

Table 4.5 displays the top 50 most upregulated genes identified in this study. These genes can be considered to be ISGs. The data showed that some of these ISGs were not expressed in the mock-infected cells, while others were present but underwent a significant increase in their expression after infection. Of the 50 genes, *Lypd8* showed the highest level of induction upon infection. The genes were identified as ISGs owing to their significant induction upon infection and considered to represent the transcriptional response to the viral infection.

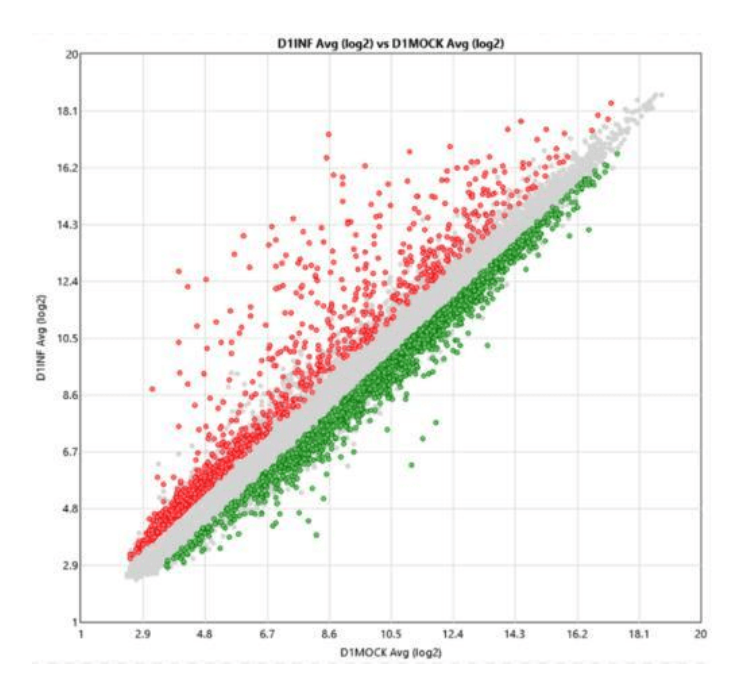


Figure 4.12. Scatter plot of the Day 0 infected mTECs

Red dots indicate the genes upregulated in the infected cells, whereas green dots show the genes lowly expressed in the infected cells.

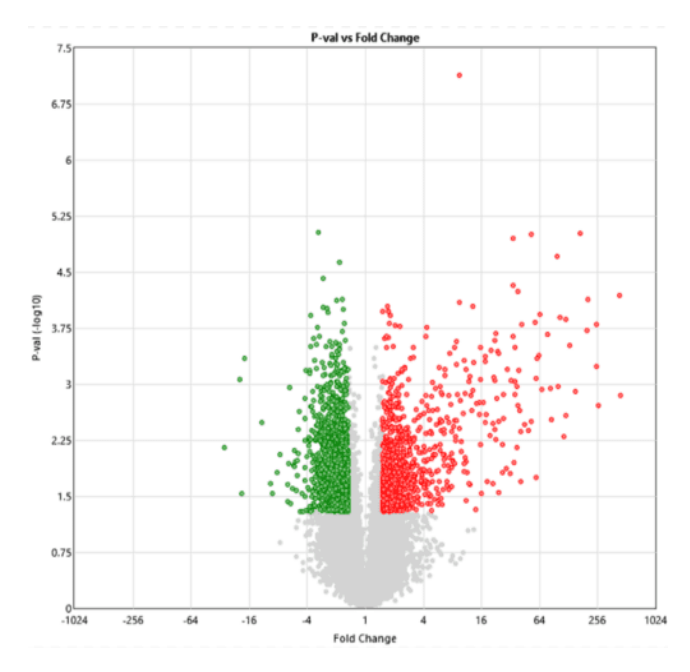


Figure 4.13. Volcano plot of the Day 0 infected mTECs

Red dots indicate the genes upregulated in the infected cells, whereas green dots show the genes lowly expressed in the infected cells.

Table 4.5. Top 50 Most Induced Genes between the Day 0 IAV- and Day 0 Mock-Infected mTECs

No	Genes	AvG D1 Mock	AvG D1 Inf	Fold Difference	pval
1	Lypd8	7.256	16.103	8.846	0.003206285
2	Mpeg1	5.326	13.353	8.026	0.000199105
3	Cxel11	3.923	11.943	8.02	0.000105558
4	Gm12250	4.41	12.403	7.993	0.000101552
5	Cxcl10	8.993	16.746	7.753	0.000564143
6	Pydc4	6.033	13.46	7.426	0.000233833
7	Gm4951	4.48	11.773	7.293	0.000181573
8	Tgtp2	8.583	15.793	7.21	0.004252527
9	Trim30a	6.403	13.59	7.186	0.001806596
10	Phfi 1a	5.966	13.086	7.12	0.000431855
11	Gm4841	5,433	12.546	7.113	1.492168-06
12	ligp1	6.163	13.26	7.096	2.43446E-06
13	Cmpk2	8.453	15.413	6.96	6.41539E-05
14	Phfi 1b	8.246	15.166	6.92	6.25153E-05
15	Rsad2	9.3	16.02	6.72	0.002507924
16	Gm12185, Tgtp1	10.053	16.666	6.613	0.004111831
17	Gbp3	8.02	14.59	6.57	0.003162469
18	Pydc3	6.136	12.606	6.47	1.09146E-05
19	Oas2	5.376	11.826	6.45	3.00255E-06
20	Ifit2	6.61	13.05	6.44	0.011743676
21	Gbp10,Gbp6	6.05	12.3	6.25	1.7427E-05
22	lgtp	7.58	13.616	6.036	4.59511E-05
23	Mx1	8.286	14.276	5.99	0.000226567
24	Sitn8	5.053	11.013	5.96	6.95887E-05
25	Sitn5	4.603	10.546	5.943	0.000286954
26	Sitn4	5.02	10.866	5.846	0.008934536
27	Gbp2b ,Gbp5	2.97	8.78	5.81	0.0010824
28	Trim30c	3.09	8.8	5,71	3.42204E-05
29	Ifit1bl2	7.773	13.403	5.63	0.000729747
30	Mx1	9.726	15.353	5.626	0.000785768
31	Gm5431	7.656	13.166	5.51	0.000827421
32	Oasit	7.333	12.716	5.383	0.003792656
34	Slfn3	3.8	9.12	5.32	0.006037914
35	H2-Q5	6.976	12.273	5.296	5.9527E-05
36	IN203	10.376	15.636	5.26	1.99959E-07
37	SIfn2	9.08	14.32	5.24	0.002937367
38	Gbp2	10.35	15.566	5.216	0.004559537
39	Trim30d	6.553	11.766	5.213	0.001255149
40	Gbp4	6.61	11.71	5.1	0.000709962
41	Gvin1	4.566	9.65	5.083	6.84753E-05
42	Irgm2	8.7	13.78	5.08	0.000865015
43	Gbp7	9.323	14.28	4.956	0.000234594
44	Irf7	10.806	15.74	4.933	0.025594766
45	F830016B08Rik	4.006	8.936	4.93	0.001180344
46	Dhx58	6.943	11.873	4.93	0.00099349
47	Gm6904	5.573	10.423	4.85	0.000256718
48	Tnfsf10	7.28	12.126	4.846	0.027209179
49	Ifi2712a	5.0166	1.196	4.786	0.008404082
50	SIfn9	9.293	0.65	4.743	5.8005E-05

The data of the ALI day 14 infected cells are depicted in scatter and volcano plots in Figures 4.14 and 4.15. A total of 7386 genes were found to be expressed; these are indicated in the plots in the form of dots. The highly differentially expressed genes are represented by coloured dots. The overexpressed genes in the day 14 mock-infected cells are indicated by green dots and the overexpressed genes in the day 14 infected cells by red dots. In the day 14 mock-infected cells, 2810 genes were highly expressed, while 4576 were lowly expressed. In the day 14 infected cells, 2405 genes were highly, while 4981 were lowly expressed.

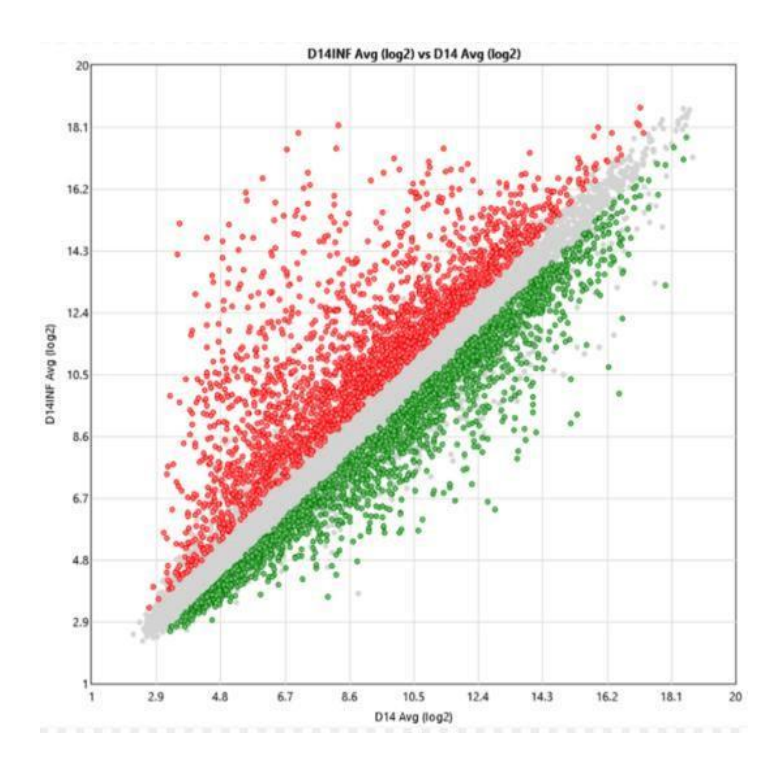


Figure 4.14. Scatter plot of the day 14 infected mTECs

Red dots indicate the genes upregulated in the infected cells, whereas green dots show the genes lowly expressed in the infected cells.

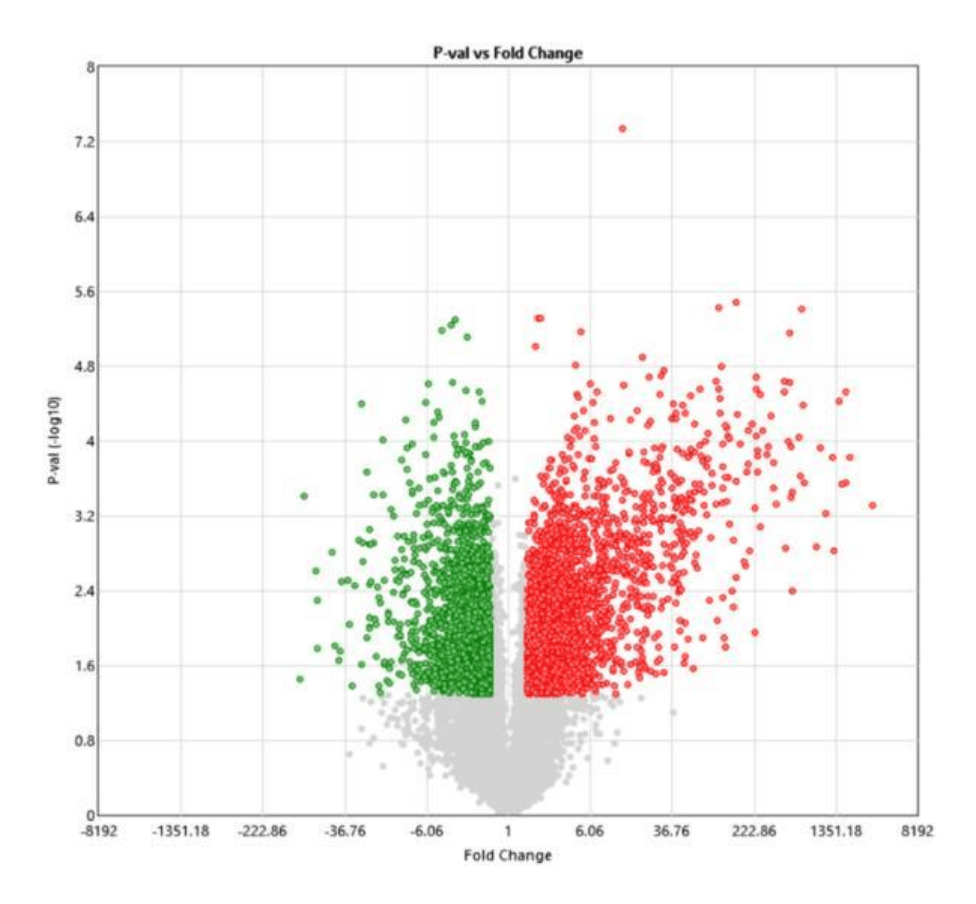


Figure 4.15. Volcano plot of the Day 14 infected mTECs

Red dots indicate the genes upregulated in the infected cells, whereas green dots show the genes lowly expressed in the infected cells.

The top 50 most induced genes are shown in Table 4.6. These genes were identified as ISGs. As seen in the RNAseq induction data (Table 4.1), some of the genes were essentially not expressed in the mock-infected cells, whereas others were expressed but also underwent a significant induction. In this data set, *Lypd8* showed the highest induction.

Table 4.6. Top 50 most induced genes between the Day 14 IAV- and Day 14 mock-infected mTECs

No	Genes	AvG D14 Mock	AvG D14 Inf	Fold Difference	pval
1	Cxcl11	3.603	14.91	11.306	0.000377111
2	Ifit3b	7.356	18.36	11.003	1.23138E-06
3	Cxcl10	6.306	17.29	10.983	5.22999E-06
4	Rsad2	6.186	16.865	10.678	7.50632E-05
5	Gbp3	5.283	15.895	10.611	2.88216E-07
6	Irf7	6.03	16.315	10.285	5.053E-06
7	Ifit3	8.33	18.555	10.225	1.98496E-09
8	Cc15	5.25	15.47	10.22	0.000690665
9	Pydc4	4.416	14.605	10.188	5.37124E-06
10	Oasi1	3.773	13.68	9.906	0.000423565
11	Cmpk2	7.043	16.85	9.806	2.61809E-06
12	lfit1bl1	7.92	17.645	9.725	1.40744E-06
13	If1203	6.943	16.38	9.436	1.79314E-06
14	ligp1	4.79	14.105	9.315	4.79613E-09
15	Sifn4	3.86	13.175	9.315	3.14784E-05
16	Gm12250	3.993	13.155	9.161	7.81061E-12
17	Phf11b	6.25	15.365	9.115	4.16272E-05
18	Ppbp	5.786	14.745	8.958	0.011819641
19	Mpeg1	5.5	14.295	8.795	1.74929E-05
20	Pydc3	4.59	13.345	8.755	6.52948E-06
21	lsg15	4.39	13.14	8.75	5.1564E-08
22	Trim30a	5.516	14.195	8.678	2.98338E-06
23	Oas1a	5.443	14.11	8.666	7.75397E-07
24	Mx2	7.26	15.845	8.585	2.53249E-06
25	Oas2	4.02	12.555	8.535	5.74738E-07
26	Sifn2	7.22	15.755	8.535	1.23419E-05
27	Gm4951	4.073	12.535	8.461	2.7685E-06
28	Xaf1	6.353	14.775	8.421	1.46077E-07
29	AI607873	7.883	16.27	8.386	0.000336073
30	Anxa10	4.833	13.185	8.351	7.06753E-06
31	Zbp1	4.68	13.025	8.345	1.00057E-06
32	Dhx58	5.12	13.445	8.325	1.98522E-08
33	SIfn9	6.623	14.925	8.301	8.02881E-07
34	Ifit2	6.546	14.725	8.178	0.001665083
35	Gbp4	5.49	13.665	8.175	7.64973E-05
36	Gbp2	8.633	16.76	8.126	0.000344299
37	Mndal	8.693	16.8	8.106	2.89802E-08
38	Apol9a	7.086	15.19	8.103	2.65375E-07
39	lgtp	6.003	14.07	8.066	3.50081E-07
40	SIfn8	4.203	12.155	7.951	1.86754E-07
41	Ddx60	7.753	15.65	7.896	1.20437E-07
42	Gm5431	6.45	14.055	7.605	4.10903E-06
43	Krt20	5.426	13.01	7.583	1.72009E-06
44	Gbp2b, Gbp5	3.566	11.135	7.568	0.000289712
45	Phf11a	5.013	12.54	7.526	0.001459063
46	Mx1	8.773	16.28	7.506	0.001521098
47	Pyhin1	8.293	15.745	7.451	0.009063837
48	Gbp10, Gbp6	6.206	13.645	7.438	1.9823E-06
49	SIfn5	4.103	11.53	7.426	0.000118341
50	Oas3	4.473	11.86	7.386	2.47225E-07

A dot plot showing the differential gene expression between the infected cell samples from the ALI day 0 and 14 cells was generated (Figure 4.16).

The data demonstrated that the day 14 infected mTECs showed a higher gene expression than did the day 0 infected cells. This confirms the data shown in Tables 4.5 and 4.6. The analysis was complicated by the fact that the two different cell cultures were phenotypically quite distinct and exhibited a significantly different transcriptional programme as outlined in Chapter 3.

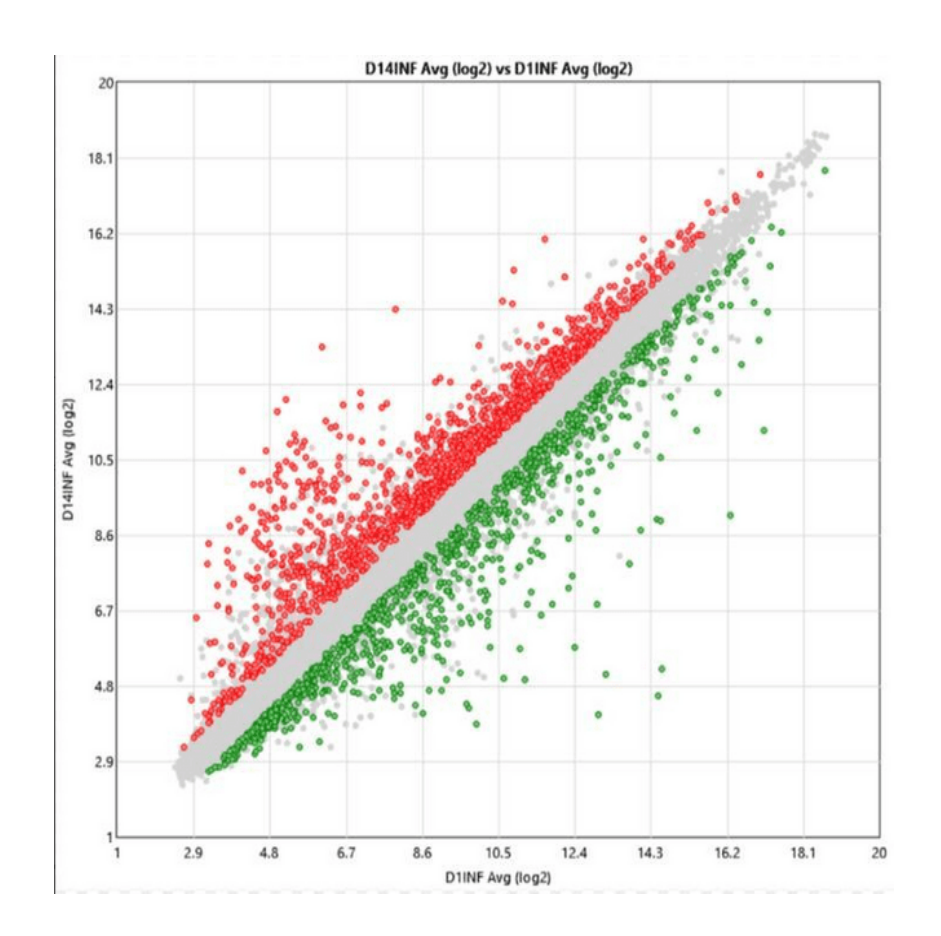


Figure 4.16. Scatter plot of the differentially expressed genes in the IAV-infected mTECs

A heat map of the genes that were >2 log2-fold differentially expressed between the different samples was generated to better understand gene induction (Figure 4.17). The data showed that there was a general similarity of the IAV-induced genes between the two conditions (Figure 4.17A). There was also a level of variability of the responses between the different samples at the same time point. The level of induction of the genes in the day 14 infected cells was higher

than that in the day 0 cells. Figure 4.17B and C shows expansions of the heat map and includes some genes that were expressed more highly in the day 0 mock-infected cells than in the day 14 mock-infected cells but were induced by infection. In the genes highlighted in Figure 4.17C, the level of induction appeared to be lower in the day 14 infected cells.

The data on the comparative expression of the top 10 most induced genes from the days 0 and 14 cells were also extracted (Figure 4.18A and B). *Lypd8* induction was higher in the day 0 infected cells than in the day 14 cells, whereas a less marked difference was seen in the other top 10 genes from the day 0 cells. Among the top 10 genes from the day 14 cells, several genes (*Cxcl11*, *Ccl5*, *Pydc4* and *Oasl1*) were more highly induced.

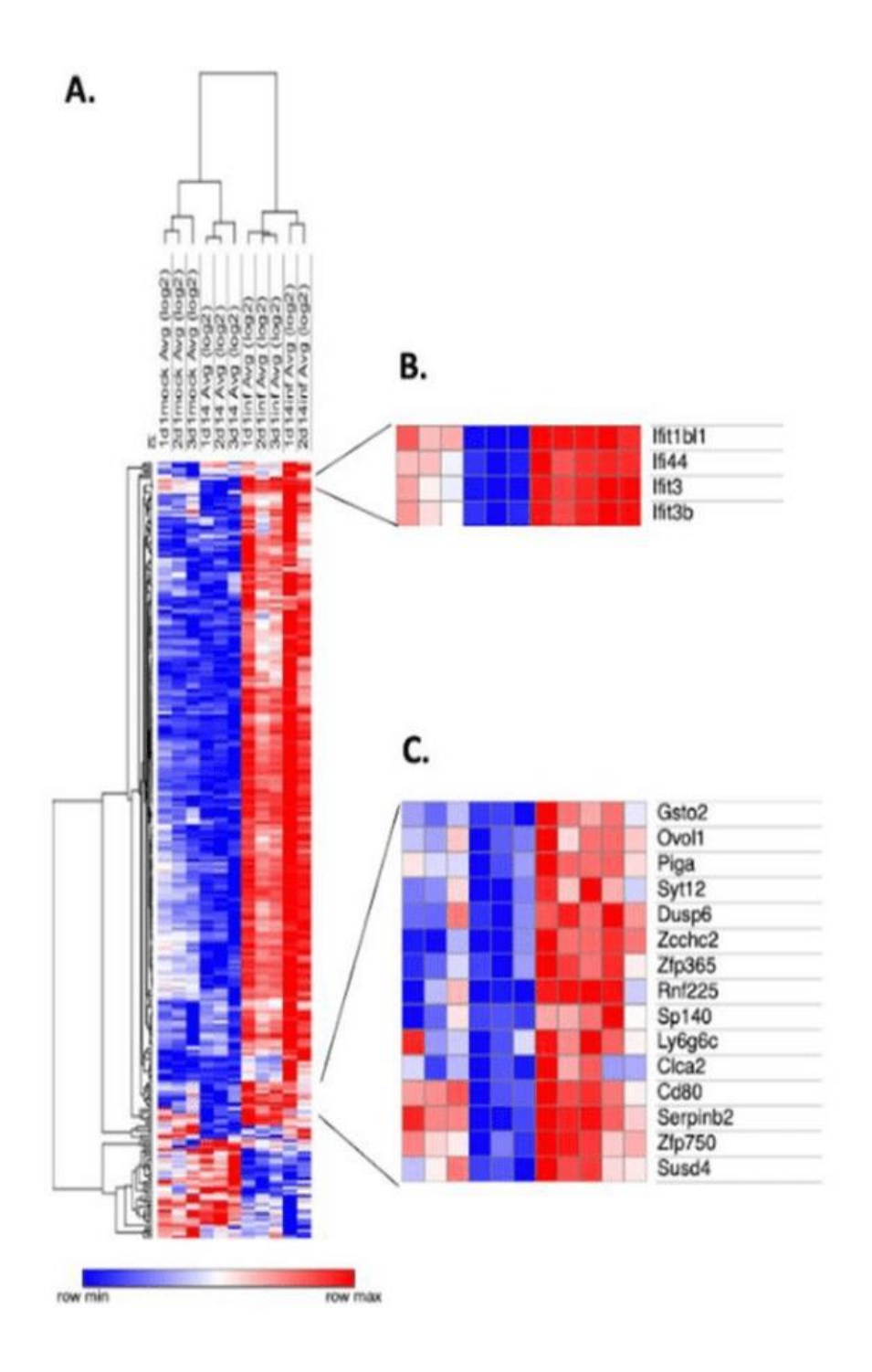


Figure 4.17. Heat map analysis of the IAV-induced genes in the undifferentiated and differentiated mTECs

(A) Comparison of all differentially expressed genes (>2 log2) among the genes in the day 0 and 14 mock-infected cells and day 1 and 14 infected cells. (B) Genes highly expressed in the day 1

and 14 infected cells and expressed in the day 0 mock-infected cells. (C) A block of genes was expressed more highly in the day 0 infected cells than in the day 14 cells.

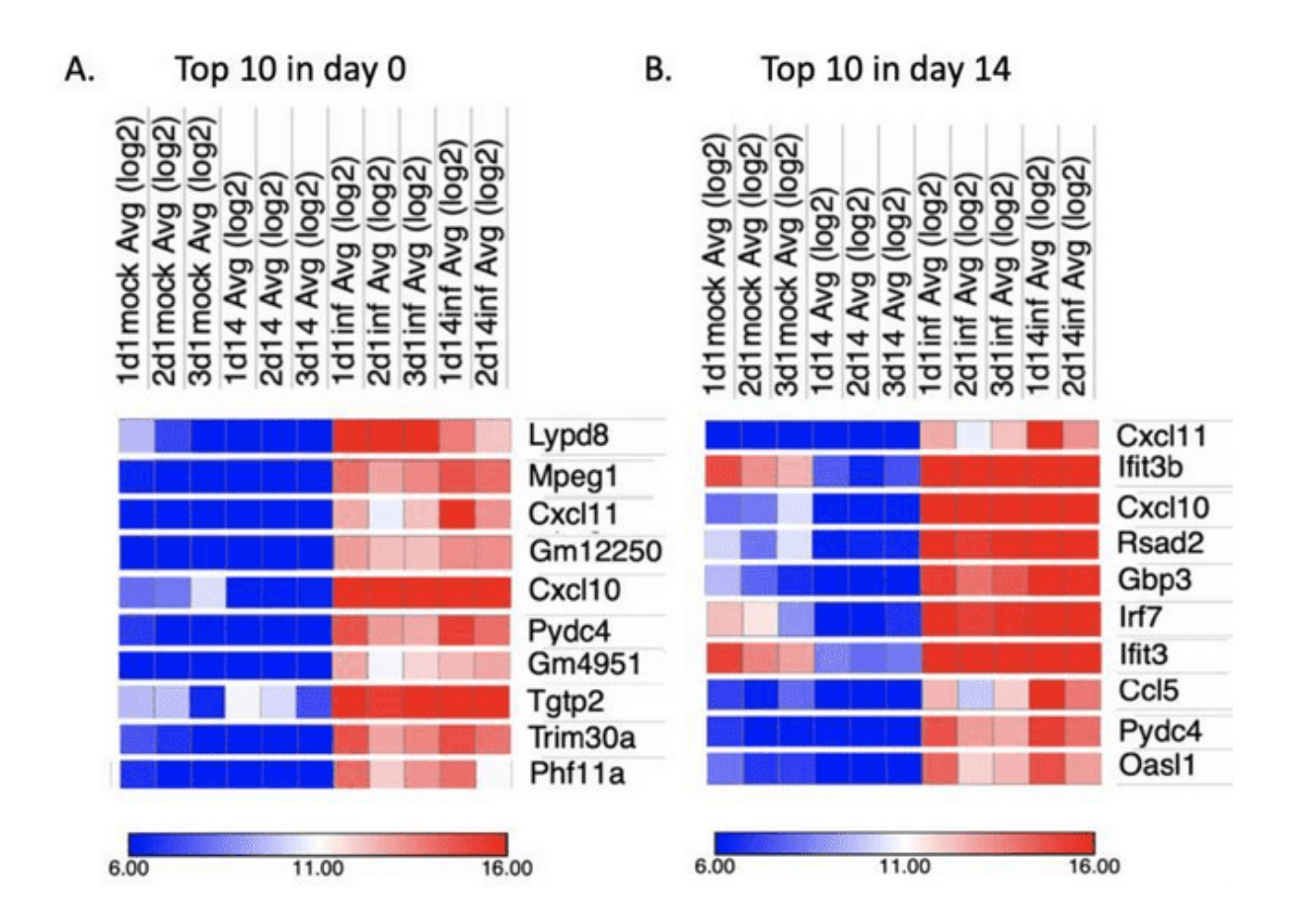


Figure 4.18. Heat map data of the top 10 most induced genes in the Day 0 and 14 mTECs

The expression data for the top 10 genes from Tables 4.5 and 4.6 are plotted. Red indicates high expression.

4.2.7 Expression of membrane-spanning proteases in the mTECs

In the study of IAV infection in the mTECs, the expression of four membrane-spanning proteases was analysed: *Tmprss2*, *Tmprs4*, *Tmprss11d* (also known as *HAT*) and *furin*. Samples were taken from the infected and uninfected mTECs on days 0 and 14, and the expression of the proteases was determined. All four genes were expressed in all samples, apart from *Tmprss11D* in the day 0 mock-infected cells. *Tmprss2* is a membrane-spanning protease that plays a role in the

infectivity of IAV. *Tmprss2* and *Tmprss4* were the most highly expressed genes. The expression of *Tmprss4* and *Tmprss11d* increased in the infected mTECs at both time points.

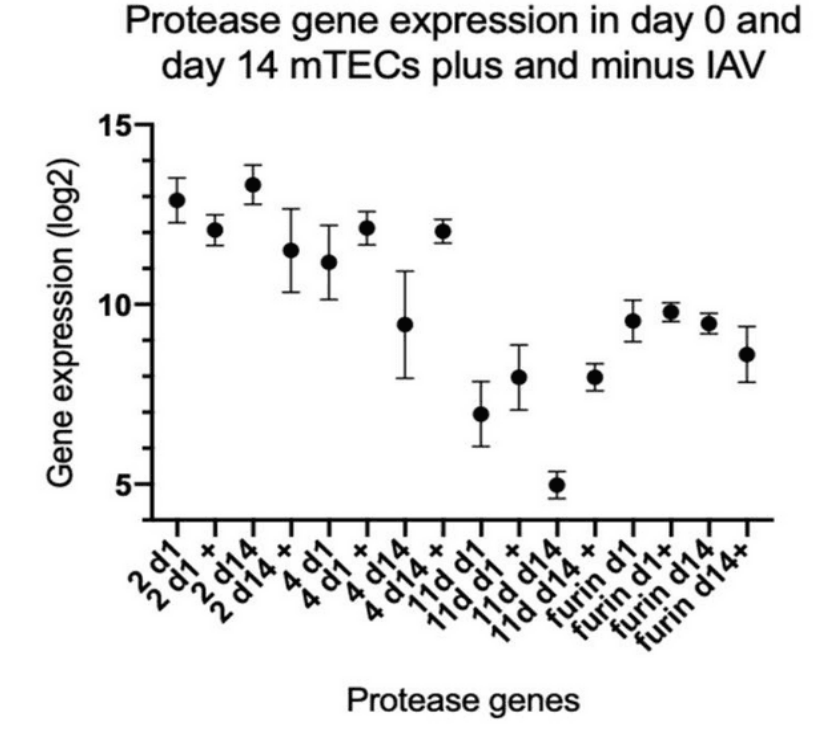


Figure 4.19. Gene expression of membrane-spanning proteases during IAV infection

The expression data for *Tmprss2* (2), *Tmprss4* (4), *Tmprss11D* (11d) and furin were extracted from the array data and are plotted as means and SDs. d = day of study; + = IAV-infected sample.

4.3 Discussion

IAV is a major cause of mortality and morbidity worldwide, particularly relative to respiratory tract infections. The exact mechanisms by which the virus infects respiratory epithelial cells and how the host protects these cells are not yet fully understood. The study hypothesis was that BPIFA1 plays a direct role in epithelial cell infection.

We initially showed that differentiated mTECs could serve as a model for IAV infection, as shown by the increased IAV-NP staining in the infected mTECs over time (Akram et al., 2018). However, the BPIFA1-positive cells showed less infection and were not infected with IAV. This led to the conclusion that BPIFA1 contributes to the protection of the airway epithelium from infection via

its release from secretory cells and that BPIFA1-positive cells are somewhat protected from initial infection.

Tracheal cell cultures from mice were obtained and cultured at the ALI to create well-differentiated mTECs to test the study hypothesis. The impact of BPIFA1 on virus infection in the mTECs was then examined. As shown in Figures 4.1 and 4.2, the reaction of the virus (0.5 MOI and 5.0 MOI) with BPIFA1 was tested for 48 and 72 h to determine the number of infections in both non-ciliated and ciliated cells. These findings are in line with the previous reports by Gerlach et al. (2004) and Quirouette et al. (2020).

However, notably, the present results are limited by the small number of replicates (only 2–3) and the variation between the different samples. Further studies with larger numbers of replicates from primary cells are mandatory to fully understand the role of BPIFA1 in IAV infection.

For investigating the genome-wide transcriptional response of the mTECs to IAV infection, RNA samples were initially taken at a single time point and MOI. Many of the genes induced were either not expressed or lowly expressed in the uninfected mTECs. The ALI day 14 infected mTECs induced a significant ISG response that resulted in the identification of the ISG gene signature. This experiment also potentially identified *Lypd8*. In general, IAV titres are reduced by *Bpifa1 in vivo*, and transmission is decreased as *BPIFA1* prevents the entry of IAV into normal epithelial cells. IAV infects both undifferentiated and differentiated mTECs, indicating that the cell specificity is unclear.

In addition to the findings that the differentiated mTECs were susceptible to IAV infection, the study also showed that the undifferentiated mTECs could also be infected, although to a lesser extent. The expression of *Bpifa1*, *Oaz-1*, *Tekt1*, *Infl2* and *Slfn4* was analysed in the infected mTECs. The *Lypd8* gene was also studied, as it appears to be induced by IAV and may play an undiscovered role in IAV infection. Figure 4.6 shows a decrease in *Tekt1* expression in the infected cells compared with the controls and a slight decrease in *Bpifa1* expression in the infected cells. The expression of *Oaz1* was relatively unchanged during infection. In contrast, *Ifnl2*, *Slfn4* and *Lypd8* showed robust expression in the infected cells at 24 h and remained elevated at 48 and 72 h, confirming, and validating the RNAseq data. By 72 h, there was a slight, but non-significant,

decline in the expression of *Tekt1*, *Bpifa1* and *Oaz1* in the infected cells compared with the controls.

The gene IfnI2 showed a high expression, leading to an elevated mRNA expression of *IFN-8*, *IL-29* (*IFN-y1*) and *IL-28A* (*IFN-y2*). Generally, AT2 epithelial cells are the main source of type II IFN proteins and this is demonstrated in Figure 7 (Wang, Oberley-Deegan et al. 2009). *Lypd8* is expressed in intestinal and colonic epithelial cells and plays a crucial role in bacterial infections in the gut by binding to flagellated bacteria and blocking bacterial invasion of the colonic mucosa (Okumura, Kurakawa et al. 2016). In a previous study, *Lypd8* in HEJ mice was upregulated for 1 day, suggesting that it may contribute to RSV resistance through regulation of cellular growth, epidermal development, mucosal protection and anti-inflammatory processes (Marzec, Cho et al. 2019).

Following infection, the transcription level of different genes in mTECs would be expected to change over time. In this regard, a comparative transcriptional analysis of the day 1 and 14 mTECs infected with IAV was performed. However, as shown in Figure 4.10, the extent of infection varied based on the amount of virus present. Indicating that the level of virus determines the extent of infection, as both differentiated and undifferentiated cells can be infected. Both the day 1 and 14 cells induced significant levels of ISGs, but the day 14 cells had a higher level of induction than the day 1 cells. Such differences were to be expected, as the level of virus and number of IFN genes that would be induced generally increase over time. In the analysis, most genes had similar expression patterns to their earlier phases, except for *Lypd8*, which showed a high expression after infection, an upregulation on the first day and a reduced expression during the second and third replication phases. In contrast, *Ccl5*, *Pydc4* and *Oasl1* showed the highest expression on day 14. Taken together, differential gene expression is critical for host cell responses; therefore, genes whose expression is increased by day 14 can be expected to counter the infection level.

The group of genes whose expression can be important to induce the immune response to IAV are those encoding membrane spanning proteases (Shen, Mao et al. 2017). In this study, the expression of protease genes during infection and mock infection conditions on days 1 and 14 was analysed, and the results showed that some protease genes had a high expression, while

others had a low expression at the same time. The expression of trypsin and matrix metalloproteases increased in various endothelial cells. The interaction between host cellular factors, influenza virus, cytokines and proteases is the major mechanism behind a pathologically increased permeability of blood vessels and failure of major organs in severe influenza cases (Gopal, Marinelli et al. 2020). Thus, *in vitro* mTEC models accurately mimic the response of the tracheal epithelium to viral infection. In this study, both the differentiated and undifferentiated mTECs were affected by IAV, and the extent of IAV infection was dependent on both time and dosage; further, the infection did not require differentiation to occur. However, the level of infection varied, with the undifferentiated cells being less affected than the differentiated cells. IAV infection had been shown to occur in BPIFA1-negative secretory cells and to be present in small amounts in ciliated cells. Limited information is currently available on the *Lypd8* protein in mice, but it blocks flagellated microbiota, and its levels are higher at the start of infection (Okumura, Kurakawa et al. 2016).

4.4 Summary

The *in vitro* mTEC model shows sensitivity to IAV infection and resembles the original tracheal epithelium. IAV infects both differentiated and undifferentiated mTECs, although the cell specificity remains unclear. IAV regulation of genes is linked to the differentiation status in some cases. The results show that IAV infection can occur in both differentiated and undifferentiated mTECs.

Chapter 5: Generation of FLAG-tagged BPIFA1-VR1255 Constructs for functional studies

5.1 Introduction

The exact function of *BPIFA1* remains elusive, but there are several proposed roles for the protein. Evidence suggests that BPIFA1 primarily acts as a defence mechanism for the RS. The various defensive functions include regulating the ion transport and regulating the surface tension of the airway secretion (McGillivary 2010, Rollins, Garcia-Caballero et al. 2010, Garland, Walton et al. 2013, Liu, Di et al. 2013), some antimicrobial activities such as decrease in microbial growth (Chu, Thaikoottathil et al. 2007, Chu, Gally et al. 2010, Gally, Di et al. 2011) and some chemotactic and immunomodulatory properties (Gakhar, Bartlett et al. 2010, Liu, Di et al. 2013). In my host laboratory, *BPIFA1* has been previously shown to play a role in the host defence against IAV infection. The data may support the role of BPIFA1 in respiratory host defence, but the exact underlying mechanism is still not understood.

BPIFA1 has structural similarity with the BPI/LBP protein superfamily (Bingle and Craven 2002). This initial modelling result has been further investigated by groups that were able to determine the crystal structure of the protein confirming the similarity of BPIFA1 with other proteins of this family (Garland, Walton et al. 2013, Ning, Wang et al. 2014). Further work has also shown that the control of cleavage and activation of ENaC are mediated by the BPIFA1 protein, and the region responsible for this lies in amino acids G22–A39. This region is also known as the S18 region (Garcia-Caballero, Rasmussen et al. 2009, Rollins, Garcia-Caballero et al. 2010, Garland, Walton et al. 2013).

Considering current research findings on this protein, it has been proposed that BPIFA1 functions in airway host defence and does so by interacting with pathogens in the airways. Previous work from the researcher's laboratory suggests that BPIFA1 performs a protective role against influenza A and other pathogens. It seems likely that the ability of the protein to do this is attributed to the specific regions of the protein.

The BPIFA1 protein is seen among all mammalian species and has been shown to contain an N-terminal domain that is divergent among species, which seems to confirm some functional ability to the protein (Britto and Cohn 2015).

This chapter describes the bioinformatics analysis of BPIFA1 across species and the generation of a range of BPIFA1 expression constructs that can be used to understand the role of specific regions of the protein. The objective of this chapter was to understand this functionality.

BPIFA will be described in various species with a focus on the S18/N-terminal region of the protein. Based on the findings, several expression constructs that could be used to generate the recombinant BPIFA1 protein for functional studies were generated and validated.

5.2 Results

5.2.1 Sequence Analysis of BPIFA1

As the previous functional work on *BPIFA1* and IVA in host group has been undertaken in mice, the present work also focused on this protein.

The divergence seen in the N-terminal region of the *BPIFA1* protein among different species (particularly in rodents) was discussed in the introduction section. Several multiple sequence alignments were then performed to further study the region of the protein.

Initially, a Basic Local Alignment Search Tool (BLAST) search was conducted using the reference sequence of the mBPIFA1 protein (NP_035256.2) against the NCBI non-redundant protein database. The schematic output is shown in Figure 5.1. In this output, sequence dissimilarity is shown by red, and spaces are shown in white. As only the top 100 sequences are shown, the alignment does not show the human protein. Blue brackets show where the sequences are inserted into the alignment. Based on the findings, the most significantly different region is the N-terminal region of *BPIFA1*, which is mostly seen in several rodent species.

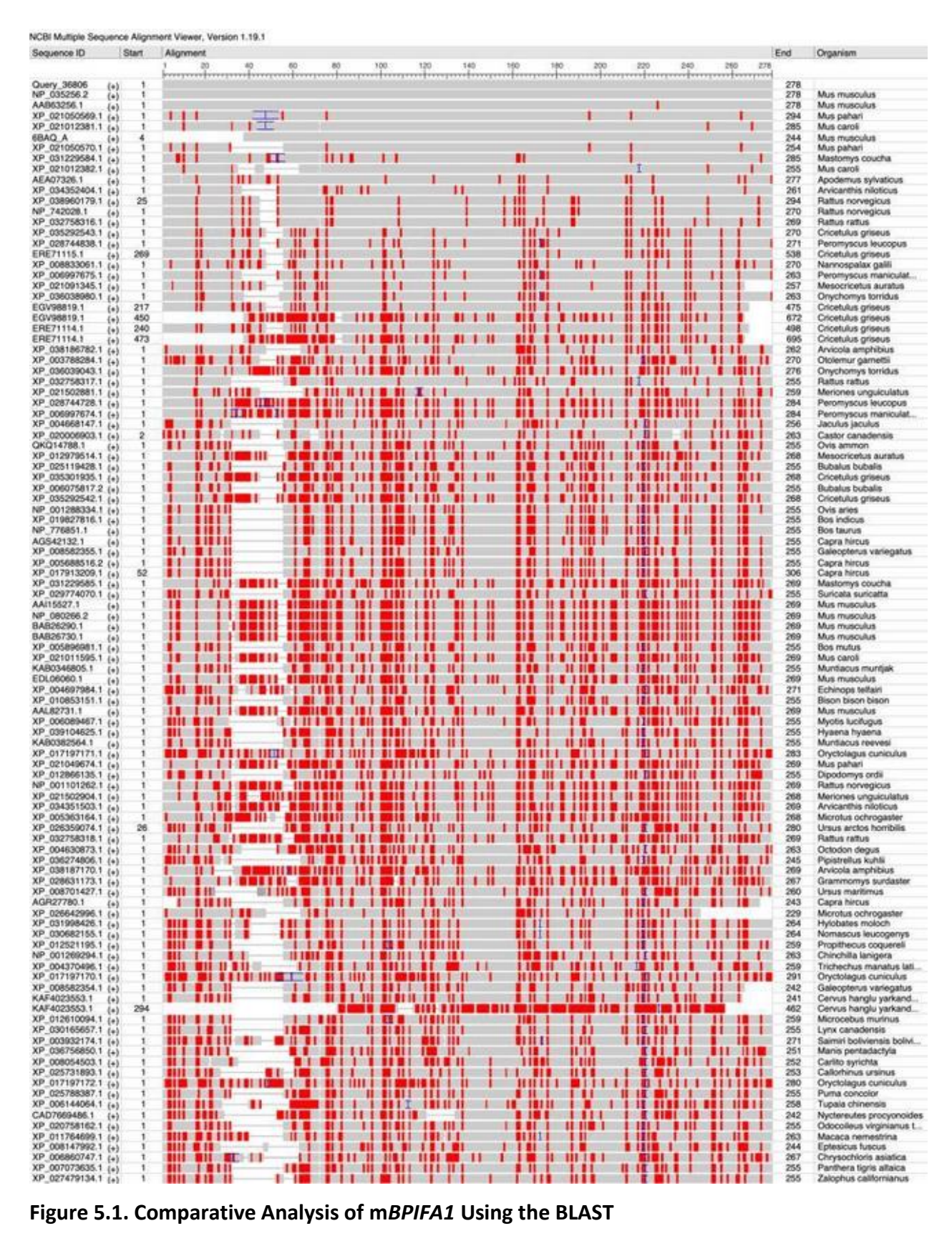


Figure 5.1. Comparative Analysis of mBPIFA1 Using the BLAST

A comparative analysis of mBPIFA1 was conducted using the BLAST. The analysis was performed on the NCBI non-redundant protein database. The results are displayed with different amino acids in red, gaps in the sequence in white and insertions in blue brackets.

The BPIFA1 sequences were compared across different rodent species using a multiple sequence alignment. The source of these sequences was either the NCBI or Ensembl. The comparison showed that compared with BPIFA1 the house mouse (*Mus musculus*), BPIFA1 from the Ryukyu mouse (*Mus caroli*), Gairdner's shrew mouse (*Mus pahari*) and Algerian mouse (*Mus spretus*) had insertions within their sequences, with 8, 16 and 16 extra amino acids, respectively. In contrast, BPIFA1 from the deer mouse (*Peromyscus maniculatus bairdii*), wood mouse (*Apodemus sylvaticus*) and Norway rat (*Rattus norvegicus*) had sequences that were 16, 8 and 8 amino acids shorter, respectively.



Figure 5.2. Alignment of the N-terminal region of selected rodent BPIFA1 proteins

A multiple sequence analysis was undertaken with a selection of rodent *BPIFA1* proteins using Clustal Omega. The alignment shows the N-terminal region of the proteins. Colours of the amino acids are based on their physicochemical properties: red = small + hydrophobic, blue = acidic, magenta = basic, green = hydroxyl + sulfhydryl + amine.

Figure 5.2 identifies these eight amino acid blocks as (L/P)PLPL(N/G)QG repeats in the N-terminal region of *BPIFA1*, which seem to be specific to rodents, because their occurrence is seen in the

BPIFA1 proteins of wood mice, deer mice and rats. This repeat region is not present in the crystal structure of m*BPIFA1*, which means that it may be unstructured (Little and Redinbo 2018).

5.2.2 BPIFA5 is a close paralogue of BPIFA1 but does not conserve the N-terminal regions

BPIF proteins show relatively low sequence similarity between paralogues (Bingle, LeClair et al. 2004); however, BPIFA5 in rodents is an exception. BPIFA5 is a lineage-restricted BPIFA protein that is found in some rodents (LeClair, Nomellini et al. 2004) and that has arisen from a recent gene duplication event (see the phylogenetic tree in Figure 5.3). Mouse BPIFA1 and BPIFA5 are 62% identical (LeClair, Nomellini et al. 2004). Figure 5.4 shows a multiple sequence alignment with mouse, rat and human BPIFA1 and mouse and rat BPIFA5. This figure shows the overall conservation of the two types of proteins and that the N-terminal region showed the greatest difference between BPIFA1 and BPIFA5. Mouse BPIFA5 is 270 amino acids long, whereas BPIFA1 is 278 amino acids long. The alignment also shows three predicted N-glycosylation sites in mBPIFA, two of which are conserved in the rat protein but are absent from hBPIFA1.

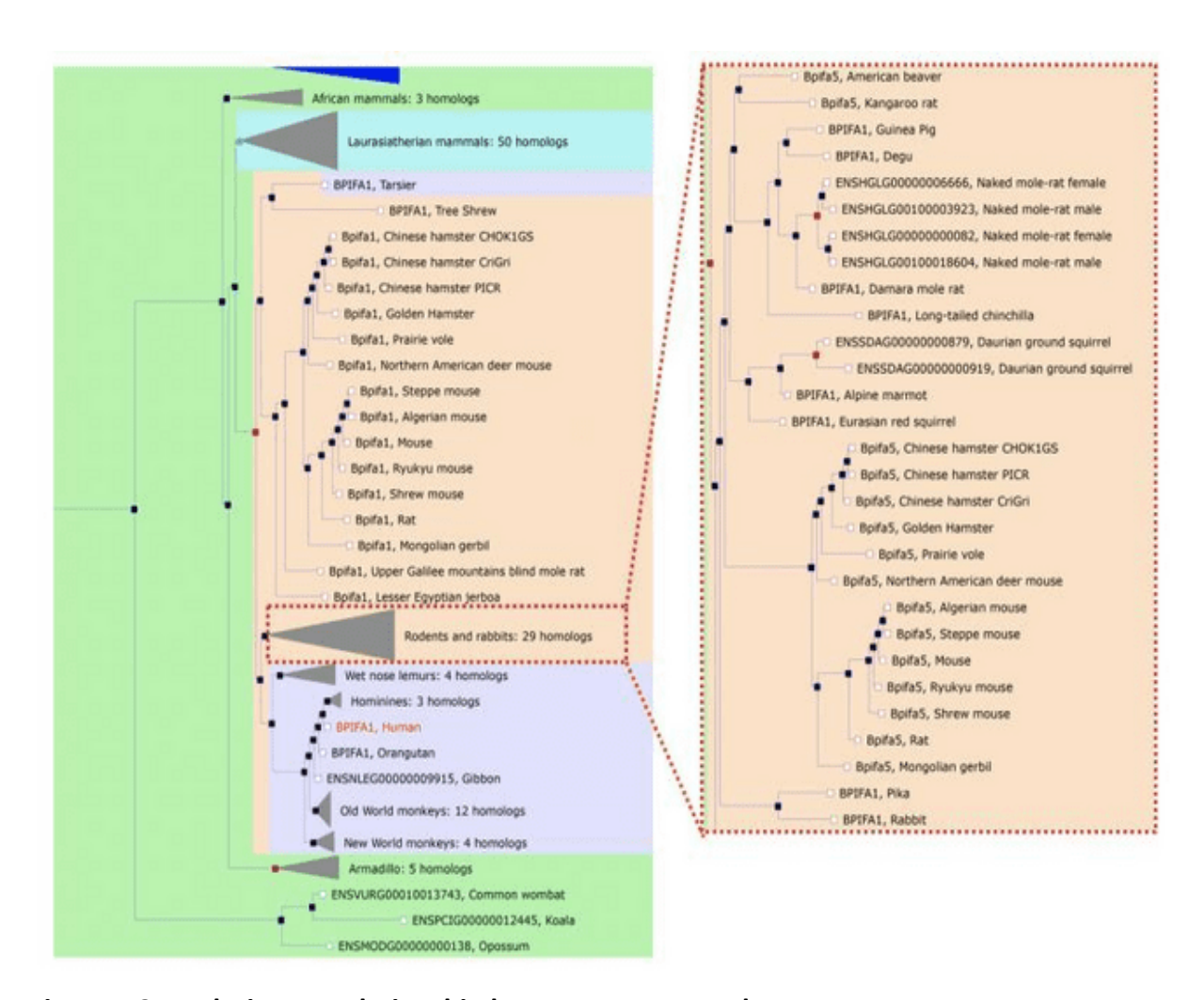


Figure 5.3. Evolutionary relationship between BPIFA1 and BPIFA5

A phylogenetic tree of a subportion of the BPIFA1 proteins was obtained from Ensembl (https://www.ensembl.org/). The expansion of the tree containing the BPIFA5 subtree is highlighted (red dots).

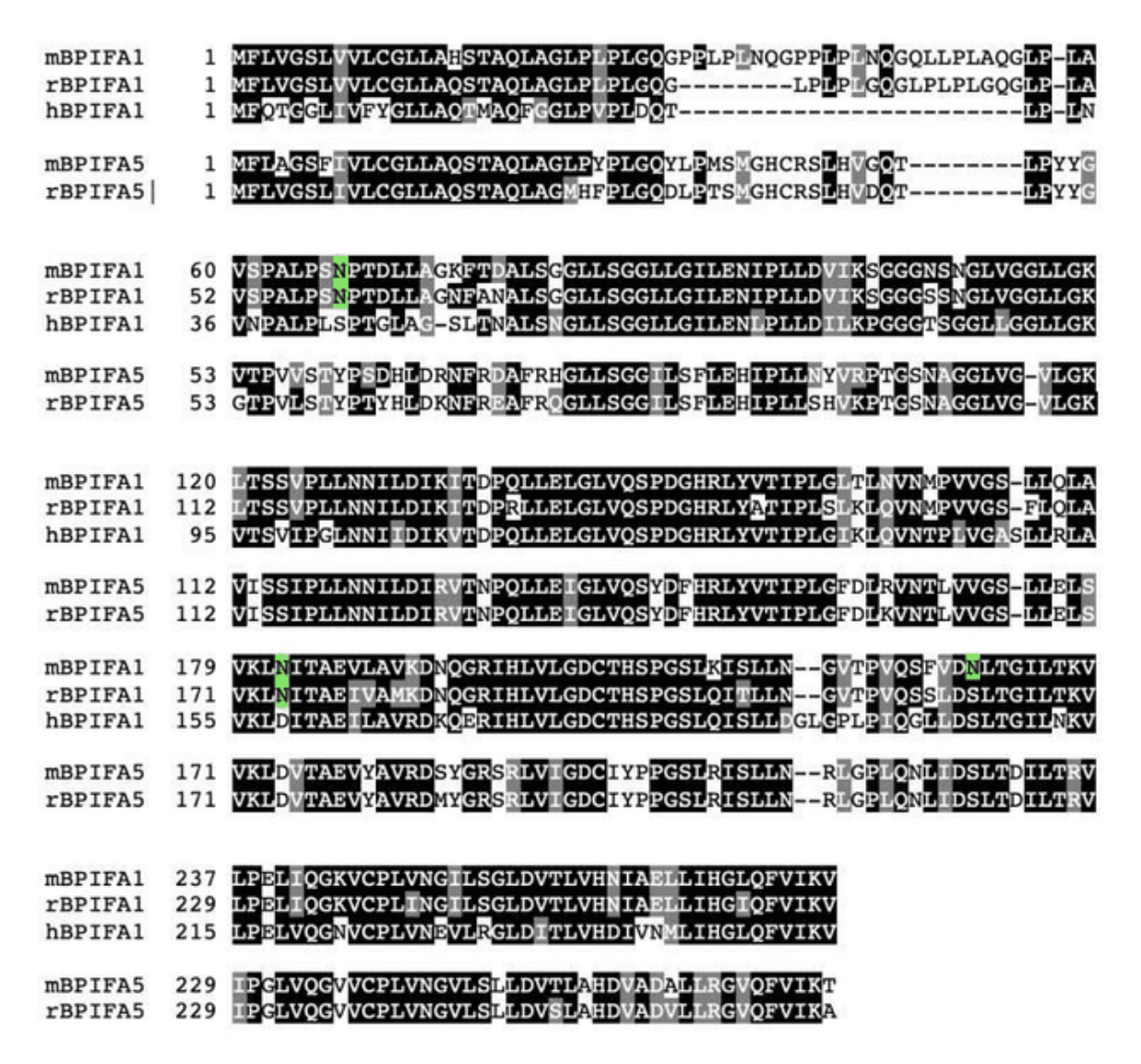


Figure 5.4. Lack of conservation of the N-terminal domains between rodent *BFIFA1* and *BPIFA5* A multiple sequence alignment of mouse, rat and human BPIFA1 and mouse and rat *BPIFA5* was performed using Clustal Omega. White letters on a black background represent the identical residue, whereas those on a grey background represent conserved residues. Gaps (-) are introduced to reach the maximal alignment. Green highlights the N-glycosylation sites.

These observations suggest that *BPIFA1* and *BPIFA5* are unlikely to share functions, which is consistent with their differential expression patterns. *BPIFA5* is expressed in the papillary structures of the tongue (LeClair, Nomellini et al. 2004), while BPIFA1 is abundant in the airways.

5.2.4 Generation of FLAG-Tagged BPIFA1 constructs in the VR1255 Vector

After the establishment that the N-terminal domains of mBPIFA1 were distinct and given the importance of the same region in the human protein, recombinant murine proteins were designed for this study. Four different constructs were utilised as shown in Figures 5.5 and 5.6, including a full-length protein, a short-deletion protein without the expanded rodent-specific region, a long-deletion protein that omitted the same region and the S18 flanking region and a mutant protein with the three N-glycosylation sites replaced by the amino acids present in the human protein. Additionally, a similar protein construct for human *BPIFA1* that had already been created in the laboratory was used. Figure 5.6 presents the expected protein products of the expression constructs. The Flag tag was added to the C-terminal end of the protein, as it was expected that this region would not impact the structure of the proteins.

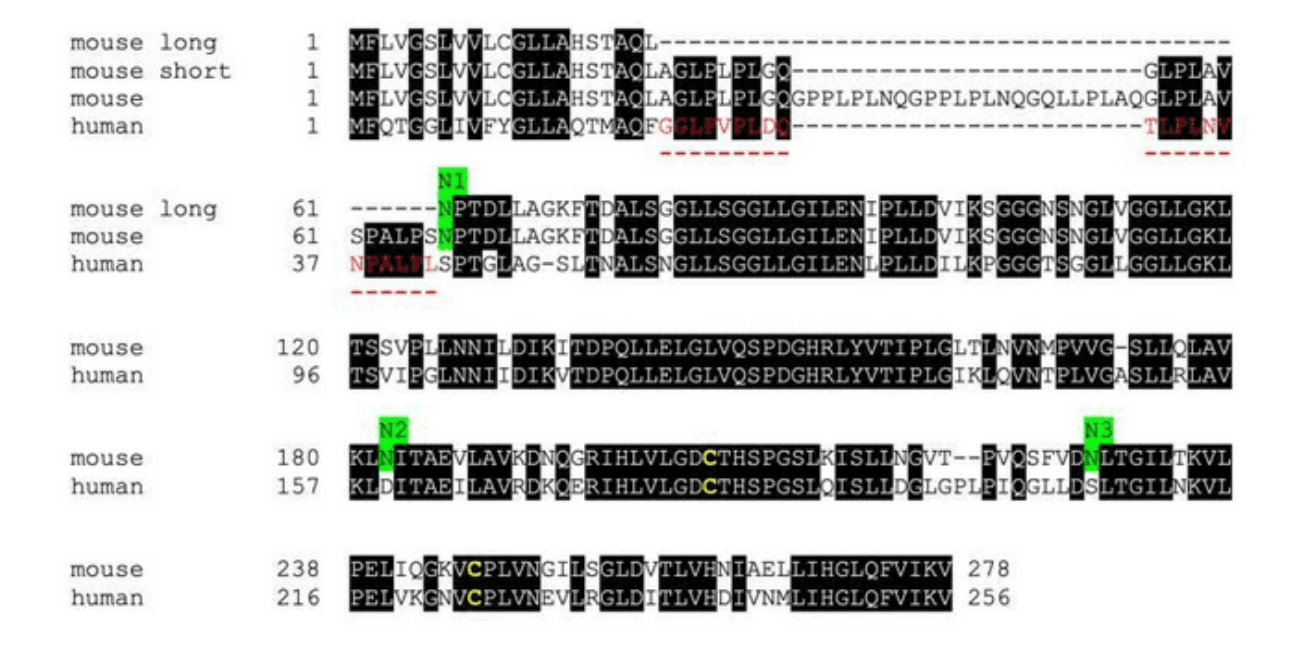


Figure 5.5. Sequences of BPIFA1 for construct production

This figure shows the *BPIFA1* sequences for the FLAG-tagged expression construct. The S18 region of the human protein is shown in red and the N-glycosylation sites in green.



Figure 5.6. Schematic diagram of the BPIFA1-FLAG constructs

The sequences of hBPIFA1—FLAG, *mBPIFA1*, *mBPIFA1* Gly Mut, mBPIFA1 SD and mBPIFA1 LD are displayed. The FLAG tag at the C-terminus is indicated in red, while the glycosylation sites are represented by the letter 'G. Gly Mut, glycosylation mutant; SD, short deletion; LD, long deletion

5.2.5 Production of VR1255 DNA for cloning reactions

BPIFA1 constructs were made in the mammalian expression vector VR1255 (Figure 5.7) (Jayawardane, Russell et al. 2008). Initially, VR1255 was produced as a vector to deliver a DNA vaccine (Hartikka, Sawdey et al. 1996). However, it has been employed for the synthesis of recombinant proteins in high quantities (Hartikka, Sawdey et al. 1996, Norman, Hobart et al. 1997).

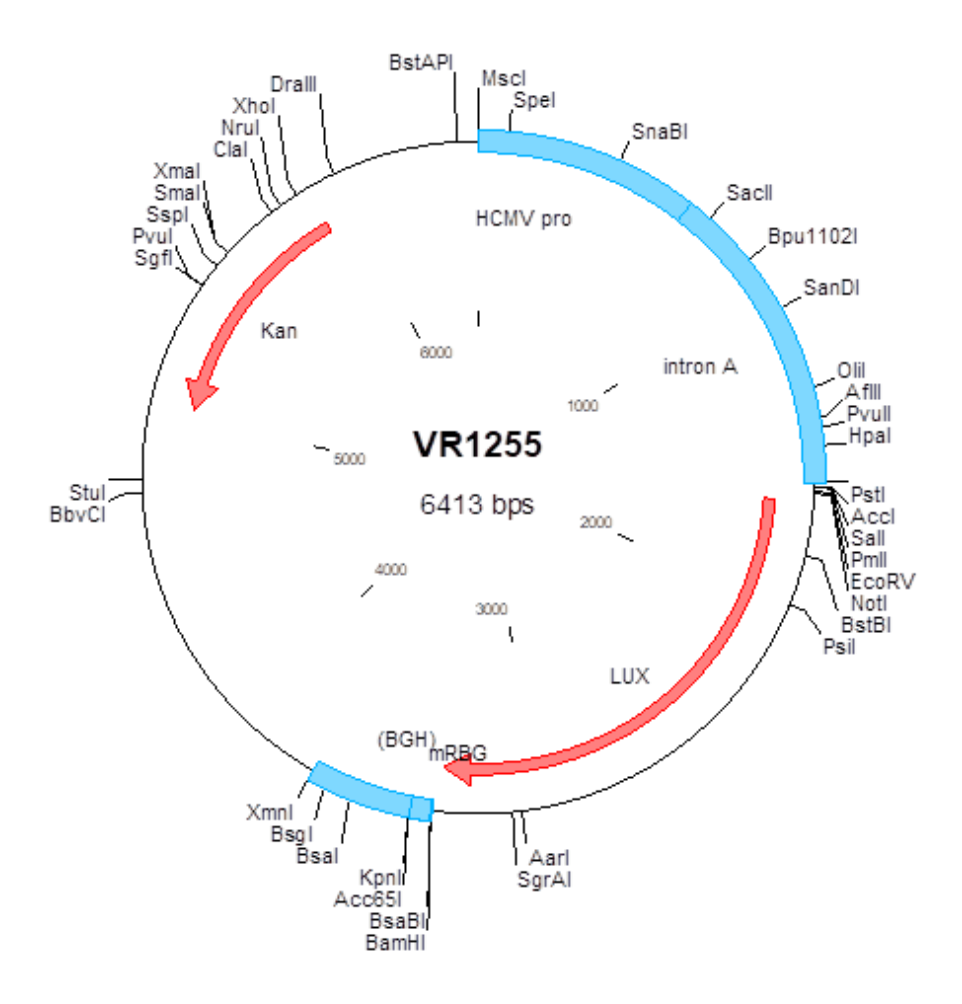


Figure 5.7. Map of the mammalian VR1255 expression plasmid

The luciferase sequence can be removed by digestion with BamHI and Not1.

After the VR1255 DNA was transformed into bacteria (*E. coli*), a maxi-prep was performed to obtain enough DNA for cloning. The plasmid was digested using NotI and BamHI enzymes to remove the luciferase sequence, producing a linear DNA that was suitable for cloning by gel recovery. Figure 5.8A shows the results of the digestion, with visible bands of 1652 bp and 4761 bp. The cut vector was recovered from the gel, and the linearised VR1255 DNA fragment sized

4761 bp was visualised through agarose gel electrophoresis to assess the quality of the DNA (Figure 5.8B).

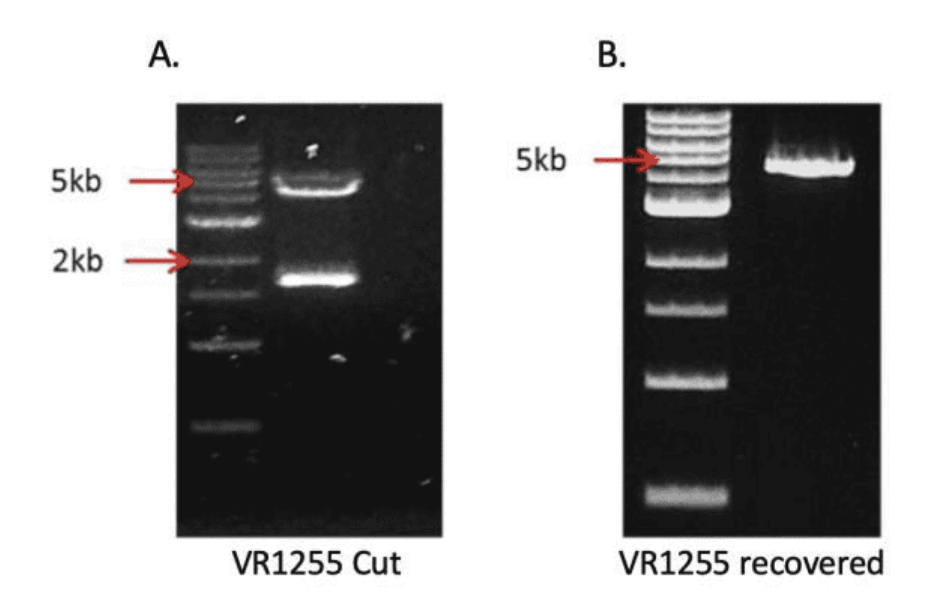


Figure 5.8. VR1255 DNA digest for initiating cloning

NotI and BamHI enzymes were used for cutting a VR1255 maxi-prep. Consequently, fragments sized 1652 bp and 4761 bp were resolved on the gel (A). The larger vector fragment was recovered from the agarose gel, and a second gel was used with the extracted plasmid DNA to assess its quality (B)

5.2.6 Generation of the mouse full-length *BPIFA1*—FLAG construct

The full-length mouse *BPIFA1* sequence was generated using RT-PCR with RNA from the differentiated mTECs. The RNA was treated with DNase to remove any genomic DNA and then reverse-transcribed into cDNA. PCR was then performed using the primer pairs shown in Figure 5.9.

mA1 Not I Forward:

Not I Kozak

5'-ATGCGGCCGCCGCCACCATGTTTCTAGTTGGGAGCCT-3'

mA1 Stop Reverse:

BamH I Stop FLAG tag

5'-GCGGATCCTTACTTGTCATCGTCCTTGTAGTCAACTTTGATGACAAACTGTAG-3'

Figure 5.9. Primers for the generation of the mBPIFA1-FLAG construct

The primer sequences include NotI and BamHI sites, with the forward primer containing a Kozak sequence (highlighted in yellow) and the reverse primer including a FLAG tag (highlighted in cyan) and a stop codon (highlighted in green). The Kozak sequence, located upstream of the start codon in a mRNA, is known to enhance the expression of a protein in some cases. The Kozak sequence is recognised by the ribosome and helps to initiate translation efficiently, leading to increased expression of the target protein. However, the impact of the Kozak sequence on the expression level can vary depending on many factors, including the specific organism, cell type and presence of other regulatory elements in the mRNA.

After RT-PCR, the *BPIFA1* fragment was cloned into pCRII-TOPO and fully sequenced to confirm its identity. The product was then digested from the plasmid using NotI and BamHI and subcloned into the pre-cut VR1255 vector. The identity of the cloned products was confirmed through minipreps and digestion, followed by full sequencing to ensure completeness. The original cloning of full-length *BPIFA1* was performed by Renata Caikauskaite.

5.2.7 Generation of FLAG-Tagged mBPIFA1 Mutant Constructs in VR1255

SDM was performed using the Q5 Site-Directed Mutagenesis Kit (NEB) to induce mutations in the mBPIFA1 sequence as outlined in Figure 5.6. The intention was to introduce two deletions around the N-terminal domain and to allow the removal of the three N-glycosylation sites. Following the

manufacturer's guidelines, NEBaseChanger was used to generate five mutagenic PCR primer pairs (http://nebasechanger.neb.com/). Table 5.1 shows the primer sequences. The initial amplification step was performed using a specific primer pair and the sequenced VR1255 mBPIFA1—FLAG construct DNA as a template as outlined in the materials and methods section. The resulting products were recovered following transformation, and mini preps of the plasmid DNA were produced and sequenced to determine whether mutations had been made.

It was initially intended to introduce three separate mutations at the N-glycosylation sites through PCRs in a sequential manner, with each mutation being introduced in an iterative manner, so that different combinations of glycosylation sites could be generated.

Table 5.1. Primer sequence used in PCR for site-directed mutagenesis -

m <i>BPIFA1</i> SDM1R	m <i>BPIFA1</i>	GCTGGGTTACAGCCAAA
m <i>BPIFA1</i> SDM1F	m <i>BPIFA1</i>	ACTGCCTTCAAAACCCAC
m <i>BPIFA1</i> SDM2R	m <i>BPIFA1</i>	GCCAATTGCAAAAGACTT
m <i>BPIFA1</i> SDM2F	m <i>BPIFA1</i>	TGTGAAGCTGAAAATTAC
m <i>BPIFA1</i> SDM3R	m <i>BPIFA1</i>	CTTTGAACAGGAGTGACT
m <i>BPIFA1</i> SDM3F	m <i>BPIFA1</i>	CTTTTTAGACAAACTCACA
m <i>BPIFA1</i> Del1R	m <i>BPIFA1</i>	CAGCTGTGCTGTG
m <i>BPIFA1</i> Del1F	m <i>BPIFA1</i>	AATCCCACAGATCTTCTTG
m <i>BPIFA1</i> Del2R	m <i>BPIFA1</i>	CTGGCCCAGGGGCAATGG
m <i>BPIFA1</i> Del2F	m <i>BPIFA1</i>	GGTCTGCCTTTGGCTGTAA

The results of the SDM experiments were variable. I was unable to introduce single mutations into the N-glycosylation sites of mBPIFA1—FLAG. PCR and transformation were undertaken on several occasions. Various annealing temperatures were determined from the technical datasheet and applied to attempt to optimise the PCR conditions.

However, even these changes did not yield any successfully mutated products. The SDM reactions to introduce the two deletions in *mBPIFA1*–FLAG was more successful. In both cases,

the required mutations were produced, which were confirmed by sequencing. An example of a sequencing reaction and the translation of the product are shown in Figure 5.10.

Given that I was unable to generate the required N-glycosylation site mutations via SDM, gene synthesis was used to generate these. Biomatik generated a single sequence in which the three glycosylation sites were mutated in the pBSK (+) simple, an amp resistance vector. They performed sequencing and restriction digestion for the verification of the mutant construct. The sequence incorporated mA1F1NotI and mA1RSTOP sequences identical to the PCR primers at each end of the mutant mBPIFA1 gene. The DNA of the synthesised product was double digested with NotI and BamH1, and the recovered product was cloned into the double-digested VR1255 plasmid. Recombinants were mini prepped and fully sequenced to confirm that the constructs were 100% correct.

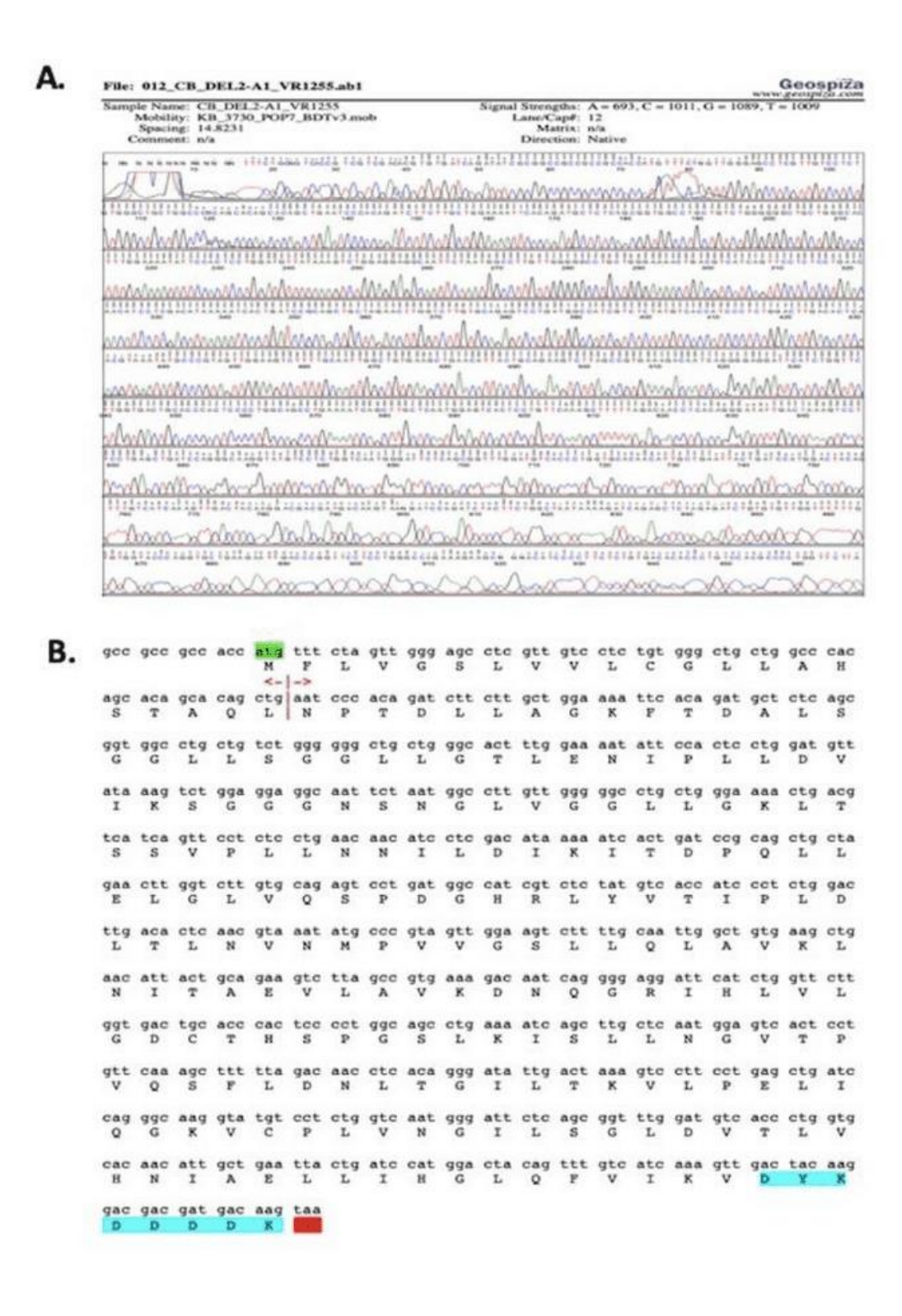


Figure 5.10. Sequencing of the mBPIFA1 long deletion clone from SDM

The sequencing plot from FinchTV is shown (A), and the translation of the final construct shows the deletion of the N-terminal region (red arrows), the FLAG tag and the start and stop codons (B). The peaks in panel A indicate the quality of the sequencing.

5.2.8 Generation of Pig and M. pahari BPIFA1 Flag-Tagged Constructs

As it was previously shown that some rodents had longer N-terminal regions, and it was intended that the function of one of these longer proteins was to be investigated, the protein from *M. pahari* (Gairdner's shrew mouse) was selected. In the multiple sequence analyses, some species appeared to be even shorter than the human protein in this region. As an example of one of these shorter sequences, the pig (*Sus scrofa*) sequence was also selected. Pig *BPIFA1* is 241 amino acids long. The multiple sequence alignment of the four sequences as well as the position of the eight amino acid repeats is shown in Figure 5.11.

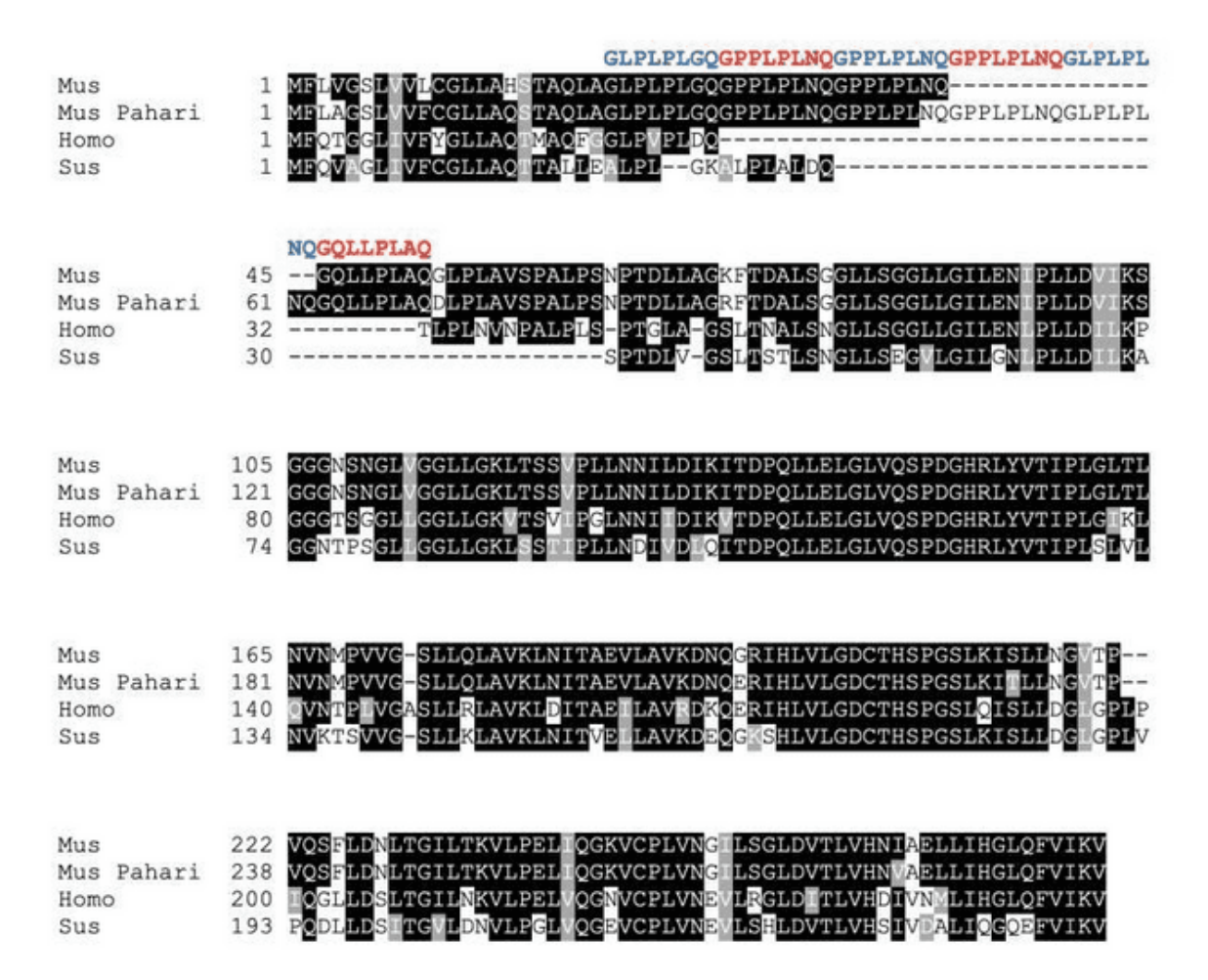


Figure 5.11. Alignment of BPIFA1 proteins for functional analysis

Mouse (mus), *Mus pahari*, human (homo) and pig (sus) *BPIFA1* were aligned. The alternating blue and red sequences identify the LPLPL repeat motifs.

The FLAG-tagged pig and *M. pahari BPIFA1* sequences were synthesised by Biomatik in the pBSK (+) simple vector. Both sequences contained a 5' *Not*I and Kozak sequence, and the 3' end had an in-frame FLAG tag, a stop codon and a *Bam*HI site. The DNA of both synthesised products was digested with *Not*I and *Bam*H1 and the product cloned into the double-digested VR1255 plasmid. Recombinants were miniprepped and fully sequenced to confirm that the constructs were 100% as expected.

After all required constructs were successfully generated and validated, they were maxi-prepped and underwent a diagnostic digest prior to use in the transfection assays (Figure 5.12).

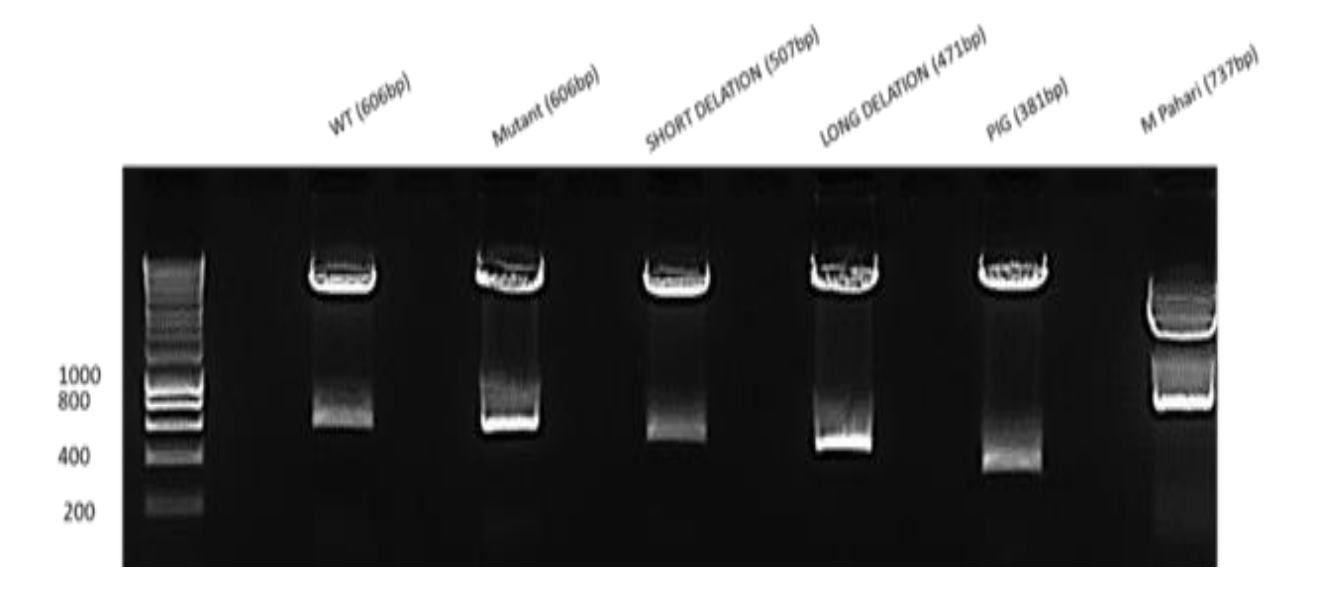


Figure 5.12. Diagnostic Digest of BPIFA1 Expression Constructs

Restriction digests were undertaken with WT mBPIFA1, long-deletion mBPIFA1, short-deletion mBPIFA1, glycosylation mutant mBPIFA1 and pig BPIFA1 with PstI, while Mus pahari BPIFA1 was cut with HindIII and NotI.

5.2.9 Transfection of the BPIFA1-VR1255 plasmids into HEK Cells

Transient transfections of HEK293T cells were performed using all FLAG-tagged *BPIFA1*–VR1255 constructs to produce recombinant proteins. HEK293T cells were selected for this purpose owing to their extensive use in the laboratory for this type of experiment. The transfections were conducted using DMEM containing 10% foetal bovine serum. An EGFP plasmid was also included in all transfection experiments as a marker, allowing the visualisation of successful transfections by imaging green cells using a ZOE fluorescent cell imager (Bio-Rad). Figure 5.13 demonstrates the successful transfection of the DNA into HEK293 cells as indicated by the green fluorescence in each image. The cells were observed 24 h after transfection with WT m*BPIFA1*.

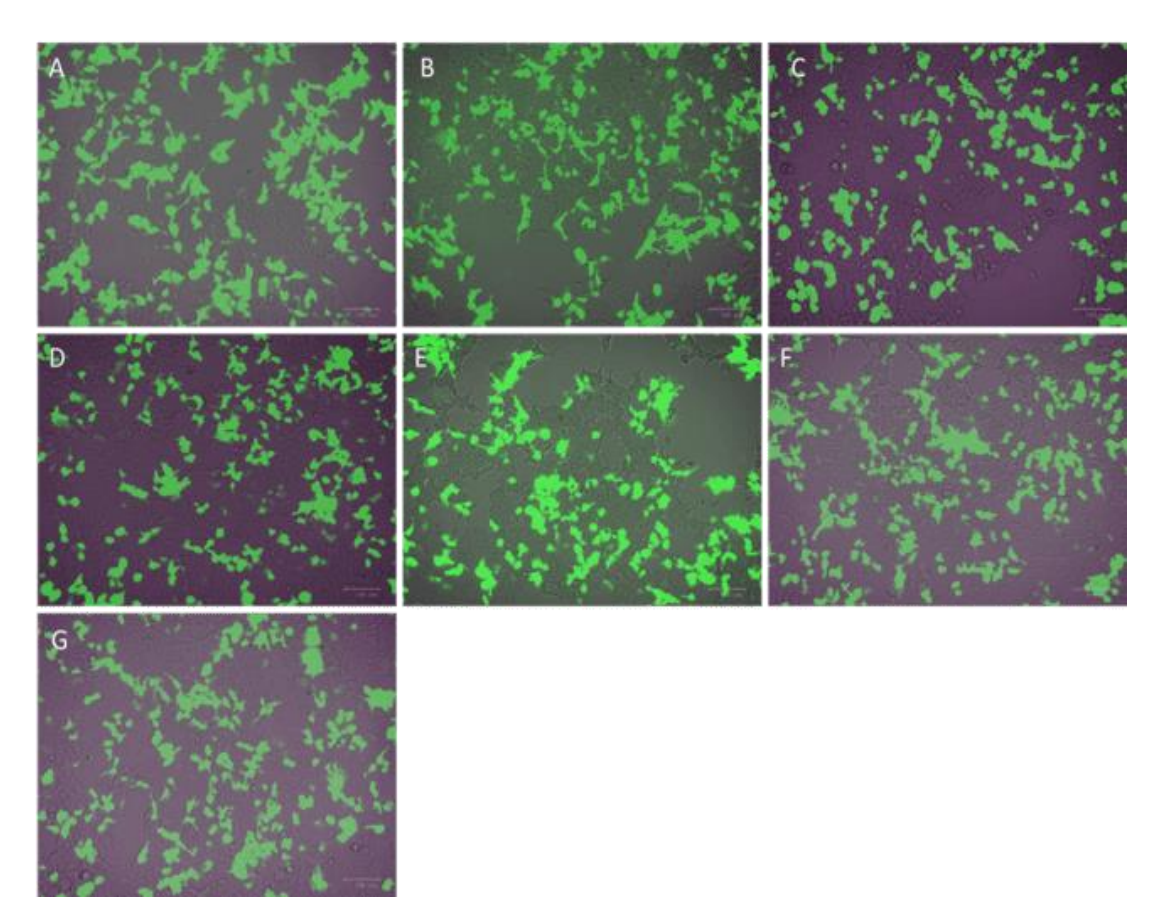


Figure 5.13. Transient transfections of HEK293T cells

Transfection of the cells was monitored based on the GFP expression as an indicator of DNA uptake by the cells. The transfections included (A) GFP as a control, (B) WT mBPIFA1, (C) long deletion, (D) glycosylation mutation, (E) short deletion, (F) Mus pahari and (G) pig. The images were captured after different time periods.

5.2.10 Production and secretion of the BPIFA1-FLAG recombinant proteins

The transient transfection of the HEK293T cells with the Flag-tagged *BPIFA1*–VR1255 constructs was undertaken to examine whether proteins were expressed and released into the conditioned media.

Initially, a T25 flask of HEK293T cells was transfected with FLAG-tagged m*BPIFA1*–VR1255 DNA to confirm that proteins were secreted. SDS-PAGE and western blotting were used to test the conditioned media. The media were collected 1, 2 and 3 days after the transfection, and the same total volume was added to the gel. Following SDS-PAGE, transfer of the blot proteins was

identified in the medium samples using an anti-FLAG antibody (Figure 5.14). In this experiment, the recombinant protein was detected in serum-supplemented conditions. The results showed the flag-stagged mBPIFA1 protein was secreted into the conditioned media for up to 72 h.

Figure 5.14. Secretion of mBPIFA1-Flag into HEK conditioned media

Equal volumes of conditioned media collected from transiently transfected HEK cells after 24, 48 and 72 h were western blotted using an antibody against FLAG as described in the materials and methods section.

Next, similar transient transfection experiments were conducted with each of the different BPIFA constructs under the same conditions, and the conditioned media were collected at 24, 72 and 96 h after transfection. Protein secretion in the media was identified by dot blotting followed by antibody detection with the Flag antibody (Figure 5.15). Immunoreactivity was detected in most of the samples, revealing that the recombinant proteins had been produced by the cells, although the amount of protein appeared to be variable. Notably, dot blotting does not provide any information about the size of secreted products. As this part of the study was conducted immediately prior to the COVID-19 lockdown, I was unable to run the samples on SDS-PAGE gels.

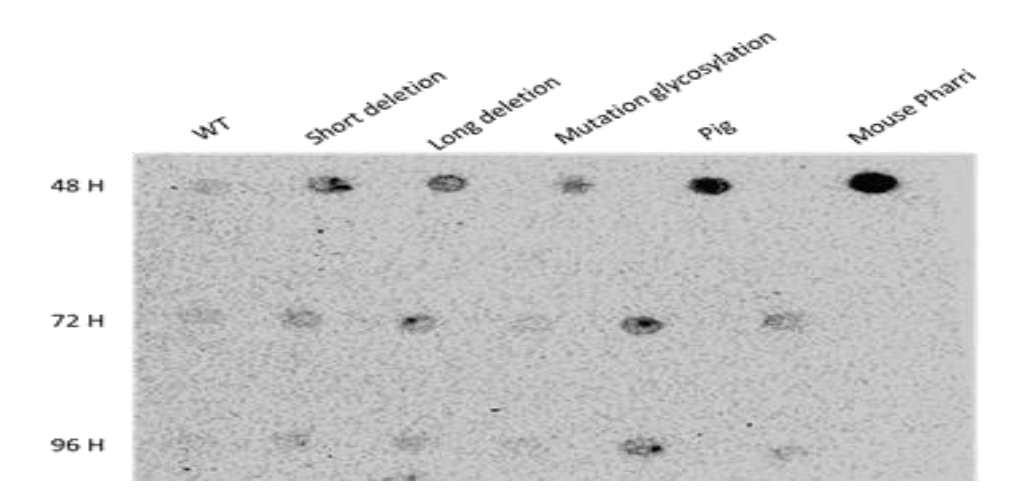


Figure 5.15. Secretion of different BPIFA1-Flag proteins into conditioned media

The conditioned media were collected from different transfections at 48, 72 and 96 h, and equal amounts were dotted onto a membrane. The proteins were then detected using the anti-FLAG antibody as described in the materials and methods section.

5.2.11 Planned experiments with recombinant proteins

As the expression constructs were generated, and the initial transfections were performed just prior to the COVID-19 lockdown, I was unable to complete the experiments planned to complete this chapter.

I had planned to investigate how the different proteins function to prevent IAV infections by doing the following:

- 1. Confirm the secretion of full-length BPIFA1 proteins using western blotting.
- 2. Scale up transfections into T75 or T175 flasks to produce more secreted proteins. These transfections would have been conducted in serum/phenol red-free media to remove potential contaminants that might interfere with the functional assay.
- 3. Evaluate the concentration and/or purification of the recombinant proteins. 10 kDa molecular mass cut off filters would have been used to concentrate the BPIFA1 proteins in the media and anti-Flag affinity resin used for batch-wise purification of the tagged BPIFA1 proteins.
- 4. Establish a functional assay to study how BPIFA1 proteins could influence IAV infection in mTECs. This assay would have been because undifferentiated mTECs can be infected by IAV as described in Chapter 4. Recombinant *BPIFA1* proteins would have been added to the IAV-infected undifferentiated mTECs, and the level of infection would have been monitored via staining and quantitation of IAV-NP or direct quantitation of the virus levels using qPCR. Dr Priyank Anujan showed the basis for this assay (Figure 5.16).

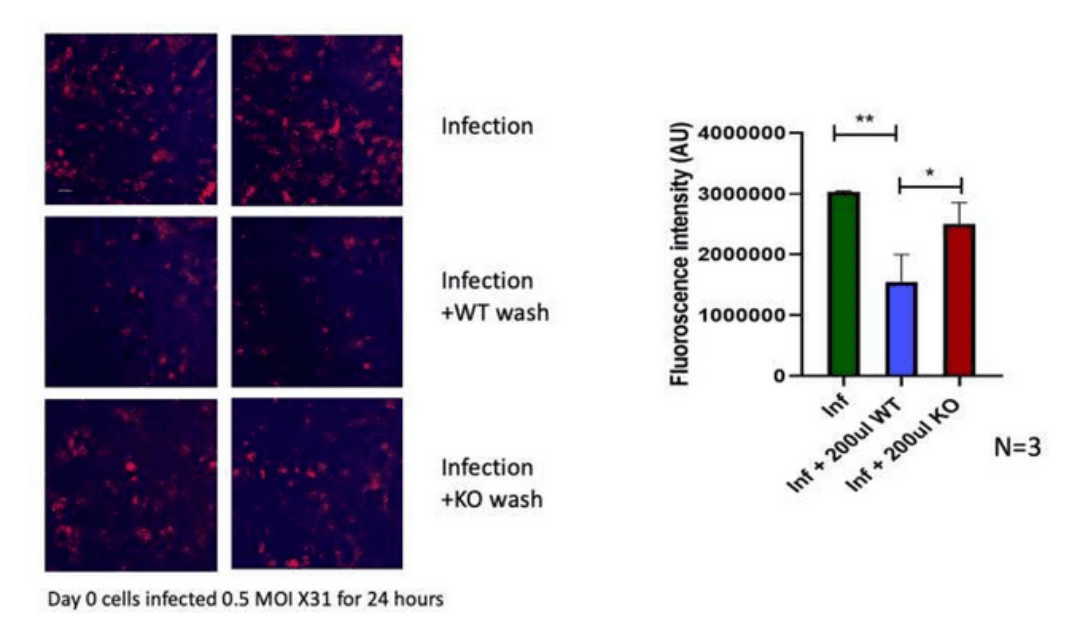


Figure 5.16. Development of a functional assay: BPIFA1 containing ALI secretions block IAV infection

In this experiment, day 0 undifferentiated mTECs were infected with 0.5 MOI of IAV X31, and apical washes from WT and *Bpifa1*-/- differentiated mTECs were added to the cells. IAV-NP was detected in the cells after 24 h, and the results were quantitated. The data suggest that BPIFA1 containing apical washes restrict IAV infection of mTECs (data from Priyank Anujan).

5. Identify the role of specific residues in *BPIFA1* using blocking peptides. Several specific peptides derived from the S18/N-terminal region of *BPIFA1* were generated. Initially, a peptide corresponding to the S18 region of human *BPIFA1* along with a scrambled peptide control was designed. Eight amino acid peptides corresponding to the three different repeats seen in the expanded N-terminal region of the mouse protein along with corresponding scrambled controls were also designed. These peptides would have been added to the functional assay outlined above.

Human S18 GGLPVPLDOTLPLNVNPA Human S18sc NLOVPPTVPLLNGPDLAN This corresponds to the S18 region of the human BPIFA1 protein Mouse 1st GLPLPLGO 1st sc LGPPOLLG Mouse 2nd GPPLPLNQ 2nd sc **PGPPQNLL** Mouse 4th GQLLPLAQ 3rd sc LOOPALGL

These correspond to the short regions with in the variable region of mouse BPIFA1

Figure 5.17. BPIFA1-derived peptides for functional studies

The sequences of specific peptides and the scrambled controls are given. The differences from the first repeat sequence are highlighted in yellow.

5.2.15 Discussion

The function of BPIFA1, the most abundant protein secreted by non-ciliated cells in the pharynx and URT, is not yet clear. Herein, the structure of BPIFA1 was analysed using bioinformatics tools to better understand its role in immune functions.

A BLAST analysis was performed using the protein sequence obtained from the NCBI, and the results showed that most regions with differences possessed N-terminal regions. Further, a multiple sequence analysis using Clustal Omega was conducted based on the sequences from selected rodents, and the results indicated that the alignment showed the N-terminal region based on the physiochemical properties. The disulphide bond of mouse BPIFA1 and BPI was found in the same location within the protein structure. Mouse BPIFA1 has two cysteine residues (C204 and C246) that participate in the disulphide bond, which is conserved across all organisms and has been documented as critical to produce bioactive BPI protein. This implies that the disulphide bond is essential for the function of BPIFA1.

The human and mouse BPIFA1 protein arrangements were examined in greater detail, and the results showed conserved regions, positions, and residues. In mouse BPIFA1, N-glycosylation targets seen in humans were found. The loss of glycosylation in human orthologues indicates that this post-translation modification is not critical for the function of BPIFA1 or that at least its absence does not lethally impact the organism.

The most interesting observation was the identification of eight amino acid block repeats in the N-terminal region of the protein, which are specific to rodents and vary in number. No similar protein repeats are found in other species, and it will be interesting to see how these function. The repeats occurred in the region of the S18 peptide, which has been previously shown to be important for ENAC activation. The crystal structure of both the human and mouse proteins did not identify either region, suggesting that the proteins are not structured. The structural paralogue of BPIFA1 and BPIFA5 found in rodents has evolved through gene duplication events and shows the highest level of conservation in the protein family, but the N-terminal region is most diverse between BPIFA1 and BPIFA5. Hence, it is unlikely that BPIFA5 functions in the same way as BPIFA1, which is consistent with their differential expression patterns, with BPIFA5 being expressed in the tongue.

After the unique N-terminal domains of the BPIFA1 proteins were confirmed, the study focused on generating recombinant murine proteins. To this end, four different types of constructs were generated, two of which involved deletion of parts of this region, and one had the three N-glycosylation sites removed. The initial plan was to create all mutant constructs through SDM, but the results were inconsistent. In particular, the researcher was unable to make any mutations in the case of the glycosylation sites. Instead, deletions were successfully introduced using this system.

Given that some rodents produced longer N-terminals containing expansions of the eight amino acid repeats, BPIFA1 from *M. pahari* was used. A construct of pig BPIFA1 was also made, as it lacked any complete repeats to cover different lengths of the expanded N-terminal region. I also planned to use synthetic peptides that corresponded to these repeats. All clones were verified by sequencing and produced for transfections.

Transient transfection of HEK293T cells was performed using all FLAG-tagged *BPIFA1*–VR1255 constructs to generate recombinant proteins. Transfection efficiency was visualised using a fluorescent cell imager (Bio-Rad). Recombinant proteins were detected from transient transfection of the HEK293T cells using western blotting of conditioned media and proteins identified by anti-FLAG antibody. All proteins appeared to be secreted, although only the mouse protein was detected in western blotting, and the other proteins were detected in dot blotting. The output of the purification of the BPIFA1 recombinant proteins was inconsistent, which may be attributed to inconsistencies in the transfections (Dalton and Barton 2014). Transient transfection was utilised in the experiments, and recombinant protein production was decreased after the cells were transported to serum-free culture conditions. Recombinant protein levels have been previously shown to be low in serum-free cell culture conditions (Rezaei, Zarkesh-Esfahani et al. 2013, Liu, Garcia-Diaz et al. 2015).

This portion of the study is incomplete. Owing to the COVID-19 lockdown, I was unable to undertake any functional studies with the different constructs. Therefore, no conclusions on the functional importance of the N-terminal region of BPIFA1 in IAV infection could be drawn.

Chapter 6: General discussion

6.1 General Discussion

Multiple cells within the airway epithelium contribute to its function and are a primary means of lung defence. These cells include basal, suprabasal, goblet, club, and ciliated cells as well as rarer cells such as ionocytes and tuft cells. Together, these cells contribute to the regulation of airway homoeostasis, and their function is key to a healthy airway. In respiratory diseases such as COPD, asthma and CF, the number of goblet cells is found to increase, while that of ciliated cells is found to decrease. Airway cells synthesise and secrete multiple HDPs and mucins. MUC5B and MUC5AC are the major proteins, but others include MUC1, MUC4, MUC16, MUC20, MUC21 and MUC22. These HDPs and mucins contribute to the airway surface lining fluid, which is critical for normal lung function and mucociliary clearance.

Influenza is a major human pathogen because of its involvement in pandemics and seasonal

epidemics (Neumann, Noda et al. 2009). Once a person is infected, there is rapid replication of the virus, leading to intense pulmonary distress and potentially to death (Nie, Stadtmuller et al. 2020). IAV predominantly infects the RS and has developed a mechanism to bypass the innate defences. IAV uses surface glycoproteins HA and NA to establish infection in the airway cells, and infection and replication require proteolytic activation at multiple stages by cellular proteases. Effective antiviral responses are induced by IAV, which leads to the upregulation of ISGs, instigating inflammatory and adaptive immune responses and facilitating antiviral responses. The abundant airway surface protein BPIFA1 exhibits a high degree of tissue restriction largely limited to the nasal cavity, trachea, and airways. These areas are key sites of IAV infection and where active innate defence is critical. BPIFA1 and other family members share structural similarities with the HDPs BPI and LBP (Bingle, Singleton et al. 2002), and many studies have shown that BPIFA1 may function in host defence (Britto and Cohn 2015). BPIFA1 proteins have an extended β-barrel-like structure, and mouse and human BPIFA1 share 66% identity. Human BPIFA1 is 256 amino acids long, whereas mouse BPIFA1 is 278 amino acids long. The N-terminal sequence of mouse BPIFA1 includes a PLPL repeat region (Weston, LeClair et al. 1999), which is not present in the sequence of human BPIFA1 (Bingle and Bingle 2000). The N-terminal region of the protein is not seen in the crystal structure of either the human or mouse protein, suggesting a flexible structure. This region of the protein contains what has been described as a functionally

important region – the S18 sequence (Hobbs, Blanchard et al. 2013, Tarran and Redinbo 2014), which has been shown to modulate the proteolytic cleavage of ENaC.

The expression of *BPIFA1* is regulated by viral infection. A previous murine model study showed that the BPIFA1 levels in the BAL were considerably lower in the mice infected with IAV. *BPIFA1* is not an ISG. To examine the function of BPIFA1 in the airway epithelium, I used mTECs from *Bpifa1*-/- and WT mice. The cells from the *Bpifa1*-/- mice were more readily infected with IAV, and infection was more severe in the lungs of the *Bpifa1*-/- mice. Phenotyping of the mTECs revealed that they were substantially similar, suggesting that the difference in IAV binding and infection depends on the presence or absence of BPIFA and not on the number of cells that express IAV receptors.

The present study aimed to further understand the role of *BPIFA1* in antiviral responses against IAV. *BPIFA1* is a crucial component of the airway defence system against viral infections and serves as a functional shield. The primary objective of this research was to build upon previous laboratory findings and gain a complete understanding of the role of *BPIFA1* as an antiviral host defence mechanism. The focus of the study was to determine how BPIFA1 acts as a shield against IAV and whether the functions are solely carried out by the protein or whether the protein works in conjunction with other proteins in the ASL.

As previously noted, primary airway cells grown in 3D cultures are generally considered to be good models of the airways. Epithelial cell differentiation occurs when the confluent cell layer develops on the semi-permeable insert, and cells are fed with media from below. After this model was initially established, a genome-wide analysis of the transcriptional events associated with differentiation was conducted herein. Unsurprisingly, cellular differentiation was associated with a marked transcriptional programme, as the cells changed from the basal cell-like phenotype to a mucociliary epithelial phenotype. At this stage, the numbers of ciliated and secretory cells increased, and a strong ciliary gene expression signature occurred. Similar studies have previously been conducted in human and murine cells (Ross, Dailey et al. 2007, Tsou, Tung et al. 2018). The array analysis identified many genes that were differentially expressed under the different culture conditions, confirming that the present data are like previous reports on mTECs. Based on scRNAseq data, the potential cell types expressing different genes were identified. This

advanced technique is becoming increasingly common. The transcriptional approach also revealed that the original cell isolation was contaminated with various cell types, including inflammatory cells and cells from the tissue that contaminated the tracheas during dissection. The contaminating cells were lost from the cultures when they were maintained and differentiated. The analysis of the cells on day 14 of differentiation indicated that they were epithelial cells. Although 14 days is commonly used as the cut off for differentiation in the researcher's laboratory when working with mouse cells, it appears that ALI cells continue to differentiate over time and that a more mature epithelial cell culture could have been obtained if the cultures were kept for a longer period before using them. In the researcher's laboratory, human ALI cells are usually kept for up to 28 days at the ALI prior to use.

Bpifa1, Bpifb1, Lyz2, Scgb3a1 and Sftpa1 were seen to be expressed predominantly in the secretory cells, with some lower expression of Bpifa1 also seen in the basal cells. Sec14l3 was expressed in the basal and secretory cells but was also robustly expressed in the ciliated cells. The expression data for Bpifa1 in each cell type were extracted. Bpifa1 expression was seen in several cell types, with the highest expression seen in the secretory cells. Among various members of the Bpif family, the Bpifa1 gene exhibited the highest expression in the mTECs on day 14. Bpifa1 has also been previously reported the most highly expressed gene, followed by Bpifb1.

Given that the ALI cultures were established in the normal state, the main aim of this study was to identify the cell types specifically infected with IAV and to investigate the transcriptional consequences of IAV infection in the mTECs. Prior work from the host laboratory suggested that IAV infects BPIFA1^{-ve} cells. The present data suggest that although some ciliated cells take up the virus, most infected cells are non-ciliated. The fact that undifferentiated mTEC cultures, which do not contain ciliated cells, are infected confirms that the virus does not need to infect through this cell type. The current study showed that the level of infection was low in the undifferentiated cells. Exactly what cell type is preferentially infected or if there is any cell specificity to this can be studied further using these cultures. This would have been a major part of the present study but experiments of this nature could not be performed owing to the COVID-19 lockdown at the time of the study. The researcher was away from the laboratory for 9 months and was unable to

access the mice needed to undertake such experiments upon returning. The researcher was also unable to access *Bpifa1*-/- mice from collaborators at the University of Liverpool, as they stopped breading them in March 2020.

The other major part of the study lacking experimental results is the generation and use of recombinant proteins and peptides. As highlighted previously, the BPIFA1 protein is present in all mammalian species, and the N-terminal region is divergent among the species. This region has been suggested to be involved in the function of BPIFA1, so the study focused on this protein. The objective of this chapter was to understand the functionality of this N-terminal region. Although the N-terminal region had been highlighted before the existence of an eight-amino acid repeated sequence in this region was identified, several recombinant murine protein expression constructs were generated. These constructs corresponded to a WT protein, a short-deletion protein that lacked the expanded rodent-specific region, a long-deletion protein that deleted this same region and the S18 region that flanked it and a mutant protein that had the three N-glycosylation sites. Constructs corresponding to proteins that had the maximal (n=6; *M. pahari*) or minimal (n=0, pig) number of repeats were also made. These constructs were validated, but having made them just before the lockdown, the researcher was unable to use them in any functional studies. The researcher was also unable to use the repeat peptides generated to cover the repeat regions.

6.2 Limitations of the Study

Although the two issues described in the preceding section are the major limitations of the study, other limitations also exist.

I was unable to undertake enough studies with *Bpifa1*-/- mice to allow direct comparison of IVA infection in the mTECs. The intention had been to evaluate shorter periods of infection ranging from 2 to 24 h, as previous work has shown clear differences in the IAV infection rate at 24 h.

The transcriptional part of the study is limited by the small sample size. For technical reasons outside of the researcher's control, three replicates of each condition in the array experiments were not obtained. Inter-sample variations could also be seen, which can be considered a limiting

factor. However, there were trends in the data, and some of the differences were clear even in the group of two samples.

Lastly, the study did not validate any candidate genes with methods other than PCR. The use of protein or IHC data would have made this aspect of the study more robust.

6.3 Conclusion

In conclusion, the observations described in this thesis show that mouse tracheal epithelial cell (mTEC) cultures are an appropriate model for studying influenza A virus (IAV) infection, and that the BPIFA-1 protein plays a critical role in protecting the lungs from IAV infection. The major findings align with the study aims:

- 1. An mTEC culture was established and validated for IAV infection studies.
- 2. A genome-wide analysis of mTEC differentiation was performed.
- 3. Transcriptional responses to IAV infection were analyzed in undifferentiated and differentiated mTEC cultures.
- 4. BPIFA1-based reagents were generated and validated for functional studies.

The key findings of the study also include the following:

- IAV infection of mTECs is time- and dose-dependent, occurring without predifferentiation in BPIFA1-negative secretory cells and some ciliated cells.
- Lypd8 may play a role in IAV infection acting as an ISG
- IAV infection levels and membrane spanning protease expression vary in undifferentiated and differentiated cells.

Together, these observations support the hypothesis mTECs are an appropriate model system to investigate if BPIFA1 plays a critical role in protecting the lungs from IAV infection.

References:

- 1. Abdelwahab, S. H., B. Reidel, J. R. Martin, A. Ghosh, J. E. Keating, P. Haridass, J. Carpenter, G. L. Glish, R. Tarran, C. M. Doerschuk and M. Kesimer (2020). "Cigarillos Compromise the Mucosal Barrier and Protein Expression in Airway Epithelia." <u>Am J Respir Cell Mol Biol</u> **63**(6): 767-779.
- Ablasser, A., H. Poeck, D. Anz, M. Berger, M. Schlee, S. Kim, C. Bourquin, N. Goutagny, Z. Jiang, K. A. Fitzgerald, S. Rothenfusser, S. Endres, G. Hartmann and V. Hornung (2009). "Selection of molecular structure and delivery of RNA oligonucleotides to activate TLR7 versus TLR8 and to induce high amounts of IL-12p70 in primary human monocytes." J Immunol 182(11): 6824-6833.
- 3. Achkar, J. M. and A. Casadevall (2013). "Antibody-mediated immunity against tuberculosis: implications for vaccine development." <u>Cell Host Microbe</u> **13**(3): 250-262.
- 4. Agnese, D. M., J. E. Calvano, S. J. Hahm, S. M. Coyle, S. A. Corbett, S. E. Calvano and S. F. Lowry (2002). "Human toll-like receptor 4 mutations but not CD14 polymorphisms are associated with an increased risk of gram-negative infections." J Infect Dis **186**(10): 1522-1525.
- 5. Ahmad, S., C. S. K. Kim and R. Tarran (2020). "The SPLUNC1-betaENaC complex prevents Burkholderia cenocepacia invasion in normal airway epithelia." Respir Res **21**(1): 190.
- 6. Akram, K., Anujan, P., Mccloskey, B., Bingle, L., and Bingle, C (2014). "Validation of an in vitro tracheal model for the study of innate host defense mechanism in respiratory tract infections." European Respiratory Journal(44).
- 7. Akram, K., Moyo, N., Tompkins, M., Tripp, R., Bingle, L., Stewart, J., and Bingle (2015). "An innate defense role for BPIFA1/SPLUNC1 against influenza-A virus infection."
- 8. Al-Qadi, M. O., A. W. Artenstein and S. S. Braman (2013). "The "forgotten zone": acquired disorders of the trachea in adults." Respir Med **107**(9): 1301-1313.
- 9. Al Katy, S., Kipar, A. and Stewart, J. (2019). "Role of BPIFA1 in the pathogenesis and immune response against Influenza A virus in mice." <u>Access Microbiology(1(1A))</u>: p.650.
- 10. Al Katy, S. H. M. (2019). "Role of BPIFA1/SPLUNC1 in the pathogenesis and immune response against influenza A virus in mice." The University of Liverpool (United Kingdom).
- 11. Alexopoulou, L., A. C. Holt, R. Medzhitov and R. A. Flavell (2001). "Recognition of double-stranded RNA and activation of NF-kappaB by Toll-like receptor 3." <u>Nature</u> **413**(6857): 732-738.
- 12. Allen-Hoffmann, B. L., S. J. Schlosser, C. A. Ivarie, C. A. Sattler, L. F. Meisner and S. L. O'Connor (2000). "Normal growth and differentiation in a spontaneously immortalized near-diploid human keratinocyte cell line, NIKS." <u>J Invest Dermatol</u> **114**(3): 444-455.
- 13. Allen, J. D. and T. M. Ross (2018). "H3N2 influenza viruses in humans: Viral mechanisms, evolution, and evaluation." <u>Hum Vaccin Immunother</u> **14**(8): 1840-1847.
- 14. Arbi, M., D. E. Pefani, C. Kyrousi, M. E. Lalioti, A. Kalogeropoulou, A. D. Papanastasiou, S. Taraviras and Z. Lygerou (2016). "GemC1 controls multiciliogenesis in the airway epithelium." EMBO Rep 17(3): 400-413.
- 15. Ashcroft, G. S., K. Lei, W. Jin, G. Longenecker, A. B. Kulkarni, T. Greenwell-Wild, H. Hale-Donze, G. McGrady, X. Y. Song and S. M. Wahl (2000). "Secretory leukocyte protease inhibitor mediates non-redundant functions necessary for normal wound healing." Nat Med 6(10): 1147-1153.
- 16. Ayora-Talavera, G. (2018). "Sialic acid receptors: Focus on their role in influenza infection." <u>J.</u> Recept. Ligand Channel Res(10): pp.1-11.
- 17. Banchereau, J. and R. M. Steinman (1998). "Dendritic cells and the control of immunity." <u>Nature</u> **392**(6673): 245-252.

- 18. Baraniuk, J. N., B. Casado, L. K. Pannell, P. B. McGarvey, P. Boschetto, M. Luisetti and P. Iadarola (2015). "Protein networks in induced sputum from smokers and COPD patients." <u>Int J Chron</u> Obstruct Pulmon Dis **10**: 1957-1975.
- 19. Barjesteh, N., K. O'Dowd and S. M. Vahedi (2020). "Antiviral responses against chicken respiratory infections: Focus on avian influenza virus and infectious bronchitis virus." Cytokine **127**: 154961.
- 20. Bastola, R., P. M. Young and S. C. Das (2021). "Simulation of respiratory tract lining fluid for in vitro dissolution study." <u>Expert Opin Drug Deliv</u> **18**(8): 1091-1100.
- 21. Baum, L. G. and J. C. Paulson (1990). "Sialyloligosaccharides of the respiratory epithelium in the selection of human influenza virus receptor specificity." <u>Acta Histochem Suppl</u> **40**: 35-38.
- 22. Beamer, L. J. (2003). "Structure of human BPI (bactericidal/permeability-increasing protein) and implications for related proteins." Biochem Soc Trans **31**(Pt 4): 791-794.
- 23. Bertram, S., Glowacka, I., Steffen, I., Kühl, A., & Pöhlmann, S (2010). "Novel insights into proteolytic cleavage of influenza virus hemagglutinin." Reviews in Medical Virology (20(5)): 298-310.
- 24. Berube, K., Z. Prytherch, C. Job and T. Hughes (2010). "Human primary bronchial lung cell constructs: the new respiratory models." <u>Toxicology</u> **278**(3): 311-318.
- 25. Bhat, S. A., S. M. Ahmad, E. M. Ibeagha-Awemu, M. Mobashir, M. A. Dar, P. T. Mumtaz, R. A. Shah, T. A. Dar, N. Shabir, H. F. Bhat and N. A. Ganai (2020). "Comparative milk proteome analysis of Kashmiri and Jersey cattle identifies differential expression of key proteins involved in immune system regulation and milk quality." <u>BMC Genomics</u> 21(1): 161.
- 26. Bingle, C. D. and L. Bingle (2000). "Characterisation of the human plunc gene, a gene product with an upper airways and nasopharyngeal restricted expression pattern." <u>Biochim Biophys Acta</u> **1493**(3): 363-367.
- 27. Bingle, C. D., L. Bingle and C. J. Craven (2011). "Distant cousins: genomic and sequence diversity within the BPI fold-containing (BPIF)/PLUNC protein family." <u>Biochem Soc Trans</u> **39**(4): 961-965.
- 28. Bingle, C. D. and C. J. Craven (2002). "PLUNC: a novel family of candidate host defence proteins expressed in the upper airways and nasopharynx." <u>Hum Mol Genet</u> **11**(8): 937-943.
- 29. Bingle, C. D., E. E. LeClair, S. Havard, L. Bingle, P. Gillingham and C. J. Craven (2004). "Phylogenetic and evolutionary analysis of the PLUNC gene family." <u>Protein Sci</u> **13**(2): 422-430.
- 30. Bingle, C. D., Seal, R.L. and Craven, C.J (2011). "Systematic nomenclature for the PLUNC/PSP/BSP30/SMGB proteins as a subfamily of the BPI fold-containing superfamily."
- 31. Bingle, C. D. and A. Vyakarnam (2008). "Novel innate immune functions of the whey acidic protein family." Trends Immunol **29**(9): 444-453.
- 32. Bingle, C. D. a. C., C.J. (2004). "Meet the relatives: a family of BPI-and LBP-related proteins." <u>Trends in immunology(25(2))</u>: pp.53-55.
- 33. Bingle, L., F. A. Barnes, S. S. Cross, D. Rassl, W. A. Wallace, M. A. Campos and C. D. Bingle (2007). "Differential epithelial expression of the putative innate immune molecule SPLUNC1 in cystic fibrosis." Respir Res 8(1): 79.
- 34. Bingle, L., S. S. Cross, A. S. High, W. A. Wallace, D. A. Devine, S. Havard, M. A. Campos and C. D. Bingle (2005). "SPLUNC1 (PLUNC) is expressed in glandular tissues of the respiratory tract and in lung tumours with a glandular phenotype." J Pathol 205(4): 491-497.
- 35. Bingle, L., S. S. Cross, A. S. High, W. A. Wallace, D. Rassl, G. Yuan, I. Hellstrom, M. A. Campos and C. D. Bingle (2006). "WFDC2 (HE4): a potential role in the innate immunity of the oral cavity and respiratory tract and the development of adenocarcinomas of the lung." Respir Res 7(1): 61.
- 36. Bingle, L., V. Singleton and C. D. Bingle (2002). "The putative ovarian tumour marker gene HE4 (WFDC2), is expressed in normal tissues and undergoes complex alternative splicing to yield multiple protein isoforms." Oncogene 21(17): 2768-2773.

- 37. Bingle, L., K. Wilson, M. Musa, B. Araujo, D. Rassl, W. A. Wallace, E. E. LeClair, T. Mauad, Z. Zhou, M. A. Mall and C. D. Bingle (2012). "BPIFB1 (LPLUNC1) is upregulated in cystic fibrosis lung disease." Histochem Cell Biol **138**(5): 749-758.
- 38. Bissonnette, E. Y., Lauzon-Joset, J. F., Debley, J. S., & Ziegler, S. F. (2020). "Cross-talk between alveolar macrophages and lung epithelial cells is essential to maintain lung homeostasis." <u>frontiers</u> in Immunology **583042**(11).
- 39. Bonser, L. R. and D. J. Erle (2017). "Airway Mucus and Asthma: The Role of MUC5AC and MUC5B." J Clin Med **6**(12).
- 40. Bottcher-Friebertshauser, E., W. Garten, M. Matrosovich and H. D. Klenk (2014). "The hemagglutinin: a determinant of pathogenicity." <u>Curr Top Microbiol Immunol</u> **385**: 3-34.
- 41. Bowie, A. G. and L. Unterholzner (2008). "Viral evasion and subversion of pattern-recognition receptor signalling." Nat Rev Immunol **8**(12): 911-922.
- 42. Braiman, A. and Z. Priel (2008). "Efficient mucociliary transport relies on efficient regulation of ciliary beating." Respir Physiol Neurobiol **163**(1-3): 202-207.
- 43. Branchfield, K., L. Nantie, J. M. Verheyden, P. Sui, M. D. Wienhold and X. Sun (2016). "Pulmonary neuroendocrine cells function as airway sensors to control lung immune response." <u>Science</u> **351**(6274): 707-710.
- 44. Britto, C. J. (2022). "Charting a New Path: A Single-Cell Atlas of Porcine Cystic Fibrosis Airways at Birth." Am J Respir Cell Mol Biol **66**(6): 585-586.
- 45. Britto, C. J. and L. Cohn (2015). "Bactericidal/Permeability-increasing protein fold-containing family member A1 in airway host protection and respiratory disease." <u>Am J Respir Cell Mol Biol</u> **52**(5): 525-534.
- 46. Britto, C. J., Q. Liu, D. R. Curran, B. Patham, C. S. Dela Cruz and L. Cohn (2013). "Short palate, lung, and nasal epithelial clone-1 is a tightly regulated airway sensor in innate and adaptive immunity." <u>Am J Respir Cell Mol Biol</u> **48**(6): 717-724.
- 47. Britto, C. J., N. Niu, S. Khanal, L. Huleihel, J. D. Herazo-Maya, A. Thompson, M. Sauler, M. D. Slade, L. Sharma, C. S. Dela Cruz, N. Kaminski and L. E. Cohn (2019). "BPIFA1 regulates lung neutrophil recruitment and interferon signaling during acute inflammation." Am J Physiol Lung Cell Mol Physiol 316(2): L321-L333.
- 48. Brubaker, S. W., K. S. Bonham, I. Zanoni and J. C. Kagan (2015). "Innate immune pattern recognition: a cell biological perspective." <u>Annu Rev Immunol</u> **33**: 257-290.
- 49. Bustamante-Marin, X. M. and L. E. Ostrowski (2017). "Cilia and Mucociliary Clearance." <u>Cold Spring</u> Harb Perspect Biol **9**(4).
- 50. Butler, J. E., K. M. Lager, W. Golde, K. S. Faaberg, M. Sinkora, C. Loving and Y. I. Zhang (2014). "Porcine reproductive and respiratory syndrome (PRRS): an immune dysregulatory pandemic." Immunol Res 59(1-3): 81-108.
- 51. Byrd-Leotis, L., N. Jia, S. Dutta, J. F. Trost, C. Gao, S. F. Cummings, T. Braulke, S. Muller-Loennies, J. Heimburg-Molinaro, D. A. Steinhauer and R. D. Cummings (2019). "Influenza binds phosphorylated glycans from human lung." Sci Adv 5(2): eaav2554.
- 52. Byrd-Leotis, L., Y. Lasanajak, T. Bowen, K. Baker, X. Song, M. S. Suthar, R. D. Cummings and D. A. Steinhauer (2021). "SARS-CoV-2 and other coronaviruses bind to phosphorylated glycans from the human lung." <u>Virology</u> **562**: 142-148.
- 53. Caikauskaite, R. (2018). "Interactions with Bacteria and Their Importance for Airway Host Defence." <u>Doctoral dissertation</u>, <u>University of Sheffield</u>.
- 54. Campbell, E. P., I. K. Quigley and C. Kintner (2016). "Foxn4 promotes gene expression required for the formation of multiple motile cilia." <u>Development</u> **143**(24): 4654-4664.

- 55. Cane, J., L. Tregidgo, S. Thulborn, D. Finch and M. Bafadhel (2021). "Antimicrobial Peptides SLPI and Beta Defensin-1 in Sputum are Negatively Correlated with FEV(1)." Int J Chron Obstruct Pulmon Dis 16: 1437-1447.
- 56. Cao, Y., Guo, Z., Vangala, P., Donnard, E., Liu, P., McDonel, P., Ordovas-Montanes, J., Shalek, A.K., Finberg, R.W., Wang, J.P. and Garber, M. (2020). "Single-cell analysis of upper airway cells reveals host-viral dynamics in influenza infected adults." BioRxiv.
- 57. Cei, D., A. Doryab, A. G. Lenz, A. Schroppel, P. Mayer, G. Burgstaller, R. Nossa, A. Ahluwalia and O. Schmid (2021). "Development of a dynamic in vitro stretch model of the alveolar interface with aerosol delivery." <u>Biotechnol Bioeng</u> **118**(2): 690-702.
- 58. Chen, C. I., S. Schaller-Bals, K. P. Paul, U. Wahn and R. Bals (2004). "Beta-defensins and LL-37 in bronchoalveolar lavage fluid of patients with cystic fibrosis." J Cyst Fibros **3**(1): 45-50.
- 59. Chen, G., T. R. Korfhagen, Y. Xu, J. Kitzmiller, S. E. Wert, Y. Maeda, A. Gregorieff, H. Clevers and J. A. Whitsett (2009). "SPDEF is required for mouse pulmonary goblet cell differentiation and regulates a network of genes associated with mucus production." J Clin Invest 119(10): 2914-2924.
- 60. Chen, X., S. Liu, M. U. Goraya, M. Maarouf, S. Huang and J. L. Chen (2018). "Host Immune Response to Influenza A Virus Infection." Front Immunol **9**: 320.
- 61. Chiang, S. C., E. J. Veldhuizen, F. A. Barnes, C. J. Craven, H. P. Haagsman and C. D. Bingle (2011). "Identification and characterisation of the BPI/LBP/PLUNC-like gene repertoire in chickens reveals the absence of a LBP gene." <u>Dev Comp Immunol</u> **35**(3): 285-295.
- 62. Childs, R. A., A. S. Palma, S. Wharton, T. Matrosovich, Y. Liu, W. Chai, M. A. Campanero-Rhodes, Y. Zhang, M. Eickmann, M. Kiso, A. Hay, M. Matrosovich and T. Feizi (2009). "Receptor-binding specificity of pandemic influenza A (H1N1) 2009 virus determined by carbohydrate microarray." Nat Biotechnol 27(9): 797-799.
- 63. Choreno-Parra, J. A., S. Thirunavukkarasu, J. Zuniga and S. A. Khader (2020). "The protective and pathogenic roles of CXCL17 in human health and disease: Potential in respiratory medicine." Cytokine Growth Factor Rev **53**: 53-62.
- 64. Chu, H. W., F. Gally, J. Thaikoottathil, Y. M. Janssen-Heininger, Q. Wu, G. Zhang, N. Reisdorph, S. Case, M. Minor, S. Smith, D. Jiang, N. Michels, G. Simon and R. J. Martin (2010). "SPLUNC1 regulation in airway epithelial cells: role of Toll-like receptor 2 signaling." Respir Res **11**(1): 155.
- 65. Chu, H. W., J. Thaikoottathil, J. G. Rino, G. Zhang, Q. Wu, T. Moss, Y. Refaeli, R. Bowler, S. E. Wenzel, Z. Chen, J. Zdunek, R. Breed, R. Young, E. Allaire and R. J. Martin (2007). "Function and regulation of SPLUNC1 protein in Mycoplasma infection and allergic inflammation." <u>J Immunol</u> 179(6): 3995-4002.
- 66. Chung, K. F. (2005). "The role of airway smooth muscle in the pathogenesis of airway wall remodeling in chronic obstructive pulmonary disease." <u>Proc Am Thorac Soc</u> **2**(4): 347-354; discussion 371-342.
- 67. Clarke, L. L., K. A. Burns, J. Y. Bayle, R. C. Boucher and M. R. Van Scott (1992). "Sodium- and chloride-conductive pathways in cultured mouse tracheal epithelium." <u>Am J Physiol</u> **263**(5 Pt 1): L519-525.
- 68. Cohn, L. (2006). "Mucus in chronic airway diseases: sorting out the sticky details." <u>J Clin Invest</u> **116**(2): 306-308.
- 69. Cordes, M., K. Cante-Barrett, E. B. van den Akker, F. A. Moretti, S. M. Kielbasa, S. A. Vloemans, L. Garcia-Perez, C. Teodosio, J. J. M. van Dongen, K. Pike-Overzet, M. J. T. Reinders and F. J. T. Staal (2022). "Single-cell immune profiling reveals thymus-seeding populations, T cell commitment, and multilineage development in the human thymus." <u>Sci Immunol</u> **7**(77): eade0182.
- 70. Cristinziano, L., R. Poto, G. Criscuolo, A. L. Ferrara, M. R. Galdiero, L. Modestino, S. Loffredo, A. de Paulis, G. Marone, G. Spadaro and G. Varricchi (2021). "IL-33 and Superantigenic Activation of

- Human Lung Mast Cells Induce the Release of Angiogenic and Lymphangiogenic Factors." <u>Cells</u> **10**(1).
- 71. Croasdell Lucchini, A., N. N. Gachanja, A. G. Rossi, D. A. Dorward and C. D. Lucas (2021). "Epithelial Cells and Inflammation in Pulmonary Wound Repair." Cells **10**(2).
- 72. Curran, D. R. and L. Cohn (2010). "Advances in mucous cell metaplasia: a plug for mucus as a therapeutic focus in chronic airway disease." Am J Respir Cell Mol Biol **42**(3): 268-275.
- 73. Dahl, R. and N. Mygind (1998). "Anatomy, physiology and function of the nasal cavities in health and disease." Adv Drug Deliv Rev **29**(1-2): 3-12.
- 74. Dalton, A. C. and W. A. Barton (2014). "Over-expression of secreted proteins from mammalian cell lines." Protein Sci **23**(5): 517-525.
- 75. Davidson, D. J., F. M. Kilanowski, S. H. Randell, D. N. Sheppard and J. R. Dorin (2000). "A primary culture model of differentiated murine tracheal epithelium." <u>Am J Physiol Lung Cell Mol Physiol</u> **279**(4): L766-778.
- 76. Davies, A., and Moores, Carl (2014). "The Respiratory System [electronic Resource]: Basic Science and Clinical Conditions. 2nd ed. London." Elsevier Health Sciences UK.
- 77. Davis, J. D. and T. P. Wypych (2021). "Cellular and functional heterogeneity of the airway epithelium." <u>Mucosal Immunol</u> **14**(5): 978-990.
- 78. De Jonge, H. J., Fehrmann, R.S., de Bont, E.S., Hofstra, R.M., Gerbens, F., Kamps, W.A., de Vries, E.G., van der Zee, A.G., te Meerman, G.J. and ter Elst, A. (2007). "Evidence based selection of housekeeping genes." <u>PloS one(2(9))</u>: p.e898.
- 79. De Smet, E. G., L. J. Seys, F. M. Verhamme, B. M. Vanaudenaerde, G. G. Brusselle, C. D. Bingle and K. R. Bracke (2018). "Association of innate defense proteins BPIFA1 and BPIFB1 with disease severity in COPD." Int J Chron Obstruct Pulmon Dis 13: 11-27.
- 80. Dean, C. H. and R. J. Snelgrove (2018). "New Rules for Club Development: New Insights into Human Small Airway Epithelial Club Cell Ontogeny and Function." <u>Am J Respir Crit Care Med</u> **198**(11): 1355-1356.
- 81. Dennis, G., Jr., B. T. Sherman, D. A. Hosack, J. Yang, W. Gao, H. C. Lane and R. A. Lempicki (2003). "DAVID: Database for Annotation, Visualization, and Integrated Discovery." Genome Biol **4**(5): P3.
- 82. Deshmukh, R., Bandyopadhyay, N., Abed, S.N., Bandopadhyay, S., Pal, Y. and Deb, P.K., (2020). "Strategies for pulmonary delivery of drugs." In Drug Delivery Systems: pp. (85-129).
- 83. Di, Y. P., R. Harper, Y. Zhao, N. Pahlavan, W. Finkbeiner and R. Wu (2003). "Molecular cloning and characterization of spurt, a human novel gene that is retinoic acid-inducible and encodes a secretory protein specific in upper respiratory tracts." J Biol Chem **278**(2): 1165-1173.
- 84. Dutta, P. and S. Das (2016). "Mammalian Antimicrobial Peptides: Promising Therapeutic Targets Against Infection and Chronic Inflammation." <u>Curr Top Med Chem</u> **16**(1): 99-129.
- 85. Edwards, C. E., A. Tata and R. S. Baric (2022). "Human lung organoids as a model for respiratory virus replication and countermeasure performance in human hosts." <u>Transl Res</u> **250**: 36-45.
- 86. Eierhoff, T., E. R. Hrincius, U. Rescher, S. Ludwig and C. Ehrhardt (2010). "The epidermal growth factor receptor (EGFR) promotes uptake of influenza A viruses (IAV) into host cells." <u>PLoS Pathog</u> **6**(9): e1001099.
- 87. El-Kassas, M., M. Alboraie, M. Elbadry, R. El Sheemy, M. Abdellah, S. Afify, A. Madkour, M. Zaghloul, A. Awad, M. N. Wifi, A. Al Balakosy and M. Eltabbakh (2023). "Non-pulmonary involvement in COVID-19: A systemic disease rather than a pure respiratory infection." World J Clin Cases 11(3): 493-505.
- 88. Ellison, R. T., 3rd (1994). "The effects of lactoferrin on gram-negative bacteria." Adv Exp Med Biol **357**: 71-90.
- 89. Farr, L., S. Ghosh and S. Moonah (2020). "Role of MIF Cytokine/CD74 Receptor Pathway in Protecting Against Injury and Promoting Repair." <u>Front Immunol</u> **11**: 1273.

- 90. Fensterl, V. and G. C. Sen (2009). "Interferons and viral infections." Biofactors 35(1): 14-20.
- 91. Fernandez-Sesma, A., S. Marukian, B. J. Ebersole, D. Kaminski, M. S. Park, T. Yuen, S. C. Sealfon, A. Garcia-Sastre and T. M. Moran (2006). "Influenza virus evades innate and adaptive immunity via the NS1 protein." J Virol **80**(13): 6295-6304.
- 92. Flannagan, R. S., B. Heit and D. E. Heinrichs (2016). "Intracellular replication of Staphylococcus aureus in mature phagolysosomes in macrophages precedes host cell death, and bacterial escape and dissemination." Cell Microbiol **18**(4): 514-535.
- 93. Frank, H. N. (2014). "ATLAS OF HUMAN ANATOMY, ENHANCED INTERNATIONAL EDITION: Including Studentconsult Interactive. Ancillaries and Guides." GRUNE & STRATTON Incorporated.
- 94. Fritz, M. A., Suiter, D.M. and Postma, G.N. (2019). "DYSPHAGIA IN CHRONIC COUGH." **Chronic Cough**: p.116.
- 95. Fung, K. Y., N. E. Mangan, H. Cumming, J. C. Horvat, J. R. Mayall, S. A. Stifter, N. De Weerd, L. C. Roisman, J. Rossjohn, S. A. Robertson, J. E. Schjenken, B. Parker, C. E. Gargett, H. P. Nguyen, D. J. Carr, P. M. Hansbro and P. J. Hertzog (2013). "Interferon-epsilon protects the female reproductive tract from viral and bacterial infection." Science **339**(6123): 1088-1092.
- 96. Gakhar, L., J. A. Bartlett, J. Penterman, D. Mizrachi, P. K. Singh, R. K. Mallampalli, S. Ramaswamy and P. B. McCray, Jr. (2010). "PLUNC is a novel airway surfactant protein with anti-biofilm activity." PLoS One **5**(2): e9098.
- 97. Gally, F., Y. P. Di, S. K. Smith, M. N. Minor, Y. Liu, D. L. Bratton, S. C. Frasch, N. M. Michels, S. R. Case and H. W. Chu (2011). "SPLUNC1 promotes lung innate defense against Mycoplasma pneumoniae infection in mice." Am J Pathol **178**(5): 2159-2167.
- 98. Ganz, T., M. E. Selsted, D. Szklarek, S. S. Harwig, K. Daher, D. F. Bainton and R. I. Lehrer (1985). "Defensins. Natural peptide antibiotics of human neutrophils." J Clin Invest **76**(4): 1427-1435.
- 99. Garcia-Caballero, A., J. E. Rasmussen, E. Gaillard, M. J. Watson, J. C. Olsen, S. H. Donaldson, M. J. Stutts and R. Tarran (2009). "SPLUNC1 regulates airway surface liquid volume by protecting ENaC from proteolytic cleavage." Proc Natl Acad Sci U S A 106(27): 11412-11417.
- 100. Garcia-Sastre, A. (2011). "Induction and evasion of type I interferon responses by influenza viruses." <u>Virus Res</u> **162**(1-2): 12-18.
- 101. Garcia, S. R. (2018). "Catching cellular heterogeneity and differentiation dynamics of normal and pathological airway epithelia through single cell transcriptional profiling." **Doctoral** dissertation.
- 102. Garland, A. L., W. G. Walton, R. D. Coakley, C. D. Tan, R. C. Gilmore, C. A. Hobbs, A. Tripathy, L. A. Clunes, S. Bencharit, M. J. Stutts, L. Betts, M. R. Redinbo and R. Tarran (2013). "Molecular basis for pH-dependent mucosal dehydration in cystic fibrosis airways." Proc Natl Acad Sci U S A 110(40): 15973-15978.
- 103. Garten, W., C. Braden, A. Arendt, C. Peitsch, J. Baron, Y. Lu, K. Pawletko, K. Hardes, T. Steinmetzer and E. Bottcher-Friebertshauser (2015). "Influenza virus activating host proteases: Identification, localization and inhibitors as potential therapeutics." <u>Eur J Cell Biol</u> **94**(7-9): 375-383.
- 104. Ghafouri, B., E. Kihlstrom, B. Stahlbom, C. Tagesson and M. Lindahl (2003). "PLUNC (palate, lung and nasal epithelial clone) proteins in human nasal lavage fluid." <u>Biochem Soc Trans</u> **31**(Pt 4): 810-814.
- 105. Ghanem, R., V. Laurent, P. Roquefort, T. Haute, S. Ramel, T. Le Gall, T. Aubry and T. Montier (2020). "Optimizations of In Vitro Mucus and Cell Culture Models to Better Predict In Vivo Gene Transfer in Pathological Lung Respiratory Airways: Cystic Fibrosis as an Example." Pharmaceutics **13**(1).
- 106. Ghati, A., P. Dam, D. Tasdemir, A. Kati, H. Sellami, G. C. Sezgin, N. Ildiz, O. L. Franco, A. K. Mandal and I. Ocsoy (2021). "Exogenous pulmonary surfactant: A review focused on adjunctive

- therapy for severe acute respiratory syndrome coronavirus 2 including SP-A and SP-D as added clinical marker." <u>Curr Opin Colloid Interface Sci</u> **51**: 101413.
- 107. Giovannoni, F., I. Bosch, C. M. Polonio, M. F. Torti, M. A. Wheeler, Z. Li, L. Romorini, M. S. Rodriguez Varela, V. Rothhammer, A. Barroso, E. C. Tjon, L. M. Sanmarco, M. C. Takenaka, S. M. S. Modaresi, C. Gutierrez-Vazquez, N. G. Zanluqui, N. B. Dos Santos, C. D. Munhoz, Z. Wang, E. B. Damonte, D. Sherr, L. Gehrke, J. P. S. Peron, C. C. Garcia and F. J. Quintana (2020). "AHR is a Zika virus host factor and a candidate target for antiviral therapy." Nat Neurosci 23(8): 939-951.
- 108. Goldstein, M. E. and M. A. Scull (2022). "Modeling Innate Antiviral Immunity in Physiological Context." J Mol Biol **434**(6): 167374.
- 109. Gopal, R., M. A. Marinelli and J. F. Alcorn (2020). "Immune Mechanisms in Cardiovascular Diseases Associated With Viral Infection." Front Immunol **11**: 570681.
- 110. Gordon, S., P. R. Crocker, L. Morris, S. H. Lee, V. H. Perry and D. A. Hume (1986). "Localization and function of tissue macrophages." <u>Ciba Found Symp</u> **118**: 54-67.
- 111. Gordon, S. and A. Pluddemann (2018). "Macrophage Clearance of Apoptotic Cells: A Critical Assessment." Front Immunol **9**: 127.
- 112. Gozzi-Silva, S. C., F. M. E. Teixeira, A. Duarte, M. N. Sato and L. M. Oliveira (2021). "Immunomodulatory Role of Nutrients: How Can Pulmonary Dysfunctions Improve?" <u>Front Nutr</u> **8**: 674258.
- 113. Green, H. (1977). "Terminal differentiation of cultured human epidermal cells." <u>Cell</u> **11**(2): 405-416.
- 114. Guo, M., Y. Du, J. J. Gokey, S. Ray, S. M. Bell, M. Adam, P. Sudha, A. K. Perl, H. Deshmukh, S. S. Potter, J. A. Whitsett and Y. Xu (2019). "Single cell RNA analysis identifies cellular heterogeneity and adaptive responses of the lung at birth." Nat Commun 10(1): 37.
- 115. Guy, C. and A. G. Bowie (2022). "Recent insights into innate immune nucleic acid sensing during viral infection." <u>Curr Opin Immunol</u> **78**: 102250.
- 116. Haddad, A., M. Gaudet, M. Plesa, Z. Allakhverdi, A. K. Mogas, S. Audusseau, C. J. Baglole, D. H. Eidelman, R. Olivenstein, M. S. Ludwig and Q. Hamid (2019). "Neutrophils from severe asthmatic patients induce epithelial to mesenchymal transition in healthy bronchial epithelial cells." Respir Res 20(1): 234.
- 117. Hadzhiev, Y., S. Yordanov, D. Popova and D. Kachakova (2017). "BPIFA1 Gene Expression in the Human Middle Ear Mucosa." J Int Adv Otol **13**(3): 340-344.
- 118. Hartikka, J., M. Sawdey, F. Cornefert-Jensen, M. Margalith, K. Barnhart, M. Nolasco, H. L. Vahlsing, J. Meek, M. Marquet, P. Hobart, J. Norman and M. Manthorpe (1996). "An improved plasmid DNA expression vector for direct injection into skeletal muscle." Hum Gene Ther 7(10): 1205-1217.
- 119. Hawkins, F. J. and D. N. Kotton (2018). "Pulmonary lonocytes Challenge the Paradigm in Cystic Fibrosis." <u>Trends Pharmacol Sci</u> **39**(10): 852-854.
- 120. He, Y., G. Zhou, Y. Zhai, X. Dong, L. Lv, F. He and K. Yao (2005). "Association of PLUNC gene polymorphisms with susceptibility to nasopharyngeal carcinoma in a Chinese population." <u>J Med Genet</u> **42**(2): 172-176.
- 121. Heath, W. R. and F. R. Carbone (2001). "Cross-presentation, dendritic cells, tolerance and immunity." Annu Rev Immunol **19**: 47-64.
- 122. Heer, A. K., Shamshiev, A., Donda, A., Uematsu, S., Akira, S., Kopf, M. and Marsland, B.J., (2007). "TLR signalling fine-tunes anti-influenza B cell responses without regulating effector T cell responses." The journal of immunology(178(4)): pp.2182-2191.
- 123. Hennessy, M. a. G., D., (2016). "Surgical anatomy and physiology of swallowing." Operative Techniques in Otolaryngology-Head and Neck Surgery(27(2)): pp.60-66.

- 124. Hobbs, C. A., M. G. Blanchard, O. Alijevic, C. D. Tan, S. Kellenberger, S. Bencharit, R. Cao, M. Kesimer, W. G. Walton, A. G. Henderson, M. R. Redinbo, M. J. Stutts and R. Tarran (2013). "Identification of the SPLUNC1 ENaC-inhibitory domain yields novel strategies to treat sodium hyperabsorption in cystic fibrosis airway epithelial cultures." <u>Am J Physiol Lung Cell Mol Physiol</u> **305**(12): L990-L1001.
- 125. Hogner, K., T. Wolff, S. Pleschka, S. Plog, A. D. Gruber, U. Kalinke, H. D. Walmrath, J. Bodner, S. Gattenlohner, P. Lewe-Schlosser, M. Matrosovich, W. Seeger, J. Lohmeyer and S. Herold (2013). "Macrophage-expressed IFN-beta contributes to apoptotic alveolar epithelial cell injury in severe influenza virus pneumonia." <u>PLoS Pathog</u> 9(2): e1003188.
- 126. Holweg, A., M. Schnare and A. Gessner (2011). "The bactericidal/permeability-increasing protein (BPI) in the innate defence of the lower airways." Biochem Soc Trans **39**(4): 1045-1050.
- 127. Horani, A., S. L. Brody and T. W. Ferkol (2014). "Picking up speed: advances in the genetics of primary ciliary dyskinesia." <u>Pediatr Res</u> **75**(1-2): 158-164.
- 128. Horani, A., A. Nath, M. G. Wasserman, T. Huang and S. L. Brody (2013). "Rho-associated protein kinase inhibition enhances airway epithelial Basal-cell proliferation and lentivirus transduction." <u>Am J Respir Cell Mol Biol</u> **49**(3): 341-347.
- 129. Hosseiniyan Khatibi, S. M., K. Kheyrolahzadeh, A. Barzegari, Y. Rahbar Saadat and S. Zununi Vahed (2020). "Medicinal signaling cells: A potential antimicrobial drug store." <u>J Cell Physiol</u> **235**(11): 7731-7746.
- 130. Hou, L., J. Li, H. Qu, L. Yang, Y. Chen, Q. Du and W. Liu (2015). "[Inhibition of replication and transcription of WSN influenza A virus by IFIT family genes]." Sheng Wu Gong Cheng Xue Bao **31**(1): 123-134.
- 131. Hultmark, D., H. Steiner, T. Rasmuson and H. G. Boman (1980). "Insect immunity. Purification and properties of three inducible bactericidal proteins from hemolymph of immunized pupae of Hyalophora cecropia." <u>Eur J Biochem</u> **106**(1): 7-16.
- 132. Imai, Y., K. Kuba, G. G. Neely, R. Yaghubian-Malhami, T. Perkmann, G. van Loo, M. Ermolaeva, R. Veldhuizen, Y. H. Leung, H. Wang, H. Liu, Y. Sun, M. Pasparakis, M. Kopf, C. Mech, S. Bavari, J. S. Peiris, A. S. Slutsky, S. Akira, M. Hultqvist, R. Holmdahl, J. Nicholls, C. Jiang, C. J. Binder and J. M. Penninger (2008). "Identification of oxidative stress and Toll-like receptor 4 signaling as a key pathway of acute lung injury." Cell **133**(2): 235-249.
- 133. Ishizaka, T., Mitsui, H., Yanagida, M., Miura, T. and Dvorak, A.M., (1993). "Development of human mast cells from their progenitors." <u>Current opinion in immunology</u>(5(6)): pp.937-943.
- 134. Ivanova, N., Y. Sotirova, G. Gavrailov, K. Nikolova and V. Andonova (2022). "Advances in the Prophylaxis of Respiratory Infections by the Nasal and the Oromucosal Route: Relevance to the Fight with the SARS-CoV-2 Pandemic." Pharmaceutics 14(3).
- 135. Iwasaki, A. and R. Medzhitov (2004). "Toll-like receptor control of the adaptive immune responses." <u>Nat Immunol</u> **5**(10): 987-995.
- 136. Iwasaki, A. and R. Medzhitov (2010). "Regulation of adaptive immunity by the innate immune system." <u>Science</u> **327**(5963): 291-295.
- 137. Iwasaki, A. and R. Medzhitov (2015). "Control of adaptive immunity by the innate immune system." Nat Immunol **16**(4): 343-353.
- 138. Iwasaki, A. and P. S. Pillai (2014). "Innate immunity to influenza virus infection." <u>Nat Rev Immunol</u> **14**(5): 315-328.
- 139. Jayawardane, G., G. C. Russell, J. Thomson, D. Deane, H. Cox, D. Gatherer, M. Ackermann, D. M. Haig and J. P. Stewart (2008). "A captured viral interleukin 10 gene with cellular exon structure." J Gen Virol 89(Pt 10): 2447-2455.

- 140. Jewell, N. A., N. Vaghefi, S. E. Mertz, P. Akter, R. S. Peebles, Jr., L. O. Bakaletz, R. K. Durbin, E. Flano and J. E. Durbin (2007). "Differential type I interferon induction by respiratory syncytial virus and influenza a virus in vivo." <u>J Virol</u> **81**(18): 9790-9800.
- 141. Jiang, Y., H. Liao, X. Zhang, S. Cao, X. Hu, Z. Yang, Y. Fang and H. Wang (2020). "IL-33 synergistically promotes the proliferation of lung cancer cells in vitro by inducing antibacterial peptide LL-37 and proinflammatory cytokines in macrophages." Immunobiology 225(6): 152025.
- 142. Jin, F. Y., C. Nathan, D. Radzioch and A. Ding (1997). "Secretory leukocyte protease inhibitor: a macrophage product induced by and antagonistic to bacterial lipopolysaccharide." <u>Cell</u> **88**(3): 417-426.
- 143. Kanashiro, A., C. H. Hiroki, D. M. da Fonseca, A. Birbrair, R. G. Ferreira, G. S. Bassi, M. D. Fonseca, R. Kusuda, G. C. M. Cebinelli, K. P. da Silva, C. W. Wanderley, G. B. Menezes, J. C. Alves-Fiho, A. G. Oliveira, T. M. Cunha, A. S. Pupo, L. Ulloa and F. Q. Cunha (2020). "The role of neutrophils in neuro-immune modulation." Pharmacol Res **151**: 104580.
- 144. Karakus, U., M. O. Pohl and S. Stertz (2020). "Breaking the Convention: Sialoglycan Variants, Coreceptors, and Alternative Receptors for Influenza A Virus Entry." J Virol **94**(4).
- 145. Kawai, T. a. A., S., (2008). "Toll-like receptor and RIG-1-like receptor signaling." <u>Annals of the New York Academy of Sciences</u>(1143(1)): pp.1-20.
- 146. Kelly, A. M. and R. M. McLoughlin (2020). "Target the Host, Kill the Bug; Targeting Host Respiratory Immunosuppressive Responses as a Novel Strategy to Improve Bacterial Clearance During Lung Infection." <u>Front Immunol</u> **11**: 767.
- 147. Kesimer, M., C. Ehre, K. A. Burns, C. W. Davis, J. K. Sheehan and R. J. Pickles (2013). "Molecular organization of the mucins and glycocalyx underlying mucus transport over mucosal surfaces of the airways." <u>Mucosal Immunol</u> **6**(2): 379-392.
- 148. Keynan, Y., Fowke, K.R., Ball, T.B. and Meyers, A.F., (2011). "Toll-like receptors dysregulation after influenza virus infection: insights into pathogenesis of subsequent bacterial pneumonia." International Scholarly Research Notices.
- 149. Kim, C. S. (2016). "Short palate lung and nasal epithelium clone 1 dissociates and endocytoses the epithelial sodium channel "_(Doctoral dissertation, The University of North Carolina at Chapel Hill).
- 150. Klimov, V., N. Cherevko, A. Klimov and P. Novikov (2022). "Neuronal-Immune Cell Units in Allergic Inflammation in the Nose." Int J Mol Sci **23**(13).
- 151. Knowles, M. R. and R. C. Boucher (2002). "Mucus clearance as a primary innate defense mechanism for mammalian airways." J Clin Invest **109**(5): 571-577.
- 152. Kosciuczuk, E. M., P. Lisowski, J. Jarczak, N. Strzalkowska, A. Jozwik, J. Horbanczuk, J. Krzyzewski, L. Zwierzchowski and E. Bagnicka (2012). "Cathelicidins: family of antimicrobial peptides. A review." Mol Biol Rep **39**(12): 10957-10970.
- 153. Kotas, M. E., C. E. O'Leary and R. M. Locksley (2023). "Tuft Cells: Context- and Tissue-Specific Programming for a Conserved Cell Lineage." <u>Annu Rev Pathol</u> **18**: 311-335.
- 154. Kroes, M. M., A. Miranda-Bedate, R. H. J. Jacobi, E. van Woudenbergh, G. den Hartog, J. P. M. van Putten, J. de Wit and E. Pinelli (2022). "Bordetella pertussis-infected innate immune cells drive the anti-pertussis response of human airway epithelium." <u>Sci Rep</u> **12**(1): 3622.
- 155. Kuhaudomlarp, S. and A. Imberty (2022). "Involvement of sialoglycans in SARS-COV-2 infection: Opportunities and challenges for glyco-based inhibitors." <u>IUBMB Life</u> **74**(12): 1253-1263.
- 156. Kumar, A., J. Zhang and F. S. Yu (2004). "Innate immune response of corneal epithelial cells to Staphylococcus aureus infection: role of peptidoglycan in stimulating proinflammatory cytokine secretion." Invest Ophthalmol Vis Sci **45**(10): 3513-3522.

- 157. Kusak, B., Grzesik, E., Konarska-Gabryś, K., Pacek, Z., Piwowarczyk, B. and Lis, G., (2018). "Bronchiolitis in children-do we choose wisely." <u>Dev Period Med</u>(22(4)): pp.323-328.
- 158. Le Goffic, R., V. Balloy, M. Lagranderie, L. Alexopoulou, N. Escriou, R. Flavell, M. Chignard and M. Si-Tahar (2006). "Detrimental contribution of the Toll-like receptor (TLR)3 to influenza A virus-induced acute pneumonia." <u>PLoS Pathog</u> **2**(6): e53.
- 159. Lechner, J. F., and LaVeck, M.A., (1985). "A serum-free method for culturing normal human bronchial epithelial cells at clonal density." <u>Journal of tissue culture methods(9(2))</u>: pp.43-48.
- 160. LeClair, E. E., V. Nomellini, M. Bahena, V. Singleton, L. Bingle, C. J. Craven and C. D. Bingle (2004). "Cloning and expression of a mouse member of the PLUNC protein family exclusively expressed in tongue epithelium." <u>Genomics</u> **83**(4): 658-666.
- 161. Lee, Y., Y. H. Hwang, K. J. Kim, A. K. Park, M. J. Paik, S. H. Kim, S. U. Lee, S. T. Yee and Y. J. Son (2018). "Proteomic and transcriptomic analysis of lung tissue in OVA-challenged mice." <u>Arch Pharm Res 41(1)</u>: 87-100.
- 162. Leeming, G. H., A. Kipar, D. J. Hughes, L. Bingle, E. Bennett, N. A. Moyo, R. A. Tripp, A. L. Bigley, C. D. Bingle, J. T. Sample and J. P. Stewart (2015). "Gammaherpesvirus infection modulates the temporal and spatial expression of SCGB1A1 (CCSP) and BPIFA1 (SPLUNC1) in the respiratory tract." <u>Lab Invest</u> **95**(6): 610-624.
- 163. Lever, J. E. P. (2021). "Mucus Matters: Mucociliary Physiology in Chronic Lung Diseases." <u>Doctoral dissertation, The University of Alabama at Birmingham.</u>
- Lewis, A. L., Szymanski, C.M., Schnaar, R.L. and Aebi, M., (2022). "Bacterial and Viral Infections. Essentials of Glycobiology." **4th edition**.
- 165. Li, D. and M. Wu (2021). "Pattern recognition receptors in health and diseases." <u>Signal</u> Transduct Target Ther **6**(1): 291.
- 166. Little, M. S. and M. R. Redinbo (2018). "Crystal structure of the mouse innate immunity factor bacterial permeability-increasing family member A1." <u>Acta Crystallogr F Struct Biol</u> Commun **74**(Pt 5): 268-276.
- 167. Liu, F., P. Zhou, Q. Wang, M. Zhang and D. Li (2018). "The Schlafen family: complex roles in different cell types and virus replication." <u>Cell Biol Int</u> **42**(1): 2-8.
- 168. Liu, J., Z. Pang, G. Wang, X. Guan, K. Fang, Z. Wang and F. Wang (2017). "Advanced Role of Neutrophils in Common Respiratory Diseases." J Immunol Res **2017**: 6710278.
- 169. Liu, Q., Z. Wang and W. Zhang (2021). "The Multifunctional Roles of Short Palate, Lung, and Nasal Epithelium Clone 1 in Regulating Airway Surface Liquid and Participating in Airway Host Defense." J Interferon Cytokine Res **41**(4): 139-148.
- 170. Liu, Y., J. A. Bartlett, M. E. Di, J. M. Bomberger, Y. R. Chan, L. Gakhar, R. K. Mallampalli, P. B. McCray, Jr. and Y. P. Di (2013). "SPLUNC1/BPIFA1 contributes to pulmonary host defense against Klebsiella pneumoniae respiratory infection." Am J Pathol **182**(5): 1519-1531.
- 171. Liu, Y., M. E. Di, H. W. Chu, X. Liu, L. Wang, S. Wenzel and Y. P. Di (2013). "Increased susceptibility to pulmonary Pseudomonas infection in Splunc1 knockout mice." <u>J Immunol</u> **191**(8): 4259-4268.
- 172. Liu, Z., B. Garcia-Diaz, B. Catacchio, E. Chiancone and H. J. Vogel (2015). "Protecting Gramnegative bacterial cell envelopes from human lysozyme: Interactions with Ivy inhibitor proteins from Escherichia coli and Pseudomonas aeruginosa." <u>Biochim Biophys Acta</u> **1848**(11 Pt B): 3032-3046.
- 173. Londrigan, S. L., K. R. Short, J. Ma, L. Gillespie, S. P. Rockman, A. G. Brooks and P. C. Reading (2015). "Infection of Mouse Macrophages by Seasonal Influenza Viruses Can Be Restricted at the Level of Virus Entry and at a Late Stage in the Virus Life Cycle." <u>J Virol</u> 89(24): 12319-12329.

- 174. Lu, H., P. Anujan, F. Zhou, Y. Zhang, Y. L. Chong, C. D. Bingle and S. Roy (2019). "Mcidas mutant mice reveal a two-step process for the specification and differentiation of multiciliated cells in mammals." <u>Development</u> **146**(6).
- 175. Lucas, R., Y. Hadizamani, J. Gonzales, B. Gorshkov, T. Bodmer, Y. Berthiaume, U. Moehrlen, H. Lode, H. Huwer, M. Hudel, M. A. Mraheil, H. A. F. Toque, T. Chakraborty and J. Hamacher (2020). "Impact of Bacterial Toxins in the Lungs." Toxins (Basel) **12**(4).
- 176. Lukinskiene, L., Y. Liu, S. D. Reynolds, C. Steele, B. R. Stripp, G. D. Leikauf, J. K. Kolls and Y. P. Di (2011). "Antimicrobial activity of PLUNC protects against Pseudomonas aeruginosa infection." <u>J Immunol</u> **187**(1): 382-390.
- 177. Lumb, A. B. a. T., C.R., (2020). "Nunn's applied respiratory physiology eBook." <u>Elsevier</u> Health Sciences UK.
- 178. Lynch, T. J. (2016). "Adult stem cells in the trachea and tracheal submucosal glands."
- 179. Madsen, H. O. and J. P. Hjorth (1985). "Molecular cloning of mouse PSP mRNA." <u>Nucleic Acids Res</u> **13**(1): 1-13.
- 180. Maini, M. K. and A. R. Burton (2019). "Restoring, releasing or replacing adaptive immunity in chronic hepatitis B." <u>Nat Rev Gastroenterol Hepatol</u> **16**(11): 662-675.
- 181. Man, W. H., W. A. de Steenhuijsen Piters and D. Bogaert (2017). "The microbiota of the respiratory tract: gatekeeper to respiratory health." <u>Nat Rev Microbiol</u> **15**(5): 259-270.
- 182. Manicassamy, B., S. Manicassamy, A. Belicha-Villanueva, G. Pisanelli, B. Pulendran and A. Garcia-Sastre (2010). "Analysis of in vivo dynamics of influenza virus infection in mice using a GFP reporter virus." Proc Natl Acad Sci U S A **107**(25): 11531-11536.
- 183. Martin, C., Karkas, A. and Prades, J.M., (2017). "Tubotympanic system functioning. ." <u>European annals of otorhinolaryngology, head and neck diseases</u>,(134(3)): pp.177-184.
- 184. Marzec, J., H. Y. Cho, M. High, Z. R. McCaw, F. Polack and S. R. Kleeberger (2019). "Toll-like receptor 4-mediated respiratory syncytial virus disease and lung transcriptomics in differentially susceptible inbred mouse strains." Physiol Genomics 51(12): 630-643.
- 185. Mashbat, B., E. Bellos, S. Hodeib, F. Bidmos, R. S. Thwaites, Y. Lu, V. J. Wright, J. A. Herberg, D. S. Klobassa, W. Zenz, T. T. Hansel, S. Nadel, P. R. Langford, L. J. Schlapbach, M. S. Li, M. R. Redinbo, Y. P. Di, M. Levin and V. Sancho-Shimizu (2020). "A Rare Mutation in SPLUNC1 Affects Bacterial Adherence and Invasion in Meningococcal Disease." Clin Infect Dis **70**(10): 2045-2053.
- 186. Matrosovich, M. N., A. S. Gambaryan, S. Teneberg, V. E. Piskarev, S. S. Yamnikova, D. K. Lvov, J. S. Robertson and K. A. Karlsson (1997). "Avian influenza A viruses differ from human viruses by recognition of sialyloligosaccharides and gangliosides and by a higher conservation of the HA receptor-binding site." <u>Virology</u> **233**(1): 224-234.
- 187. Matsumiya, T. and D. M. Stafforini (2010). "Function and regulation of retinoic acid-inducible gene-I." Crit Rev Immunol **30**(6): 489-513.
- McCreary, E. K., J. R. Bariola, T. Minnier, R. J. Wadas, J. A. Shovel, D. Albin, O. C. Marroquin, M. Schmidhofer, M. K. Wisniewski, D. A. Nace, C. Sullivan, M. Axe, R. Meyers, T. Khadem, W. Garrard, K. Collins, A. Wells, R. D. Bart, K. Linstrum, S. K. Montgomery, G. Haidar, G. M. Snyder, B. J. McVerry, C. W. Seymour, D. M. Yealy, D. T. Huang and D. C. Angus (2022). "Launching a comparative effectiveness adaptive platform trial of monoclonal antibodies for COVID-19 in 21 days." Contemp Clin Trials 113: 106652.
- 189. McGillivary, G. a. B., L.O., (2010). "The multifunctional host defense peptide SPLUNC1 is critical for homeostasis of the mammalian upper airway." <u>PloS one(5(10))</u>.
- 190. Medzhitov, R., P. Preston-Hurlburt and C. A. Janeway, Jr. (1997). "A human homologue of the Drosophila Toll protein signals activation of adaptive immunity." <u>Nature</u> **388**(6640): 394-397.
- 191. Meng, S., P. Chanda, R. A. Thandavarayan and J. P. Cooke (2017). "Transflammation: Innate immune signaling in nuclear reprogramming." Adv Drug Deliv Rev **120**: 133-141.

- 192. Meraz, K. A. (2014). "Characterization of NS1 SUMOylation and its effect on influenza A viral infection.".
- 193. Meredith, M., D. Zemmour, D. Mathis and C. Benoist (2015). "Aire controls gene expression in the thymic epithelium with ordered stochasticity." Nat Immunol **16**(9): 942-949.
- 194. Mezoughi, A. B. a. E., Z.O., (2021). "The Role of Pulmonary Surfactant in COVID19 Understanding." International Research Journal of Pure and Applied Chemistry(22(6)): pp.15-30.
- 195. Miller, A. J., B. R. Dye, D. Ferrer-Torres, D. R. Hill, A. W. Overeem, L. D. Shea and J. R. Spence (2019). "Generation of lung organoids from human pluripotent stem cells in vitro." <u>Nat Protoc 14(2)</u>: 518-540.
- 196. Mirels, L. and W. D. Ball (1992). "Neonatal rat submandibular gland protein SMG-A and parotid secretory protein are alternatively regulated members of a salivary protein multigene family." J Biol Chem 267(4): 2679-2687.
- 197. Mohamed, A. A. and M. Alawna (2020). "Role of increasing the aerobic capacity on improving the function of immune and respiratory systems in patients with coronavirus (COVID-19): A review." <u>Diabetes Metab Syndr</u> **14**(4): 489-496.
- 198. Montoro, D. T., A. L. Haber, M. Biton, V. Vinarsky, B. Lin, S. E. Birket, F. Yuan, S. Chen, H. M. Leung, J. Villoria, N. Rogel, G. Burgin, A. M. Tsankov, A. Waghray, M. Slyper, J. Waldman, L. Nguyen, D. Dionne, O. Rozenblatt-Rosen, P. R. Tata, H. Mou, M. Shivaraju, H. Bihler, M. Mense, G. J. Tearney, S. M. Rowe, J. F. Engelhardt, A. Regev and J. Rajagopal (2018). "A revised airway epithelial hierarchy includes CFTR-expressing ionocytes." Nature 560(7718): 319-324.
- 199. Montoro, D. T., A. L. Haber, J. E. Rood, A. Regev and J. Rajagopal (2020). "A Synthesis Concerning Conservation and Divergence of Cell Types across Epithelia." <u>Cold Spring Harb</u> Perspect Biol **12**(11).
- 200. Morimoto, M., Liu, Z., Cheng, H.T., Winters, N., Bader, D. and Kopan, R., (2010). "Canonical Notch signalling in the developing lung is required for determination of arterial smooth muscle cells and selection of Clara versus ciliated cell fate." Journal of cell science(123(2)): pp.213-224.
- 201. Mulay, A., M. M. K. Chowdhury, C. T. James, L. Bingle and C. D. Bingle (2021). "The transcriptional landscape of the cultured murine middle ear epithelium in vitro." Biol Open **10**(4).
- 202. Mulero, J. J., B. J. Boyle, S. Bradley, J. M. Bright, S. T. Nelken, T. T. Ho, N. K. Mize, J. D. Childs, D. G. Ballinger, J. E. Ford and F. Rupp (2002). "Three new human members of the lipid transfer/lipopolysaccharide binding protein family (LT/LBP)." <u>Immunogenetics</u> **54**(5): 293-300.
- 203. Murphy, K. a. W., C., (2016). "Janeway's immunobiology." Garland science.
- 204. Murthy, K. J. R. a. S., J.G (2005). "Economic burden of chronic obstructive pulmonary disease." <u>Burden of disease in India,</u>: p.264.
- 205. Musa, M., K. Wilson, L. Sun, A. Mulay, L. Bingle, H. M. Marriott, E. E. LeClair and C. D. Bingle (2012). "Differential localisation of BPIFA1 (SPLUNC1) and BPIFB1 (LPLUNC1) in the nasal and oral cavities of mice." Cell Tissue Res **350**(3): 455-464.
- 206. Nagaoka, I., K. Suzuki, T. Murakami, F. Niyonsaba, H. Tamura and M. Hirata (2010). "Evaluation of the effect of alpha-defensin human neutrophil peptides on neutrophil apoptosis." <u>Int J Mol Med</u> 26(6): 925-934.
- 207. Nakashige, T. G., Zhang, B., Krebs, C., & Nolan, E. M. (2015). "Human calprotectin is an iron-sequestering host-defense protein." <u>Nature chemical biology</u>(11(10)): 765-771.
- 208. Narayanankutty, A., A. Sasidharan and J. T. Job (2020). "Targeting Toll like Receptors in Cancer: Role of TLR Natural and Synthetic Modulators." Curr Pharm Des **26**(39): 5040-5053.
- 209. Neumann, G. and Y. Kawaoka (2015). "Transmission of influenza A viruses." <u>Virology</u> **479-480**: 234-246.
- 210. Neumann, G., T. Noda and Y. Kawaoka (2009). "Emergence and pandemic potential of swine-origin H1N1 influenza virus." Nature **459**(7249): 931-939.

- 211. Nguyen, S. N., Bobst, C.E. and Kaltashov, I.A. (2018). "Compositions and methods for delivering agents to the central nervous system." <u>U.S. Patent 9,950,075</u>.
- 212. Nicholls, J. M. (2013). "The battle between influenza and the innate immune response in the human respiratory tract." <u>Infect Chemother</u> **45**(1): 11-21.
- 213. Nie, C., M. Stadtmuller, H. Yang, Y. Xia, T. Wolff, C. Cheng and R. Haag (2020). "Spiky Nanostructures with Geometry-matching Topography for Virus Inhibition." <u>Nano Lett</u> **20**(7): 5367-5375.
- 214. Ning, F., C. Wang, K. Z. Berry, P. Kandasamy, H. Liu, R. C. Murphy, D. R. Voelker, C. W. Nho, C. H. Pan, S. Dai, L. Niu, H. W. Chu and G. Zhang (2014). "Structural characterization of the pulmonary innate immune protein SPLUNC1 and identification of lipid ligands." <u>FASEB J</u> 28(12): 5349-5360.
- 215. Nocini, R., G. Molteni, C. Mattiuzzi and G. Lippi (2020). "Updates on larynx cancer epidemiology." <u>Chin J Cancer Res</u> **32**(1): 18-25.
- 216. Nordlund-Moller, L., O. Andersson, R. Ahlgren, J. Schilling, M. Gillner, J. A. Gustafsson and J. Lund (1990). "Cloning, structure, and expression of a rat binding protein for polychlorinated biphenyls. Homology to the hormonally regulated progesterone-binding protein uteroglobin." J. Biol Chem. 265(21): 12690-12693.
- 217. Norman, J. A., P. Hobart, M. Manthorpe, P. Felgner and C. Wheeler (1997). "Development of improved vectors for DNA-based immunization and other gene therapy applications." <u>Vaccine</u> **15**(8): 801-803.
- 218. Nugteren, S. and J. N. Samsom (2021). "Secretory Leukocyte Protease Inhibitor (SLPI) in mucosal tissues: Protects against inflammation, but promotes cancer." Cytokine Growth Factor Rev **59**: 22-35.
- 220. Okumura, R., T. Kurakawa, T. Nakano, H. Kayama, M. Kinoshita, D. Motooka, K. Gotoh, T. Kimura, N. Kamiyama, T. Kusu, Y. Ueda, H. Wu, H. Iijima, S. Barman, H. Osawa, H. Matsuno, J. Nishimura, Y. Ohba, S. Nakamura, T. Iida, M. Yamamoto, E. Umemoto, K. Sano and K. Takeda (2016). "Lypd8 promotes the segregation of flagellated microbiota and colonic epithelia." Nature 532(7597): 117-121.
- 221. Olajuyin, A. M., X. Zhang and H. L. Ji (2019). "Alveolar type 2 progenitor cells for lung injury repair." <u>Cell Death Discov</u> **5**: 63.
- 222. Ostedgaard, L. S., M. P. Price, K. M. Whitworth, M. H. Abou Alaiwa, A. J. Fischer, A. Warrier, M. Samuel, L. D. Spate, P. D. Allen, B. M. Hilkin, G. S. Romano Ibarra, M. E. Ortiz Bezara, B. J. Goodell, S. E. Mather, L. S. Powers, M. R. Stroik, N. D. Gansemer, C. E. Hippee, K. Zarei, J. A. Goeken, T. R. Businga, E. A. Hoffman, D. K. Meyerholz, R. S. Prather, D. A. Stoltz and M. J. Welsh (2020). "Lack of airway submucosal glands impairs respiratory host defenses." <u>Elife</u> 9.
- 223. Ouadah, Y., E. R. Rojas, D. P. Riordan, S. Capostagno, C. S. Kuo and M. A. Krasnow (2019). "Rare Pulmonary Neuroendocrine Cells Are Stem Cells Regulated by Rb, p53, and Notch." <u>Cell</u> **179**(2): 403-416 e423.
- 224. Parekh, K. R., J. Nawroth, A. Pai, S. M. Busch, C. N. Senger and A. L. Ryan (2020). "Stem cells and lung regeneration." Am J Physiol Cell Physiol **319**(4): C675-C693.
- 225. Pasrija, R. and M. Naime (2021). "The deregulated immune reaction and cytokines release storm (CRS) in COVID-19 disease." <u>Int Immunopharmacol</u> **90**: 107225.
- 226. Patil, G. and S. Li (2019). "Tripartite motif proteins: an emerging antiviral protein family." Future Virol **14**(2): 107-122.

- 227. Peiris, J. S., C. Y. Cheung, C. Y. Leung and J. M. Nicholls (2009). "Innate immune responses to influenza A H5N1: friend or foe?" Trends Immunol **30**(12): 574-584.
- 228. Perez-Rubio, G., M. A. Ponce-Gallegos, B. A. Dominguez-Mazzocco, J. Ponce-Gallegos, R. A. Garcia-Ramirez and R. Falfan-Valencia (2021). "Role of the Host Genetic Susceptibility to 2009 Pandemic Influenza A H1N1." <u>Viruses</u> **13**(2).
- 229. Perrone, L. A., J. K. Plowden, A. Garcia-Sastre, J. M. Katz and T. M. Tumpey (2008). "H5N1 and 1918 pandemic influenza virus infection results in early and excessive infiltration of macrophages and neutrophils in the lungs of mice." PLoS Pathog 4(8): e1000115.
- 230. Picca, A., R. Calvani, H. J. Coelho-Junior, F. Landi, R. Bernabei and E. Marzetti (2020). "Mitochondrial Dysfunction, Oxidative Stress, and Neuroinflammation: Intertwined Roads to Neurodegeneration." <a href="https://doi.org/10.1007/j.nch.2016/j.nc
- 231. Pichlmair, A., O. Schulz, C. P. Tan, T. I. Naslund, P. Liljestrom, F. Weber and C. Reis e Sousa (2006). "RIG-I-mediated antiviral responses to single-stranded RNA bearing 5'-phosphates." Science 314(5801): 997-1001.
- 232. Plasschaert, L. W., R. Zilionis, R. Choo-Wing, V. Savova, J. Knehr, G. Roma, A. M. Klein and A. B. Jaffe (2018). "A single-cell atlas of the airway epithelium reveals the CFTR-rich pulmonary ionocyte." Nature **560**(7718): 377-381.
- 233. Policelli, C. (2016). "Analyses of idiopathic pulmonary fibrosis (IPF) inpatients in the United States." (Doctoral dissertation, Rutgers University-School of Health Professions).
- 234. Poltorak, A., Ricciardi-Castagnoli, P., Citterio, S. and Beutler, B., (2000). "Physical contact between lipopolysaccharide and toll-like receptor 4 revealed by genetic complementation." <u>Proceedings of the National Academy of Sciences</u>, (97(5)): pp.2163-2167.
- 235. Prasad, S. V., K. Fiedoruk, T. Daniluk, E. Piktel and R. Bucki (2019). "Expression and Function of Host Defense Peptides at Inflammation Sites." Int J Mol Sci **21**(1).
- 236. Raja, T. I., Mozafari, M., Milan, P.B., Samadikuchaksaraei, A. and Sefat, F., (2019). "Nanoengineered biomaterials for tracheal replacement." In Nanoengineered Biomaterials for Regenerative Medicine (pp. 285-303).
- 237. Rajavelu, P., G. Chen, Y. Xu, J. A. Kitzmiller, T. R. Korfhagen and J. A. Whitsett (2015). "Airway epithelial SPDEF integrates goblet cell differentiation and pulmonary Th2 inflammation." J Clin Invest **125**(5): 2021-2031.
- 238. Rayner, R. E., P. Makena, G. L. Prasad and E. Cormet-Boyaka (2019). "Optimization of Normal Human Bronchial Epithelial (NHBE) Cell 3D Cultures for in vitro Lung Model Studies." <u>Sci</u> <u>Rep</u> **9**(1): 500.
- 239. Rezaei, M., S. H. Zarkesh-Esfahani and M. Gharagozloo (2013). "The effect of different media composition and temperatures on the production of recombinant human growth hormone by CHO cells." Res Pharm Sci 8(3): 211-217.
- 240. Richard, Z. (2023). "Toll-like receptor (TLR) 7 and TLR8 stimulation of mucosal-associated invariant T cells and gamma delta T cells: a role in HIV susceptibility."
- 241. Rock, J. R., Onaitis, M. W., Rawlins, E. L., Lu, Y., Clark, C. P., Xue, Y., . . . Hogan, B. L (2009). "Basal cells as stem cells of the mouse trachea and human airway epithelium." <u>Proceedings of the National Academy of Sciences</u>,(106(31)): 12771-12775.
- 242. Rogers, D. F. (2003). "The airway goblet cell." Int J Biochem Cell Biol 35(1): 1-6.
- 243. Rogers, G. N., J. C. Paulson, R. S. Daniels, J. J. Skehel, I. A. Wilson and D. C. Wiley (1983). "Single amino acid substitutions in influenza haemagglutinin change receptor binding specificity." Nature **304**(5921): 76-78.
- 244. Rogers, K. e. (2010). "The respiratory system." Britannica Educational Publishing.

- 245. Rollins, B. M., A. Garcia-Caballero, M. J. Stutts and R. Tarran (2010). "SPLUNC1 expression reduces surface levels of the epithelial sodium channel (ENaC) in Xenopus laevis oocytes." Channels (Austin) **4**(4): 255-259.
- 246. Rosales, C. (2018). "Neutrophil: A Cell with Many Roles in Inflammation or Several Cell Types?" Front Physiol **9**: 113.
- 247. Rosales, C. (2020). "Neutrophils at the crossroads of innate and adaptive immunity." <u>J</u> <u>Leukoc Biol</u> **108**(1): 377-396.
- 248. Ross, A. J., L. A. Dailey, L. E. Brighton and R. B. Devlin (2007). "Transcriptional profiling of mucociliary differentiation in human airway epithelial cells." <u>Am J Respir Cell Mol Biol</u> **37**(2): 169-185.
- 249. Ryan, R., M. Failler, M. L. Reilly, M. Garfa-Traore, M. Delous, E. Filhol, T. Reboul, C. Bole-Feysot, P. Nitschke, V. Baudouin, S. Amselem, E. Escudier, M. Legendre, A. Benmerah and S. Saunier (2018). "Functional characterization of tektin-1 in motile cilia and evidence for TEKT1 as a new candidate gene for motile ciliopathies." <u>Hum Mol Genet</u> **27**(2): 266-282.
- 250. Saha, B. K. and W. H. Chong (2021). "Diffuse Alveolar Hemorrhage in Cardiac Diseases." Lung **199**(2): 103-112.
- 251. Sakuragi, S., H. Liao, K. Yajima, S. Fujiwara and H. Nakamura (2022). "Rubella Virus Triggers Type I Interferon Antiviral Response in Cultured Human Neural Cells: Involvement in the Control of Viral Gene Expression and Infectious Progeny Production." Int J Mol Sci **23**(17).
- 252. Samet, S. J. (2018). "Specific Gene Constellations of Swine Influenza a Viruses and Differences in the Host Antiviral Response Influences Disease Pathogenesis in Resistant and Susceptible Murine Strains." (Doctoral dissertation, University of Georgia).
- 253. Samji, T. (2009). "Influenza A: understanding the viral life cycle." <u>Yale J Biol Med</u> **82**(4): 153-159.
- 254. Sayeed, S., L. Nistico, C. St Croix and Y. P. Di (2013). "Multifunctional role of human SPLUNC1 in Pseudomonas aeruginosa infection." <u>Infect Immun</u> **81**(1): 285-291.
- 255. Schaefer, N., X. Li, M. A. Seibold, N. N. Jarjour, L. C. Denlinger, M. Castro, A. M. Coverstone, W. G. Teague, J. Boomer, E. R. Bleecker, D. A. Meyers, W. C. Moore, G. A. Hawkins, J. Fahy, B. R. Phillips, D. T. Mauger, A. Dakhama, S. Gellatly, N. Pavelka, R. Berman, Y. P. Di, S. E. Wenzel and H. W. Chu (2019). "The effect of BPIFA1/SPLUNC1 genetic variation on its expression and function in asthmatic airway epithelium." JCI Insight 4(8).
- 256. Schiller, H. B., D. T. Montoro, L. M. Simon, E. L. Rawlins, K. B. Meyer, M. Strunz, F. A. Vieira Braga, W. Timens, G. H. Koppelman, G. R. S. Budinger, J. K. Burgess, A. Waghray, M. van den Berge, F. J. Theis, A. Regev, N. Kaminski, J. Rajagopal, S. A. Teichmann, A. V. Misharin and M. C. Nawijn (2019). "The Human Lung Cell Atlas: A High-Resolution Reference Map of the Human Lung in Health and Disease." Am J Respir Cell Mol Biol 61(1): 31-41.
- 257. Schoggins, J. W. (2019). "Interferon-stimulated genes: what do they all do?" Annual review of virology,(6): pp.567-584.
- 258. Schulz, O., S. S. Diebold, M. Chen, T. I. Naslund, M. A. Nolte, L. Alexopoulou, Y. T. Azuma, R. A. Flavell, P. Liljestrom and C. Reis e Sousa (2005). "Toll-like receptor 3 promotes cross-priming to virus-infected cells." <u>Nature</u> **433**(7028): 887-892.
- 259. Schweitzer, K. S., T. Crue, J. M. Nall, D. Foster, S. Sajuthi, K. A. Correll, M. Nakamura, J. L. Everman, G. P. Downey, M. A. Seibold, J. P. Bridges, K. A. Serban, H. W. Chu and I. Petrache (2021). "Influenza virus infection increases ACE2 expression and shedding in human small airway epithelial cells." Eur Respir J 58(1).
- 260. Scott, A., S. Weldon and C. C. Taggart (2011). "SLPI and elafin: multifunctional antiproteases of the WFDC family." <u>Biochem Soc Trans</u> **39**(5): 1437-1440.

- 261. Seo, Y. J., C. J. Pritzl, M. Vijayan, C. R. Blake, M. E. McClain and B. Hahm (2012). "Sphingosine analogue AAL-R increases TLR7-mediated dendritic cell responses via p38 and type I IFN signaling pathways." <u>J Immunol</u> **188**(10): 4759-4768.
- 262. Shahverdi, M., J. Masoumi, F. Ghorbaninezhad, N. Shajari, F. Hajizadeh, H. Hassanian, N. Alizadeh, M. Jafarlou and B. Baradaran (2022). "The modulatory role of dendritic cell-T cell crosstalk in breast cancer: Challenges and prospects." Adv Med Sci **67**(2): 353-363.
- 263. Sharma, S., I. Verma and G. K. Khuller (2001). "Therapeutic potential of human neutrophil peptide 1 against experimental tuberculosis." Antimicrob Agents Chemother **45**(2): 639-640.
- Shen, L. W., H. J. Mao, Y. L. Wu, Y. Tanaka and W. Zhang (2017). "TMPRSS2: A potential target for treatment of influenza virus and coronavirus infections." Biochimie **142**: 1-10.
- 265. Shieh, W. J., D. M. Blau, A. M. Denison, M. Deleon-Carnes, P. Adem, J. Bhatnagar, J. Sumner, L. Liu, M. Patel, B. Batten, P. Greer, T. Jones, C. Smith, J. Bartlett, J. Montague, E. White, D. Rollin, R. Gao, C. Seales, H. Jost, M. Metcalfe, C. S. Goldsmith, C. Humphrey, A. Schmitz, C. Drew, C. Paddock, T. M. Uyeki and S. R. Zaki (2010). "2009 pandemic influenza A (H1N1): pathology and pathogenesis of 100 fatal cases in the United States." Am J Pathol 177(1): 166-175.
- 266. Shimazu, R., Akashi, S., Ogata, H., Nagai, Y., Fukudome, K., Miyake, K. and Kimoto, M., (1999). "MD-2, a molecule that confers lipopolysaccharide responsiveness on Toll-like receptor 4." The Journal of experimental medicine(189(11)): pp.1777-1782.
- 267. Shtyrya, Y. A., L. V. Mochalova and N. V. Bovin (2009). "Influenza virus neuraminidase: structure and function." <u>Acta Naturae</u> **1**(2): 26-32.
- 268. Siebel, C. a. L., U., (2017). "Notch signalling in development, tissue homeostasis, and disease." Physiological reviews, (97(4)): pp.1235-1294.
- 269. Simmaco, M., G. Kreil and D. Barra (2009). "Bombinins, antimicrobial peptides from Bombina species." Biochim Biophys Acta **1788**(8): 1551-1555.
- 270. Singh, N., Suthar, B., Mehta, A., Nema, N. and Pandey, A., (2020). "Corona virus: an immunological perspective review." Int J Immunol Immunother(7): p.050.
- 271. Slepushkin, V. A., P. D. Staber, G. Wang, P. B. McCray, Jr. and B. L. Davidson (2001). "Infection of human airway epithelia with H1N1, H2N2, and H3N2 influenza A virus strains." Mol Ther 3(3): 395-402.
- 272. Sollberger, G., A. Choidas, G. L. Burn, P. Habenberger, R. Di Lucrezia, S. Kordes, S. Menninger, J. Eickhoff, P. Nussbaumer, B. Klebl, R. Kruger, A. Herzig and A. Zychlinsky (2018). "Gasdermin D plays a vital role in the generation of neutrophil extracellular traps." <u>Sci Immunol</u> **3**(26).
- 273. Sountoulidis, A., A. Liontos, H. P. Nguyen, A. B. Firsova, A. Fysikopoulos, X. Qian, W. Seeger, E. Sundstrom, M. Nilsson and C. Samakovlis (2020). "SCRINSHOT enables spatial mapping of cell states in tissue sections with single-cell resolution." <u>PLoS Biol</u> **18**(11): e3000675.
- Spanakis, N., V. Pitiriga, V. Gennimata and A. Tsakris (2014). "A review of neuraminidase inhibitor susceptibility in influenza strains." <u>Expert Rev Anti Infect Ther</u> **12**(11): 1325-1336.
- 275. Steuerman, Y., M. Cohen, N. Peshes-Yaloz, L. Valadarsky, O. Cohn, E. David, A. Frishberg, L. Mayo, E. Bacharach, I. Amit and I. Gat-Viks (2018). "Dissection of Influenza Infection In Vivo by Single-Cell RNA Sequencing." <u>Cell Syst</u> **6**(6): 679-691 e674.
- 276. Stupnikov, M. R., Y. Yang, M. Mori, J. Lu and W. V. Cardoso (2019). "Jagged and Delta-like ligands control distinct events during airway progenitor cell differentiation." <u>Elife</u> **8**.
- 277. Suzuki, Y. (1994). "Gangliosides as influenza virus receptors: variation of influenza viruses and their recognition of the receptor sialo-sugar chains." <u>Progress in lipid research(33(4))</u>: pp.429-457.
- 278. Taherali, F., F. Varum and A. W. Basit (2018). "A slippery slope: On the origin, role and physiology of mucus." <u>Adv Drug Deliv Rev</u> **124**: 16-33.

- 279. Takeda, K. a. A., S., (2005). "Toll-like receptors in innate immunity." <u>International immunology</u>(17(1)): pp.1-14.
- 280. Takeuchi, O., T. Kawai, P. F. Muhlradt, M. Morr, J. D. Radolf, A. Zychlinsky, K. Takeda and S. Akira (2001). "Discrimination of bacterial lipoproteins by Toll-like receptor 6." Int Immunol13(7): 933-940.
- 281. Tam, S. Y. J. (2022). "Exploring the Effects of Toll-Like Receptor 4 Antagonism on Gastrointestinal Mucositis and Tumour Activity." (<u>Doctoral dissertation</u>).
- 282. Tarran, R. and M. R. Redinbo (2014). "Mammalian short palate lung and nasal epithelial clone 1 (SPLUNC1) in pH-dependent airway hydration." Int J Biochem Cell Biol **52**: 130-135.
- 283. Tavares, T. D., J. C. Antunes, J. Padrao, A. I. Ribeiro, A. Zille, M. T. P. Amorim, F. Ferreira and H. P. Felgueiras (2020). "Activity of Specialized Biomolecules against Gram-Positive and Gram-Negative Bacteria." Antibiotics (Basel) **9**(6).
- 284. Teirumnieks, E., Balchev, I., Ghalot, R.S. and Lazov, L., (2020). "Antibacterial and anti-viral effects of silver nanoparticles in medicine against COVID-19-a review." <u>Laser Physics</u>(31(1)): p.013001.
- 285. Terryah, S. T., R. C. Fellner, S. Ahmad, P. J. Moore, B. Reidel, J. I. Sesma, C. S. Kim, A. L. Garland, D. W. Scott, J. R. Sabater, J. Carpenter, S. H. Randell, M. Kesimer, W. M. Abraham, W. J. Arendshorst and R. Tarran (2018). "Evaluation of a SPLUNC1-derived peptide for the treatment of cystic fibrosis lung disease." Am J Physiol Lung Cell Mol Physiol **314**(1): L192-L205.
- 286. Thakur, A., A. Sharma, H. K. Alajangi, P. K. Jaiswal, Y. B. Lim, G. Singh and R. P. Barnwal (2022). "In pursuit of next-generation therapeutics: Antimicrobial peptides against superbugs, their sources, mechanism of action, nanotechnology-based delivery, and clinical applications." International-Parameter Superbugs-4, Biol Macromol **218**: 135-156.
- 287. Thompson, A. J., R. P. de Vries and J. C. Paulson (2019). "Virus recognition of glycan receptors." <u>Curr Opin Virol</u> **34**: 117-129.
- 288. Tilley, A. E., M. S. Walters, R. Shaykhiev and R. G. Crystal (2015). "Cilia dysfunction in lung disease." Annu Rev Physiol **77**: 379-406.
- 289. Tong, S., Y. Li, P. Rivailler, C. Conrardy, D. A. Castillo, L. M. Chen, S. Recuenco, J. A. Ellison, C. T. Davis, I. A. York, A. S. Turmelle, D. Moran, S. Rogers, M. Shi, Y. Tao, M. R. Weil, K. Tang, L. A. Rowe, S. Sammons, X. Xu, M. Frace, K. A. Lindblade, N. J. Cox, L. J. Anderson, C. E. Rupprecht and R. O. Donis (2012). "A distinct lineage of influenza A virus from bats." Proc Natl Acad Sci U S A 109(11): 4269-4274.
- 290. Torre, P. and A. I. Flores (2020). "Current Status and Future Prospects of Perinatal Stem Cells." <u>Genes (Basel)</u> **12**(1).
- 291. Townsend, L., A. H. Dyer, K. Jones, J. Dunne, A. Mooney, F. Gaffney, L. O'Connor, D. Leavy, K. O'Brien, J. Dowds, J. A. Sugrue, D. Hopkins, I. Martin-Loeches, C. Ni Cheallaigh, P. Nadarajan, A. M. McLaughlin, N. M. Bourke, C. Bergin, C. O'Farrelly, C. Bannan and N. Conlon (2020). "Persistent fatigue following SARS-CoV-2 infection is common and independent of severity of initial infection." <u>PLoS One</u> 15(11): e0240784.
- 292. Travaglini, K. J., A. N. Nabhan, L. Penland, R. Sinha, A. Gillich, R. V. Sit, S. Chang, S. D. Conley, Y. Mori, J. Seita, G. J. Berry, J. B. Shrager, R. J. Metzger, C. S. Kuo, N. Neff, I. L. Weissman, S. R. Quake and M. A. Krasnow (2020). "A molecular cell atlas of the human lung from single-cell RNA sequencing." Nature **587**(7835): 619-625.
- 293. Tsou, Y. A., M. C. Tung, K. A. Alexander, W. D. Chang, M. H. Tsai, H. L. Chen and C. M. Chen (2018). "The Role of BPIFA1 in Upper Airway Microbial Infections and Correlated Diseases." Biomed Res Int 2018: 2021890.
- 294. Tykalová, M. H. (2022). "Interaction of tick-borne encephalitis virus with host and vector cells." <u>Doctoral dissertation, Academy of Sciences of the Czech Republic</u>.

- 295. Tyner, J. W., E. Y. Kim, K. Ide, M. R. Pelletier, W. T. Roswit, J. D. Morton, J. T. Battaile, A. C. Patel, G. A. Patterson, M. Castro, M. S. Spoor, Y. You, S. L. Brody and M. J. Holtzman (2006). "Blocking airway mucous cell metaplasia by inhibiting EGFR antiapoptosis and IL-13 transdifferentiation signals." J Clin Invest **116**(2): 309-321.
- 296. Ugonna, K., C. D. Bingle, K. Plant, K. Wilson and M. L. Everard (2014). "Macrophages are required for dendritic cell uptake of respiratory syncytial virus from an infected epithelium." <u>PLoS</u> One **9**(3): e91855.
- 297. Ulevitch, R. J. and P. S. Tobias (1995). "Receptor-dependent mechanisms of cell stimulation by bacterial endotoxin." <u>Annu Rev Immunol</u> **13**: 437-457.
- 298. Ulfig, A. and L. I. Leichert (2021). "The effects of neutrophil-generated hypochlorous acid and other hypohalous acids on host and pathogens." Cell Mol Life Sci **78**(2): 385-414.
- 299. Ushakumary, M. G., Riccetti, M. and Perl, A.K.T., (2021). "Resident interstitial lung fibroblasts and their role in alveolar stem cell niche development, homeostasis, injury, and regeneration." Stem cells translational medicine(10(7)): pp.1021-1032.
- 300. Utkin, Y., A. Siniavin, I. Kasheverov and V. Tsetlin (2022). "Antiviral Effects of Animal Toxins: Is There a Way to Drugs?" Int J Mol Sci **23**(7).
- 301. Vachon, E., Y. Bourbonnais, C. D. Bingle, S. J. Rowe, M. F. Janelle and G. M. Tremblay (2002). "Anti-inflammatory effect of pre-elafin in lipopolysaccharide-induced acute lung inflammation." Biol Chem **383**(7-8): 1249-1256.
- 302. Van Poucke, S. G., J. M. Nicholls, H. J. Nauwynck and K. Van Reeth (2010). "Replication of avian, human and swine influenza viruses in porcine respiratory explants and association with sialic acid distribution." Virol J **7**: 38.
- 303. Vance, S. J., R. E. McDonald, A. Cooper, B. O. Smith and M. W. Kennedy (2013). "The structure of latherin, a surfactant allergen protein from horse sweat and saliva." <u>J R Soc Interface</u> **10**(85): 20130453.
- 304. Vareille, M., E. Kieninger, M. R. Edwards and N. Regamey (2011). "The airway epithelium: soldier in the fight against respiratory viruses." <u>Clin Microbiol Rev</u> **24**(1): 210-229.
- 305. Varela-Fernandez, R., X. Garcia-Otero, V. Diaz-Tome, U. Regueiro, M. Lopez-Lopez, M. Gonzalez-Barcia, M. Isabel Lema and F. Javier Otero-Espinar (2022). "Lactoferrin-loaded nanostructured lipid carriers (NLCs) as a new formulation for optimized ocular drug delivery." <u>Eur</u> J Pharm Biopharm **172**: 144-156.
- 306. Vargas, P. A., P. M. Speight, C. D. Bingle, A. W. Barrett and L. Bingle (2008). "Expression of PLUNC family members in benign and malignant salivary gland tumours." Oral Dis **14**(7): 613-619.
- 307. Veloso, P., A. Fernandez, J. Astorga, D. Gonzalez-Quintanilla, A. Castro, A. Escobar, A. Hoare and M. Hernandez (2022). "Lipopolysaccharide from Porphyromonas gingivalis, but Not from Porphyromonas endodontalis, Induces Macrophage M1 Profile." Int J Mol Sci 23(17).
- 308. Wang, H., L. He, B. Liu, Y. Feng, H. Zhou, Z. Zhang, Y. Wu, J. Wang, Y. Gan, T. Yuan, M. Wu, X. Xie and Z. Feng (2018). "Establishment and comparison of air-liquid interface culture systems for primary and immortalized swine tracheal epithelial cells." <u>BMC Cell Biol</u> **19**(1): 10.
- 309. Wang, J., R. Oberley-Deegan, S. Wang, M. Nikrad, C. J. Funk, K. L. Hartshorn and R. J. Mason (2009). "Differentiated human alveolar type II cells secrete antiviral IL-29 (IFN-lambda 1) in response to influenza A infection." J Immunol **182**(3): 1296-1304.
- 310. Wang, Y., Hong, J., Liu, X., Yang, H., Liu, R., Wu, J., Wang, A., Lin, D. and Lai, R., (2008). "Snake cathelicidin from Bungarus fasciatus is a potent peptide antibiotics." <u>PloS one(3(9))</u>: p.e3217.
- 311. Wanner, A., M. Salathe and T. G. O'Riordan (1996). "Mucociliary clearance in the airways." Am J Respir Crit Care Med **154**(6 Pt 1): 1868-1902.

- 312. Ward, P. P. and O. M. Conneely (2004). "Lactoferrin: role in iron homeostasis and host defense against microbial infection." <u>Biometals</u> **17**(3): 203-208.
- 313. Webb, N. E., B. Bernshtein and G. Alter (2021). "Tissues: the unexplored frontier of antibody mediated immunity." <u>Curr Opin Virol</u> **47**: 52-67.
- 314. Wegen, S., L. van Heek, P. Linde, K. Claus, D. Akuamoa-Boateng, C. Baues, S. J. Sharma, K. Schomacker, T. Fischer, K. S. Roth, J. P. Klussmann, S. Marnitz, A. Drzezga and C. Kobe (2022). "Head-to-Head Comparison of [(68) Ga]Ga-FAPI-46-PET/CT and [(18)F]F-FDG-PET/CT for Radiotherapy Planning in Head and Neck Cancer." Mol Imaging Biol **24**(6): 986-994.
- 315. Weiss, J., P. Elsbach, I. Olsson and H. Odeberg (1978). "Purification and characterization of a potent bactericidal and membrane active protein from the granules of human polymorphonuclear leukocytes." J Biol Chem 253(8): 2664-2672.
- 316. Weston, W. M., E. E. LeClair, W. Trzyna, K. M. McHugh, P. Nugent, C. M. Lafferty, L. Ma, R. S. Tuan and R. M. Greene (1999). "Differential display identification of plunc, a novel gene expressed in embryonic palate, nasal epithelium, and adult lung." <u>J Biol Chem</u> **274**(19): 13698-13703.
- 317. Whitsett, J. A. (2018). "Airway Epithelial Differentiation and Mucociliary Clearance." <u>Ann</u> Am Thorac Soc **15**(Suppl 3): S143-S148.
- 318. Whitsett, J. A. and T. Alenghat (2015). "Respiratory epithelial cells orchestrate pulmonary innate immunity." Nat Immunol **16**(1): 27-35.
- 319. Widdicombe, J. H. (2019). "Early studies of airway submucosal glands." <u>Am J Physiol Lung</u> Cell Mol Physiol **316**(6): L990-L998.
- 320. Wilschanski, M. and P. R. Durie (2007). "Patterns of GI disease in adulthood associated with mutations in the CFTR gene." <u>Gut</u> **56**(8): 1153-1163.
- Winkelmann, A. and T. Noack (2010). "The Clara cell: a "Third Reich eponym"?" <u>Eur Respir</u> J **36**(4): 722-727.
- 322. Wolf, D. and S. P. Goff (2008). "Host restriction factors blocking retroviral replication." Annu Rev Genet **42**: 143-163.
- 323. Wu, L., Q. Wei, J. Brzostek and N. R. J. Gascoigne (2020). "Signaling from T cell receptors (TCRs) and chimeric antigen receptors (CARs) on T cells." <u>Cell Mol Immunol</u> **17**(6): 600-612.
- 324. Wu, N. H., W. Yang, A. Beineke, R. Dijkman, M. Matrosovich, W. Baumgartner, V. Thiel, P. Valentin-Weigand, F. Meng and G. Herrler (2016). "The differentiated airway epithelium infected by influenza viruses maintains the barrier function despite a dramatic loss of ciliated cells." <u>Sci</u> Rep **6**: 39668.
- 325. Wu, Q., D. Jiang, M. Minor and H. W. Chu (2014). "Electronic cigarette liquid increases inflammation and virus infection in primary human airway epithelial cells." <u>PLoS One</u> **9**(9): e108342.
- 326. Wu, R., Y. H. Zhao and M. M. Chang (1997). "Growth and differentiation of conducting airway epithelial cells in culture." <u>Eur Respir J</u> **10**(10): 2398-2403.
- 327. Wu, T., J. Huang, P. J. Moore, M. S. Little, W. G. Walton, R. C. Fellner, N. E. Alexis, Y. Peter Di, M. R. Redinbo, S. L. Tilley and R. Tarran (2017). "Identification of BPIFA1/SPLUNC1 as an epithelium-derived smooth muscle relaxing factor." Nat Commun 8: 14118.
- 328. Yan, N. and Z. J. Chen (2012). "Intrinsic antiviral immunity." Nat Immunol **13**(3): 214-222.
- 329. Yang, I. V., L. H. Burch, M. P. Steele, J. D. Savov, J. W. Hollingsworth, E. McElvania-Tekippe, K. G. Berman, M. C. Speer, T. A. Sporn, K. K. Brown, M. I. Schwarz and D. A. Schwartz (2007). "Gene expression profiling of familial and sporadic interstitial pneumonia." <u>Am J Respir Crit Care Med</u> **175**(1): 45-54.

- 330. Yang, J., B. J. Hernandez, D. Martinez Alanis, O. Narvaez del Pilar, L. Vila-Ellis, H. Akiyama, S. E. Evans, E. J. Ostrin and J. Chen (2016). "The development and plasticity of alveolar type 1 cells." Development **143**(1): 54-65.
- 331. You, Y., T. Huang, E. J. Richer, J. E. Schmidt, J. Zabner, Z. Borok and S. L. Brody (2004). "Role of f-box factor foxj1 in differentiation of ciliated airway epithelial cells." <u>Am J Physiol Lung</u> Cell Mol Physiol **286**(4): L650-657.
- 332. You, Y., E. J. Richer, T. Huang and S. L. Brody (2002). "Growth and differentiation of mouse tracheal epithelial cells: selection of a proliferative population." <u>Am J Physiol Lung Cell Mol Physiol</u> **283**(6): L1315-1321.
- 333. Youssef, N., A. A. Kassem, R. M. Farid, F. A. Ismail, M. A. E. El-Massik and N. A. Boraie (2018). "A novel nasal almotriptan loaded solid lipid nanoparticles in mucoadhesive in situ gel formulation for brain targeting: Preparation, characterization and in vivo evaluation." Int J Pharm 548(1): 609-624.
- 334. Zanna, M. Y., A. R. Yasmin, A. R. Omar, S. S. Arshad, A. R. Mariatulqabtiah, S. H. Nur-Fazila and M. I. N. Mahiza (2021). "Review of Dendritic Cells, Their Role in Clinical Immunology, and Distribution in Various Animal Species." Int J Mol Sci 22(15).
- 335. Zaragosi, L. E., M. Deprez and P. Barbry (2020). "Using single-cell RNA sequencing to unravel cell lineage relationships in the respiratory tract." <u>Biochem Soc Trans</u> **48**(1): 327-336.
- 336. Zasloff, M. (1987). "Magainins, a class of antimicrobial peptides from Xenopus skin: isolation, characterization of two active forms, and partial cDNA sequence of a precursor." Procure Natl Acad Sci U S A 84(15): 5449-5453.
- 337. Zegels, G., G. A. Van Raemdonck, W. A. Tjalma and X. W. Van Ostade (2010). "Use of cervicovaginal fluid for the identification of biomarkers for pathologies of the female genital tract." Proteome Sci **8**: 63.
- 338. Zepp, J. A., W. J. Zacharias, D. B. Frank, C. A. Cavanaugh, S. Zhou, M. P. Morley and E. E. Morrisey (2017). "Distinct Mesenchymal Lineages and Niches Promote Epithelial Self-Renewal and Myofibrogenesis in the Lung." <u>Cell</u> **170**(6): 1134-1148 e1110.
- 339. Zhang, J. and K. Nawata (2017). "A comparative study on predicting influenza outbreaks." <u>Biosci Trends</u> **11**(5): 533-541.
- 340. Zhang, W. J., K. Y. Li, B. H. Huang, H. Wang, S. G. Wan and S. C. Zhou (2022). "The hepatocyte in the innate immunity." <u>Virology</u> **576**: 111-116.
- 341. Zhou, X., J. Cui, V. Macias, A. A. Kajdacsy-Balla, H. Ye, J. Wang and P. N. Rao (2007). "The progress on genetic analysis of nasopharyngeal carcinoma." <u>Comp Funct Genomics</u> **2007**: 57513.